HYDRODYNAMIC CHARACTERISTICS OF GAS/LIQUID/FIBER THREE-PHASE FLOWS BASED ON OBJECTIVE AND MINIMALLY-INTRUSIVE PRESSURE FLUCTUATION MEASUREMENTS

A Dissertation
Presented to
The Academic Faculty

by

Tao Xie

In Partial Fulfillment
of the Requirements for the Degree
Doctor of Philosophy in the
School of Mechanical Engineering

Georgia Institute of Technology
August 2004

HYDRODYNAMIC CHARACTERISTICS OF GAS/LIQUID/FIBER THREE-PHASE FLOWS BASED ON OBJECTIVE AND MINIMALLY-INTRUSIVE PRESSURE FLUCTUATION MEASUREMENTS

APPROVED BY:

Dr. S. Mostafa Ghiaasiaan, Chair

Dr. Seppo Karrila

Dr. D. William Tedder

Dr. Minami Yoda

Dr. Andrei G. Fedorov

Dr. Tom McDonough

Date Approved: 08/30/2004

ACKNOWLEDGMENTS

First and foremost, I would like to thank my advisor, Dr. S. Mostafa Ghiaasiaan, and my former co-advisor, Dr. Seppo Karrila. The successful completion of this investigation and subsequent thesis would not have been possible without their constant support and guidance during my studies at Georgia Tech. And I would also like to thank my thesis committee members, Dr. Tom McDonough, Dr. Andrei Fedorov, Dr. Minami Yoda, and Dr. Daniel Tedder for their insightful comments and suggestions. Special thanks go to Dr. T. J. Heindel for his guidance in my earlier days of this PhD program.

I cannot fully express my gratitude to the exceptional team at Institute of Paper Science and Technology. For their generous assistance in the research of this thesis, I would like to acknowledge Chris Nelson, Clark Woitkovich, Mark Szlemko, and Mike Buchanan.

I am very grateful to U.S. Department of Energy for funding this research under grant DE-FC07-00ID13871 through Institute of Paper Science and Technology.

I would also thank Georgia Institute of Technology. This institute will forever be part of who I am since I have spent five years here for my graduate work.

Last but not least, I would be remiss if I did not mention my parents, Xie, Guanrong and Zeng, Guangze, who have been the greatest inspiration of all through their strength, nobility, and fortitude. And I would not forget to thank my sister, Xie, Lan, for encouraging me and not allowing me to give up when I am feeling overwhelmed.

To all of you, I humbly dedicate this thesis.

TABLE OF CONTENTS

LIST OF FIGURES

FIGURE **PAGE**

LIST OF TABLES

TABLE **PAGE**

NOMENCLATURE

Notations

A	Flow cross-sectional area (m^2)
$\mathbf{A}$	Coefficient matrix
Bo	Boiling number
$\mathbf{C}$	Column vector
C_0	Drift flux distribution coefficient
D	Channel Diameter (m)
D_H	Hydraulic diameter (m)
d	Bias in neuron activation function; Discrete time shift
f	Frequency (*Hz*); Friction factor
f_s	Sampling frequency (*Hz*)
G	Mass flux ($kg/m^2 s$)
g	Gravitational acceleration (m/s^2)
h	Specific enthalpy (J/kg)
h_{fg}	Specific heat of vaporization (J/kg)
I	Gamma-ray count
I_G, I_L	Gamma-ray counts with pure gas and pure liquid, respectively
j	Pressure time series coordinate
$K_{L,i}a_i''$	Interfacial volumetric mass transfer coefficient ($kg/m^3 s$)
$K_{L,P}a_P''$	Interphase-liquid bulk volumetric mass transfer coefficient ($kg/m^3 s$)

k	Discrete time shift
L	Length (m)
l	Chord length (m)
N	Total number of counts in Gamma-ray densitometry; Finite length of a discrete time signal
O_2	Oxygen
O_3	Ozone
P	Pressure (Pa)
$p*$	Normalized pressure signal
P_x	Power spectral density function (dB)
p_f	Wetted perimeter (m)
p_H	Heated perimeter (m)
q''	Heat flux (W/m^2)
R_x	Autocorrelation function
S	Slip ratio; Correlation term
s	Neural network input
T	Temperature (K); The second-order correlation term
U	Velocity (m/s)
u	Threshold in activation function
U_G	Gas phase velocity (m/s)
U_{GS}	Superficial gas velocity (cm/s)
U_{LS}	Superficial pulp-water liquid velocity (cm/s)

V	Average velocity (m/s)
V_{GJ}	Gas drift velocity (m/s)
W	Weight factor
X_{tt}	Martinelli factor
$x(n)$	Discrete time signal
$\boldsymbol{Y}$	Column vector containing the state variables
y	Neuron output
Z	Ohnesorge number
z	Axial coordinate (m)

Greek Letters

α	Void fraction
β	Slope parameter in transfer function
γ	Constant
δ	Local gradient of network
δ_F	Film thickness
ε	Gas holdup (void fraction), roughness
ε_i	Chord-average void fraction for chord i
ζ	Fiber consistency in mixture (%); Statistic defined in Equation; Relative error
η	Constant
θ	Unit step function; Angle of inclination with respect to the horizontal plane
μ	Viscosity

ν	Kinematic viscosity
ξ_i	Uncertainty in ε_i
ρ	Density
σ_f^2	Variance of spectrum
τ	Time shift (s); Shear stress
τ_d	Wall shear stress

Superscripts

-	Cross-section average
T	Transpose
*	Dimensionless

Abbreviations

ANN	Artificial neural network
CHF	Critical heat flux
FPM	First-principle model

SUMMARY

Experiments were performed in an instrumented three-phase bubble column to investigate the flow patterns and void fractions in gas-water-pulp three-phase flows in a vertical, upward column, with gas and gas-water slurry through-flows. The investigation is novel, and examines the hydrodynamics of gas-liquid-fiber mixtures over a relatively wide range of superficial phase velocities not investigated in the past. Flow regimes were identified, and gas holdup (void fraction) was measured. The range of pulp consistency (i.e., weight fraction of dry pulp in the pulp-water mixture) in the experiments was varied in the 0.0~1.5% range, which represents the low consistency (LC) pulp suspension range. Empirical flow regime maps were developed, and the void fraction data were correlated using the Drift Flux Model (DFM) (Xie et al., 2003a).

The aforementioned test facility, with some modifications, was subsequently used (Xie et al., 2003b), whereby local pressure fluctuations recorded by a single high-sensitivity dynamic pressure transducer at a particular location on the test section wall (1.2 m above the test section inlet) were recorded and utilized for the development of an ANN-based method for flow regime classification. Two different feed-forward back-propagation artificial neural networks were designed, trained and tested to demonstrate the feasibility of flow regime identification based on signals recorded by a single sensor. The inputs were statistical properties of pressure signal: the standard deviation, coefficients of skewness and kurtosis, and several time shift autocorrelations of normalized pressure signals. The results successfully demonstrated the suitability of the developed ANN-based method for flow regime characterization.

Although the aforementioned study had clearly shown that ANNs are capable of learning to recognize flow regimes based on pressure fluctuation and some other flow-induced signals, it was noted that a number of important issues needed to be resolved before ANNs could find widespread industrial applications. Practical functional transportability of trained ANNs is among these crucial issues. This *transportability is defined* here as the capability of a single ANN to function with several sensors in the following sense: trained with a sensor, and/or a scaled-down system, it performs acceptably with another reasonably similar sensor and/or a prototypical-scale system. The ANN must then use somewhat sensor-independent, invariant characteristics of the input signals; we thus need to help it along by preprocessing these signals to promote such invariance in the inputs.

Using the data obtained with the aforementioned test facility (Xie et al., 2003b), the transportability of an ANN trained for regime classification, between pressure signals obtained from three separate but in principle similar sensors, was examined. The sensors represented different observation points in the flow that was not fully developed, and their signal characteristics were therefore somewhat different. In addition, differences were present in the sensor calibration (zero, gain, and linearity), and in the physical installations of the sensors. These differences can evidently affect their signals. Transportability with respect to multiple similar sensors applied to the same system scale (i.e., no scale-change difference) was considered here. This type of transportability is important, it must be emphasized, since small differences among similar sensors (caused by sensor drift, for example) are often inevitable. An ANN was developed that used the power spectral characteristics of the normalized pressure fluctuations as input, and its

transportability was successfully shown. An ANN-based method was furthermore developed that enhanced the transportability of the aforementioned ANNs. While a redundant system with multiple sensors is an obvious target application, such robustness of algorithms that provides transportability will also contribute to performance with a single sensor, shielding against effects of calibration changes or sensor replacements.

The hybrid artificial neural network-first principle modeling (ANN-FPM) is a flexible and useful methodology that has recently found applications for complex multiphase flow processes. In this method the flow state variables are obtained from the solution of conservation equations using first principle-based closure relations whenever possible, and using trained artificial neural networks for poorly-understood constitutive relations and rate processes for which experimental data are available. The available qualified dryout heat flux data representing uniformly-heated circular microchanels (channels with diameters of around or slightly larger than 1mm) are compared with two widely-used critical heat flux (CHF) correlations that are well known for their accuracy, showing poor agreement. An ANN-FPM method was developed, whereby the boiling and two-phase flow processes in the heated channels were predicted based on a simple slip-flow technique which constituted the first-principle model component. Dryout heat flux was assumed to depend on local thermal and hydrodynamic parameters predicted by the aforementioned first-principle model. A feed-forward, back-propagation artificial neural network was then designed and trained for predicting the conditions that lead to dryout, and was coupled to the first-principle model. The developed ANN-FPM was shown to predict all the data and their trends very well.

CHAPTER 1

INTRODUCTION

1.1 Background

Multiphase flows and their related technology play an important role in the chemical and process industry. Handling systems involving two or more phases is common in areas from the processing of fuels and chemicals to the production of food, paper, pharmaceuticals and specialty materials. Despite the wide usage of multiphase systems, the current methodology adopted for the design and operation of multiphase flow systems is by and large based on intuition and rules of thumb rather than on first principles. The main reason for this state of affairs is that the local flow structures are typically extremely complex and the link between the micro and macro-scales has not been clearly established. Consequently, our understanding of the numerous hydrodynamic problems encountered in multiphase systems remains incomplete. The main reasons for the inability to treat these flows purely from a theoretical basis are the lack of detailed structural and dynamic information at the micro-scale, and the mathematical difficulties associated with the methods for handling the randomness of the multiphase media. Successful approach towards the understanding of such complex flows requires reliable data, which in turn depends on the implementation of sophisticated sensors and measuring techniques capable of non-invasive measurements, as well as the ability to record the required information associated with the entire flow field (Chaouki et al., 1997).

Multiphase flows have many important applications in paper-making industry, one of which is a fibrous slurry flow in bubble columns subject to the flow of paper pulp and water with a throughput of gas. This gas-liquid-pulp fiber slurry flow occurs in a number of systems in paper-making and recycling, including flotation deinking, delignification and bleaching (Smook, 1992). Gas-liquid-pulp mixtures exhibit hydrodynamics that are much more complex than what is observed in typical gas-liquid flows, and even in gas-non-Newtonian liquid two-phase flows. Pulp fibers in an aqueous suspension swell by absorbing water, and in the simplest interpretation a pulp-water mixture can be considered a yield-pseudoplastic fluid (Duffy and Titchener, 1975; Duffy et al., 1976; Bennington et al., 1995), acting as a solid when shear stress is below some threshold, and as a non-Newtonian liquid otherwise. Flocculation (entanglement of fiber groups to conformations that possess mechanical strength, usually called flocs) is the main cause for the complexity in pulp slurries as well as in gas-liquid-pulp three-phase flow systems, and can be observed at consistencies (weight fractions of dry pulp in the water-pulp mixture) as low as 0.5%. At consistencies higher than about 1%, three-dimensional networks of pulp form in the mixture (Bennington et al., 1989) that can be broken down by high shear only. These networks can trap small bubbles (Walmsley, 1992), and often they lead to the channeling phenomenon in flotation devices whereby the gas preferentially flows through inter-floc passages (Lindsay et al., 1995). The size and strength of flocs increase as consistency is increased. Flocculation, which is facilitated by the high aspect ratio of fibers, thus renders gas-liquid-pulp systems drastically different in their behavior compared with other gas-solid-liquid three-phase

systems, as well as non-Newtonian liquid-gas two-phase flows. Some rather complicated flow regimes are induced, even in uniformly aerated bubble columns.

Basically, in multiphase flow systems different flow morphological configurations can occur, and the hydrodynamic and kinematical characteristics of the system vary with different flow regimes. For design and modeling of bubble columns and other multiphase flow systems, therefore, it is of theoretical and practical significance to identify the major flow regimes or flow patterns, and develop a method to predict the parameter ranges of occurrence of each regime. In many engineering problems, it is imperative to develop a reliable, objective and quantitative instrumentation-based indicator of flow regime (Xie et al, 2003b).

Artificial neural networks (ANNs) are analytical tools that imitate the neural aspect of the human brain, whereby learning is based on experience and repetition rather than the application of rule-based principles and formulas. An ANN consists of a layered network of neurons (nodes), with each neuron connected to a large number of others. The input signal to the network is passed among the neurons, with each neuron calculating its own output using weighting associated with connections. Learning is achieved by the adjustment of the weights associated with inter-neuron connections. ANNs provide capabilities such as learning, self-organization, generalization (response to new problems using incomplete information), and training; and are excellent for pattern recognition and trend prediction for processes that are highly nonlinear, poorly-understood, and/or too complex for accurate mathematical modeling. They are thus ideal for application in multiphase flow systems, and when properly designed and trained, can be used for on-

line monitoring and diagnostics. ANNs are now increasingly applied in various branches of finance, science, and industry.

Attempts at the identification of two-phase flow patterns using objective sensor response-based methods have been made in the past. The patterns of the variations and fluctuations of local absolute and differential pressures (Hubbard et al., 1966; Weisman, et al., 1979; Matsui, 1984; Matsui, 1986; Lin and Hanratty, 1986; Spedding and Spence, 1993; Cai et al., 1996), and cross-sectional average electric capacitance of the flow field (Mi et al., 1998), for example, have been found to be strongly regime-dependent. The pressure fluctuations that result from the passage of gas and liquid pockets, and their statistical characteristics (power spectral density, probability density function, auto and cross-correlation functions), are particularly attractive for flow pattern classification because the required sensors are robust, inexpensive, and relatively well-developed, and are thus more likely to be applied in the industrial systems.

Although the application of neural networks to multiphase flow problems has started only recently, the published studies have clearly demonstrated their enormous potential. Mi et al. (1998) applied a neural network for two-phase flow regime identification in a vertical channel using signals from electric capacitance probes with excellent results. Gupta et al. (1999) successfully applied a hybrid method based on four neural networks along with simple first-principles models (the latter meant to render the model independent of specific device geometry), for the prediction of attachment rate constant in flotation columns.

Neural network-based techniques thus provide a vast potential for the study of basic hydrodynamics, and non-intrusive monitoring and diagnostics of multiphase flow

systems, in particular for large, opaque, and/or hazardous material-containing systems where direct visual and intrusive observation and monitoring are difficult.

1.2 Objectives of This Investigation

The primary objective of this investigation is to develop and demonstrate objective and minimally-intrusive flow regime classification methods for gas/water/paper pulp three-phase slurries, based on artificial neural network-assisted recognition of patterns in the statistical characteristics of pressure fluctuations. The transportability of the developed method, whereby an artificial neural network trained and tested with a set of data is manipulated and used for the characterization of an unseen and different but plausible similar data set, is also to be examined.

1.3 Outline of This Thesis

The reminder of this dissertation continues as follows:

In chapter 2, the literature dealing with the fundamental two-phase flow and the hydrodynamic characteristics of gas/liquid/fiber pulp slurry three-phase flows in bleaching systems, as well as their flow regimes, are briefly reviewed in Sections 2.1, 2.2 and 2.3, respectively, and are followed by a brief discussion of artificial neural networks and their recent applications in chemical and process engineering in Sections 2.4 and 2.5.

The experimental system and analytical methods that were used in this study are then explained in Chapter 3.

Chapter 4 presents a detailed description of flow regimes observed in this study.

Chapter 5 provides the neural network models developed for flow pattern classification using pressure fluctuation signals, and discusses their transportability and offers recommendations for future neural network-based identification technique research.

Chapter 6 concludes this study and offers recommendations.

Appendix I contains void fraction data. Appendix II contains artificial neural network data for flow regime identification. Appendix III presents the description of a hybrid artificial neural network-first principle model used for predicting critical heat flux in mini-channels. Appendix IV outlines FORTRAN codes that were developed for the artificial neural network-first principle modeling (ANN-FPM) of critical heat flux. Appendix V contains experimental data for dryout in the studied mini-channels. Appendix VI lists the published papers based on this thesis work.

CHAPTER 2

LITERATURE REVIEW

2.1 Two-Phase Flow

Two-phase flow has been extensively investigated in the past. A study of the characteristics of three-phase flow could not be accomplished without understanding of the state-of-the-art with respect to two-phase flow dynamics. An overview of the two-phase flow dynamics is presented in this section.

A two-phase flow system, one in which gas and liquid are simultaneously present within a single system, is of interest here. The phases can be flowing co-currently, counter-currently, or the gaseous phase could be flowing through a stationary liquid. The void distribution patterns, and the flow regimes, of two-phase systems have been extensively studied by many researchers, and have been found to depend on parameters such as the system pressure, individual phase flow rates, channel geometry, and the direction of the flow with respect to gravity.

Two-phase flow regimes in vertical flows are usually divided into five major patterns: bubbly, slug, churn, annular, and dispersed annular regimes (Collier and Thome, 1994). Figure 2.1 is a pictorial description of those flow regimes.

A bubbly regime can be described as a distribution of small vapor or gas bubbles in a continuous liquid phase. Slug flow is characterized by large gas bubbles, or plugs, which are separated from each other by slugs of liquid. Small bubbles may also be present in this regime. Churn flow is similar to slug flow, but the plugs are more chaotically dispersed and they typically have a highly deformed shapes. Annular flow

occurs when the liquid travels exclusively along the walls of the channel and the gas phase occupies the core of the channel. Dispersed annular flow arises when liquid droplets are dispersed in the gaseous core of an annular flow regime.

The primary flow regimes of horizontal flow include bubbly, plug, stratified, wavy, slug, and annular regimes. For the purposes of this study, however, only the two-phase regimes in vertical channels with upward flow will be treated with further detail.

The flow regimes of two-phase vertical upward flow have mostly been defined in one-dimensional channels. These studies have given rise to one-dimensional flow regime maps used to define flow pattern transition points. Many flow regime maps have been proposed in the past. Reviews of these maps can be found in monographs such as Govier and Aziz (1972) and Hsu and Graham (1986). Most flow regime maps are purely empirical. One popular map of this type is that of Hewitt and Roberts (1969), who developed their map based on air-water data. Their empirical data identified the aforementioned regimes. Hewitt and Roberts (1969) also suggested an additional wispy annular flow regime in which water droplets form clouds within an annular flow.

Mechanistic models for predicting conditions leading to flow regime transitions have also been derived. The flow regime model of Taitel et al. (1980) is a representative example and its predictions for air-water flow in a 5cm-diameter pipe are shown in Figure 2.2. Taitel et al. (1980) extensively studied two-phase flow regimes and found some discrepancies in several flow maps. Therefore they developed a flow regime model based on theoretical analysis of gas-liquid flow systems. The transition lines in the aforementioned model are generated by equations that represent specific processes.

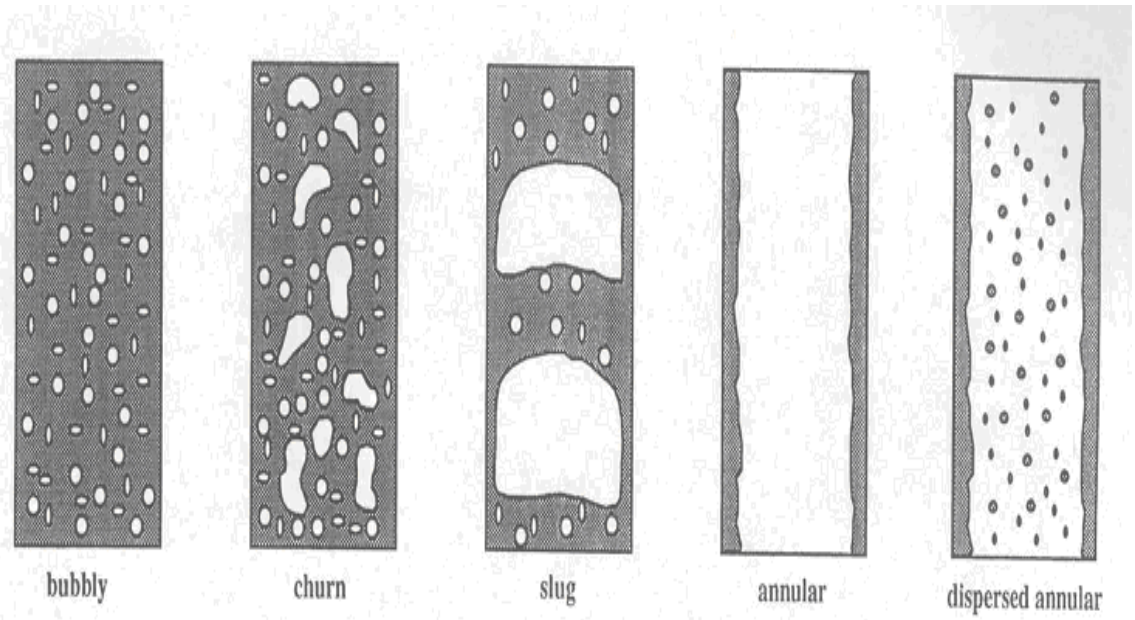

Figure 2.1: Flow regimes for two-phase vertical flow

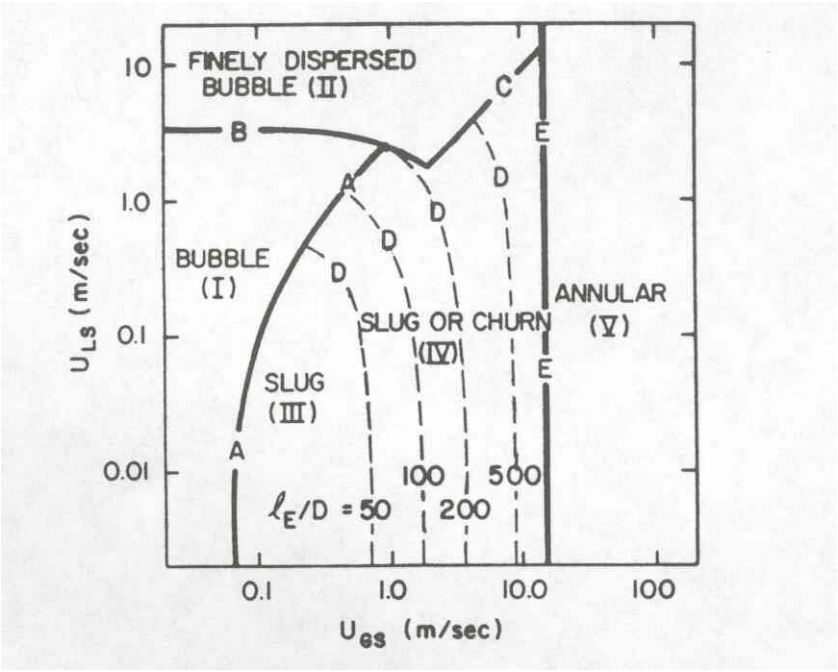

Figure 2.2: Flow regime transition lines from Taitel et al. (1980) for air-water flow in a 5cm-diamter tube

Flow regime maps, along with the relevant constitutive relations such as inter-phase transfer coefficients, are necessary for the closure of multiphase conservation equations. Derivation and solution of the multiphase conservation equations, however, is often needed for the study of the dynamics of multiphase systems. A brief review of two-phase flow models is therefore given below.

Two-phase flow dynamics are usually modeled using three major approaches, which include the homogenous equilibrium mixture (HEM) model, the thermal equilibrium mixture model, and the two-fluid (separate flow) model. Discussion of these models can be found in textbooks such as Todreas and Kazimi (1990). The HEM model, which is the simplest among all models, requires that the two phases flow with the same velocity, exist only at the same temperature, and therefore allows for them to be treated as a single fluid. The thermal equilibrium mixture model allows for the two phases to have different velocities, but requires that they exist at the same local temperature. The drift flux model is a widely used model of this type. Zuber and Findlay (1965), Bankoff (1960), Armand and Treschev (1959), and others have contributed to the development of the drift flux model. The two-fluid model allows for thermal non-equilibrium as well as different phase velocities.

In the thermal equilibrium mixture model explained above, the momentum equations are required in general, one for each phase. However, the problem can be reduced to one mixture momentum equation, provided an auxiliary relation is available to supplant the velocity slip between the phases. This is often done by rendering an empirical void-quality relation. The void-quality relationship of one-dimensional two-phase flow has been examined by Dix (1971), Zuber and Findlay (1965), and Martinelli

and Nelson (1948). The correlation of Zuber and Findlay (1965) is actually the drift flux model.

Another important relationship studied in two-phase flow systems is the pressure-drop relation. The total pressure drop in a vertical channel is the sum of three separate pressure drop components, due to friction, gravity, and acceleration. Lockhart and Martinelli (1949), Martinelli and Nelson (1948), Thom (1964), Jones (1961), and many other researchers have examined these relationships yielding various empirical methods for determining pressure drop parameters. Discussions of these two-phase flow relations can be found in many monographs and textbooks such as Todreas and Kazimi (1990), Wallis (1969), and Collier and Thome (1994).

2.2 Hydrodynamic Characteristics of Pulp Fiber-Liquid Slurries

Special attention will now be given to the characteristics of pulp fiber-liquid flows in bubble columns, which are evidently more relevant to this study. No other non-Newtonian fluid is pumped in larger volumes than pulp fiber suspensions, and yet these suspensions remain one of the least understood industrial flows (Dence and Reeve, 1996). The unique characteristics of pulp suspensions in pipe flow have been reported by many researchers, and will only be touched upon here.

Pulp suspensions are continuous mixtures of liquid and fiber networks which exhibit structure and strength caused by interaction between neighboring fibers. Pulp fibers have a density close to the density of water and, when dispersed as isolated particles, can quickly respond to local velocity gradients and turbulent eddies (Lindsay et al., 1995). Pulp suspensions are characterized by flocs, which are three-dimensional

structures that are formed by the tendency of fibers to form networks. Flocs appear at consistencies as low as 0.5%, and increase in frequency, size and strength as consistency is increased. In suspensions with consistencies greater than 0.5%, cohesive strength occurs from mechanical forces caused by the bending and hooking of fibers (Kerekes et al., 1985). As the consistency of the suspension increases, the level of fiber/fiber interactions increases which in turn strengthens the network. However, the distribution of fibers within the network is not always uniform, and local mass concentrations of fibers give rise to flocs within the suspension. Because network strength is dependent on the quantity of fiber contacts, flocs exhibit a higher strength than their surrounding. Therefore, flocs not only form regions of higher mass concentration, but also form regions of greater strength in the suspension. As a consequence, flocs may behave as independent entities in a flowing suspension.

Pulp suspensions can be divided into three categories based on their consistency (the mass fraction of the pulp in the pulp-liquid mixture). In low-consistency (LC) mixtures, where the consistency is in the 0-4% range, the fibers and flocs are surrounded by abundant liquid, and can be pumped and mixed relatively easily. In the medium consistency (MC) range, which usually refers to the 8-16% consistency range, fiber network strength and flow resistance are significant, and the mixture approaches a wet fiber aggregate surrounded by gas as the higher limit of consistency is approached. The volume of entrained gas in medium-consistency suspensions may exceed 10% (Dosch et al., 1986). The content of gas can be significantly increased if gases are intentionally supplied to the suspension.

In the high consistency (HC) range, typically covering consistencies of 20-40%, the suspension resembles a damp fiber aggregate. The void ratio in this range is relatively high so that the network can be considered as a porous medium having a much lower resistance to gas flow in the inter-floc spaces than in the intra-floc passages. Thus, fiber flocs in this consistency range present an "aerodynamic specific surface" to a flowing gas substantially less than the specific surface of an individual fiber, approximately 15-60 m^2/kg compared with approximately 350-1000 m^2/kg (Garner and Kerekes, 1978). Therefore, although a gas readily flows through the suspension, there may be little contact between the gas and most fibers unless the flocs are broken up in some manner (Dence and Reeve, 1996).

For the interest of this research, only the pulp suspension behavior in low consistency flows will be reviewed here. A noted earlier, the physics of pulp suspension flow relies on the ability of fibers to entangle and form a network. The fibrous network may result in high head losses at low velocities, sometimes even lead to clogging – especially when flowing through contracting channels or small passages, and entrain gas bubbles. As was mentioned earlier, the characteristics of the pulp suspension depend strongly on consistency and flow rate within a given channel. Loosely following Duffy et al. (1976), several basic effects are depicted in Figure 2.3, which is a typical logarithmic head loss-velocity curve for a low-consistency pulp suspension. In the region from A to B, plug flow of the fibrous network occurs. Near or slightly beyond B, at a higher velocity, a clear annulus of water with laminar flow may form around the plug: the annulus tends to be thin, typically less than a fiber length. (In some short-fibered or mechanical pulps, the maximum at point B may be suppressed.) Near C, turbulence in the

annulus is apparent, and the fibers still form a plug in the center. The plug is increasingly disrupted and begins to shrink at some point between C and E.

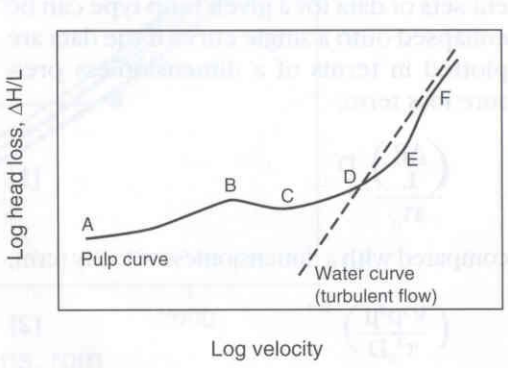

Figure 2.3: Comparison of head loss curves for water and a pulp suspension

At point D, the pressure drop in the suspension is the same as in pure water at the same liquid velocity. This marks the onset of drag reduction for, at higher velocities, the friction losses are less than for pure water in spite of the higher apparent viscosity of the suspension. The point of maximum drag reduction occurs at point E. increases in velocity continue to disrupt the plug until the flow is fully turbulent, perhaps at point F. Drag reduction still occurs although the degree of drag reduction tends to decrease as velocity increases further. Details of the head loss curve for pulp suspensions can vary widely depending on fiber properties, slurry concentration, and even configuration of the flow loop used in the measurements (Dence and Reeve, 1996).

The behavior of a pulp suspension is closely related to the network strength of the flocs. A useful parameter is τ_d, the wall shear stress at the point where the pulp frictional losses and the water frictional losses are equal (point D in Fig. 2.3). This factor is a measure of the stress required to disrupt the network. Moller (1976) found that different

sets of data for a given pulp type can be collapsed onto a single curve if the data are plotted in terms of a dimensionless pressure loss term,

$$\frac{\left(\frac{\Delta P}{L}\right)D}{4\tau_d} \tag{2-1}$$

compared with a dimensionless velocity term,

$$\left(\frac{V^5\rho^2\mu}{\tau_d^3 D}\right)^{1/6} \tag{2-2}$$

where ΔP/L is the pressure drop per unit distance, D is the pipe diameter, V is the average velocity, ρ is the liquid density, and μ is the viscosity.

Details of flow behavior are related to characteristics of the pulp fibers themselves, meaning that flow properties vary with species (especially between hardwoods and softwoods), pulping method (e.g., kraft compared with mechanical pulping), the degree of refining, and even the bleaching process (if any) that has been applied to the pulp.

2.3 Flow Regimes in Pulp Fiber-Liquid-Gas Three-phase Flows

Compared to two-phase flow, three-phase flow systems have not been adequately studied due to its intrinsic complexity. A review of three-phase flow systems encountered in the pulp and paper industry will now be presented. The three phases of interest here are solid, liquid, and gas. Once again, the solid of interest is made of wood pulp fibers, while

the liquid will be water in most cases, and the gas will vary depending upon its intended use.

Published studies dealing with three-phase flows involving fibrous slurries are scarce, and mostly deal with the hydrodynamics of gas-sparged fibrous slurries. Some of the studies focused on the three-phase pulp-water-gas systems and its associated flow regimes in pipe flow. Robertson and Mason (1957) and Sanders and Meyer (1971) studied the frictional pressure loss for turbulent fiber suspension flows. Various three-phase flow regimes for tube flow were defined. In a similar study, Gullichsen and Harkonen (1981) identified several flow regimes experienced at medium fiber consistencies prior to the onset of turbulent flow.

Investigations have shown that the addition of air to the pulp-liquid pipe flow has a significant effect in reducing drag force. Lee and Duffy (1976) showed that, at high suspension flow rates in turbulent conditions, the addition of air had a positive effect on drainage rates, leading to a reduction in drag. Under highly turbulent conditions, however, the fibers had a great tendency to entangle themselves due to the more turbulent motion, and the contribution of entrained air becomes insignificant (Lee and Duffy, 1976). Longhill and Duffy (1988) experimentally studied the dynamic effect of air injected into pulp flow at medium stock concentrations ranging from 12% to above 15%. They found that the air trapped between the pipe wall and the fiber suspension reduced the frictional resistance in the flow.

Besides its capability to reduce drag under certain conditions, the presence of air/gas in pulp suspensions has other applications in the pulp and paper industry. Processes such as flotation deinking and bleaching rely heavily on the presence of gas or

air bubbles, which are used for introducing chemical reactants, as well as for causing effective mixing. Nevertheless, the mechanisms by which the gas bubbles interact with fibers in pulp suspensions have received little attention and are poorly understood. In pulp bleaching where gaseous chemicals are used, which is evidently of interest to this study, extensive and sustained contact between the gaseous chemicals and the fiber is desired. This is particularly true for low-solubility chemicals such as oxygen and ozone, for which a three-phase (gas-water-fiber) system with a significant interfacial area concentration is needed, and this is done in low and medium consistencies by creating highly turbulent conditions.

Despite the crucial role of effective mixing, it should be noted however, that current design methods for bleaching mixers are essentially empirical because little is known about the hydrodynamics of the three-phase flow systems that occur in bleaching with gaseous chemicals. For bleaching, the ideal flow regime is one characterized by a homogeneous mixture of micro-bubbles and the fibrous suspension. Such a flow pattern is often not sustainable, however, due to the tendency of bubbles to coalesce, leading to the churn and slug flow regimes that are dominated by large bubbles. Channeling, furthermore, may occur at higher consistencies, whereby the gas preferentially flows through certain areas in the mixture, bypassing most of the fibers. There is substantial evidence showing that many current pulp fiber-liquid-gas flow systems in paper bleaching do not work in their optimal conditions.

Some recent studies dealing with gas/pulp/water three-phase flow systems are now reviewed. Isler and Widmer (1979) studied the activity of air bubbles entrained in a horizontal pulp flow. They noticed that the rising bubbles had a tendency to carry pulp

fibers toward the top of the pipe when the pulp was flowing at low velocities. As the flow velocity increased, the fibers became more evenly distributed across the cross-section of the pipe. Isler and Widmer (1979) also observed a tendency for the larger bubbles with diameters between 80 μm and 300 μm to rise, while the smaller bubbles, less than 60 μm in diameter, appeared to be adhering to the pulp fibers.

Pelton and Piette (1992) further examined the effects of pulp fiber suspensions on the air bubble hold-up using a vertical bubble column reactor. They measured the probability that a single bubble would escape the fibrous network and reach the surface. They stated two different mechanisms that would inhibit bubble rise. The first mechanism is the bubble adhesion to the fiber surface and the second mechanism is entrapment of the bubble in a fiber network. The first mechanism requires the existence of a gas-solid interface at which adhesion takes place, whereas the second does not. Pelton and Piette (1992) defined a "bubble escape diameter" which corresponds to the diameter of the bubbles that had a 50% probability of escaping. This "bubble escape diameter" increases with pulp consistency. Microscopic observations, however, eliminated adhesion as a mechanism responsible for indefinite entrapment of the bubbles, and proved that all long term gas hold-up is due to bubble entrapment within the fiber networks. The experiments also led to the conclusion that the higher the pulp consistency, the larger the air bubbles which are unable to escape from the pulp suspensions. Since the experiment was performed with one bubble at a time, the last conclusion holds without considering the effect of channeling.

Walmsley (1992) performed experiments using batch fiber suspensions with 0-2% consistency, and identified several flow regimes associated with his bubble column

experiments. Two common ones were bubbly and churn-turbulent flow regimes. The former flow regime occurred at a gas velocity less than 10 cm/sec and was characterized by a uniform distribution of tiny bubbles. When the gas velocities were increased to 10 cm/sec and above, the latter flow regime occurred featuring chaotic bubble coalescence and distribution. Walmsley (1992) also showed that the addition of only 0.1% weight pulp caused significant hydrodynamic changes, where fibers induced bubble coalescence and caused the regime transition from bubbly to churn to take place at lower gas flow rates.

Lindsay et al. (1995) experimentally studied the flow regimes and gas holdup in a column containing a vertical and quiescent pulp slurry 0.66 m high and 12.7 cm in diameter, and in a vertical column 1.5m long and 13 cm in diameter that had through-flow of pulp-water slurry and air. They used Gamma-ray densitometry for the measurement of multiple chord-average void fractions. With the quiescent column (no through-flow of pulp-liquid slurry), the pulp promoted transition from bubbly flow to churn flow by enhancing bubble coalescence. With a slurry through-flow (co-current flow), tests were performed with 0% and 1% consistency. Although flow regimes could only be seen at the near-wall zone of the test section, bubbly, plug, and a transition regime separating them could be recognized. Bubbly flow was seen at very low gas superficial velocities only, where bubbles were entrapped in and carried by flocs. They noted that in the system without slurry through-flow the fibers promoted bubble coalescence and regime transition to churn, while in the experiments with slurry through-flow the presence of fibers appeared to lead to greater gas holdup and interfacial surface area.

A more detailed experimental study of the hydrodynamics of gas-sparged columns containing pulp-water slurry (without a pulp slurry through-flow) was conducted more recently by Reese, Jiang and Fan (1996), with a scope and objective similar to the aftermentioned study by Lindsay et al. (1995). A cylindrical column 10.7 cm in diameter and 2.2 m high, and a 7.5cm × 3.9cm rectangular column 1.0 m high, were used with pulp slurry consistencies in the 0~1% range. An intrusive light transmission probe, and a particle image velocimetry (PIV) system were used in the two test sections for studying the bubble characteristics. They noted that even at a consistency as low as 0.1%, bubbles behaved differently than those in pure water. Their results showed that the presence of pulp in the column enhanced bubble coalescence, and caused a reduction of gas holdup.

Heindel (1999) and Heindel and Garner (1999, 2000) used flash X-ray photography to study the bubble size characteristics in gas-liquid-cellulose fiber flows with consistencies up to 1.5%. They could divide the bubbles into two large and small categories. The relative number of large bubbles increased with increasing fiber consistency. The size distribution of the small bubbles, however, was approximately log-normal, and was independent of fiber consistency.

2.4 Basic Concepts and Operating Principles of Artificial Neural Networks

As one branch of artificial intelligence, the theory of artificial neural networks was first introduced in the middle of the 20th century and numerous advances have been made since then. Researchers from many scientific disciplines are designing artificial neural networks to solve various problems, including pattern recognition, optimization,

control, forecasting and prediction, etc. In this section, important concepts and facts related to artificial neural networks will be briefly reviewed.

2.4.1 What Are Artificial Neural Networks?

Artificial neural networks are inspired by the natural neurons that are in the human brain. Mathematically, they are very similar. Physically, each real neuron is constituted as shown in Figure 2.4.

The natural neuron owns a certain number of connections, called dendrites. Each neuron has between 1000 and 10000 dendrites. Through these, the neuron reveives thousands of electrical stimulations called local potentials. If the coefficient of a signal is positive, it is called an excitation signal. If the coefficient is negative, the signal is said to be an inhibitor. The dendrites meet at a common point: the cellular body. If the sum of all local potentials is high enough to excite the cellular body, these are transformed into a big electrical stimulation. The stimulation then propagates quickly on the output part of the neuron: the axon. The axon is then spanned into several little links, which lead to synaptic connections with other neurons. All these operations are chemically realized. Billions of neurons are interconnected with each other to form the human brain neural network. These interconnected neurons send information back and forth to each other through connections; the result is an intelligent being capable of learning, analysis, prediction, and recognition.

Artificial neural networks are formed from up to thousands of simulated neurons that are connected in much the same way as the brain's neurons and are thus able to learn in a similar manner to human beings. In artificial neural networks, what needs to be done

is to mimic the chemical reactions within biological neuron with a computational model: each neuron receives signals from the others. Before entering a neuron, a signal is multiplied by a coefficient, called a synaptic coefficient in analogy to the biological ones. Then, pondered signals are added together. A particular function is applied to this sum, so that in output the response from the neuron is obtained, which can become the input for other neurons.

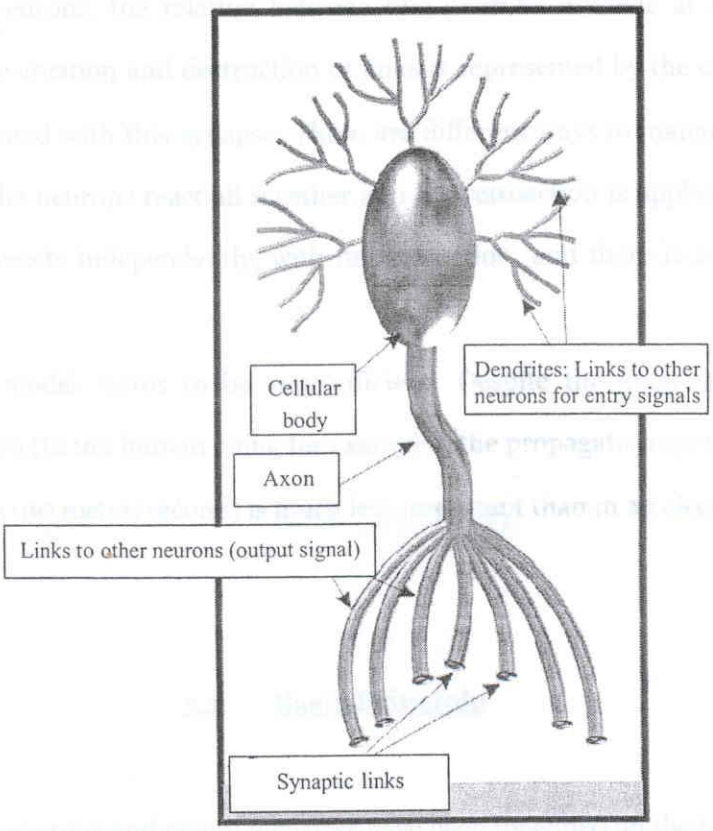

Figure 2.4: Biological neuron cell

2.4.2 Why Use Artificial Neural Network?

Artificial neural networks are good at pattern recognition, trend prediction, modeling, control, signal filtering, noise reduction, image analysis, classification, and evaluation. In fact, the uses for neural networks are so numerous and diverse that these applications may seem to have nothing in common. However, they all share the ability to make associations between known inputs and outputs by observing a large number of examples.

An artificial neural network is an excellent candidate for any application requiring pattern recognition. A pattern may consist of visual, numeric, or symbolic data. Artificial neural networks are able to recognize patterns even when the data are noisy, ambiguous, distorted, or have a great amount of variation. To train a neural network to recognize patterns, many sample inputs coupled with the correct identification or classification are needed. Pattern recognition is quite possibly the easiest thing to train a neural network to do. If the problem involves recognition or classification, a neural network will do it faster, more consistently, and often better than a person.

The prediction of trends, particularly financial forecasting, is actually a special case of pattern recognition in which the element of time is involved in the input patterns. Given historical data, an artificial neural network can predict the Standard & Poor's stock market index next week, the price of supplies used in an industry six months from now, and many other things that make a business more profitable and decision-making easier.

Artificial neural networks are considered clever and intuitive because they learn by example rather than by following programmed rules. An artificial neural network can be used to solve a problem, even though one may have only a general understanding of

what the important factors are. One need not even know exactly how these factors interact. One must know which information is important so that one can select a good variety of data to train a network with. One does not need to be certain how important each type of data is. One can train a neural network to learn the relationships, and then ask it questions such as "What effect does the price of gasoline have on this stock, given values for the other inputs?" or, "Which factors are most important or have the biggest effect on this prediction?"

Problems that are difficult to compute and do not require perfect answers, but quick good answers, are also handled very well by neural networks. Conventional computational techniques are known for their precision, but this precision is not always desirable. It is sometimes more important, for example, that a robot arm be moved quickly in some general direction rather than slowly in exactly the right direction. In conventional robotics, programs and mathematics become quite complicated. A program that uses complicated formulas to calculate direction, speed, volume, or any other quantity can be a lot slower to respond than a neural network. A neural network does not need detailed measurements or calculations, because it learns the positions and angles in space directly. It can make generalizations about the spatial relationships after learning from a few examples, and it can relearn with new values as the equipment wears and changes with age.

Artificial neural networks are thus used instead of traditional programming methods when the rules are not certain or when they change over time. Artificial neural networks are an addition to, not a replacement for conventional computer programs. They are currently ineffective in performing serial logic and precise complicated arithmetic.

Serious attempts are being made to better understand the biological mechanisms of thought and to incorporate them into artificial neural networks.

2.4.3 Computational Models of Neuron

Neurons process input and produce output. Each neuron takes in the output from many other neurons. Once inside the neuron, the weighted signals are summed to a net value. In most models, they are simply added together. The inhibitory signals have a negative weight value. Thus, when added in with excitatory signals they reduce to the overall signal input.

The equation below is basic to all neural networks:

$$net_i = \sum_{j=1}^{p} (w_{ij} * x_j) \qquad (2\text{-}3)$$

The equation means the net value for neuron i, net_i, equals the sum of the weight times the input signal for all the inputs to the neuron i from neuron j starting at output of neuron j = 1 and ending at j = p. More simply, it means adding up all of the signals that are coming into this neuron, taking the connection strengths of each signal into account.

After finding the weighted sum of its inputs (net_i), the neuron calculates its output by applying an activation function, which produces an activation level (a_i) inside the neuron. The neuron calculates its output by finding the weighted sum of its inputs (net_i) and then applying an activation function, which produces an activation level (a_i) inside the neuron. The activation is passed through an output, or transfer function f_i, which produces the actual output for that neuron for that time, $y_i(t)$.

In the simplest models, the activation function is the weighted sum of the neuron's inputs; the previous state is not taken into account. In more complicated models,

the activation function also uses the previous output value of the neuron, so that the neuron can self-excite. These activation functions slowly decay over time; an excited state slowly return to an inactive level. Sometimes the activation function is stochastic, i.e. it includes a random noise factor.

The state of activation is a way to refer to the state of the neural network at a given time. Each neuron has an individual activation value which can be written as $a_i(t)$, where a means activation, i is the neuron and (t) is a particular time. The activation function specifies what the neuron is to do with the signals after the weights have had their effect. The activation function could even be used to do some sort of time integration of the inputs, so that the neuron and the network exhibit time dependent behavior. This behavior is an area of active research (Lawrence, 1994), but there are generally no useful results or understanding yet.

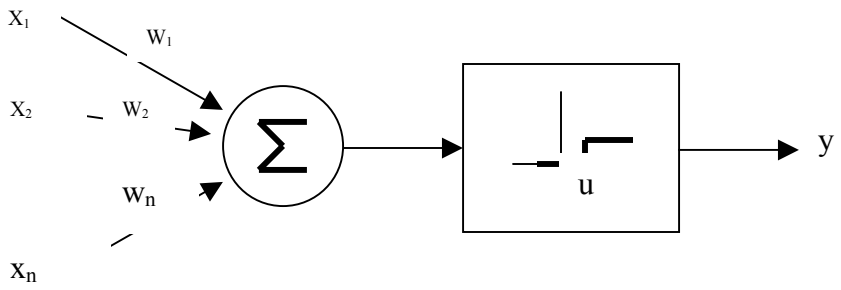

Figure 2.5: McCulloch-Pitts model of a neuron

The activation is passed through a transfer function, which produces the actual output for that neuron. The transfer function of a neuron defines how the activation value is output. McCulloch and Pitts (1943) proposed a binary threshold unit as the transfer function. Their model is shown in Figure 2.5. Mathematically, it can be represented as:

$$y_i = \theta\left(\sum_{j=1}^{p} w_{ij} x_j - u\right) \tag{2-4}$$

where y_i is the output of the neuron i, $\theta(\ )$ is a unit step function, and w_{ij} is the synapse weight associated with j-th input. For simplicity of notation, the threshold u can be considered as another weight w_o and be attached to the sum with a constant input $x_o = 1$. McCulloch and Pitts (1943) proved that, in principle, suitably chosen weights let a synchronous arrangement of such neurons perform universal computation. This model contains a number of simplifying assumptions, however, that do not reflect the true behavior of biological neurons (Jain et al., 1996).

The McCulloch and Pitts neuron has been generalized in many ways. One of them is to use a transfer function other than the threshold function, such as piecewise linear, sigmoidal, or Gaussian, as shown in Figure 2.6. The most common is the sigmoid function. It is a strictly increasing function that exhibits smoothness and has the desired asymptotic properties. The standard form is the logistic function, defined by

$$f(x) = 1/(1 + \exp\{-\beta x\}), \tag{2-5}$$

where, β is the slope parameter.

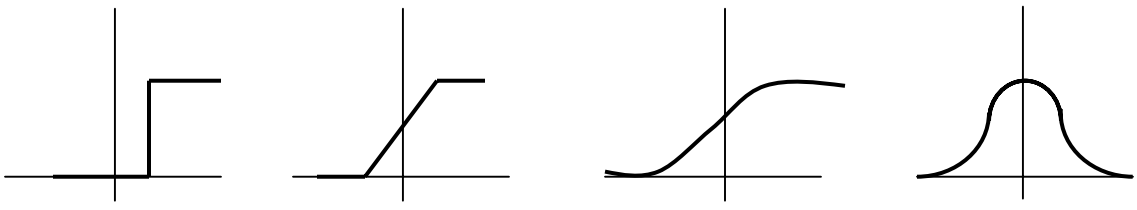

(a) (b) (c) (d)

Figure 2.6: Different types of transfer functions: (a) threshold, (b) piecewise linear, (c) sigmoidal, and (d) Gaussian.

The sigmoid function is a particularly useful nonlinear transfer function. This transfer function is a saturation function; excitation above some maximum firing level has no further effect. The sigmoid function has a high and a low saturation limit, and a proportional range in between. This function usually produces a 0 when the activation value is a large negative number, and a 1 when the activation value is a large positive number, and makes a smooth transition in between. The sigmoid transfer function thus produces an output from –1 to +1 in some networks.

Regardless of the exact transfer function, a neuron fires when it recognizes a particular value combination of incoming signals. In other words, the operation of a neuron is defined by laws for determining a match between the input vector, consisting of incoming signals, and a weight vector of internal parameter set.

2.4.4 Neural Network Architecture

Artificial neural networks can be viewed as weighted and directed graphs in which artificial neurons are nodes and directed edges (with weights) are connections between neuron outputs and neuron inputs (Jain et al., 1996). Based on their connection patterns, neural networks can be grouped into two categories:

- feed-forward networks, in which no loop exists,
- feedback (recurrent) networks, in which loops occur because of feedback connections.

Feed forward networks are less often considered to be associative memories than the feedback networks, although they can provide exactly the same functionality. It can

be shown mathematically that any feedback network has an equivalent feed forward network which performs the same task (Lawrence, 1994).

Nowadays, the most commonly used neural networks are nonlinear feed-forward models. Current feed forward network architectures in fact work better than current feedback architectures. The capacity of feedback networks has not thus far proved to be very impressive. In running mode, feed forward models are also faster, since they only need to make one pass through the system to find a solution. Feedback networks must cycle repetitively until the neuron outputs stop updating, which typically takes anywhere from 3 to 1,000 cycles.

Feed forward neural networks can be supervised or unsupervised. A supervised network compares its answers during training to known correct answers, whereas and unsupervised network (self-organizing) does not.

Different network architectures require different learning algorithms. The next section will discuss the most common learning processes.

2.4.5 Learning Algorithms

The ability to learn is a fundamental trait of artificial neural networks. The most attractive characteristics of artificial neural networks is their ability to mathematically learn by examples and repetitions.

There are basically two learning paradigms: supervised learning and unsupervised learning. Supervised learning is the most elementary form of adaptation. During training, it requires an *a priori* knowledge of what the result should be. Output neurons are told what the ideal response to input signals should be. For one-layer networks in which the

stimulus-response relation can be controlled closely, this is easily accomplished by monitoring each neuron individually. In multi-layer networks, supervised learning is more difficult. It is harder to correct the hidden layers. On the contrary, unsupervised learning does not have specific corrections made by an observer. Supervised and unsupervised learning are methods used exclusive of each other.

In the supervised learning, there exists a "teacher" or "trainer", which may be implemented in various ways. This trainer corrects the network's responses to a set of inputs. Pairs of inputs and outputs are presented to the network. The network takes each input and produces an output, which it then compares to the correct output. The trainer causes the network to construct an internal representation that captures the regularities of the data in a distributed and generalized way. This is the form of learning which is best understood, and is presently most suitable to real applications.

In unsupervised learning, no "teacher" is involved. Instead, the network is simply exposed to a number of inputs. The network organizes itself in such a way as to come up with its own classifications for inputs.

Next, we will use examples to illustrate the differences between the two learning algorithms: gradient-descent backpropagation (supervised) and Kohonen's network (self-organizing).

2.4.5.1 Backpropagation

The gradient-descent backpropagation originates from error-correction rule. The idea behind this rule is that the learning algorithm modifies the parameters of the network in the direction in which the total error decreases most rapidly for the current point. The

back-propagation algorithm creates an N-dimensional error function, which can be thought of as an error surface, where N is the number of weights and biases in the network. The algorithm changes synaptic weights and biases of the network in search of the global minimum of the error function. It moves across the error surface in the direction of steepest descent, the direction in which a change in network parameters will decrease the error most. This is a stochastic process, which means that it zig-zags its way about the true direction to the minimum of the error surface. Baldi et al. (1989) proved that for a multiple-layer linear feedforward network using back-propagation learning, there is only one minimum and all other critical points are saddle points.

Gradient-descent backpropagation cannot guarantee convergence in all cases, because it can be caught in a local minimum or diverge. It is also a relatively slow learning algorithm. For those reasons, there are modifications of the gradient-descent backpropagation algorithm that improve the speed and/or convergence. A momentum term can be added in order to prevent the training from getting stuck in local minima. This momentum term makes the algorithm take the running average of the gradient to make it less sensitive to small fluctuations. Also, the learning rate can be modified dynamically. Dynamic modification of the learning rate allows the network to learn faster when the error gradient is large but keeps it from overshooting when the gradient is small. Finally, batch training can be used instead of sequential training to make the training process less sensitive to anomalous data points. Batch-mode training is generally more stable than pattern-mode training because the effect of anomalous data points is small when they are aggregated with a large number of "normal" data points. Gori et al.

(1992) proved that, for linearly separable patterns, using batch ordinary differential equation (ODE) training ensures convergence to an optimal solution.

In the learning process, the multiple-layer perceptron network uses two different kinds of signals: function signals and error signals. Function signals are signals that enter the network through the input nodes, propagate through the network, and emerge as output signals. Error signals are signals that originate at the output layer of the network and propagate backwards though the network (Haykin, 1999). To train a multiple-layer perceptron, a function signal is padded through the network, and its output is compared to some desired output. The comparison creates an error signal, which is passed backward through the network. In the forward pass, when the function signal is passing through the network, the weights and biases of the network are fixed. The function signal appearing at the output of neuron i at iteration n is computed as

$$y_i(n) = \theta(a_i(n)) \tag{2-6}$$

where $a_i(n)$ is the net internal activation level of neuron i, defined by

$$a_i(n) = \sum_{j=0}^{p} w_{ji}(n) y_j(n) \tag{2-7}$$

where p is the total number of inputs (excluding the threshold) applied to neuron j, and $w_{ji}(n)$ is the synaptic weight connecting neuron j to neuron i, and $y_j(n)$ is the input signal of neuron i or, equivalently, the function signal appearing at the output of neuron j (Haykin, 1999). This can also be written as the dot product of $\boldsymbol{w}$ and $\boldsymbol{y}$ vectors.

In the backward pass, when the error signal is passing backward through the network, the weights and biases of the network are modified. The synaptic weights of the network in layer l are adjusted for the $n+1$ iteration according to the rule:

$$w_{ji}^{(l)}(n+1) = w_{ji}^{(l)}(n) + \gamma[w_{ji}^{(l)}(n) - w_{ji}^{(l)}(n-1)] + \eta\delta_i^{(l)}(n)y_j^{(l-1)}(n-1) \qquad (2\text{-}8)$$

where γ and η are constants and $\delta_i^{(l)}$ is the local gradient of network for the *i*th neuron in the *l*th layer and is computed from

$$\delta_i^{(l)}(n) = y_i^{(l)}(n)[1 - y_i^{(l)}(n)]\sum_k \delta_k^{(l+1)}(n)w_{kj}^{(l+1)}(n) \qquad \text{for any layer } l \qquad (2\text{-}9)$$

$$\delta_i^{(L)}(n) = e_i^{(L)}(n)o_i(n)[1 - o_i(n)] \qquad \text{for output layer } L \qquad (2\text{-}10)$$

where $o_i(n)$ is the *i*th output at iteration *n* and $e_i^{(L)}(n)$ is the error of that output, defined as

$$e_i^{(L)}(n) = d_i(n) - y_i(n) \qquad (2\text{-}11)$$

with the desired output $d_i(n)$ at iteration *n* (Haykin, 1999).

The gradient descent back-propagation algorithm is the most commonly used training algorithm. It is a recursive algorithm, which means that the points can be given to the algorithm one at a time. It is mostly stable, but it is slow.

2.4.5.2 Kohonen's Self-Organizing Map Network

Kohonen's (1989) model of self-organization is based on the idea that the brain tends to compress and organize sensory data spontaneously. Self-organization is Kohonen's term for unsupervised learning. The essential mechanism of the Kohonen scheme causes the system to modify itself so that nearby neurons respond similarly. The neurons compete in a modified winner-take-all manner. The neuron whose weight vector generates the largest dot product with the input vector is the winner and is permitted to provide the output. However, in this model, the weights of not only the winner, but also its nearest neighbors (in the physical sense) are adjusted.

The purpose of Kohonen's self-organizing mappings is that patterns of high dimension (i.e., long vectors) are transformed into one or two-dimensional patterns. For example, in a situation where input units are mapped onto corresponding output units, a self-organizing system would give a localized response – that is, a single output unit responding most, with activation falling off in the units around it, for each input pattern provided.

The way this is accomplished is as follows: each output unit has a vector of weights that connect it with the input units. These weight vectors are initially random. At each time step, the dot product of the weight vector of each unit with the current input vector is formed:

$$a_i = \sum w_{ji} x_j \tag{2-12}$$

where x_j is the jth component of the input vector, a_i is the activation of the ith output unit, and the w_{ji} are the weights connecting them.

After the activation of each output unit is computed, the output unit with the maximum activation level is selected. This is the unit whose weight vector is most similar to the input vector. This weight vector is then adjusted to be even more similar to the input vector by the rule

$$\Delta a(t_{n+1}) = \alpha(t_n)(x(t_n) - a(t_n)) \tag{2-13}$$

in which x and a are the input and output vectors respectively, α is the learning rate, Δa is the change in a, and t_n and t_{n+1} are the nth and $(n+1)$th time step respectively.

2.4.6 Limitations of ANNs

Although artificial neural networks are very powerful tools for dealing with complex problems, they are not cure-all. Artificial neural networks heavily rely on their training samples. If the training samples are insufficient or do not cover all the typical conditions of the problem, errors can be large with testing samples. If the training samples are too much, they can also cause the overfitting problem.

The most important limitation of ANNs is that they do not reveal the exact nature of the relationship between inputs and outputs; in other words, the ANN models are hard to interpret or convert to rules. Besides, confidence intervals for predictions are not always available. Multiple models can be created from the same training data, as the nonlinear multivariable optimization for weight and biases is a "hard problem" with no guarantee of finding the global optimum. Interrupted training can be criticized as a method that depends on the optimization algorithm (only used with back-propagation). Regularization of weights relates to "maximum margin classifiers" but introduces one more tunable parameter. Due to compounding nonlinearity, furthermore, the model behavior could be erratic in localized regions of the multidimensional input space.

2.5 Recent Applications of Artificial Neural Network in Engineering

Although the application of neural networks to multiphase flow problems has started only recently, the published studies have clearly demonstrated their enormous potential.

Multiphase flows in pipes can lead to a large number of different geometric configurations and phase fractions. This obviously poses an intractable problem, because

it is difficult to determine a priori which configuration the flow will assume. Bishop et al. (1993) reported the use of the backpropagation network to extract the appropriate phase configuration and, in addition, the phase fractions of oil and water directly from gamma ray attenuation data.

Similarly, the backpropagation network has also been trained to infer flow regimes and phase flow rates of liquid/gas multiphase flows using gamma ray densitometry by Burns et al. (1993).

Cai et al. (1994) attempted to build an objective flow regime classifier based on neural network method for air-water two-phase flow. The absolute pressure signals were sampled at 40 Hz from a 2-inch horizontal air-water flow loop. Eight stochastic features, including standard deviation, skewness, kurtosis (amplitude-domain features) and linear prediction coefficients and prediction residue error (frequency-domain features), served as input vectors for a Kohonen self-organizing neural network. A total of 366 measurements were taken covering slug, wavy/stratified, bubble, and intermittent flow. They compared the output of the neural network to their visual observation and Mandhane flow map boundaries (1974) and concluded that the technique was capable of sub-classifying flow regimes.

Peng et al. (1996) proposed a method based on fuzzy logical neural network to recognize oil-gas two-component flow patterns. They first used electrical capacitance tomography (ECT) to monitor the flour main flow patterns inside the pipeline, which were stratified, annular, slug, and bubble flow. For each flow condition, 28 (N*(N-1)/2, N=8 is the electrode number) dependent measured capacitance values were obtained using an 8-electrode capacitance transducer and fed into a fuzzy logic module, which

converted the input data to fuzzy format and constituted the input for a back-propagation feed forward neural network. The output of the network was sent to another module, which used the maximum likelihood criterion and estimated the most likely flow regime. They claimed good agreement was achieved but no quantitative result was given.

Mi and Ishii (1996, 1997, 1998, 2001) conducted one of the most comprehensive investigations on two-phase flow regime identification using neural networks to date. Their efforts involved both horizontal and vertical pipe flow. In 1997, Mi et al. (1997) presented a fuzzy logic and neural network-based model to conduct nonlinear mapping from impedance measurements to a horizontal two-phase flow pattern. They used an impedance void-sensor which consisted of a probe with a set of electrodes and a circuit for impedance measurements. Eight symmetrically arranged and flush-mounted electrodes on the horizontal test section provided the capability of measuring the diagonal and neighboring impedances. To model the relation between the measurement and its statistical characteristics, the time series of the diagonal and neighboring impedence were online supplied to a three-layer neural network with six output nodes. Two of the output nodes merely repeated the input, hence providing the neural network with some auto-associative characteristics. Two nodes were used to estimate the standard deviation in the signal patterns of diagonal and neighboring impedances. The other two nodes estimated the mean of inputs. The six outputs flowed into a fuzzy-rule logic which was based on the relation between probability density function of impedance and the corresponding flow regime. Following their previous work, Mi et al. (1998, 2001) successfully implemented two-phase flow regime identification in a 5.08 cm diameter vertical channel using artificial neural networks. The mean and standard deviation values of the impedence

between diagonal electrodes were selected to represent the input to the neural network. Both supervised and self-organizing neural network approaches were applied and provided an accurate solution to the otherwise complex modeling problem.

Sun et al. (2002) developed a neural network scheme to identify flow regimes and measure quality in gas-liquid two-phase flow systems using differential pressure signals. They produced a two-phase flow on a horizontal steel pipe with a diameter of 20 mm by pumping gas and water through at a gas flow rate of 1.6 - 54 m^3/hr and water flow rate of 0.2 - 5.0 m^3/hr, respectively. The inlet length of the test section was 3.50 m and the outlet was 2 m that guaranteed to achieve fully developed flow regimes. They installed two pressure taps on the top of the test section with a distance of 1000mm. Differential pressure signals were sampled at a frequency of 400Hz and 20000data points were acquired at a time. They applied wavelet analyses to the measured differential pressure signals and extracted a feature called scale energy ratio (SER). A three-layer back-propagation neural network was then adopted to map the multi-scale data to the flow regimes they observed, which included annular, bubbly, plug, and slug flow. SER at six different scales were populated to the neural network as inputs. Binary outputs were expected to represent the flow regimes. Their tests showed an acceptable correct identification rate from 81.3% to 90.0%.

Wu et al. (2001) studied intelligent identification systems for flow regimes of oil-gas-water multiphase flow in oil transportation pipelines. Their research was featured with fractal theory and denoising technique. The test section was a plexi-glass tube with inner diameter of 40 mm. It had an inlet length of 3.25 m (L/D = 81.25) and the outlet length was 3 m (L/D = 75). Through tubing, a piezo-resistance differential pressure

transducer was connected with two pressure taps, which were 205 mm apart. The instantaneous pressure drops were measured and denoised by using wavelet theory. Accordingly, the noise component was first eliminated based on the discrepancy between the wavelet spectrum of noise and the "polished" signal at different scales (Mallat and Hang, 1992), then signals were reconstructed without noise using the algorithm of wavelet reconstruction. The denoised signal pattern was characterized by a fractal dimension, in view of the fact that multiphase flow exhibits unique characteristics of fractal. Nine correlation dimensions were computed and extracted for each work condition of flow of interest, and arranged as input vectors for an improved back-propagation neural network model. To simplify the problem, the oil-gas-water system was considered as a two-phase flow. Stratified, intermittent, and annular flow were defined as output of the neural network. Their results showed that the methodology offered a potentially useful computational tool to analyze two-phase flow regimes. The most important merits of the method were simplicity, fast response, and high accuracy.

Otawara et al. (2002) developed an artificial neural network model to reveal the dynamic behavior of a three-phase fluidized bed. They carried out experiments in a transparent acrylic resin column with an inner diameter of 9.184 m and a height of 2.0 m, in which air, tap water, and glass beads served as the gas, liquid, and solid phases, respectively. Superficial gas velocity were 2.3 cm/sec, 4.5 cm/sec, or 7.8 cm/sec. The volume fraction of the beads was set at 0.05. An optical transmittance probe was employed to emit a laser beam across the channel and the intensity received by the detector was converted by phototransistor into voltage signals. In the three-phase flow, the particles passage through the laser beam were recognized as spike signals while

bubble passages were recognized as broad oscillating signals. An artificial neural network was trained with the superficial gas velocity plus seven time-series data comprising the proceeding and current temporal intervals, I_{n-6}, I_{n-5}, I_{n-4}, I_{n-3}, I_{n-2}, I_{n-1}, I_n. Each of them was the time period between two sequential signals representing bubble or particle passage and generated from the optical probe voltage output. The output of the network was the succeeding temporal interval, I_{n+1}. Eleven hidden nodes were chosen to circumvent over-training. The trained ANN successfully generated bifurcation diagrams indicating bubble and particle motions by recurrently feeding back its output to one of the input neurodes and pushing one input neuron value to the adjacent one. With the conjecture that those neurons corresponded to the parameters characterizing the non-linearity properties of the state variable of the three-phase flow, they examined the activation values of the 11 hidden nodes inside the network. Results implied that the flow regimes could be clearly identified through the judicious evaluation of activation levels of the hidden neurons of the artificial neural network system.

Besides the application of artificial neural networks to fluids, they have also proved beneficial in modeling heat transfer problems. The following are examples of recently-published investigations.

Moon and Chang (1994) used the non-linear mapping capability of ANNs for correlating critical heat flux (CHF) data. In other applications ANNs have even been used as fast calculation alternatives for well-understood but time-consuming theoretical models (Jambunathan et al., 1996) and equations of states (Normandin et al., 1993). Jambunathan et al. (1996)'s back-propagation model also overcame the limitation that predictions are only based on a fixed set of initial conditions.

Using the Korea Advanced Institute of Science and Technology (KAIST) database, Moon et al. (1996) developed an ANN-based method for predicting CHF in round, vertical and uniformly heated channels with water. The parameters representing the heated channel inlet, exit, or local conditions were selected as input to train the artificial neural network. In a follow-up paper, Lee et al. (2000) used an innovative ANN-based technique for deriving an expression for the effect of the heated length on CHF.

The hybrid, ANN-FPM method is a simple approach for modeling complex processes that are highly non-linear functions of local parameters that themselves must be calculated from the solution of conservation equations. In this method the conservation equations are solved using primarily first principles with minimal assumptions introduced in the development and closure of these conservation equations. The complex and poorly understood closure relations, in particular the rate-controlling transport processes, which are typically poorly understood non-linear functions of local state variables, are represented by trained neural networks. Several investigators have recently applied the ANN-FPM approach to complex physical and chemical processes, everywhere with success (Qi et al., 1999; Fullana et al., 1999; Molga and Cherbanski, 1999; Gupta et al., 1999).

CHAPTER 3

EXPERIMENTAL APPARATUS

3.1 Test Loop

A schematic of the experimental facility is shown in Figure 3.1. The main components of the loop include a feed tank, a receiving tank, a re-circulation pump, a Hydrosonic pump (also known as a Shock Pulse Generator or SPG), and the test section. Pulp of the proper consistency is first loaded into the feed tank and the receiving tank. The pulp used in this study was washed, unbleached softwood. Since dilute cellulose fiber suspensions have the propensity to separate when left stagnant for an extended time period, the water-fiber slurry is gently stirred by a variable speed Lightnin mixer in each tank to maintain the fiber consistency at a constant value. The two consecutive tanks are 0.144 m^3 in volume, and are both exposed to atmosphere. The long residence time of fluid in these tanks provides for the bulk of the entrained gas to leave the system. Visual observation confirmed that there were virtually no visible bubbles near the pipe intakes in the tanks. Small bubbles may of course be trapped in the fiber networks and remain in the tank. The volume fraction of these entrapped bubbles is not more than a few percent even under quiescent flow conditions, however (Pelton and Piette, 1992; Taylor, 1993), and their effect is therefore neglected. The water-fiber mixture is then circulated at a continuous basis by a 1-hp, 1725-rpm Discflo pump, which is tested to operate at up to 11% consistency with no plugging.

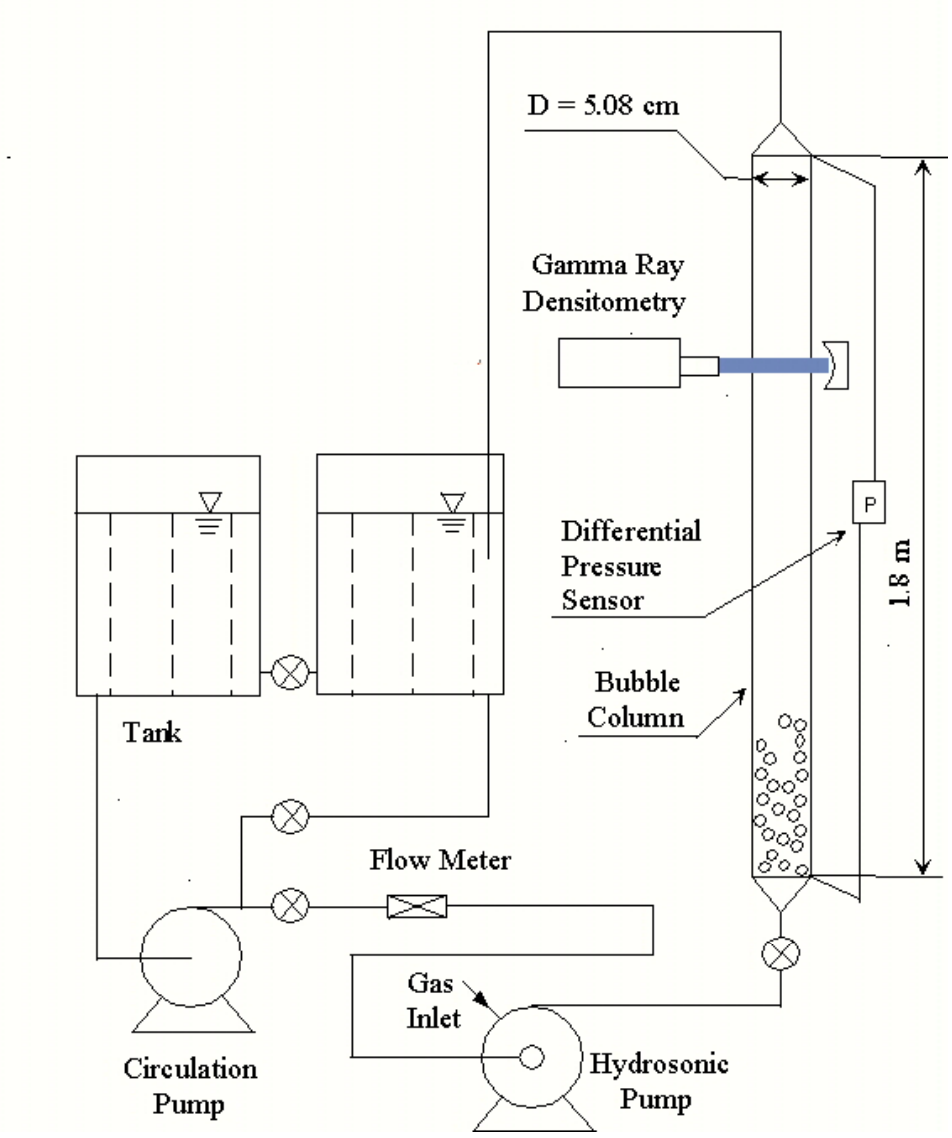

Figure 3.1: Schematic of the experimental facility

Filtered air from the building is injected into the flowing liquid in a 2.5 cm diameter tube prior to the Hydrosonic pump.

A co-current flow system was designed to study multiphase flow characteristics. The test section is a PVC schedule 40 pipe that is 1.80 m in length and has a 5.08 cm inner diameter. A differential pressure transducer (Validyne DP15) is attached to the bottom and the top of the test section, which measures the pressure drop in the test section. It should be noted that industrial paper-making systems in which gas-liquid-pulp three-phase flow takes place are typically much larger than our test section. The geometric configuration of industrial systems, furthermore, precludes fully-developed flow conditions. The unavailability of general scaling laws for multiphase flows renders the experimental simulation of prototypical systems very difficult. This experimental study is thus meant to shed light on the fundamental hydrodynamic issues associated with the multiphase flows of interest, rather than directly simulating prototypical systems.

The flow system is flexible, in the fact that, the test section can be positioned in a horizontal or a vertical configuration. The vertical configuration is shown in Fig. 3.2 and the horizontal configuration is shown in Fig. 3.3. The column is mounted onto a sturdy pipe frame made of extruded aluminum. The pipe frame, which houses the guided carriage, is connected to the base frame by a single joint, which allows for the column to pivot between the two configurations. The guided carriage is a piece of equipment that is rigidly affixed to the pipe frame by a stainless steel ball screw. It is held in place between two beams, and is designed to travel linearly along the length of the PVC pipe on bearings.

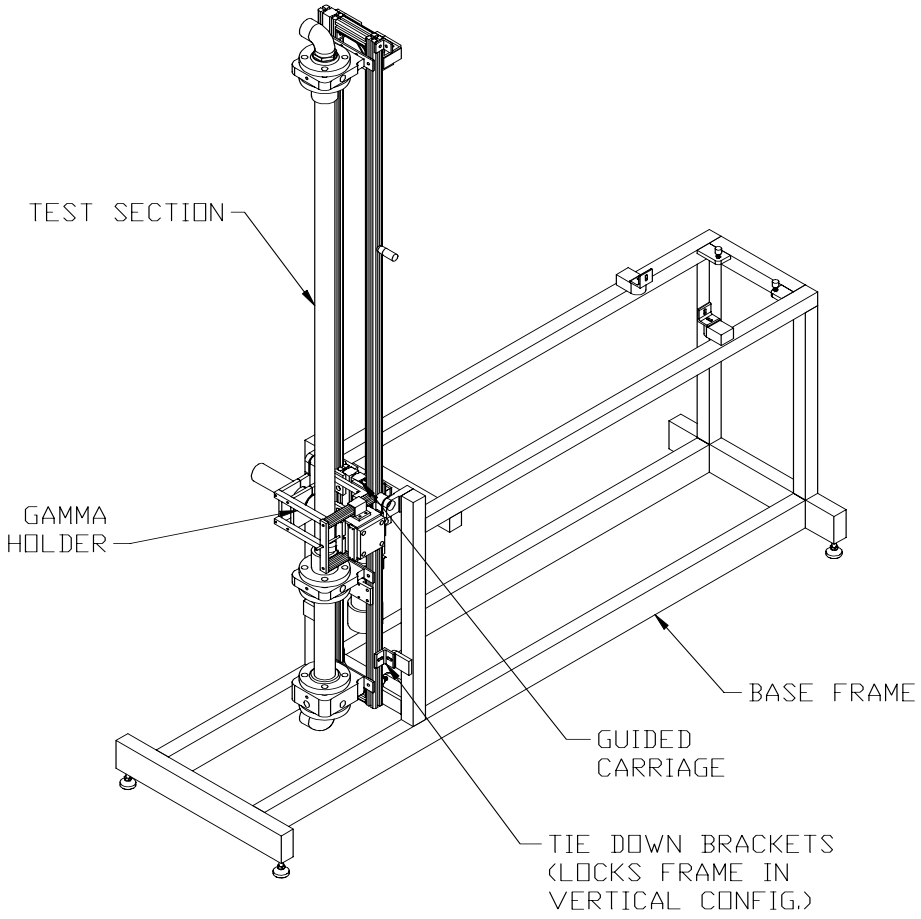

Figure 3.2: Bubble Column Vertical Configuration

The purpose of the guided carriage is to hold the x-ray film cassette and the gamma holder assembly for fluid dynamic observations of the flow conditions in the test section. These attachments are securely attached to the guided carriage by four grade eight cap screws. The guided carriage has been designed to travel along the length of the test section for flexible measurement at different locations.

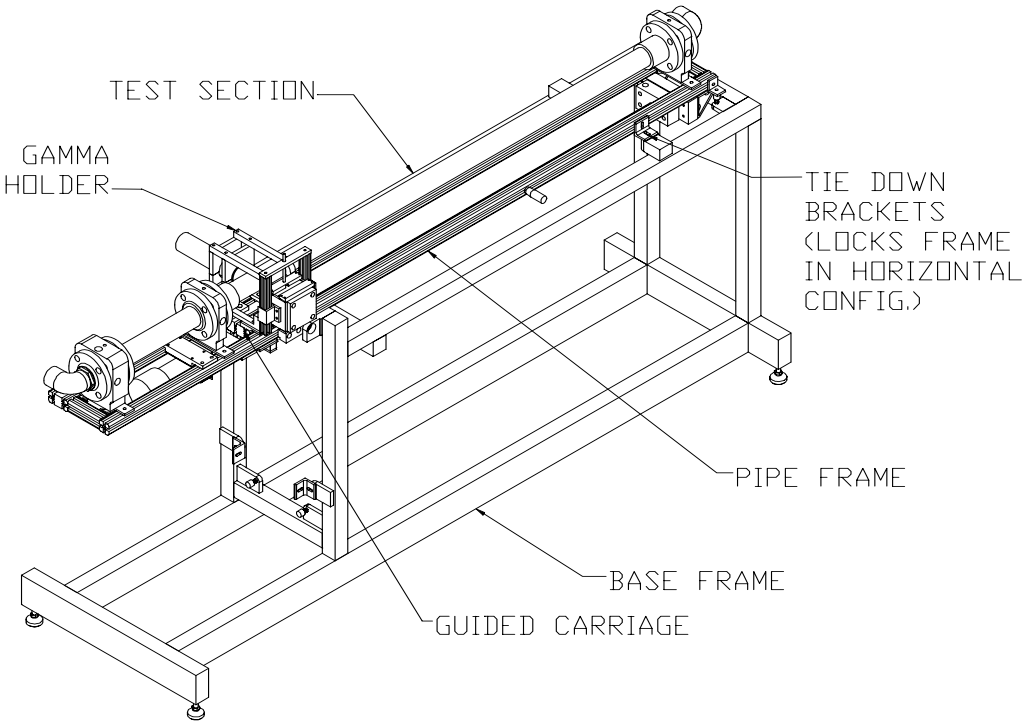

Figure 3.3: Bubble Column Horizontal Configuration

The gas-liquid-fiber mixture exiting from the column is channeled by a conical constriction followed by a conical expansion at the top of the test section into an 8 cm diameter pipe. The pipe is constructed as a "T" section with one end open to atmosphere in order for gas to escape, and the other end is connected to a 10 cm o.d. PVC pipe, which is lower than the column exit to allow for the mixture to enter the receiving tank.

The hydrosonic pump (Hydrodynamics Inc., Rome, Georgia) is a patented mixer design that uses a proprietary technology for mechanical-to-thermal energy conversion

based on shock waves. Pressurized air is introduced to the hydrosonic pump. In converting mechanical to thermal energy at a very high and efficient rate, the hydrosonic pump generates intimate mixing of the gas and liquid, and breaks down the gas phase into micro-bubbles.

3.2 Instrumentation and Measurements

The test facility schematic provided in Figure 3.1 also depicts the major measurement instruments. These instruments are now explained.

The pulp flow rates are monitored with a *Krohne IFC080 Smart* magnetic flow meter and encompass a range of 0~2.0 *l/s*.

The air flow rate is measured by two Top Trak flow meters. One of them has a measurement range of 0~40 slpm (standard liter per minute), while the other with a range of 0-1 slpm. They can be switched from one to the other in order to accommodate different gas flow rates.

The Gamma-ray densitometer, described previously by Lindsay et al. (1995), is used for the measurement of chord-average void fractions at various locations in the test section. The densitometer includes a 45mCi Americium-241 source and an Ortec Model 276 detector. The Am-241 sealed source was mounted in the rubber-lined clamp on the gamma holder assembly, as shown on Figure 3.4. The Ortec gamma-ray detector was also mounted on the gamma holder assembly. The gamma holder assembly with the mounted source and detector is what is referred to herein as the GRD prototype. The sealed source and detector are positioned within a few millimeters of opposite sides of the PVC pipe. The narrow beam of radiation (approximately 5 millimeters in diameter) follows a

source-to-detector pathway that directly traverses the PVC pipe and its contents. The sealed source and detector can be moved manually in both lateral directions via thumbscrews so that measurements can be made at various chord positions across any given cross sectional plane of the PVC pipe. By performing void fraction measurement on several chords at a given location, the cross section-average void fraction can be calculated, and radial distribution of void fraction can be estimated (Lindsay et al., 1995).

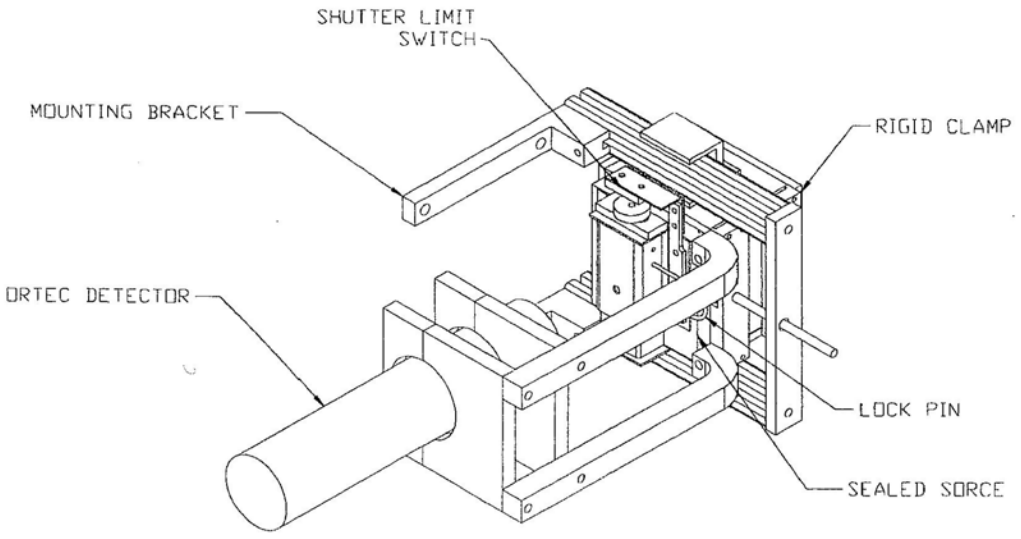

Figure 3.4: GRD prototype consisting of Am-241 sealed source and Ortec radiation detector mounted in gamma holder assembly

The pressure transducers used to record dynamic pressure in the test section are ENDEVCO® Model 8510B (shown in Figure 3.5). They are rugged, miniature, high sensitivity piezoresistive pressure transducers.

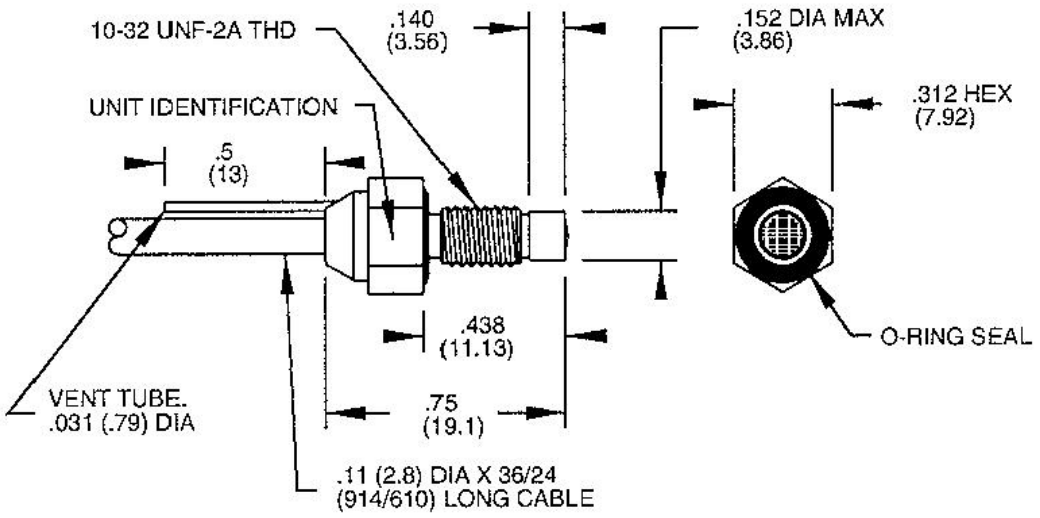

Figure 3.5: ENDEVCO® Model 8510B

The piezoresistive sensing element is a solid-resistor, which changes electrical resistance in proportion to applied mechanical stress. Since it is a single crystal it is not only strong but virtually free of mechanical hysteresis with inherently good linearity. The significant characteristic of this element is that its change of resistance is largely relative to its change in length. It has a gage factor many times greater than the typical wire strain gage. Piezoresistive element gage factors range typically from 50 to 200.

Three Endevco pressure sensors are installed onto the test section in a row with a spacing of 10 cm, starting at the location of 120 cm from the column inlet. The typical installation is shown in Fig. 3.6.

To couple with piezoresistive pressure transducers, the ENDEVCO Model 136 DC Amplifier, which is a three-channel signal conditioner, are employed. The unit provides an AC output voltage proportional to the voltage input, and is powered by 90-240 VAC.

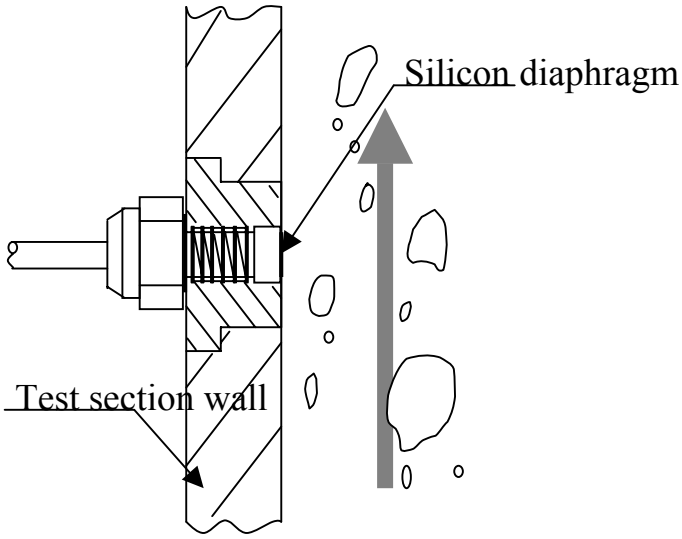

Figure 3.6: Typical installation of dynamic pressure transducer

The Endevco Model 136 has a fixed 10 Hz 4-pole Butterworth high-pass filter that can be selected or bypassed. It has a plug-in 4-pole low pass filter whose corner can be set by an internal header module, which offers multiple corner frequencies.

Key features:

- Three-channel DC differential Voltage Amplifier;
- 100 kHz Bandwidth (-3dB corner);
- 10 Volt Full Scale Output;
- Auto-zero and Shunt Calibration;
- Four selectable excitation voltage levels;
- Gain range from 0 to 1000;
- RS-232 Serial Interface;

- Optional Low Pass Filter corners available (standard default filter is a 10 kHz Butterworth);
- Filter option available for J211 and ISO6487 requirements.

3.3 Data Acquisition (Labview) and Software (NeuroShell 2)

3.3.1 PC-based Data Acquisition System

Data from all electronic sensors were first input into a shield I/O connector block National Instruments Model SCB-68, which was interfacing I/O signals to plug-in DAQ devices with 68-pin connectors. The output of SCB-68 were collected and recorded using the National Instruments model PCI-MIO-16E-4 data acquisition card with 16 channel multiplexer/amplification boards. The board digitized all analog signals at a maximal sampling rate of 25 kS/s and provided for software averaging of the digitized values to remove potential AC noise pick-up. The data acquisition system was running using a LabVIEW 5.1 program on a 120-MHz Pentium computer that utilized Microsoft Windows 98 as an operating environment. This data acquisition program, shown in Figure 3.10, enabled the operator to control the sampling rate and data logging time at which the dynamic pressure sensor signal was sampled. The data acquisition system recorded all data for a particular experiment to a prescribed text file on the Pentium computer for future analysis.

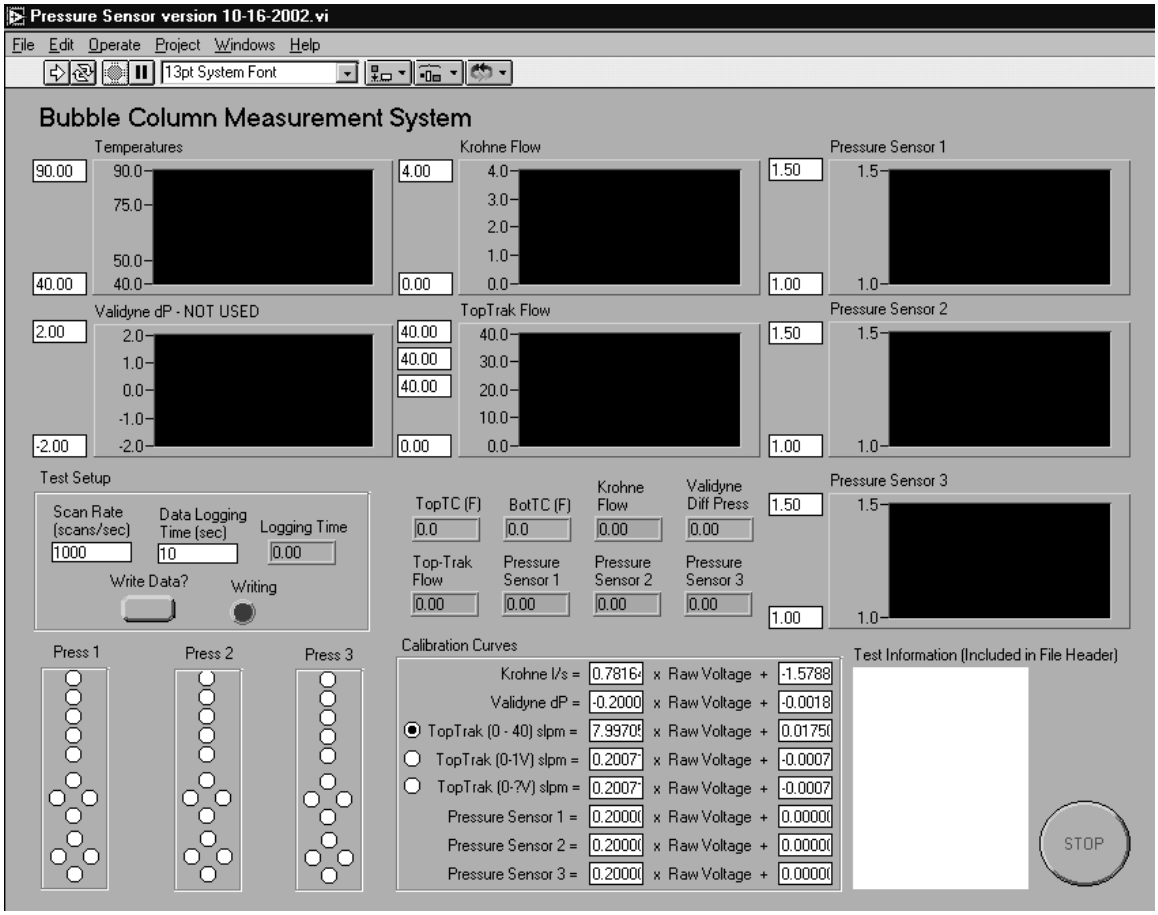

Figure 3.7: Data acquisition program

3.3.2 Software (NeuroShell 2)

NeuroShell 2 was used to undertake the task of designing artificial neural networks. It combines powerful neural network architectures, a Microsoft Windows icon driven user interface, sophisticated utilities, and popular options to give users the ultimate neural network experimental environment. It is recommended for those users who are concerned with classic neural network paradigms like back-propagation.

The NeuroShell 2 Advanced Options screen, which displays the independent modules that may be used to create a neural network application, is shown in Figure 3.8.

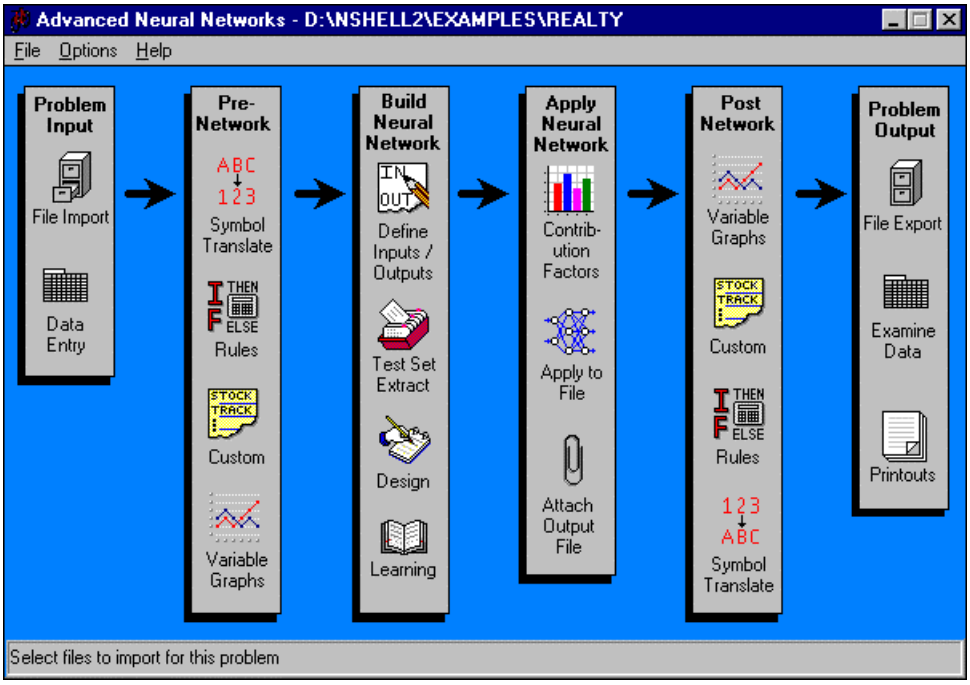

Figure 3.8: NeuroShell 2 user interface

3.4 Experimental Procedures

3.4.1 Characterization of Pulp Used for Flow Tests

It is well known that depending on fiber slenderness, length, and flexibility, different paper making pulps have different levels of tendency to flocculate and to plug piping. The unbleached kraft pulps used in this study as a mixture were of South African origin, available at IPST as dry lap pulp.

The average freeness after dispersion with a Valley beater was measured at 682.5 CSF. Freeness is a term used to define how quickly water is drained from the pulp. The surface tension, which has a significant effect on bubble/liquid interactions, of the water phase from the pulp suspension, was determined to be 62.0 dyne/cm.

The fiber properties were measured with Optest FQA (Fiber Quality Analyzer) equipment and the results are summarized in Table 3-1.

Table 3-1: The accumulated results of FQA

Percent fines		Mean length			Mean curl		Mean kink		
Arith-metic (%)	Length weighted (%)	Arithmetic (mm)	Length weighted (mm)	Weight weighted (mm)	Arith-metic	Length weighted	Kink index (1/mm)	Total kink angle (^{o})	Kinks per mm
23.42	2.35	0.716 ±0.031	2.451	3.483	0.133 ±0.008	0.161	1.43	53.0	0.72

The size range reported as fines is 0.072 to 0.100mm. The arithmetic percent fines is the account of all material in that size range divided by the total count. The length–weighted percent fines is a calculated approximation of the weighted percent of fines. The percent fines determination with FQA does not represent an official method, however. The results are useful on a relative basis.

Individual fiber length measurements are grouped into different given length fractions. The arithmetic average is the sum of individual fiber lengths divided by the number of fibers. It is biased toward the low end, where there are more individuals. The length-weighted mean length is most commonly used to represent the average fiber length because it removes some of this bias by putting a weight on each fraction proportional to the length measured. The weight-weighted average length is second order weighing.

Curl is the gradual and continuous curvature of a fiber. The curl index is the ratio of the fiber length to its longest linear dimension, decreased by one. The value increases with curl from zero (a straight fiber).

The kink index is a measure of the abrupt changes in the fiber curvature. It is weighted by the kink angles.

The Kraft softwood pulp fibers are typically about 30 microns in thickness.

3.4.2 Installation and Operation of Gamma-ray Densitometer

Before flow tests, the sealed gamma source was carefully taken out from its storage cabinet. With radiation safety officer (RSO) present, the GPD prototype was bolted onto the guided carriage. The clamps holding the source, and those holding the detector, were next loosened slightly to allow final positioning of the source and detector. The source and detector should each be approximately 3 mm from the PVC pipe. Once final positioning was achieved, all mounting clamps were re-tightened. At this point, the RSO conducted a Geiger survey count and a wipe test to test for leakage or contamination.

During the flow test, the shutter on the source was open to release gamma ray. The shutter on the Am-241 sealed source was safely opened by pulling the lock pin, lifting the shutter until the magnet on the top contacts the limit switch, and inserting the lock pin into the upper hole. When this protocol was followed, a warning light flashed on the front panel of the electrical enclosure on the wall whenever the shutter was open. In addition, a warning window would flash on the data acquisition computer screen. The shutter was only opened when densitometry measurements were being made.

3.4.3 Flow Tests

Flow regimes and gas holdup values were recorded over $21 \le \overline{U_{LS}} \le 51\,\text{cm/s}$ and $0 \le \overline{U_{GS}} \le 26\,\text{cm/s}$ ranges. In each test series the pulp-water mixture superficial velocity would be set at a constant and stable value. The gas superficial velocity would then be

increased in steps, starting from a very small value. The flow patterns were visually identified. A digital camera (Canon Powershot, 4 Mega Pixels) was used, whereby video images would be analyzed for flow regime identification. For each selected $\overline{U_{LS}}$ value, once the predominant and easily distinguishable regimes (to be described later) were identified, sufficiently fine adjustments to the flow rate were done to make sure that each regime was spanned by at least 3 or 4 data points. The pressure fluctuations of the test section at 1.2 m, 1.3 m, and 1.4 m from the inlet of the section were recorded using the three dynamic pressure sensors, which were described in earlier section.

Gas holdup measurements were performed by the Gamma-ray densitometer at a height of 1.45 m above the test section inlet. These measurements were done in the tests where flow regimes and their transition conditions were the objective, as well as in separate tests meant to examine repeatability. Chord-average void-fraction was measured at the following 5 lateral positions: the test section cross-section center line (l_1=D=5.08 cm, with l_1 representing the chord length); 1 cm to the left and right of the centerline (l_2=l_4=4.67 cm); and 2 cm to the left and right of the centerline (l_3=l_5= 3.13 cm). The cross-section average gas holdup, $\bar{\varepsilon}$, was then calculated from:

$$\bar{\varepsilon} = \frac{\sum_{i=1}^{5} \varepsilon_i l_i}{\sum_{i}^{5} l_i} \tag{3-1}$$

A detailed discussion of the principles of Gamma-ray densitometry can be found in Hewitt (1978), and a method for the estimation of the uncertainty in the measured void fractions resulting from photon statistical fluctuations can be found in Honan & Lahey

(1978) and Vince & Fincke (1983). Accordingly, the chord-average void fraction is related to Gamma-ray counts as:

$$\varepsilon_i = \frac{\ln(I / I_L)}{\ln(I_G / I_L)} \tag{3-2}$$

where I_L, I_G, and I respectively represent the Gamma-ray counts (all measured over the same time period) with pure water, pure gas, and the three-phase mixture of interest. (The small solids fraction suspended in the liquid can in our case be neglected.) Gamma-ray counts were recorded for periods of 10 seconds, and were repeated 10 times at each chord. The uncertainty in the measured $\bar{\varepsilon}$ could be estimated from (Lindsay et al., 1995):

$$\xi_i = \frac{\Delta\varepsilon_i}{\varepsilon_i} = \frac{1}{\sqrt{N}} \frac{[2(1-\varepsilon_i+\varepsilon_i{}^2)]^{1/2}}{\varepsilon_i \ln(I_G / I_L)} \tag{3-3}$$

where, N is the product of the number of counts and number of repeated count measurements. In view of Equation (3-2), the uncertainty in the cross section-average gas holdup is estimated by:

$$\frac{\Delta\bar{\varepsilon}}{\bar{\varepsilon}} = \frac{1}{\bar{\varepsilon}} \frac{\sum_{i=1}^{5} \varepsilon_i l_i \xi_i}{\sum_{i=1}^{5} l_i} \tag{3-4}$$

All gas holdup calculations were based on the reasonable assumption that Gamma-ray attenuation was not affected by the pulp (Lindsay et al., 1995).

As mentioned earlier, the hydrosonic pump generates fine mixtures of micro-bubbles and slurry at the test section inlet. Bubble size characteristics in the test section have been measured by flash X-ray photography (Rezak, 2002). The X-ray flash photography system used for this purpose has been discussed previously (Zavaglia and Lindsay, 1989; Rezak, 2002), and will not be described here. Although flash X-ray

photography can ideally provide two-dimensional images, we could apply the method to bubbly flow as long as the bubble number density was relatively small. When two bubbles overlap but the front bubble does not completely cover the bubble behind it, one can distinguish the individual bubbles because their common area has a different gray scale in the image. The smallest bubble diameter that could be resolved is approximately 2 mm. Figure 3.9 depicts typical cumulative number-based bubble size distributions, obtained from the analyses of X-ray images taken from the test section at a height of 140 cm above its entrance. The displayed figures of course only depict the bubbly flow pattern. The typical visible bubble size is of the order millimeters, however, indicating that at the time of observation the initial gas dispersion to micro-bubbles has evolved by bubble coalescence to reasonably large bubble sizes. In a clear water suspension the micro-bubbles generated by the mixer have the appearance of a fog that makes the suspension appear "cloudy", while these measured bubble sizes represent clearly distinguishable individual bubbles.

The typical and maximum uncertainties associated with phase superficial velocities were $\pm 3.0\%$ and $\pm 4.5\%$ for $\overline{U_{LS}}$; and $\pm 9.6\%$ and $\pm 33.0\%$ for $\overline{U_{GS}}$, respectively. The uncertainties in gas holdup associated with Gamma ray densitometry were everywhere small in comparison with the gas holdup data scatter.

The signal processing of pressure fluctuations will be presented in chapter 5.

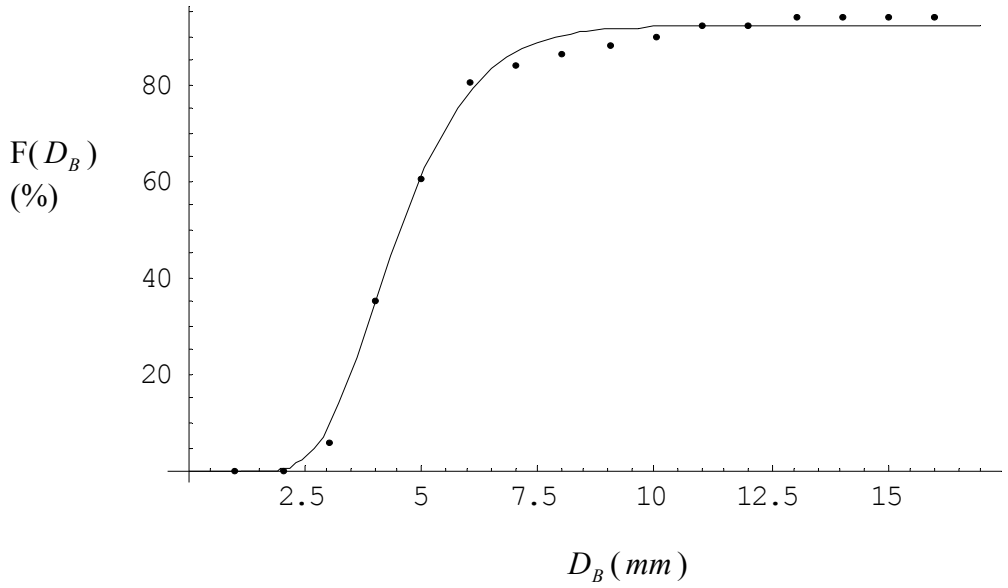

(a)

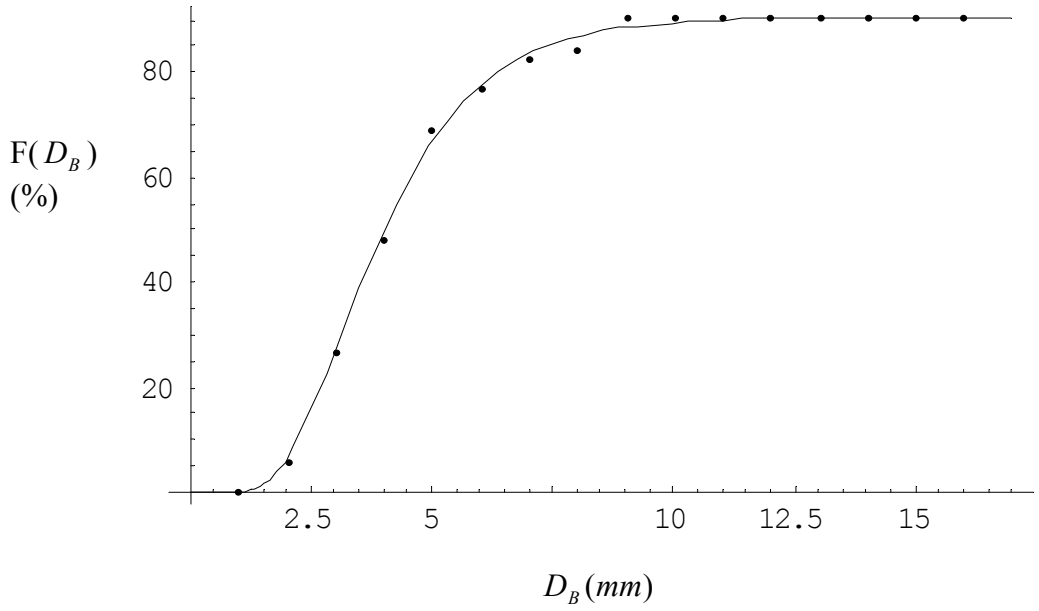

(b)

Figure 3.9: Typical bubble size distributions at 140 cm height, obtained by X-ray flash photography and image analysis (Rezak et al., 2002): (a) at 1.0% pulp consistency, superficial gas velocity is 15 cm/sec; (b) at 2.0% pulp consistency, superficial gas velocity is 15 cm/sec. (Axis X: bubble size (mm), Axis Y: cumulative distribution of the number of bubbles (%).)

CHAPTER 4

FLOW REGIMES & VOID FRACTIONS

4.1 Introductory Remarks

To study the hydrodynamic characteristics of the bubble column, especially various flow regimes and their transition lines, flow tests were performed using the test loop described in Chapter 3 and shown in Figure 3.1. Flow regimes were investigated by varying superficial liquid velocity ($21 \le \overline{U_{LS}} \le 51$ cm/s) and superficial gas velocity ($0 \le \overline{U_{GS}} \le 26$ cm/s). In each test series the pulp-water mixture superficial velocity would be set at a constant and stable value. The gas superficial velocity would then be increased in steps, starting from a very small value. In these tests, the hydrosonic pump was used to assist generating small bubbles. The flow patterns were visually identified. For each selected $\overline{U_{LS}}$ value, once the predominant and easily distinguishable regimes (to be described later) were identified, sufficiently fine adjustments to the flow rate were done to make sure that each regime was spanned by at least 3 or 4 data points.

Gas holdup measurements were performed by the Gamma-ray densitometer at a height of 1.45 m from the test section inlet. Chord-average void-fraction was measured at the following 5 lateral positions: the test section cross-section center line; 1 cm to the left and right of the centerline; and 2 cm to the left and right of the centerline.

4.2 Flow Regimes

Six different flow patterns could be identified based on the video pictures. These flow patterns are schematically displayed in Fig. 4.1. The small arrows in these figures are meant to show the apparent direction of motion of small bubbles. The faint large arrows, furthermore, display the curvilinear passage of large bubbles. As noted, in the flow regimes depicted in Figs. 4.1(c) and 4.1(d) the motion of large bubbles was spiral.

At very low gas superficial velocities the dispersed bubbly regime, depicted in Fig. 4.1(a) was observed. Fine bubbles with small diameters that appear to be trapped in fiber networks, rise in the test section, without any visible breakup or coalescence. Bubbles were not uniformly distributed in the test section, however. This regime was not observed at very low $\overline{U_{LS}}$ or very low consistencies. The entrapment of bubbles in fiber networks is consistent with previously reported observations (Pelton, 1992; Lindsay et al., 1995), and can evidently occur only when the bubbles remain small and network structures large enough to entrap such bubbles are present.

With increasing gas superficial velocity, the dispersed bubbly regime would be replaced by the layered bubbly flow, displayed schematically in Fig. 4.1(b). This flow regime is not typically observed in gas-liquid two-phase flows, and was characterized by a flocculated core and an essentially fiber-free annular zone that was 3~4 mm thick. Dispersed bubbles trapped in the flocculated core could be sporadically seen, while the fiber-free annulus contained distorted bubbles moving in rectilinear fashion. Bubble collisions occasionally occurred, without apparent coalescence. Furthermore, the flocculated core was periodically disturbed by tightly grouped bubble clusters, typically with 1~2 Hz frequency.

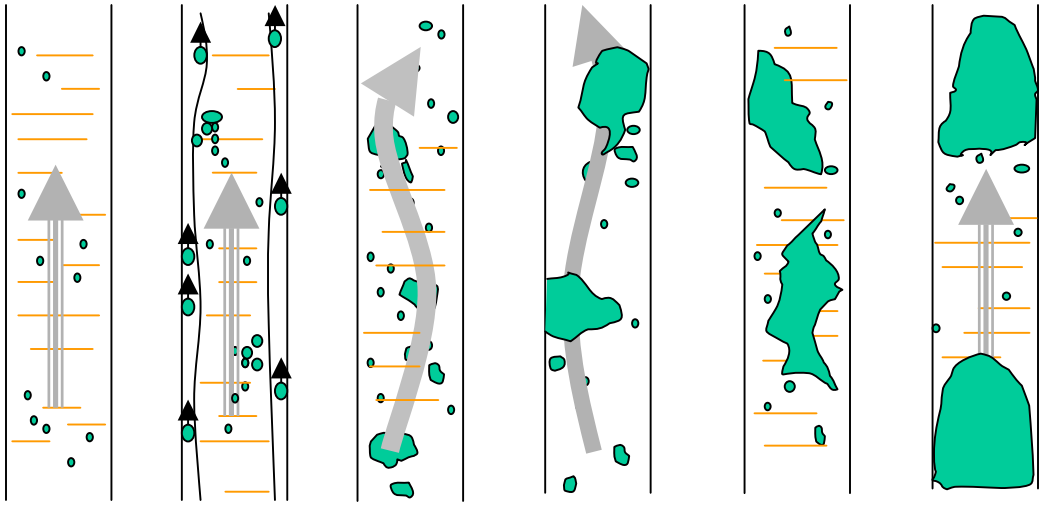

Figure 4.1: Schematics of the flow regimes: (a) Dispersed bubbly flow; (b) Layered bubbly flow; (c) Incipient Plug flow; (d) Plug flow; (e) Churn-Turbulent flow; (f) Slug flow.

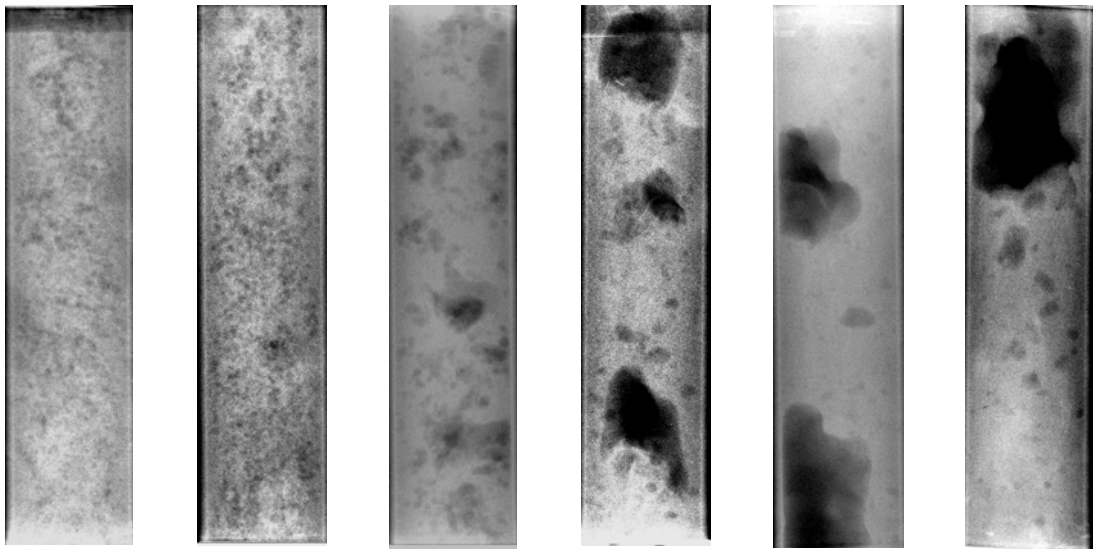

Figure 4.2: Close-ups from X-ray. (a) Dispersed bubbly flow; (b) Layered bubbly flow; (c) Incipient Plug flow; (d) Plug flow; (e) Churn-Turbulent flow; (f) Slug flow.

Further increasing $\overline{U_{GS}}$ would lead to the plug flow pattern, displayed in Fig. 4.1(c) and 4.1(d). The flow pattern in Fig. 4.1(c), referred to here as the incipient plug flow pattern, represents transition from bubbly to plug. It is characterized by clusters of small bubbles, and large, irregular-shaped gas plugs with 2-3 cm in dimension that move in swirling spiral manner and disturb the flow field. Swarms of small bubbles often trail the air plugs, and the small bubbles do not coalesce. The air plugs could even be seen very near the test section entrance, and appeared to dominate the flow field. The plugs would collect solitary bubbles that sporadically appeared to be caught in fiber networks. In their gas-liquid-spherical beads experiments in a 10.2 cm-diameter bubble column, Chen et al. (1994) could identify a vortical-spiral flow regime. The flow field in this flow regime contains four flow zones, including a descending zone adjacent to the wall, a vortical-spiral zone characterized by downward liquid and solid streams, a fast bubble flow zone where strong bubble coalescence and breakup took place, and a central plume zone. Large bubbles with spiral trajectories occurred in their experiments. While the latter observation is similar to the behavior of air plugs in our incipient plug flow regime, the aforementioned flow field zones could not be observed in our experiments.

At higher $\overline{U_{GS}}$ the plug flow pattern had the appearance depicted in Fig. 4.1(d). Large air plugs with dimensions comparable with the channel diameter totally dominated the flow field, although isolated small bubbles could be also seen. The plugs mostly stayed near the channel wall. With increasing $\overline{U_{GS}}$, the spiral motion of plugs would gradually give way to straight, upward motion. The plugs caused churning and back-mixing.

The churn-turbulent flow pattern, displayed in Fig. 4.1(e), represented the transition from plug to slug flow. This flow pattern is consistent with the known hydrodynamic characteristics of churn-turbulent flow in gas-liquid two-phase channel flow (Collier and Thome, 1994) and two-phase flow in bubble column (Deckwer, 1985), and is characterized by irregular-shaped large gas pockets near the channel centerline that carry smaller bubbles in their wakes, repeatedly collide and coalesce with smaller bubbles, and cause an oscillatory and unstable flow field. This flow pattern could be considered as the channel entrance region flow field for the development of slug flow, in accordance with the observation of Taitel et al (1980) for gas-liquid flow, as described below.

With further increasing $\overline{U_{GS}}$, the slug flow pattern, depicted in Fig. 4.1(f) is established. The flow field in this regime is dominated by bullet-shaped bubbles that resemble Taylor bubbles in gas-liquid two-phase flow. Transition from churn-turbulent regime to slug flow was gradual, i.e., as $\overline{U_{GS}}$ was increased, bullet-shaped bubbles resulting from the coalescence and growth of smaller bubbles could first be recognized near the exit of the test section. The location of regime transition from churn-turbulent to slug flow moves downwards in the test section as $\overline{U_{GS}}$ is increased.

4.3 Flow Regime Maps

Tests were performed with air and water (free of pulp) in order to develop a flow regime map for comparison with the gas-liquid-fiber flow regime data. The air and water flow regime map, plotted in $\overline{U_{LS}}$ and $\overline{U_{GS}}$ coordinates, is displayed in Fig. 4.3. Also depicted in the figure is the flow regime transition line for bubbly to churn/slug regime

change according to Taitel and Dukler (1980). The flow regime in the bubbly zone of Fig. 4.3 was characterized by the typical small and distorted bubbles in zig-zag motion. In the zone designated as bubbly/plug, however, the flow field contained randomly distributed large air plugs that resembled the air plugs depicted in Fig. 4.1(c). Our regime transition line representing transition to churn flow is evidently relatively close to the model of Taitel and Dukler (1980). Usually, relatively large air plugs intermittently pass through bubbly flow, and the flow regime zone we have designated as bubbly/plug may be considered to simply represent transition from bubbly to churn and therefore incorporated in the bubbly flow zones. We decided to distinguish this zone from bubbly and churn, however, due to the significant role of the air plugs in the flow regime depicted in Fig. 4.1(c). It should be emphasized, however, that our test section is relatively short and the flow regimes reported here are affected by the test section entrance. The churn flow regime, furthermore, may be considered as the entrance region flow pattern that would eventually lead to slug flow if the channel was sufficiently long (Taitel and Dukler, 1980).

The flow regime data, based on phasic superficial velocities as coordinates, are shown in Fig. 4.4(a), (b) and (c), for 0.5%, 1.0%, and 1.5% consistencies, respectively. The incipient plug and plug flow patterns are presented together, since clear demarcation of a boundary between the two is difficult. Dispersed bubbly and layered bubbly regimes only occupy very small portions of the regime maps, and are encountered at very low gas superficial velocities. Plug, churn and slug flow patterns, in combination, occupy virtually the entire flow regime maps for $\overline{U_{GS}} \geq 1$ cm/s. Absent in the flow regime maps

is annular flow, which would need gas superficial velocities significantly higher than the upper limit of $\overline{U_{GS}}$ in our experiments.

The flow regime transition lines are sensitive to consistency, in particular when the 0.5% consistency data are compared with data representing higher consistencies. All regime transitions evidently take place at considerably lower gas superficial velocities for 0.5% consistency slurry than for higher consistency slurries. In comparison, the regime transition lines for 1% and 1.5% slurries are relatively close. Nevertheless, overall, increasing consistency monotonically shifts the regime transition lines towards higher $\overline{U_{GS}}$ values. Transition from dispersed bubbly to layered bubbly depends primarily on the capability of the fiber networks to entrap bubbles and oppose their accumulation in the near-wall zone where the hydrodynamic resistance opposing bubble rise is lower due to lower fiber concentration. With 1% and 1.5% consistencies the fiber networks are evidently better capable of entrapping the small bubbles. Transition from bubbly to plug, furthermore, depends on the capability of fibers in preventing coalescence among bubbles and the consequent formation of gas plugs. It is therefore reasonable that the transition from layered bubbly to plug flow also occurs at higher $\overline{U_{GS}}$ values for the higher 1% and 1.5% consistencies. The monotonic shifting of all other regime transition lines as consistency is increased can be also attributed to the stronger retardation of bubble coalescence as consistency is increased.

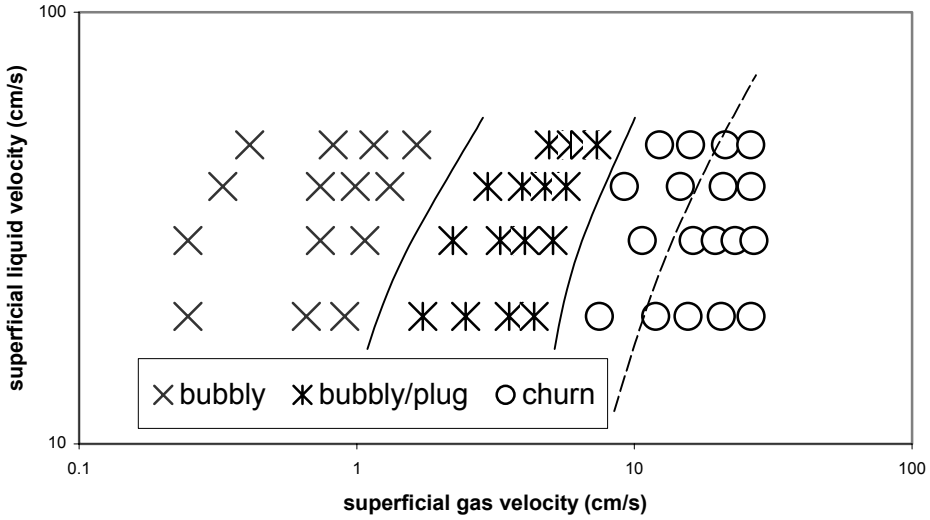

Figure 4.3: The flow regime map for air and water mixture. The broken line represents the bubbly-to-churn transition according to Taitel and Dukler (1980).

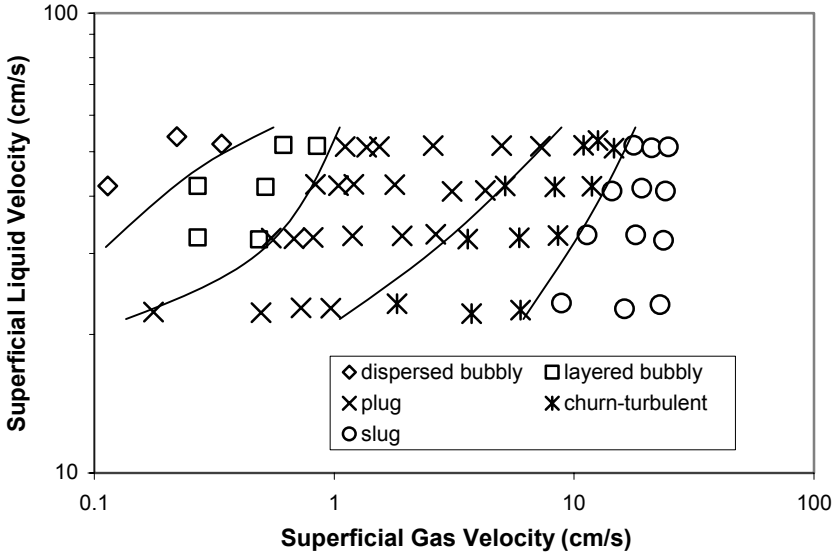

(a)

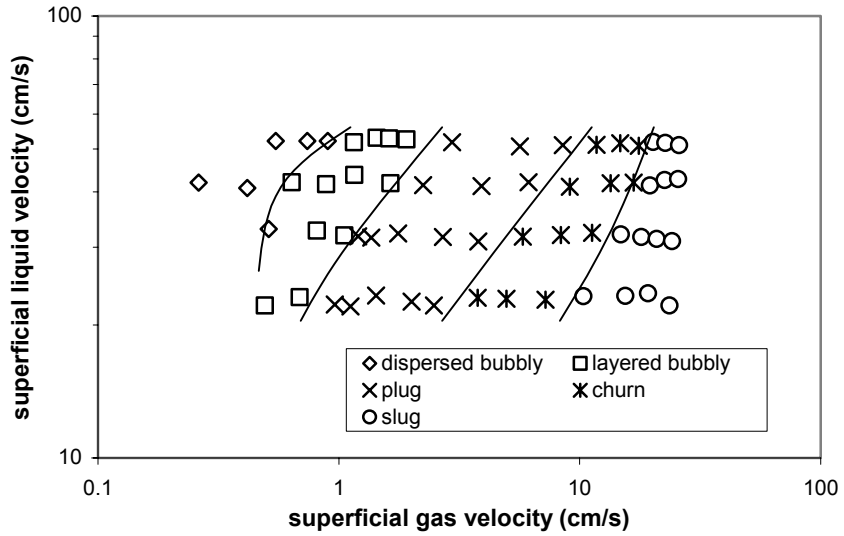

(b)

Figure 4.4: Flow regime maps: (a) pulp consistency = 0.5%; (b) pulp consistency =1.0%; (c) pulp consistency = 1.5%. Logarithmic scales are used on each axis, which results in nearly linear transition boundaries.

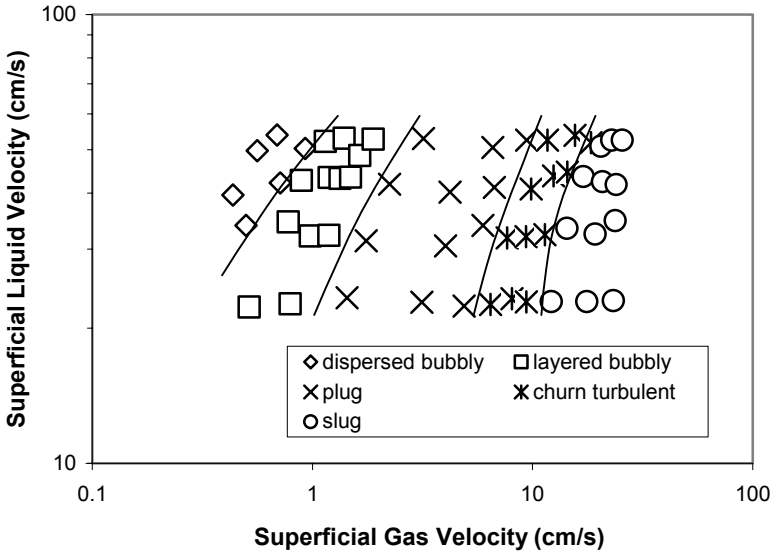

(c)

Figure 4.4(Continued)

The subjective nature of visual identification of flow patterns should be emphasized, which inevitably leads to uncertainty with respect to the regime transition lines. Successful, objective flow regime identification methods have been demonstrated for gas-liquid two-phase flow, most of them based on the statistical characteristics of pressure fluctuation signals (Matsumi, 1984; Lin and Hanratty, 1986; Wambsganss et al., 1994; Cai et al., 1996). Artificial neural network-based methods for classification and recognition of statistical patterns of such signals associated to the major two-phase flow regimes have also been successfully demonstrated (Cai et al., 1994; Mi et al., 1998). These techniques have not been applied to three-phase pulp-liquid-gas flows thus far, however.

4.4 Gas Holdup (Void Fraction)

Gas holdup data presented and discussed in this section represent Gamma-ray densitometry measurements at 140 cm location along the test section from the inlet. Typical chord-average gas holdup distributions in the channel cross-section are depicted in Fig. 4.5. For bubbly and layered bubbly regimes the relatively uniform cross-sectional distributions of gas holdup is consistent with the presence of fiber networks which prevent mixing and the resulting migration of bubbles towards the channel center. The void fraction profiles for all other regimes have their familiar overall shapes with their maxima at the channel center, and confirm the mixing caused by churning and the motion of large gas plugs.

Fig. 4.6 and 4.7 depict the parametric effects of consistency and phase superficial velocities on the measured cross section-average gas holdups. Each data point in fact

represents the average of two separate repetitions of the same experiment to ensure repeatability. At very low gas superficial velocities, where bubbly flow occurs, specific trends are difficult to identify due to the very small gas holdups and the relatively large data scatter. Clear trends can be recognized at higher gas holdups, however. With consistency maintained constant, $\bar{\varepsilon}$ increases monotonically with $\overline{U_{GS}}$ when $\overline{U_{LS}}$ is held constant, and it decreases monotonically with increasing $\overline{U_{LS}}$ when $\overline{U_{GS}}$ remains unchanged. The effect of pulp consistency on gas holdup is more complicated, however. The gas holdup profiles for 1% and 1.5% consistency are in fact relatively close, and with the exception of the highest $\overline{U_{GS}}$ depicted in Fig. 4.7, the cross section-average gas holdup for 1% consistency is everywhere only slightly lower than that for 1.5% consistency. This trend is reversed for $\overline{U_{LS}}$ =51 cm/s data, likely due to subtle changes in the characteristics of the slug flow pattern. The gas holdup values obtained with 0.5% consistency, on the other hand, are everywhere significantly lower. It should be mentioned that the monotonic and smooth dependency of $\bar{\varepsilon}$ on consistency and phase superficial velocities observed in these experiments were possible since significant channeling (preferential flow of gas through low hydraulic resistance "channels" where fiber networks are weaker) did not occur in the experiments. More complicated parametric dependence of $\bar{\varepsilon}$ (and other related parameters such as interfacial area concentration and phasic residence time in the system) may occur at higher consistencies and/or larger-diameter columns, where strong and large three-dimensional fiber networks can easily form.

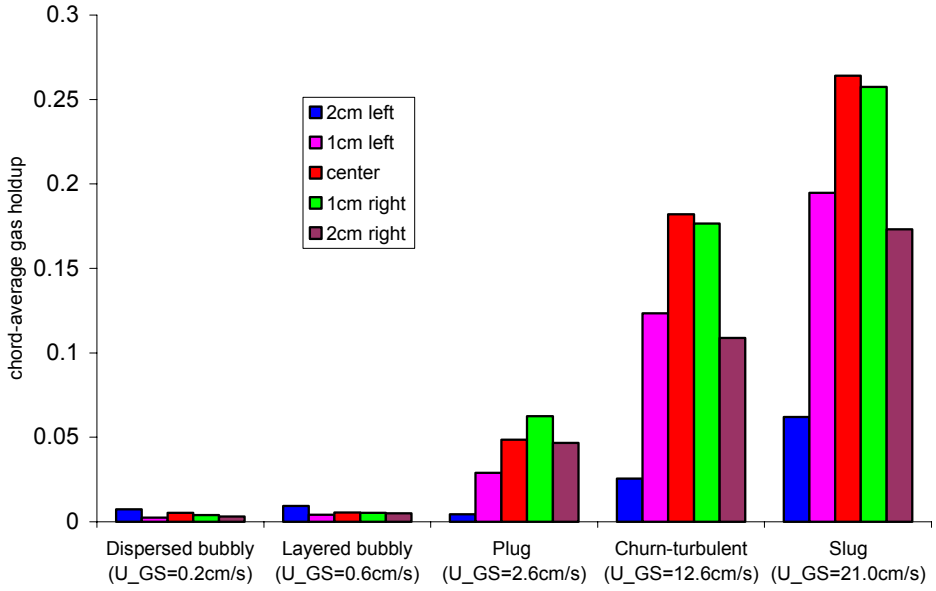

(a)

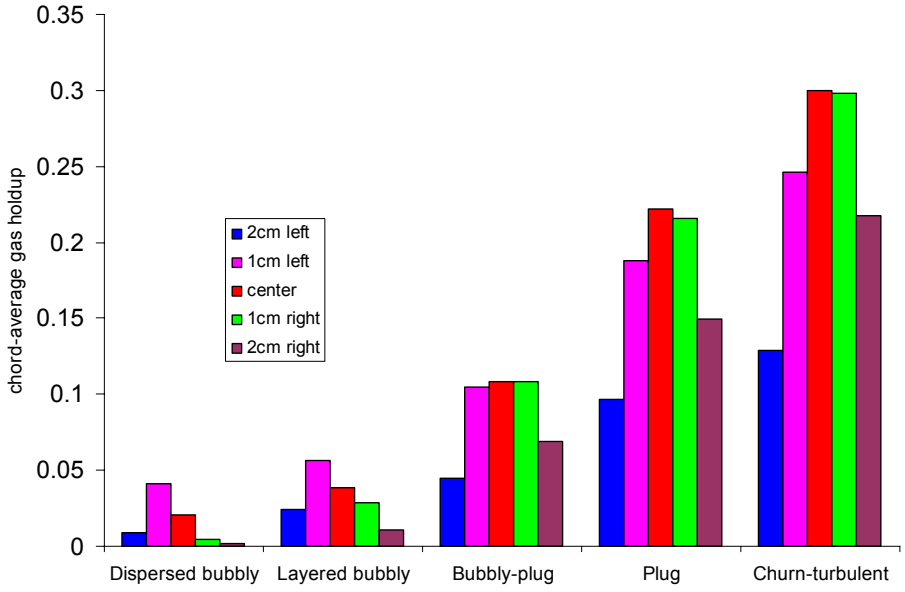

(b)

Figure 4.5: Typical chord-average gas holdup profiles at a superficial liquid velocity of 51 cm/s: (a) for *0.5%* consistency; (b) for *1.5%* consistency.

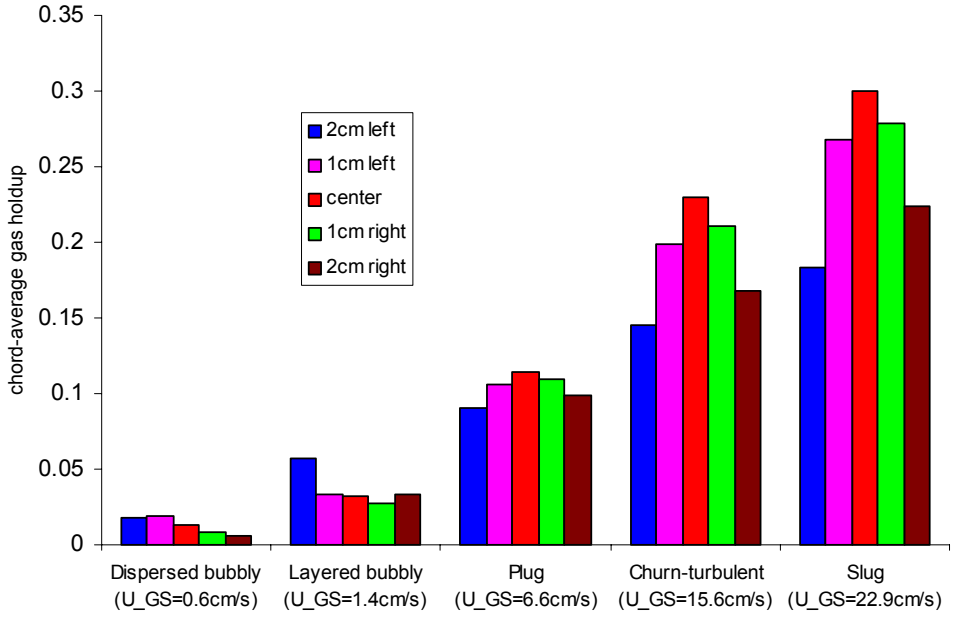

(c)

Figure 4.5 (Continued)

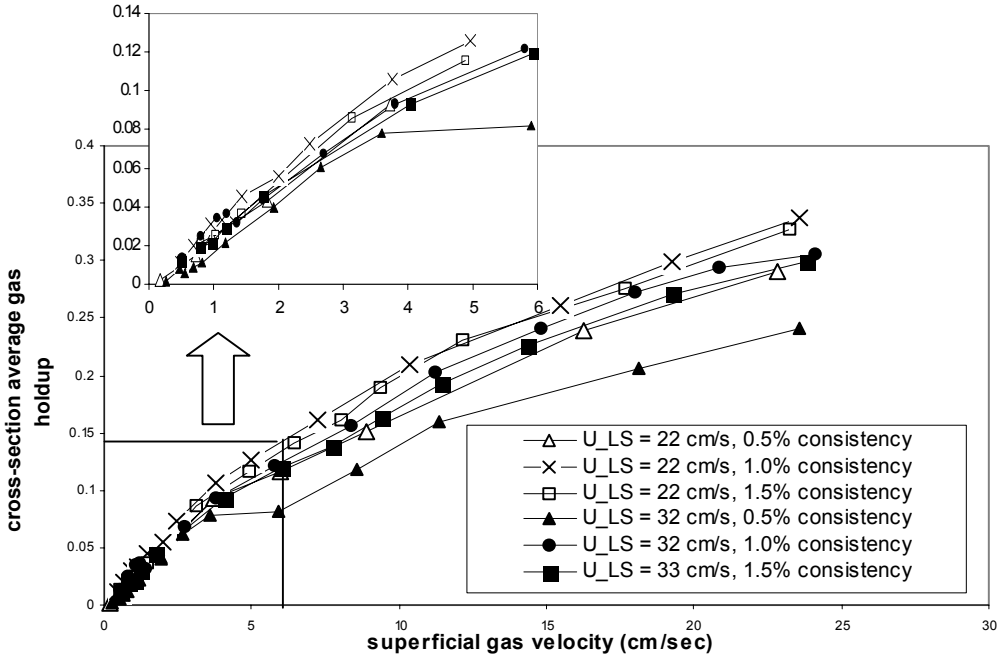

Figure 4.6: Cross-section average gas holdups

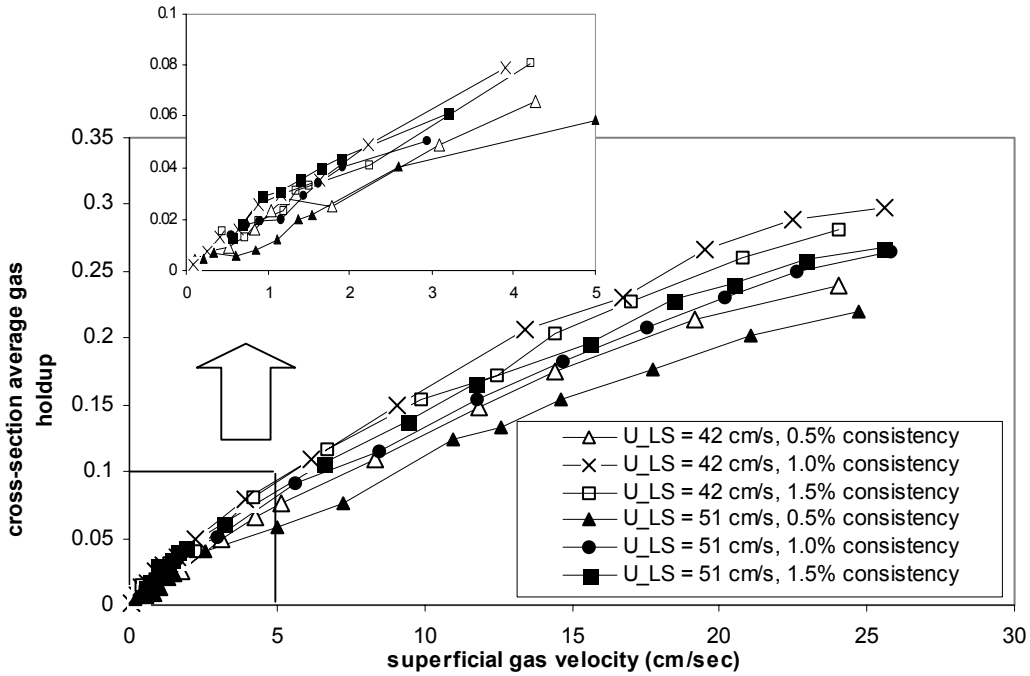

Figure 4.7: Cross-section average gas holdups

The cross section-average gas holdups were small and highly scattered for dispersed and layered bubbly regimes. Figure 4.8 compares the measured gas holdups for these flow patterns, with the predictions of the homogeneous flow model, which assumes that the two phases are well mixed and have the same axial velocity everywhere:

$$\bar{\varepsilon} = \frac{\overline{U_{GS}}}{\overline{U_{GS}} + \overline{U_{LS}}} \tag{4-1}$$

The agreement, notwithstanding the large scatter in the data, is reasonable.

Significant velocity slip occurs in other flow regimes. The Drift Flux Model (DFM) (Zuber and Findlay, 1965; Wallis, 1969) has been found useful for the correlation of gas holdup in gas-non-Newtonian liquid two-phase flow (Chhabra et al., 1984; Welsh et al., 1999). The gas holdup data for these flow regimes were therefore correlated using DFM, according to which:

$$\bar{\varepsilon} = \frac{\overline{U_{GS}}}{C_0(\overline{U_{GS}} + \overline{U_{LS}}) + V_{GJ}} \tag{4-2}$$

The parameter C_0 represents the global slip, and is defined as:

$$C_0 = \frac{<\varepsilon(U_{GS} + U_{LS})>}{\bar{\varepsilon} < U_{GS} + U_{LS} >} \tag{4-3}$$

The gas drift velocity, V_{GJ}, is an indication of local slip, and is defined as:

$$V_{GJ} = \frac{<\varepsilon[V_G - (U_{GS} + U_{LS})]>}{\bar{\varepsilon}} \tag{4-4}$$

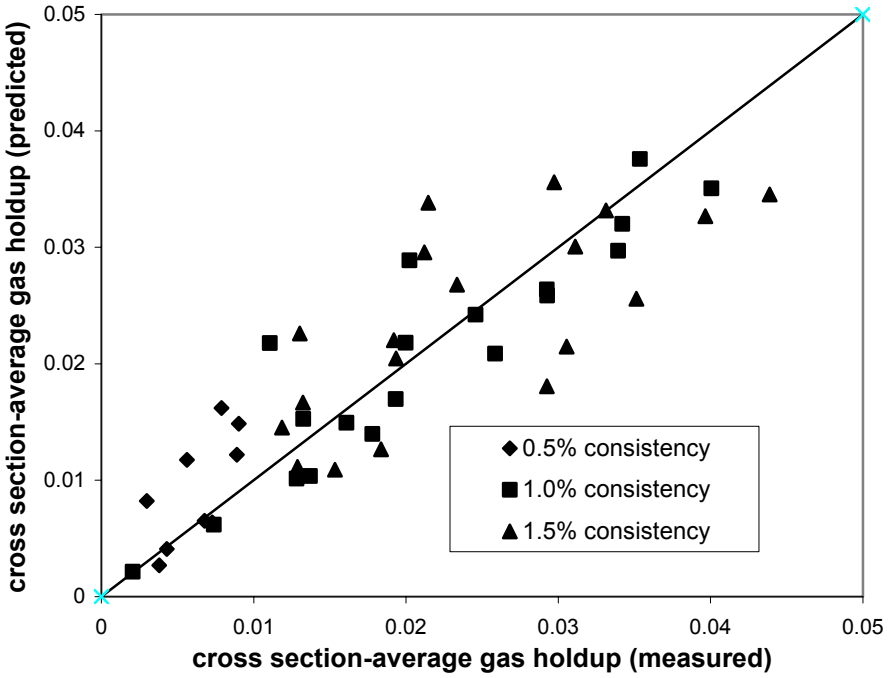

Figure 4.8: Comparison of gas holdups in dispersed bubbly and layered bubbly regimes with the predictions of homogeneous flow model

Note that in the above expressions the notation <> implies flow cross-sectional averaging. Thus, for any arbitrary property η:

$$\bar{\eta} = <\eta> = \frac{1}{A}\iint_A \eta dA \tag{4-5}$$

Parameters C_0 and V_{GJ} can be rigorously calculated only for flow fields with well-known hydrodynamic characteristics. In practice, for most cases C_0 and V_{GJ} are treated as empirical coefficients, and can be estimated using experimental gas holdup data following a simple procedure (Wallis, 1969).

Correlations of the data representing the plug, churn-turbulent and slug flow regimes, in various combinations, was attempted. The DFM parameters are generally dependent on the liquid properties (Chhabra et al., 1984). The DFM parameters were thus found to be sensitive to consistency, and since only three consistencies were used in the experiments, separate correlations were attempted for each consistency. Excluding separate correlation parameters for each of the flow patterns (which would provide the most accurate correlations, at the expense of the largest number of empirically-adjusted parameters), the following was found to be the most reasonable combination. For each pulp consistency, the plug and churn flow regimes could be combined into one group, and represented by a single set of C_0 and V_{GJ} values. This can be interpreted to imply that the aforementioned regimes are similar, at least with respect to their phase velocity slip characteristics. The slug flow regime, however, was noticeably different from the other regimes, and was therefore correlated separately. A similar distinction between slug flow and other regimes is also common for non-fibrous slurries (Chhabra et al., 1984).

Values of C_0 and V_{GJ} found in this way are summarized in Table 4-1, where the mean and standard deviation of the following statistic are also provided:

$$\zeta = \left| 1 - \frac{\bar{\varepsilon}_{\mathrm{mod}\,el}}{\bar{\varepsilon}_{\exp}} \right| \tag{4-6}$$

Figures 4.9 and 4.10 compare the experimental and predicted gas holdups.

Table 4-1: Drift Flux Model parameter values

Regime	Consistency (%)	C_0	V_{GJ} (cm/s)	$\bar{\zeta}$ (%)	σ_ζ
Bubbly-Plug/Plug/Churn	0.5	1.11	18.5	17.9	20.8
	1.0	1.08	5.7	6.7	4.8
	1.5	1.01	10.3	7.8	6.2
Slug	0.5	1.15	23.7	4.1	3.0
	1.0	1.10	13.5	5.0	3.0
	1.5	1.05	14.4	4.9	3.9

As mentioned earlier, C_0 is a measure of global slip, or non-uniformity of void fraction profile over the column cross-section; C_0 = 1 implies a flat gas holdup profile, while increasing non-uniformity leads to higher C_0 values. As noted in Fig. 4.5(b), the void fraction profiles are relatively flat in bubbly, layered-bubbly and plug flow, and the data show that the profiles become more uniform in these flow regimes as consistency is increased. These trends are consistent with the magnitudes and the trend of variation of C_0 with consistency depicted in Table 4-1, where C_0 is only slightly larger than unity, and approaches 1 as consistency is increased. For slug flow, the well-accepted value of C_0 is 1.2 for gas-liquid two-phase flow. Table 4-1 implies that flatter gas holdup profiles are obtained as the fiber consistency is increased, and this trend is consistent with Fig. 4.5. The parameter V_{GJ} represents local slip. Fibers can have two opposing effects on

V_{GJ}. On one hand, higher fiber consistency implies stronger fiber network-bubble entanglement, hence lowers velocity slip. On the other hand, higher consistency can lead to larger and therefore more buoyant bubbles by enhancing coalescence, thereby tending to increase velocity slip. The rather complicated trend in the V_{GJ} values in Table 4-1 results from the combined effect of the above processes.

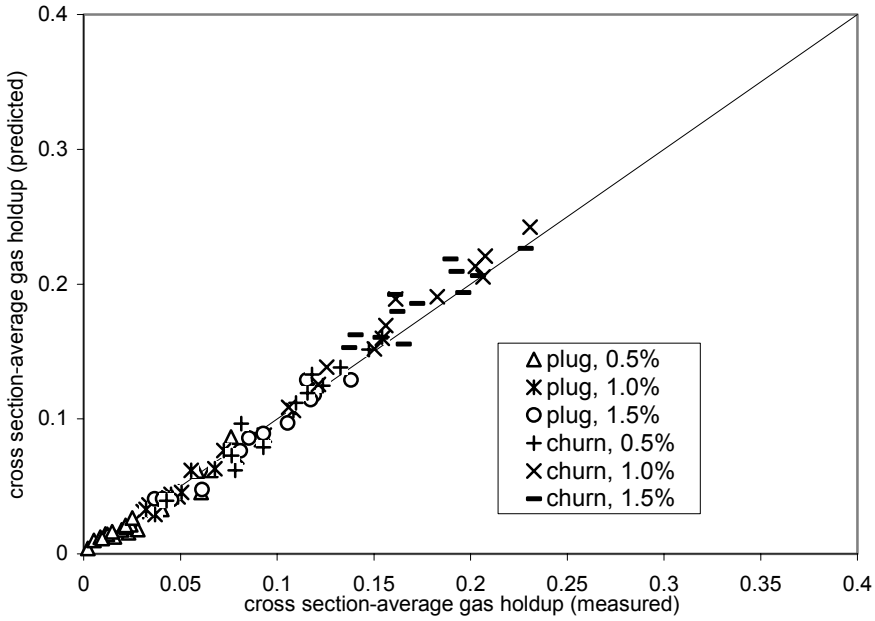

Figure 4.9: Comparison of gas holdups with the drift flux model predictions for plug and churn flow regimes

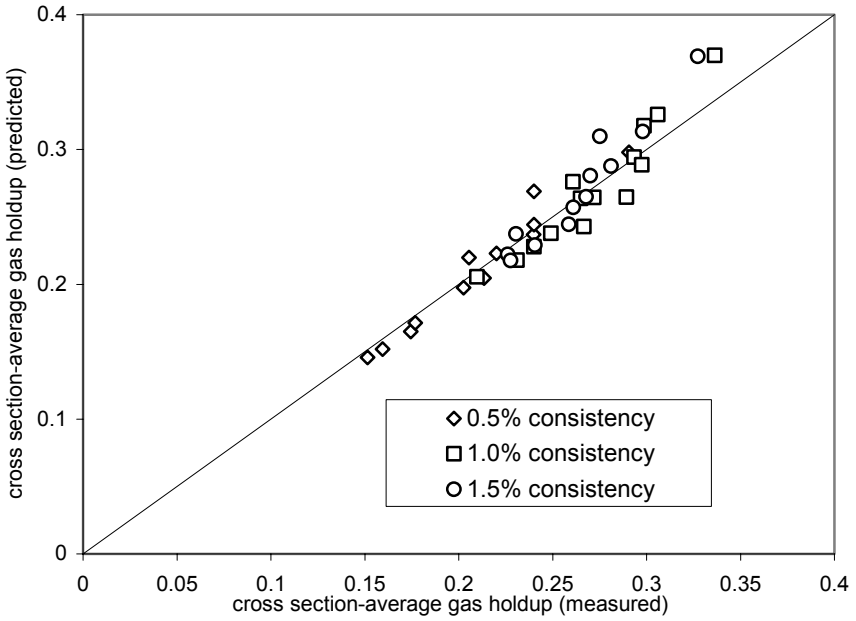

Figure 4.10: Comparison of gas holdups with the drift flux model predictions for slug flow regime

In summary, our experimental results showed that cross section-average gas holdup agreed with the predictions of homogeneous flow model for bubbly and layered bubbly regimes. The Drift Flux Model (DFM) could be applied to other regimes, when plug and churn-turbulent regimes were treated together, and slug flow was treated separately. The drift flux parameters were functions of consistency, however.

CHAPTER 5

ARTIFICIAL NEURAL NETWORK-BASED FLOW REGIME IDENTIFICATION

5.1 Introductory Remarks

In this chapter, the results for flow regime identification using various artificial neural networks are presented. The flow regime data were obtained using the test loop depicted in Figure 3.1. The following modifications were made, however.

The hydrosonic pump was removed to avoid fiber clogging inside the pump. The gas was introduced and mixed with the pulp-liquid prior to the test section.

Five holes were drilled on the test section to host the dynamic pressure sensors mentioned in Section 3.2. They are spaced 10 cm from each other in a row, starting from 120 cm above the inlet of the test section. Those orifices were designed to provide the flexibility of recording pressure signal at various locations, and the combinations of using any three of them were able to offer simultaneous recordings of pressure fluctuations inside bubble column. In our study, three holes positioned at 120 cm, 130 cm, and 140 cm respectively were used to mount the dynamic pressure transducers, whereby the rest two holes were plugged and not used.

The remainder of this chapter is organized as follows. In Section 5.2, typical pressure measurements for each major flow regime were presented. In Sections 5.3 - 5.4, the results of an ANN-based method, using the statistical characteristics of the normalized pressure fluctuations recorded by a single sensor at 120 cm height, are presented. A different, and more robust ANN-based method, based on the frequency-

domain analysis of the normalized pressure signals, is described in Sections 5.5 – 5.8. Finally, in Sections 5.8 – 5.10, the important issue of transportability of ANNs is addressed. It is shown in these sections that the frequency-domain based ANNs have promising characteristics with respect to transportability.

5.2 Pressure Sensor Measurements

In the experiments, tests were carried out over $21 \le \overline{U_{LS}} \le 51\,\text{cm/s}$ and $0 \le \overline{U_{GS}} \le 26\,\text{cm/s}$ superficial velocity ranges for the liquid slurry and the gas phase, respectively. Flow regimes were identified using video pictures, and gas holdup values were measured in the tests following the aforementioned procedures. In every test, the pressure fluctuations were recorded using the aforementioned dynamic pressure sensors, located at heights of 120 cm (Sensor 1), 130 cm (Sensor 2), and 140 cm (Sensor 3) from the inlet of the bubble column. Acquisition frequency and length of time series data are important factors for the estimation of statistical properties of random data. The former was selected as 100 samples/sec so that the Nyquist rate exceeded the maximum frequency contained in the data, as prior literature suggests that the most informative pressure fluctuations in the bubble columns occur in the range from 0 to 20 Hz (Drahos et al., 1991). The record length of 2000 data points (20 seconds duration) was chosen on the basis of preliminary experiments to satisfy wide-sense stationarity.

Typical pressure traces for each major flow regime (to be discussed shortly) are shown in Figure 5.1(a) – (d). (Figure 5.1(a) represents the dispersed bubbly flow depicted schematically in Figure 4.1(a), hence the approximately uniform signal frequency.)

In this investigation, the flow regimes were identified by direct visualization with assistance of flash X-ray images and Gamma-ray densitometry. Based on visual observations six distinct flow regimes could be identified, as schematically depicted in Fig. 4.1. The faint large arrows in these figures display the curvilinear passage of large bubbles. A detailed description of each flow pattern has been offered in Chapter 4.

However, analysis with ANNs, described in the forthcoming section, indicated that the flow regimes depicted in Figure 4.1(a), 4(b) and 4(c) had essentially similar statistical pressure fluctuation characteristics that could not be readily distinguished from one another by the neural networks, suggesting that their common basic hydrodynamic characteristics are more significant than their apparent morphological differences. Accordingly, the three flow regimes depicted in Figure 4(a), 4(b) and 4(c) will be addressed as the bubbly flow regime in the forthcoming discussions.

The experimental data points generated in this study are depicted in Figure 5.2(a), (b) and (c), for 0.5%, 1.0% and 1.5% water-pulp consistencies, respectively. The data points, 200 in total number, are shown in gas and liquid/pulp mixture superficial velocity coordinates, leading to the displayed experimental flow regime transition lines.

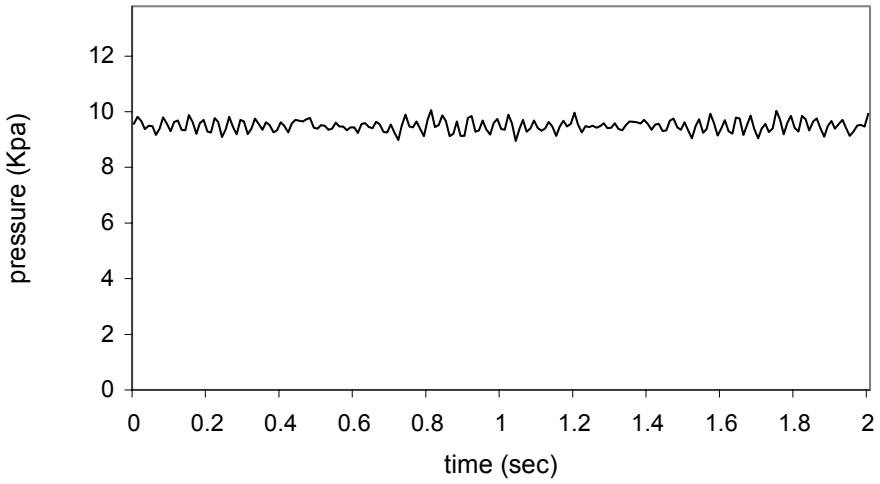

(a)

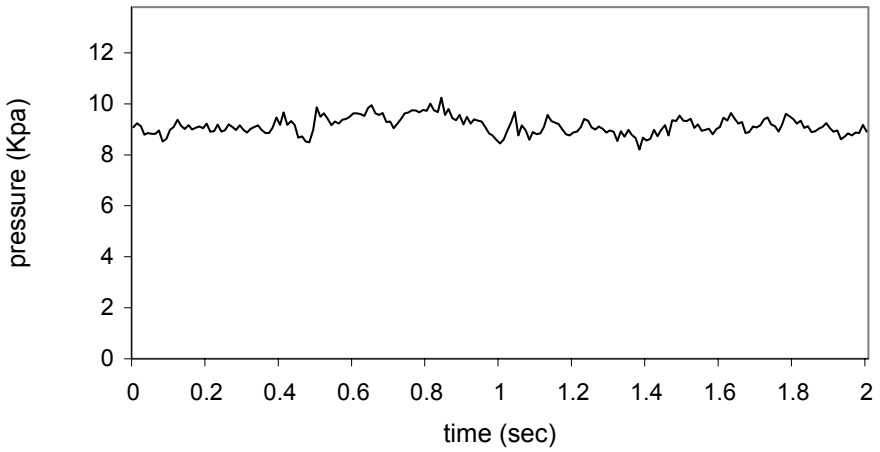

(b)

Figure 5.1: Pressure transducer measurements: (a) bubbly flow; (b) plug flow; (c) churn-turbulent flow; (d) slug flow

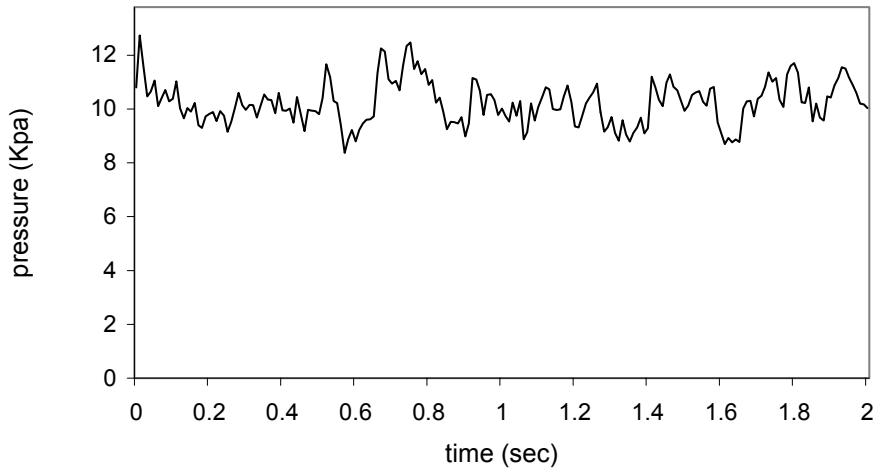

(c)

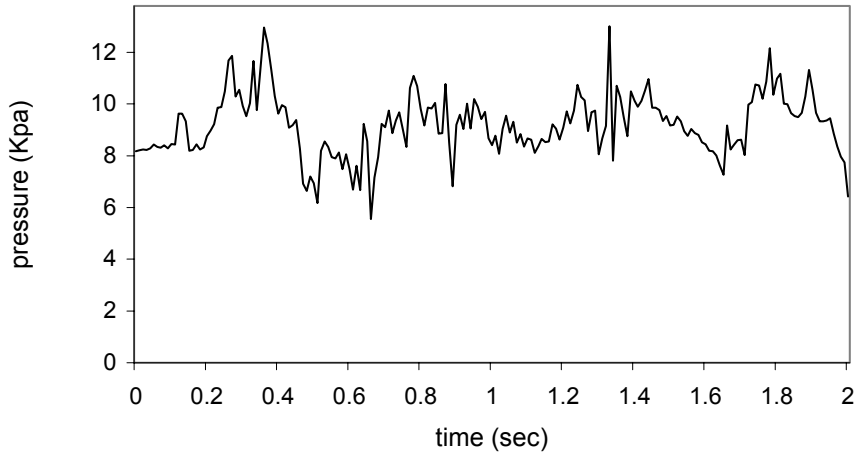

(d)

Figure 5.1 (Continued)

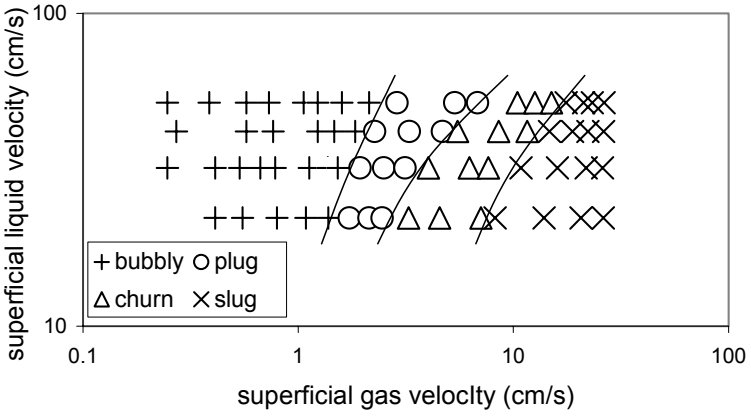

(a)

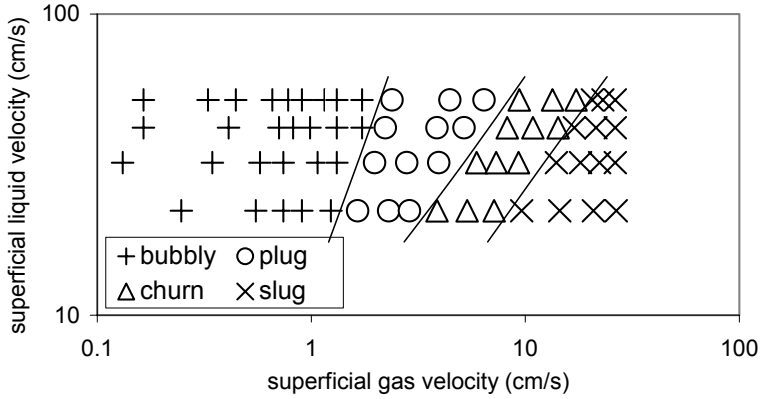

(b)

Figure 5.2: Experimental flow regime data: (a) 0.5% pulp consistency; (b) 1.0% pulp consistency; (c) 1.5% pulp consistency

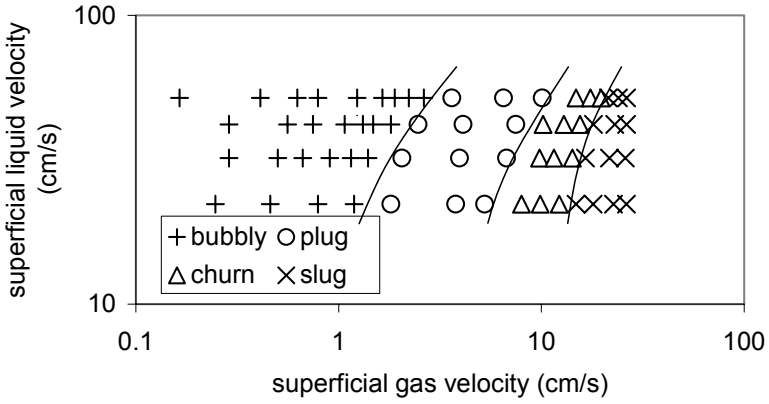

(c)

Figure 5.2 (Continued)

5.3 Time-Domain Parameters

As described earlier, artificial neural networks constitute a class of algorithms that may be able to use flow statistical parameters in order to perform flow regime identification. To some extent, a neural network pattern recognition approach involves a trainable black box. It can be trained to learn the correct output or classification for each of the training samples. After training, the neural network can interpolate (or even extrapolate) when faced with new, similarly behaving patterns.

Supervised neural networks, which are often used as associative memories or classifiers, were developed to function as a classifier for identifying flow regimes. The principles of ANNs have been described in Chapter 2, and will not be repeated here, and only the major characteristics of the design are presented. The standard deviation, coefficient of skewness, coefficient of kurtosis, and second-order correlation terms T(2),

T(5), T(10), T(20), T(50), T(100), and T(200), of the normalized pressure signals are chosen to represent characteristics of pressure fluctuations, and used as input to the neural network. The commonly accepted mathematical definitions of standard deviation, skewness, and kurtosis were used. The second-order correlation terms of normalized pressure signals are:

$$T(d) = \overline{p^*(t)p^*(t+\tau)} \tag{5-1}$$

Where, the normalized pressure fluctuation p^* is defined as

$$p^* = (p - \overline{p}) \Big/ \sqrt{\overline{(p-\overline{p})^2}} \tag{5-2}$$

The parameter τ is the time shift, and is defined as $\tau = d / N$, where N represents the rate of pressure signal measurements (100 Hz in these experiments).

The rationale for the selection of the above input parameters was as follows. We want our classification algorithm to be, as much as possible, independent of the run length or logging frequency of the pressure signals. To achieve this type of invariance, we pre-process the signals in a manner that, at least for high enough logging frequencies, leads to invariant intermediate variables. The pattern recognition algorithm is then trained to use these variables as its inputs. The second order correlations of equation (5-1) are appropriate invariants, provided that the shift *d* is properly scaled with the logging frequency. Those terms embody the translation invariant relationships between the input data stream and the output (Giles and Maxwell, 1987).

The output of the system is an indicator of flow regimes, including bubbly flow, plug flow, churn-turbulent flow, and slug flow. The ANN was feed-forward, and has three neuron layers (i.e., one hidden layer). The neurons in the input layer had a piecewise linear activation function, while the neurons in the hidden and the output layers

use a sigmoidal activation function. The back-propagation learning paradigm was used. NeuroShell 2 was used for the design and training of the neural network models.

Two neural network structures were developed each using a different output layer configuration, and their schematics are shown in Figure 5.3(a) and 5.3(b). In configuration A, the targeted output values were designated to 0.3, 0.5, 0.7, and 0.9 corresponding to bubbly flow, plug flow, churn-turbulent flow, and slug flow, respectively. The flow regime is treated like an ordinal variable in this configuration, having a natural ordering based on the observed typical sequence of regime transitions – a more typical approach to classification treats the classes symmetrically without assumed ordering. The output value of this configuration is continuous, and 0.4, 0.6, and 0.8 were set as the decision boundaries between the flow regimes. This design was consistent with the nearly linear transition boundaries in the flow regime maps depicted in Figure 5.2.

The ANN with configuration B has four neurons in the output layer, each of which represents a distinct flow regime. During training and calibration, the output of the neuron corresponding to the correct flow regime is assigned the value 1, while the others are assigned zero. The outputs of the trained network can be perceived as probabilities of each flow regime for any given set of input parameters, with the node possessing the largest output showing the most probable regime. The number of hidden layer neurons was experimented with, and the optimal number of nodes was found to be 7 for both of configurations.

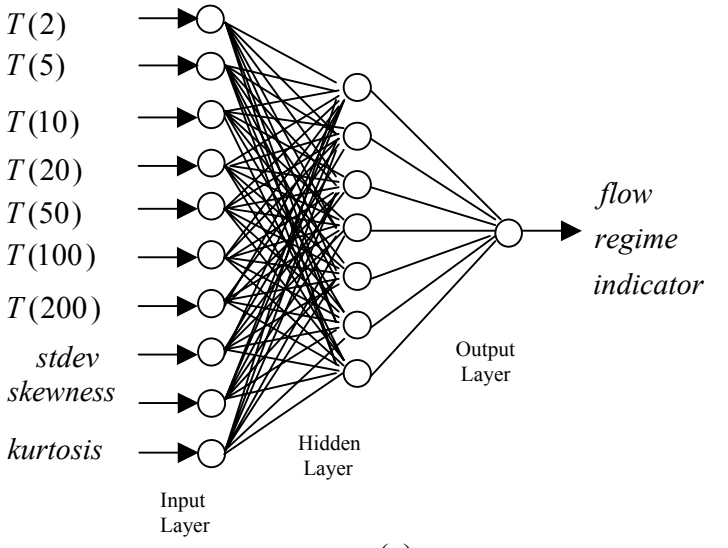

(a)

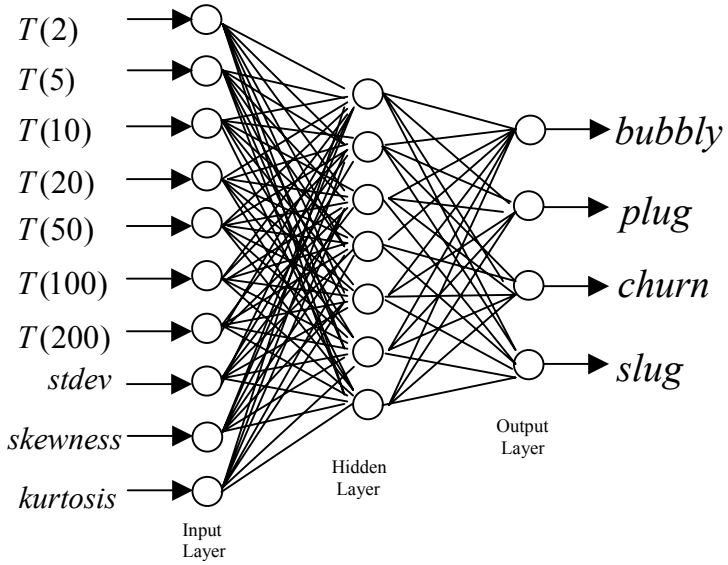

(b)

Figure 5.3: Schematics of neural networks: (a) Configuration A; (b) Configuration B

5.4 Performance of ANNs That Are Based on Time-Domain Parameters

The training data set is a subset of all the possible examples of the mapping. Following common practice, a fraction of the obtained data (60%) was used for training the ANNs and another 17% of the samples were used for calibration (i.e., validation of the data set), which prevented the networks from being over-trained. The remainder of the data (45 data points), which the networks had never "seen" during the training process, was used to test the networks. The test set of data was randomly chosen to avoid a memorized-patterns effect. For each network type, the training was stopped when either 20,000 training events were reached, or the validation error showed incipient over-training.

The predictions of the ANN with configuration A are compared with the test subset of the experimental data in Figures 5.4(a), 5.4(b), and 5.4(c), for the three consistencies of 0.5%, 1% and 1.5%, respectively. In these figures the depicted regime transition lines are experimental, and are the same as those in Figures 5.2. The data points, however, are what the ANN predicts. Similar results, depicting the performance of the ANN with configuration B, are shown in Figures 5.5(a), 5.5(b) and 5.5(c). As noted, both ANNs predict the flow regimes well, with either model misclassifying only 4 out of the 45 test data points. However, the misclassified cases only confused neighboring flow regimes. The misclassified cases, furthermore, all evidently represent near-transition conditions for two adjacent flow regimes. This is particularly important for the ANN with configuration B, since it was not aware of which flow regimes are adjacent on the flow regime map based on the information it had been trained with. For both configurations, furthermore, all misclassifications occur with respect to the plug flow regime. A possible

reason for the observed misclassifications is that plug flow regime itself represents a transition between bubbly and churn flow regimes.

Figure 5.6 presents contribution factors for each input of the ANN with configuration A; these factors provide a rough measure of the importance of each input variable towards the network's output, relative to the other inputs. The higher the contribution factor, the more that variable is contributing to the classification. The contribution factors were calculated based on the internal weights using a proprietary algorithm in the commercial neural network package. It should be noted, however, that these contribution factors can sometimes be misleading for nonlinear models due to the local nature of any linearization. For nonlinear models it is well known that the feature selection problem is very complicated, and a variable that seems insignificant within one group of inputs can shine when pooled with some other inputs. Therefore, any typical method of estimating an input's significance is at best suggestive, and should not be the basis for hard decisions. A discussion of saliency measures in ANNs is available in Duda et al. (2000).

The above results clearly support the feasibility of using a single, minimally-intrusive pressure sensor for flow regime identification. However, more experiments are needed. In particular, the feasibility of this method for much larger industrial systems needs experimental verification. Furthermore, the transportability of trained ANNs, whereby an ANN trained with a sensor, and/or a scaled-down system, can be manipulated and applied with another similar sensor and/or a prototypical-scale system, needs to be investigated.

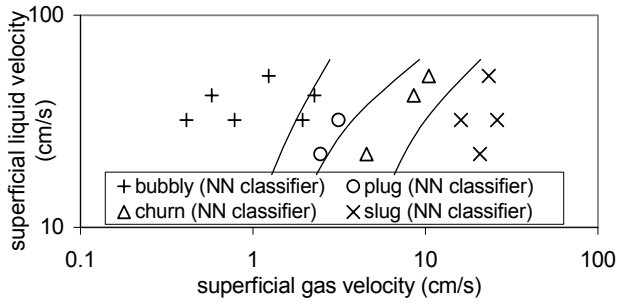

(a)

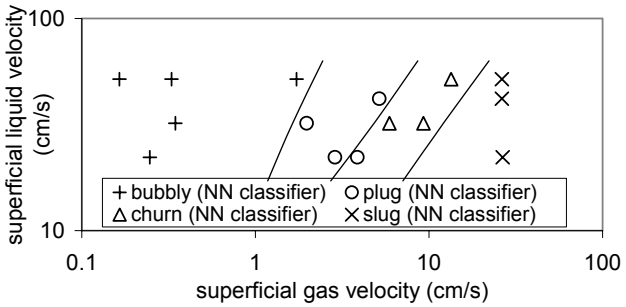

(b)

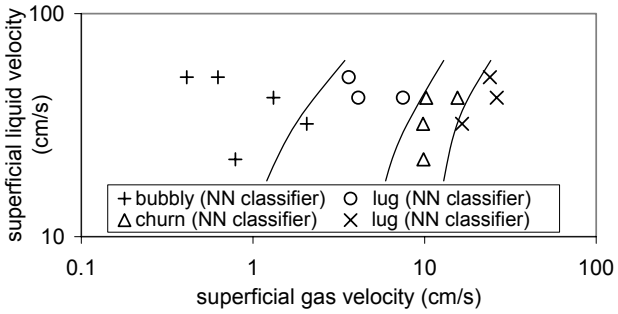

(c)

Figure 5.4: Comparison between the predictions of the ANN with configuration A and the test subset of the data: (a) 0.5% pulp consistency; (b) 1.0% pulp consistency; (c) 1.5% pulp consistency

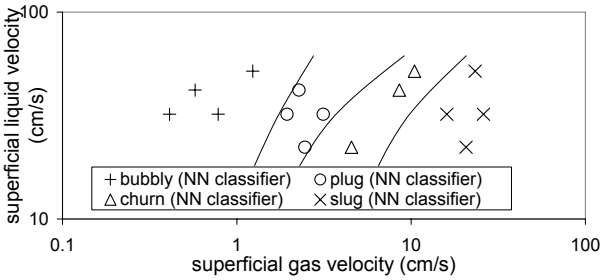

(a)

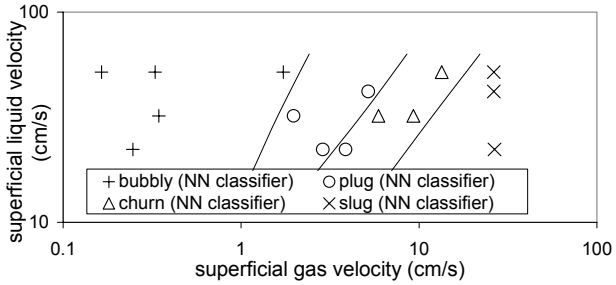

(b)

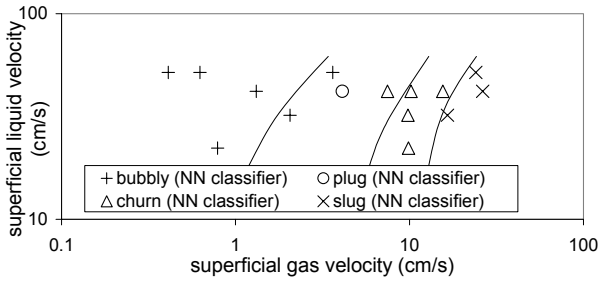

(c)

Figure 5.5: Comparison between the predictions of the ANN with configuration B and the test subset of the data: (a) 0.5% pulp consistency; (b) 1.0% pulp consistency; (c) 1.5% pulp consistency

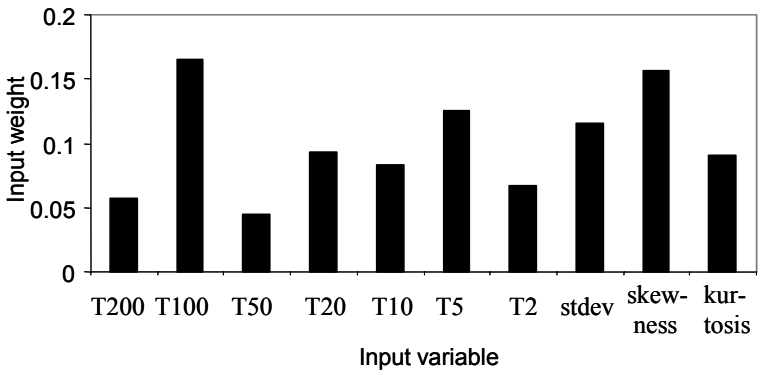

Figure 5.6: Contribution factor analysis for the ANN with configuration A

5.5 Frequency-Domain Parameters

The feasibility of an ANN for regime identification was demonstrated in the proceeding sections, using as inputs the standard deviation, coefficients of skewness and kurtosis, and several second-order correlation terms of the normalized pressure signals recorded by a single sensor. The feasibility of using normalized pressure power spectral characteristics is now examined, as our current goal is to promote a certain type of invariance (indifference to zero and gain at least).

Periodic phenomena pervade in engineering systems, and the hydrodynamic processes in bubble columns are no exception. Spectral analysis is commonly used to reveal the periodicity in a time-series. The power spectral density is a frequency domain characteristic of a time series and is appropriate for the detection of frequency composition in a stochastic process (Matsumoto and Suzuki, 1984). Assuming the process to be stationary and ergodic, the power spectral density function $P_x(f)$ of a discrete-time signal $x(n)$ is defined as the Fourier transform of the autocorrelation sequence $R_x(k)$:

$$P_x(f) = \sum_{k=-\infty}^{\infty} R_x(k) e^{-i2\pi kf/f_s} \tag{5-3}$$

where, f_s is the sampling frequency.

For an autocorrelation-ergodic real-valued process and an unlimited amount of data, the autocorrelation sequence may in theory be approached by a time-average:

$$R_x(k) = \lim_{N\to\infty} \frac{1}{2N+1} \sum_{n=-N}^{N} x(n+k)x(n) \tag{5-4}$$

The record length of the signal we actually work with is of course limited. To diminish the distortion of the spectrum due to finite length of data record, the averaged modified

periodogram method (Welch's method) was adopted. If $x(n)$ is only measured over a finite interval, say n = 0, 1, …, N-1, then periodogram method estimates the power spectral density as:

$$\hat{P}_x(f) = \sum_{k=-N+1}^{N-1} \hat{R}_x(k) e^{-i2\pi kf/f_s} \tag{5-5}$$

where, the autocorrelation is given as:

$$\hat{R}_x(k) = \frac{1}{N} \sum_{n=0}^{N-1-k} x(n+k)x(n) \tag{5-6}$$

Welch (1967) modified the periodogram method by subdividing the N-point sequence into overlapping segments. He then applied window function to each data segment and computed the corresponding periodograms for each segment. Finally, he averaged the periodograms to obtain the power spectrum estimate. More details of this method are available in Proakis et al. (1996).

In our study, the normalized pressure fluctuations, defined below, were the time series of interest.

$$p^* = (p - \overline{p}) \Big/ \sqrt{\overline{(p - \overline{p})^2}} \tag{5-7}$$

The power spectrum was estimated using segments with a length of 256 points and a Hanning window of the same size in order to lower the variance of the estimate. All the power spectrum analyses were performed using the signal processing toolbox of Matlab 6.1 (MATLAB 6.1 Tutorial, The Mathworks, Inc., 2003).

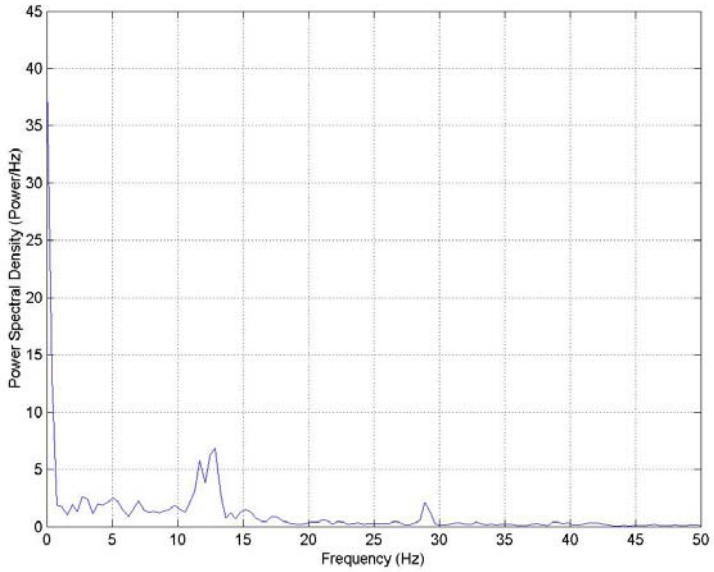

(a)

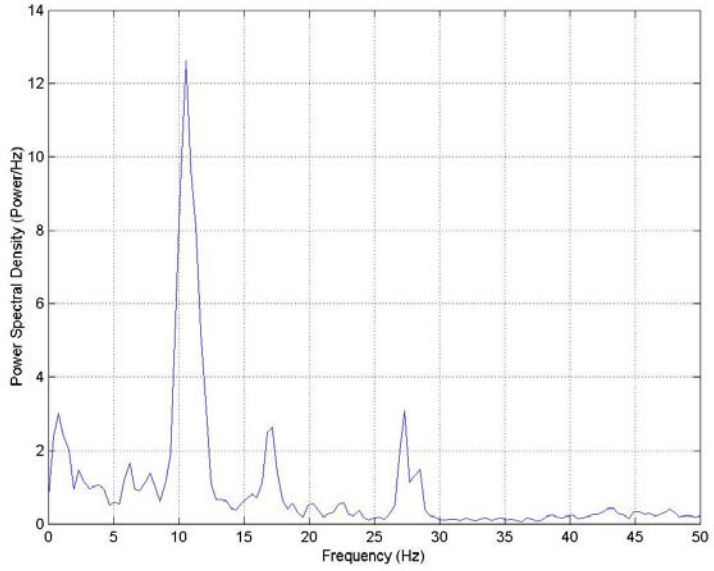

(b)

Figure 5.7: Examples of the power spectral density functions of pressure fluctuation: (a) bubbly flow; (b) plug flow; (c) churn-turbulent flow; (d) slug flow.

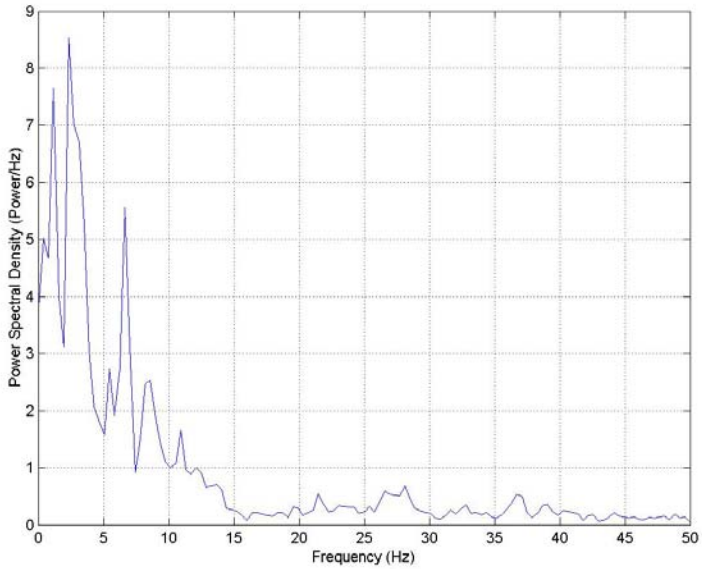

(c)

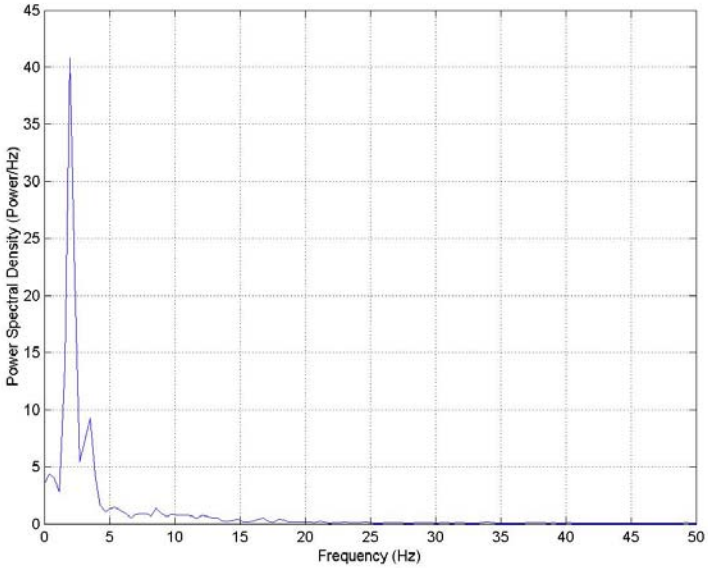

(d)

Figure 5.7 (Continued)

Examples of power spectra for all the major flow regimes are shown in Figure 5.7(a), 5.7(b), 5.7(c) and 5.7(d). The power spectrum in the bubbly flow regime exhibits two clear peaks (approximately at 13 Hz and 27 Hz for the depicted case), which may correspond to the frequency of gas bubbles at two different sizes. In the plug flow regime, the lower-frequency peak becomes more dominant. This may represent the passing-by of large gas plugs with dimensions comparable to the channel diameter. The power spectrum of churn flow regime shows several peaks spread over a wide frequency range from 0 to 15 Hz except for strong peaks at the small frequency range (less than about 3 Hz). The peaks may represent the coalescence and collisions of gas pockets. The slug flow regime has a very strong spike (at about 2 Hz in the displayed case), corresponding to the macroscopic periodic oscillations of the bullet-shaped bubbles that resemble Taylor bubbles in gas-liquid two-phase flow. It is also noted that the frequency components over 30 Hz do not contribute much to the power spectral density.

The above examples indicate that the power spectral structure of each hydrodynamic regime in a gas-liquid pulp mixture flow is distinct, and therefore it may be possible to identify the hydrodynamic regimes of the gas-liquid-pulp slurry fiber flow in a bubble column based on their estimated pressure power spectral characteristics.

To characterize the hydrodynamics of the flow based on the power spectral density function, it is necessary to first implement parameterization of the information contained in the spectral patterns. Based on the recorded power spectra, we focus on a frequency range up to 30 Hz. Each spectrum is normalized to one in its integral over the 0 – 30 Hz range (which provides invariance against changes in gain). The frequency range over 0-30 Hz is then divided into five bandwidths: 0-3 Hz, 3-8 Hz, 8-13 Hz, 13-25 Hz,

and 25-30 Hz. According to Parseval's relation, the integral of the power spectral density across the entire band is a measure of the total energy of the signal. To approximate the percentage of energy the signal has in a given frequency band, we need to sum the estimated average power spectral density over the desired frequency band. The mean value of power in each of the aforementioned bands, denoted as P^*_{0-3Hz}, P^*_{3-8Hz}, P^*_{8-13Hz}, $P^*_{13-25Hz}$, and $P^*_{25-30Hz}$, respectively, is then used as representative of the individual band.

It should be mentioned that the number of frequency windows and the ranges of the windows were judicious. Increasing the number of windows, or equivalently reducing the frequency ranges of the windows, would in principle improve the predictions at the expense of extra computation. Furthermore, the smaller the number of input parameters, the more practically appealing a model would be. An optimization analysis would therefore be warranted in order to determine the smallest number of frequency bands that are needed for accurate representation of the system hydrodynamics. Although we did not perform an optimization analysis, nevertheless the selected input parameters for the forthcoming ANN, as will be shown, are adequate. The selection of appropriate input parameters would in fact be considered as an important contribution of this research. Other parameters of interest are mean frequency, $\bar{f}$, given by:

$$\bar{f} = \frac{\sum_i f_i P_x(f_i)}{\sum_i P_x(f_i)}, \tag{5-8}$$

and spectrum variance $\sigma_f{}^2$, estimated from:

$$\sigma_f{}^2 = \frac{\sum_i (f_i - \bar{f})^2 P_x(f_i)}{\sum_i P_x(f_i)}. \qquad (5\text{-}9)$$

The above 7 discrete parameters, suggested by Drahos et al. (1989), were selected to represent the characteristics of power spectrum of pressure fluctuations. Along with the fiber consistency of the three-phase flow ζ, they constitute the inputs to the forthcoming neural networks – the consistency is regulated and known in real process applications, and provides essential prior information. The output of the neural network is an indicator of flow regimes. The commercial software package (NeuroShell 2) was used for the design and training of the neural network models. Based on the experience described in Xie et al. (2003b), the targeted output values were designated to 0.3, 0.5, 0.7, and 0.9 corresponding to bubbly flow, plug flow, churn-turbulent flow, and slug flow, respectively. The flow regime is therefore treated like an ordinal variable in the neural network, having a natural ordering based on the observed typical sequence of regime transitions. The output value from the ANN is continuous, and 0.4, 0.6, and 0.8 were set *a priori* as the decision boundaries between the flow regimes. This design was consistent with the nearly linear transition boundaries in the (log-log plotted) flow regime maps.

5.6 Supervised ANNs Based on Frequency-Domain Parameters

A three-neuron-layer ANN was designed. The neurons in the input layer had a piecewise linear activation function, while the neurons in the hidden and the output layers used the logistic activation function. The back-propagation learning paradigm was used. The number of neurons in the hidden layer was experimented with, and the optimal

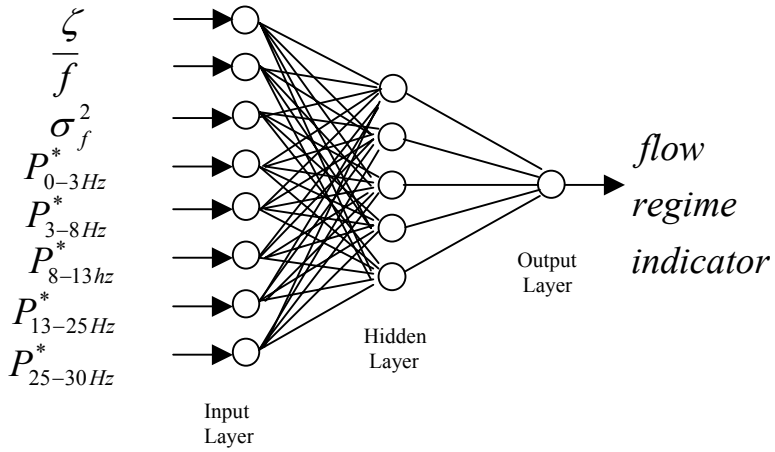

Figure 5.8: Schematic of the configuration of ANN-1

number of nodes was found to be 5. The configuration of this neural network (referred to as ANN-1) is shown in Figure 5.8.

The pressure data measured by Sensor 1 were used first. A total of 197 data records were available. Following common practice, a fraction of the obtained data (77%, or 152 data records) was selected for training ANN-1, which constituted the so-called 'calibration data'. The remainder of the data (45 data records), which the network had never 'seen' during the training process, was used to test the network. The test set of data was of course randomly chosen to avoid a memorized-patterns effect. During training, to prevent incipient over-training, the process was stopped when 20,000 training events since the minimum average error for the calibration data set were reached.

The predictions of the designed and trained ANN are compared with the test subset of the experimental data in Figures 5.9(a), (b), and (c), for the three consistencies of 0.5%, 1% and 1.5%, respectively. In these figures the depicted regime transition lines are experimental. The data points, however, are what the ANN predicts. The solid lines in

these figures represent the observed flow regime transitions in the experiments where the aforementioned pressure signals were also recorded (Xie et al., 2003b). The dashed lines are the regime transitions observed in an earlier series of experiments using essentially the same test facility (Xie et al, 2003a). With the exception of bubbly-plug transition in Fig 5.9(a), the two sets of regime transition lines are in agreement. In the analysis of the data associated with the latter tests, three different bubbly flow patterns (dispersed bubbly, layered bubbly, and incipient bubbly) were reported (Xie et al., 2003a). Analysis with ANNs, however, indicated that these flow patterns had similar pressure fluctuation characteristics (Xie et al., 2003b). The apparent discrepancy between the bubbly-plug transition lines in Fig 5.9(a) is likely due to difficulty associated with distinction between incipient plug and plug flow patterns in our earlier experiments (Xie et al., 2003a). The experimental regime transition lines depicted in all the forthcoming figures are the same as the solid lines in Figs 5.2(a-c).

As noted in Figs 5.9(a)-(c), the neural network ANN-1 predicts the flow regimes successfully, misclassifying only 5 out of the 45 test data records. Only neighboring flow regimes were confused: the misclassified cases in fact all represent near-transition conditions. It is also worth noting that most of the misclassification cases occur in experiments with the highest consistency (1.5%), which may indicate that the data with 1.5% consistency were contaminated with an interfering signal, and that the noise level in the pressure signals can be significantly boosted by the presence of more fiber. The interfering noise displayed low frequency characteristics and could not be fully eliminated by low-pass filtering during signal processing.

The above results further support the feasibility of using a single, minimally-intrusive pressure sensor for flow regime identification. However, more experiments are needed. In particular, the feasibility of this method for much larger industrial systems needs experimental verification.

5.7 Voting Scheme with Multiple Sensors

Using the ANN-1 design, a voting scheme was developed and tested with the objective of improving the regime predictions by taking advantage of the multiplicity of the pressure sensors. Accordingly, three separate ANNs, all having the configuration depicted in Figure 5.8, were used, each trained using the signals recorded by one of the three sensors. The training was done using a common set of 158 data points. The signals recorded by each sensor for the remainder of the data points (the test data) were then used as input for that particular sensor. The correct flow regime associated with each test data would then depend on the majority vote among the three ANNs.

The results of this method are compared with the test data in Figs 5.10(a)-(c). Overall, these predictions show an improvement over those depicted in Figs 5.9(a)-(c), as expected. The relatively high confusion rates associated with the $\zeta = 1.5\%$ consistency persist, however, confirming that these confusions may be caused by noise.

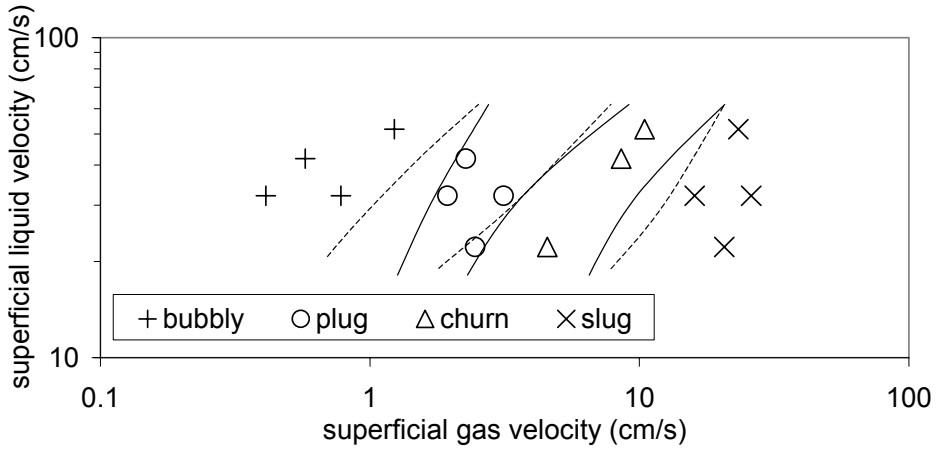

(a)

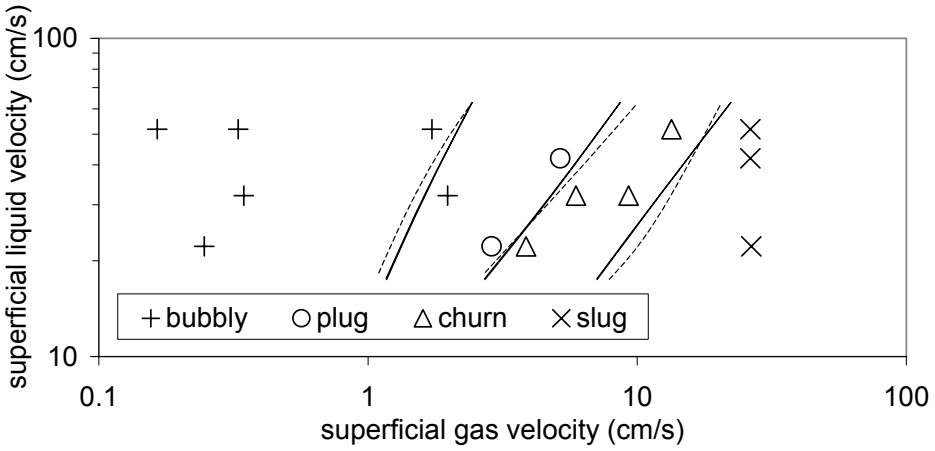

(b)

Figure 5.9: Comparison between the predictions of ANN-1 and the test subset of the data: (a) 0.5% pulp consistency; (b) 1.0% pulp consistency; (c) 1.5% pulp consistency. Transition lines are experimental and symbols are ANN predictions. Dashed lines are from the previous experiments (Xie et al., 2003a).

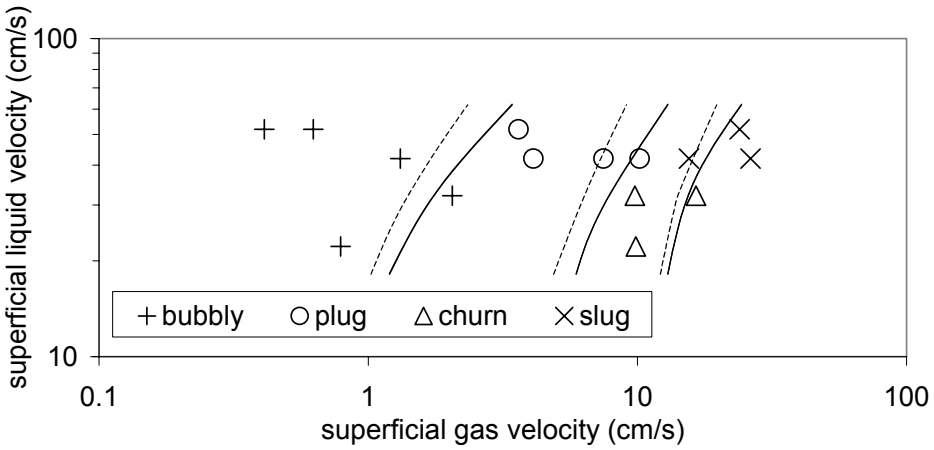

(c)

Figure 5.9 (Continued)

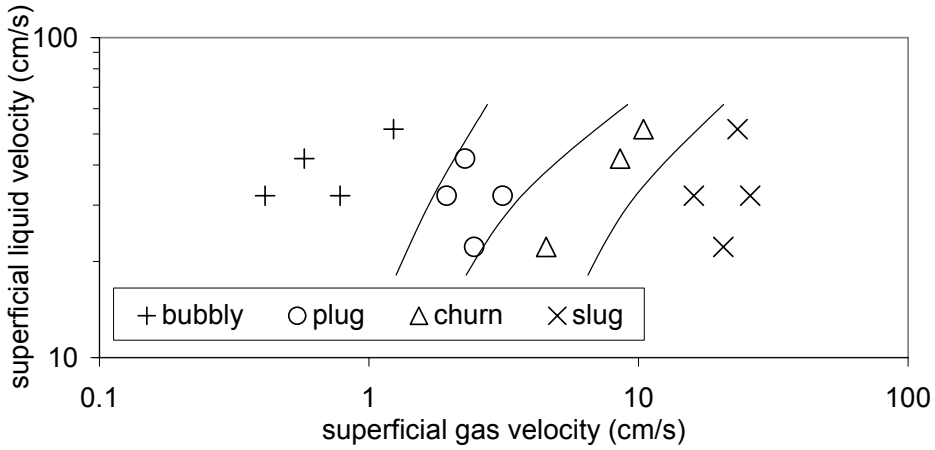

(a)

Figure 5.10: Comparison between the predictions based on the voting scheme and experiment: (a) 0.5% pulp consistency; (b) 1.0% pulp consistency; (c) 1.5% pulp consistency. (Regime boundaries are from experiments; symbols are model predictions.)

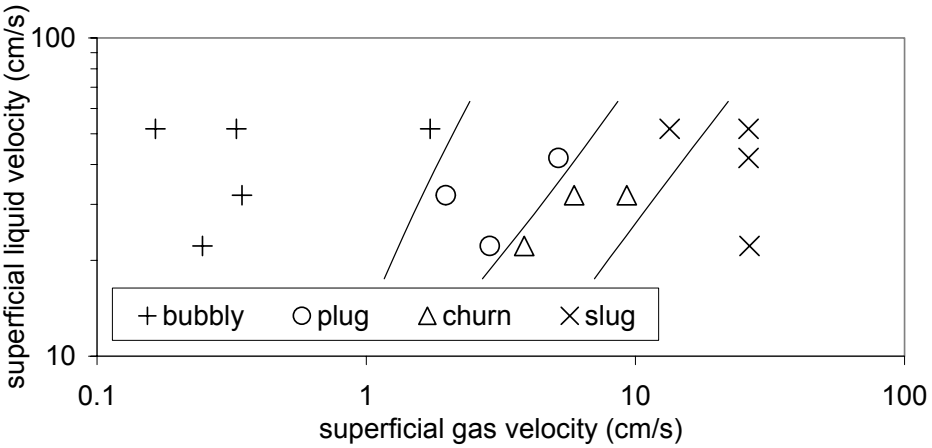

(b)

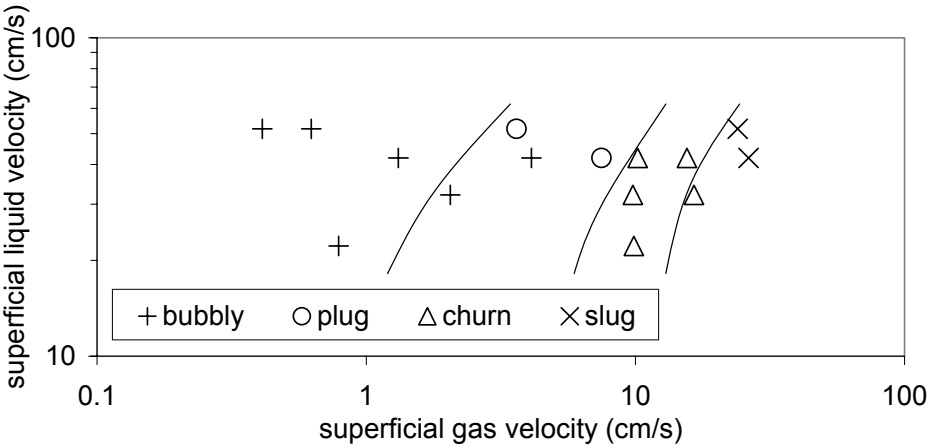

(c)

Figure 5.10 (Continued)

5.8 Self-Organizing ANN Based on Frequency-Domain Parameters

To further examine the distinct identity of the flow regimes and the experimental regime transition boundaries, an unsupervised neural network system using Kohonen Self-Organizing Map (KSOM) technique was also developed (Kohonen, 1989; Zeidenberg, 1990). In an unsupervised learning process, no "teaching" is required. Instead, the network is simply exposed to a number of inputs data sets, and is asked to classify them into a pre-determined number of groups. In Kohonen's model of self-organization, which is the same as unsupervised learning, the neurons have competition in a modified winner-take-all manner. The neuron whose weight vector produces the largest dot product with the input vector is the winner and is allowed to provide the output. However, in this model, the weights of not only the winner, but also its nearest neighbors (in the physical sense) are adjusted correspondingly.

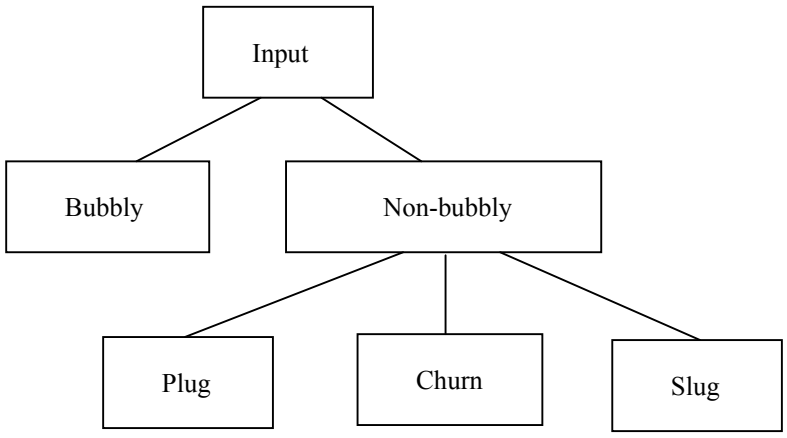

Figure 5.11: Schematic of the self-organizing neural network classifier

The data clustering was done in two stages, according to the schematic of Figure 5.11, using the aforementioned parameters P^*_{0-3Hz}, P^*_{3-8Hz}, P^*_{8-13Hz}, $P^*_{13-25Hz}$, $P^*_{25-30Hz}$, $\bar{f}$, and σ_f^2 as inputs for the KSOM networks. In the first stage the data were divided into two clusters using a two-layer KSOM network. Examination of the results showed that one cluster corresponded to bubbly flow, and the other included all other regimes. In the second stage, another two-layer KSOM network with three output nodes was used to separate all non-bubbly data. Examination of the results showed that the patterns grouped by the three output nodes corresponded to plug, churn and slug flow regimes. The unsupervised clustering methodology was applied to the entire data for three consistencies 0.5%, 1.0%, and 1.5%. The results for 0.5% and 1% consistencies are depicted in Figs. 5.12(a) and 5.12(b) respectively, where the regime border lines are experimental and the data are the clustering outcomes. The clustering of these data points is evidently good for 0.5% and 1.0% consistencies, and all the mismatches are at regime transition boundaries. The fact that clustering the data by the KSOM network found nearly similar regimes and regime boundaries as had been experimentally observed is very encouraging, and indicates that our visually-based regime boundary definitions were reasonably objective.

The clustering of the 1.5% consistency data is shown in Figure 5.12(c). As noted, these results are inferior to those shown in Figs. 5.12(a) and 5.12(b). This is essentially consistent with the observations of our supervised neural network performances. One of the reasons would be that the 1.5% consistency data confused the KSOM due to its inherent high noise level. Higher energy consumption level of the circulation pump was required to circulate the fiber suspension inside the system as pulp consistency increased.

It was observed that the roaring or rumbling type noise, which was an indication of operating the pump away from the preferred range of operation, started to pick up at 1.5% pulp consistency, and the vibration on our test section became way much stronger. It is possible that the highly-sensitive pressure sensors attached to the test section wall sensed the vibration and the quality of their measurements was damaged to some extent.

On the other hand, the aforementioned KSOM's training was evidently dominated by the trends in the lower consistency data, in view of the fact that the data representing 1.5% consistency were outnumbered by lower consistency data by a factor of 2. It is therefore not surprising that the above KSOM could not adequately cluster the 1.5% consistency data. Thus, given the above-mentioned differences between the hydrodynamic characteristics of the 1.5% consistency mixture and those of the lower consistency mixtures, it was decided to reapply the KSOM to the 1.5% consistency data, separately. In other words, the latter data would be analyzed this time by themselves, and not as part of the entire data pool.

Our attempt of applying KSOM to specifically cluster the 1.5% consistency data led to Figure 5.13. As noted, this time we had a better match between the visually-identified flow regimes and the KSOM clustering, compared to those shown in Fig. 5.12(c). The improvement caused by individual treatment of 1.5% consistency data further confirms that our definition of regime boundaries are basically correct, but unambiguous classification may not be feasible with data as limited as those used here, at higher consistencies.

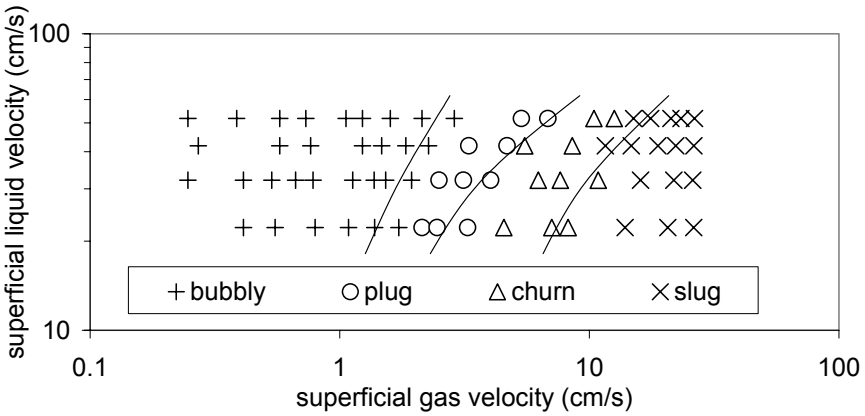

(a)

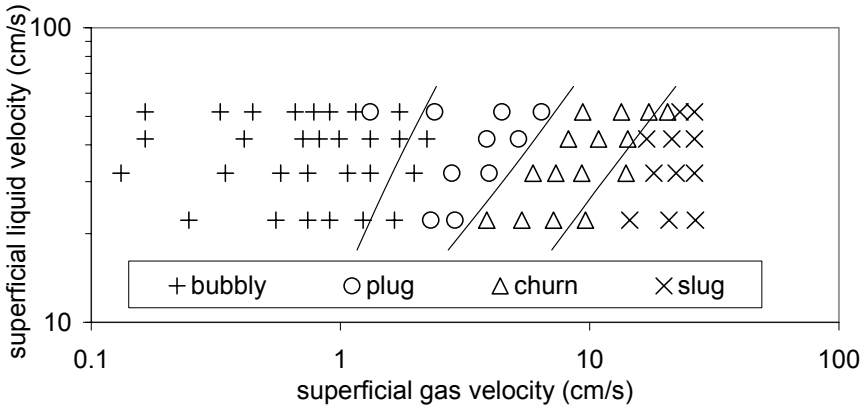

(b)

Figure 5.12: Comparison between the predictions of self-organizing network model and the test data: (a) 0.5% pulp consistency; (b) 1.0% pulp consistency; (c) 1.5% pulp consistency. (Regime boundaries are from experiments; symbols are model predictions.)

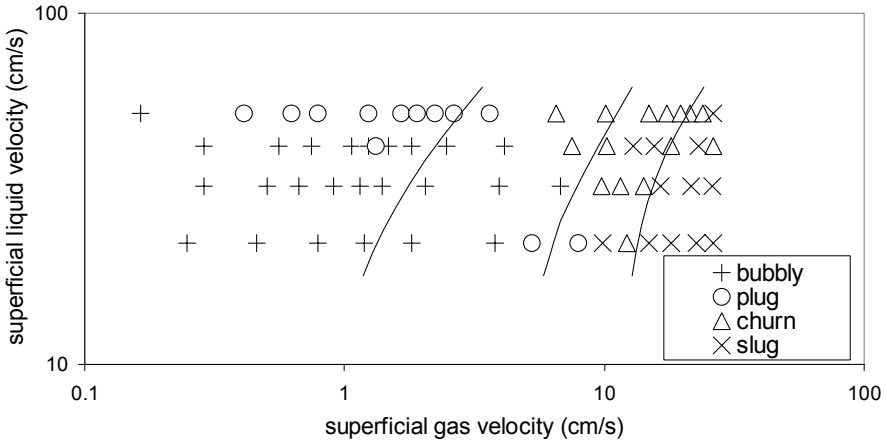

(c)

Figure 5.12 (Continued)

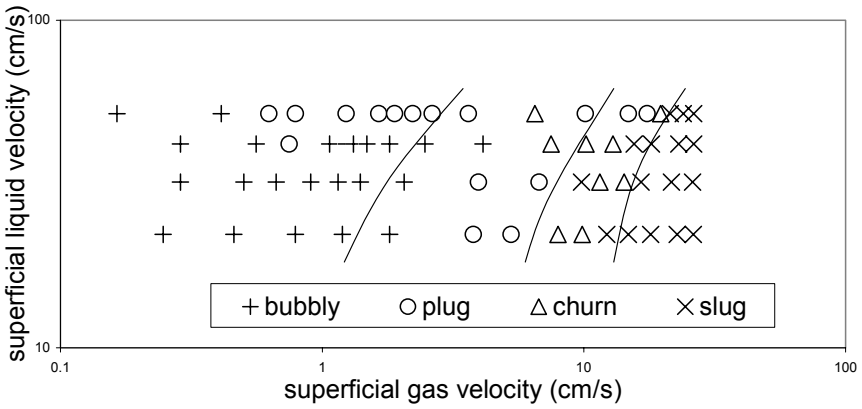

Figure 5.13: Comparison between the clustering of self-organizing network model and the test data, which only included 1.5% pulp consistency. (Regime boundaries are from experiments; symbols are model predictions.)

5.9 Transportability

The potential benefits promised by the pressure sensor-neural network technique could be realized by fulfilling certain requirements. One necessity is the continued improvements in the development of more robust, more specific, and faster sensors. Another need is that results from one sensor must be transferable to another similar pressure sensor. Before any wide use of a prediction model can be encouraged, its transportability, which is often defined as the capability to produce accurate predictions of data not included in the development of the prediction model, and drawn from a different but plausible related population (Justice et al., 1999), needs to be assessed. This will allow simultaneous accumulation of data on frequency characteristics of flow regime samples from bubble columns of the same scale operated at different sites, and the sharing and distribution of these databases. Without this capability, each bubble column must develop its own database, and can use it only in the particular sensor that generated the data. If there is sensor shift, not even the sensor could be used after some time. Sources addressing this issue are scarce in the literature. Clear methods must be developed to assure seamless transportability of data and information between similar sensors. A possible scenario would be as follows (Balaban et al, 2000):

1. A series of appropriate operating conditions that are easy-to-prepare, easy-to-replicate, relatively stable, and almost spanning over the normal working conditions would be established as standards for the bubble columns of particular type in question, and agreed upon by all the interested parties.
2. One bubble column having a particular sensor, referred to as ‘central bubble column and central sensor’, would be constructed or chosen, in order to prepare

these standards to initiate the central database. The corresponding flow regimes would be studied and a classification model using neural networks would be designed and validated.

3. Each interested party having same type of bubble column with similar sensors would use their own sensor to read these standards to establish 'calibration'. When sensor data needs to be shared by another party having a similar sensor, the 'calibration' data would be sent together with it. The receiving party, having read the same standards using their sensor, would generate a function to convert the incoming data into their sensor, and another function to transform their data into the sensor of the former party.
4. Several interested parties could contribute to the central database in a similar manner. Data in the database would be transferable to any bubble column inclusively, since the transformation functions are known.
5. Periodically, each sensor would read the standards, and adjust its reading for sensor drift. This would allow accumulation of data over time, corrected for temporal changes.
6. The central database would be able to correctly classify unknown samples read by the sensor of any bubble column, make it available to all interested parties.

For ANNs of interest in flow regime classification, where the system scale and the characteristics of the sensor are also important, the transportability concept needs to be extended to not only address a different but plausible population, but the system scale and sensors as well. A transportable ANN-based method should ideally be trained on a reference system using a set of reference sensors, and be able to correctly classify the

flow regimes when applied to a system with a significantly different scale and using somewhat different sensors, but subject to a similar flow field. The signals recorded in the latter (prototypical) system may evidently need to be manipulated before they can be used as input to the trained reference ANN. The development of a method appropriate for this manipulation is a crucial step towards transportability.

5.10 Test of Transportability for Frequency-Domain Parameter-Based ANN

As a first step towards the above goals, the objectives of this study were to evaluate the neural network approach (ANN-1) for its ability to satisfactorily predict flow regimes using transformed data read from another sensor. In our investigation, the data from another bubble column of the same scale were not available. So we studied the transportability of ANN-1 using the preprocessed data from the two sensors located on different axial positions. We are particularly interested in the frequency relevance of the flow conditions, i.e., its ability to support decision-making for flow regimes displaying distinctive power spectrum patterns.

In this effort, using the data obtained with the aforementioned test facility (also described in Xie et al., 2003b), the transportability of an ANN trained for regime classification, between pressure signals from three separate but in principle similar sensors, is addressed. The sensors represent different observation points in flow that is not fully developed, and their signal characteristics are therefore somewhat different in addition to differences in calibration (zero, gain, and linearity) – also minor differences in the physical installation of the sensors can affect their signals. Transportability with respect to multiple similar sensors applied to the same system scale (i.e., no scale-change difference) is considered here. This type of transportability is important since small

differences among similar sensors (caused by sensor drift, for example) are often inevitable. An ANN is developed that uses the power spectral characteristics of the normalized pressure fluctuations as input, and is shown to have good transportability. An ANN-based method is furthermore developed that enhances the transportability of the aforementioned ANNs. While a redundant system with multiple sensors is an obvious target application, such robustness of algorithms that provides transportability will also contribute to performance with a single sensor, shielding against effects of calibration changes or sensor replacements.

Firstly, the transportability of the ANN-1 for the interpretation of the signals recorded by Sensor 2 and Sensor 3 without any manipulation of the ANN and data, was examined. Accordingly, the pressure signals recorded by Sensor 2 and Sensor 3 were normalized and were directly (without any manipulation) used for the calculation of input parameters for ANN-1. The predictions of ANN-1 are compared with the entire experimental data in Figs 5.13(a)-(c) and Figs 5.14(a)-(c) for Sensor 2 and Sensor 3, respectively. The agreement is encouraging, and only about 13% of the data are misclassified, with the misclassified data points all representing conditions close to regime transition.

A similar test was performed using the ANN discussed in Section 5.3. The latter ANN, as mentioned earlier, uses the standard deviation, coefficients of skewness and kurtosis, and several time-shift auto correlations of normalized pressure signals from a sensor as input. The result obtained by directly applying the ANN trained and tested for Sensor 1 to the data recorded by Sensors 2 and 3 (not shown here for brevity) were inferior to those depicted in Figs 5.14 and 5.15, and led to about 16% mismatches. This

particular net was using inputs that were not indifferent to gain and shift of zero point: the standard deviation is proportional to gain.

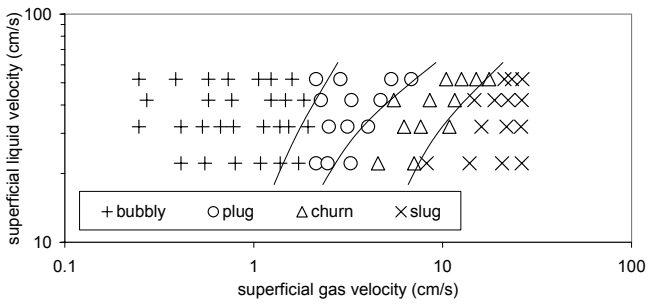

(a)

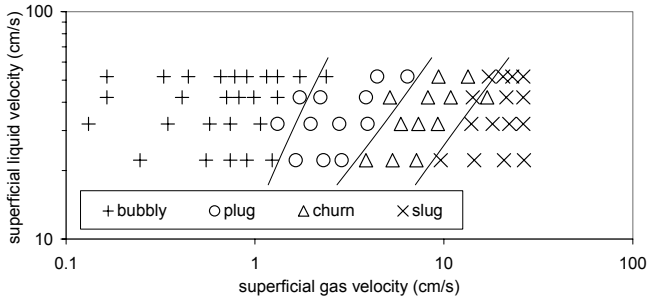

(b)

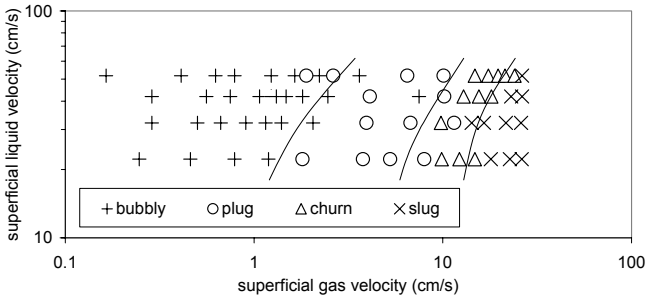

(c)

Figure 5.14: Comparison between the predictions of ANN-1 and the experimental data when pressure signals of Sensor 2 are directly used for the calculation of NN input parameters. (Regime boundaries are from experiments; symbols are model predictions.)

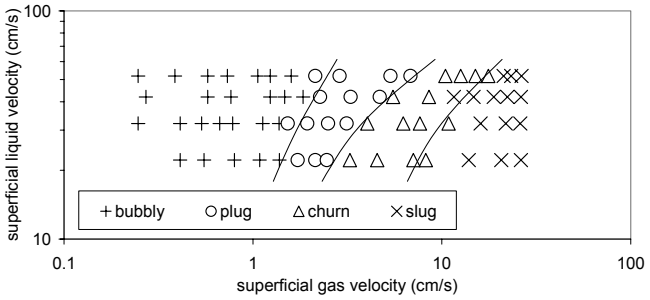

(a)

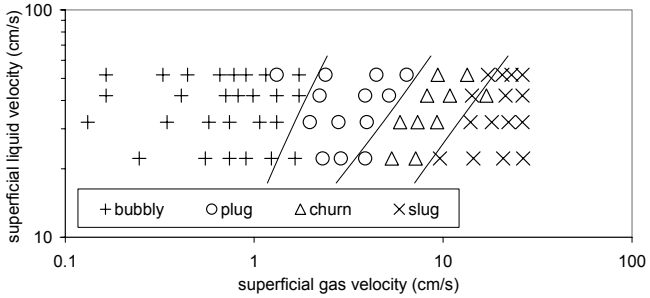

(b)

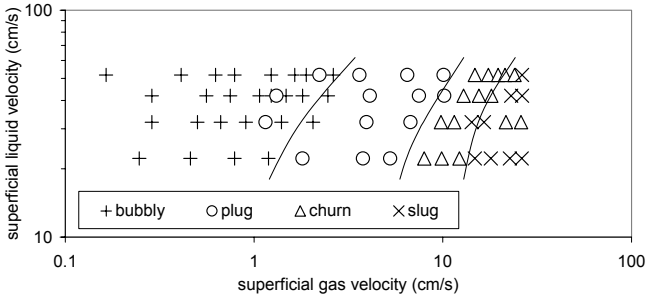

(c)

Figure 5.15: Comparison between the predictions of ANN-1 and the experimental data when pressure signals of Sensor 3 are directly used for the calculation of NN input parameters. (Regime boundaries are from experiments; symbols are model predictions.)

5.11 Improvement of Transportability of the Frequency-Domain Parameter-Based ANN Method

To further improve the transportability of ANN-1 to Sensor 2 and 3, a method similar to the one proposed by Balaban et al. (2000) was attempted. The pressure signals from Sensor 2 and Sensor 3 were normalized and their power spectra were obtained. The three-layer back-propagation ANN depicted in Fig. 5.16 (hereafter referred to as ANN-2) was then developed. ANN-2 was meant to be trained in order to convert all the input parameters needed by ANN-1 that represent either Sensor 2 or Sensor 3, such that they could be correctly interpreted by ANN-1. An ANN similar to ANN-2 was trained for each of Sensor 2 and Sensor 3. For training ANN-2 with respect to Sensor 2, the 7 parameters representing the power spectral density characteristics associated with 152 data points ('calibration data' subset) obtained with Sensor 2 were used as input to ANN-2, while the corresponding parameters obtained with Sensor 1 constituted the outputs. Once trained in this way, ANN-2 was then utilized for the conversion of the 45 unseen Sensor 2 data records, and the output parameters generated by ANN-2 were then used as input for ANN-1. The predictions of ANN-1 for the latter 45 data records are compared with the experimental data in Figs. 5.17(a)-(c). A similar procedure for Sensor 3 led to Figs. 5.18(a)-(c). The results, as noted, are good. The misclassifications are few, and represent relatively minor confusion for data points associated with regime transition zones. It is also worth emphasizing that mismatches associated with $\zeta = 1.5\%$ are more severe, confirming the added complexity of the flow field due to higher consistency.

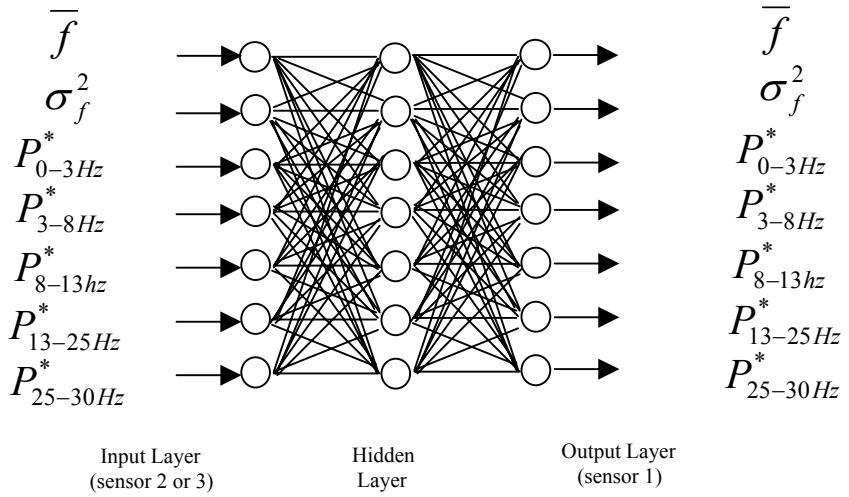

Figure 5.16: Representation of the configuration of ANN-2. For training, input parameters are from either Sensor 2 or Sensor 3, while output parameters are from Sensor 1.

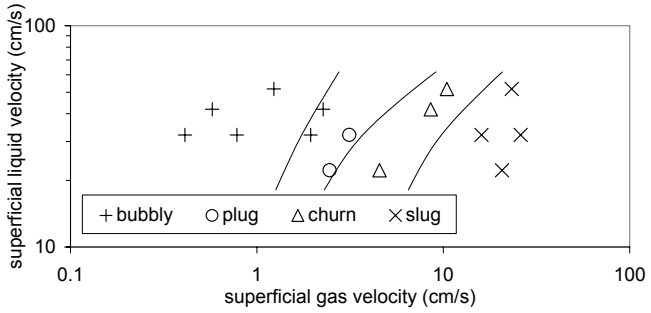

(a)

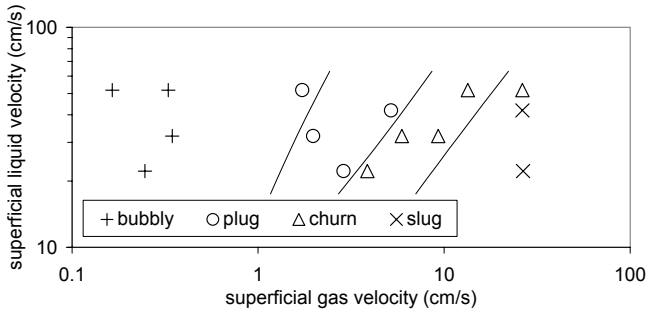

(b)

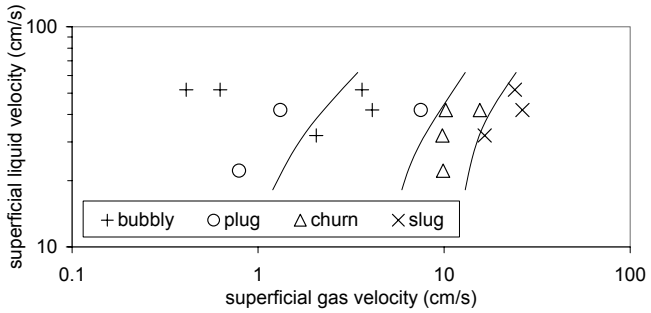

(c)

Figure 5.17: Comparison between the prediction of the ANN and the test subset of data for Sensor 2: (a) 0.5% pulp consistency; (b) 1.0% pulp consistency; (c) 1.5% pulp consistency. (Regime boundaries are from experiments; symbols are model predictions.)

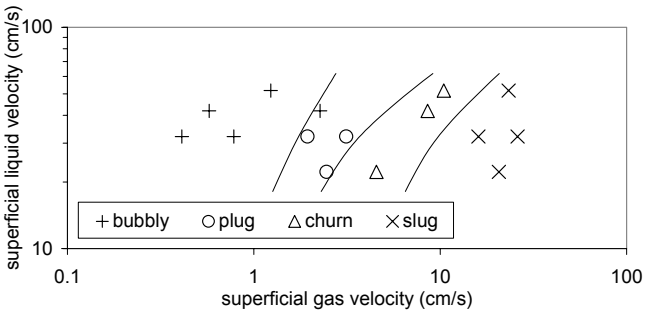

(a)

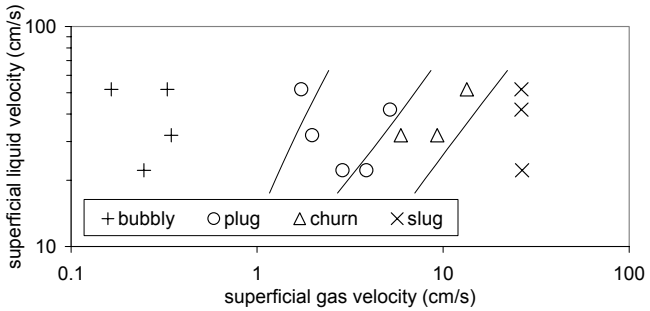

(b)

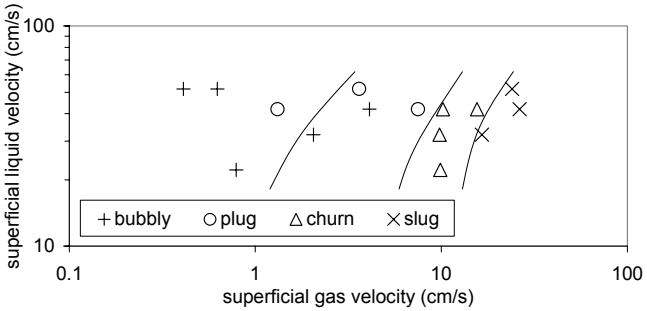

(c)

Figure 5.18: Comparison between the prediction of the ANN and the test subset of data for Sensor 3: (a) 0.5% pulp consistency; (b) 1.0% pulp consistency; (c) 1.5% pulp consistency. (Regime boundaries are from experiments; symbols are model predictions.)

5.12 Conclusion and Recommendation

In this chapter, the feasibility of using ANNs for the identification of major flow regimes in three-phase gas/liquid/pulp fiber systems based on the pressure signals recorded by high-sensitivity pressure sensors was examined. Experimental data were obtained using an instrumented test loop, that included a transparent vertical column (test section) that was 1.8 m long and had an inner diameter of 5.08 cm, with upward through flows of mixed air and aqueous Kraft softwood pulp suspensions. The aqueous pulp suspensions had consistencies of 0.5%, 1.0%, and 1.5%. Flow regimes, including bubbly, plug, churn and slug, were identified visually. Measurements included pressure fluctuations recorded at a sampling rate of 100 Hz by three similar highly sensitive sensors installed near the test section wall at 1.2 m, 1.3 m, and 1.4 m above the test section inlet, respectively. A total of nearly two hundred data records covering bubbly, plug, churn, and slug flow regimes were obtained.

Two supervised, feed-forward ANNs were designed and trained against a subset of the data for flow regime identification using several easily calculated statistical characteristics of the normalized dynamic pressure signals from a single sensor (Sensor 1, the one located at a height of 1.2 m) as input parameters. The designed networks predicted the flow regimes in the remainder of the data points (the test subset of the data) very well. It was concluded that an ANN-aided flow regime classifier based on a single pressure sensor may be feasible for industrial systems. Experimental verification in industrial systems, which are typically much larger than the test section used in this study, was recommended.

Furthermore, the feasibility of using a transportable artificial neural network-based technique for the identification of flow regimes in a gas/liquid/pulp fiber three-phase flow system was examined. A three-layer, feed-forward ANN was designed that used seven input parameters all representing the characteristics of the spectral power density distributions of normalized pressure fluctuations associated with a single pressure sensor (Sensor 1), and was shown to perform well. A voting scheme, whereby ANNs trained for the three sensors (Sensor 1, Sensor 2, and Sensor 3) would be used for regime identification for an unseen data set based on the majority vote, resulted in an improvement in the accuracy of the predictions. The ANN that had been trained based on signals recorded by one of the sensors (Sensor 1), furthermore, was directly applied to the signals recorded by the other two sensors, and was shown to predict the flow regimes reasonably well. An ANN-based method was then developed for the conversion of the spectral power density characteristics of one sensor such that they approximated similar characteristics obtained with another sensor, to enable the use of a classification algorithm created for the latter sensor. The results were good, and confirmed the suitability of the proposed method for improving transportability.

The results of this investigation indicate that the developed ANN-based regime classification method that uses the normalized pressure power spectral density characteristics is reasonably transportable when high-sensitivity sensors are used on analogous systems of the same size scale. Transportability with respect to sensors that are significantly different, and with respect to systems with different size scales remains to be resolved, however, and further investigations are recommended.

CHAPTER 6

CONCLUSIONS AND RECOMMENDATIONS

6.1 Concluding Remarks

Gas-liquid-fiber three-phase flows are common in a number of applications of paper production and recycling, including delignification and bleaching. These flows constitute one of the most complicated and least-understood areas of fluid mechanics. The main cause of complexity of pulp slurry hydrodynamics is flocculation (entanglement of fiber groups to conformations that possess mechanical strength) that leads to the formation of flocs that resist shear, block the passage gas bubbles through the networks, and complicate the mixture hydrodynamics. No reliable analytical or empirical predictive methods are available to classify complex flow patterns observed in these systems, despite relatively extensive experimental investigations in the past. The objectives of this study were to perform an experimental investigation of the hydrodynamics characteristics of gas-liquid-fiber three-phase flows, and to develop objective techniques for the classification of these characteristics.

In the experiments, all of which were conducted in a transparent vertical column 5.08 cm in inner diameter and 1.8 m tall, with upward through flows of mixed air and aqueous Kraft softwood pulp suspensions, various flow regimes and void fractions were identified and measured using visual observation and gamma-ray densitometer. The transitions of flow regimes were observed and recorded by controlling superficial gas velocity ($0 \le \overline{U_{GS}} \le 26$ cm/s) and superficial liquid velocity ($21 \le \overline{U_{LS}} \le 51$ cm/s). Water

constituted the liquid phase, air was the gas phase, and pulp fiber was the solid phase. The aqueous pulp suspensions had consistencies of 0.5%, 1.0%, and 1.5%.

Six distinct flow regimes were identified, including dispersed bubbly, layered bubbly, incipient plug, plug, churn-turbulent, and slug. Bubbly flow occurred only at very low liquid-pulp slurry superficial velocities. The flow regime transition lines were sensitive to pulp consistency. Empirical flow regime maps were then developed in terms of superficial gas velocity and superficial liquid velocity.

Cross section-average gas holdups (void fractions) agreed with the predictions of the homogeneous flow model for bubbly and layered bubbly regimes. The void fraction data could be correlated using the Drift Flux Model (DFM) for other regimes, when plug and churn-turbulent regimes were treated together and slug flow was treated separately. The results showed that the drift flux parameters were functions of pulp consistency.

The aforementioned test facility was subsequently modified, and instrumented by a single high-sensitivity dynamic pressure transducer installed at a particular location on the test section wall (1.2 m above the test section inlet). Local pressure fluctuation signals were recorded at the rate of 100 Hz, and then utilized for the development of artificial neural network (ANN)-based methods for flow regime identification. Although ANN-assisted methods have been attempted for gas-liquid two-phase flow in the past, no such attempt has been reported for liquid/gas/fiber three-phase flows. A total of two hundred data records covering bubbly, plug, churn, and slug flow regimes were collected.

Two different supervised, feed-forward ANNs were designed and trained against a subset of the data for flow regime identification using several easily-calculable statistical characteristics of the normalized dynamic pressure signals as input parameters:

the standard deviation, coefficients of skewness and kurtosis, and several time shift autocorrelations of normalized pressure signals. The designed networks predicted the flow regimes in the remainder of the data points (the test subset of the data) very well. It was concluded that an ANN-aided flow regime classifier based on a single pressure sensor may be feasible for industrial systems.

To study the transportability of artificial neural network (ANN)-based techniques for the identification of flow regimes in the aforementioned flow system, more experiments were performed including simultaneously measuring pressure fluctuations with three similar dynamic pressure sensors mounted at 1.2 m, 1.3m, and 1.4 m above the test section inlet, respectively. A three-layer, feed-forward ANN was designed that used seven input parameters all representing the characteristics of the spectral power density distributions of normalized pressure fluctuations associated with a single pressure sensor, and was shown to perform well. Besides, a voting scheme, whereby ANNs trained for the three sensors would be used for regime identification for an unseen data set based on the majority vote, resulted in an improvement in the accuracy of the predictions. The ANN that had been trained based on signals recorded by one of the sensors (Sensor 1), furthermore, was directly applied to the signals recorded by the other two sensors, and was shown to predict the flow regimes reasonably well. An ANN-based method was then developed for the conversion of the spectral power density characteristics of one sensor such that they approximated similar characteristics obtained with another sensor, to enable the use of a classification algorithm created for the latter sensor. The results were good, and confirmed the suitability of the proposed method for improving

transportability. Overall, these ANNs were superior to the aforementioned ANNs that used statistical characteristics of the normalized pressure fluctuations.

The results of this investigation indicate that the developed ANN-based regime classification method that uses the normalized pressure power spectral density characteristics is reasonably transportable when high-sensitivity sensors are used on analogous systems of the same size scale. We thus conclude that ANNs using the characteristics of the power spectral density distribution of pressure fluctuations are very promising for future applications in prototypical systems.

Another focus of this thesis was to explore the applicability of hybrid, ANN-FPM methodology to complex boiling and two-phase flow phenomena (see Appendix III). In this method the conservation equations are solved using primarily first principles with minimal assumptions introduced in the development and closure of these conservation equations. The complex and poorly understood closure relations, in particular the rate-controlling transport processes, which are typically poorly understood non-linear functions of local state variables, are represented by trained neural networks.

The methodology was first applied to a small set of experimental critical heat flux data previously obtained in a heated horizontal, thin annular test section cooled with water, with good results. Next, another hybrid artificial neural network-first principle model (ANN-FPM) was developed for the prediction of dryout heat flux in microchannels cooled with water. The dryout data associated with water flow in circular microchannels (with diameters of around or slightly larger than 1 mm) in the PU-BTPFL CHF database (Hall and Mudawar, 1998) were used for model development and comparison. A simple slip-flow model was used to predict the thermal and hydrodynamic

parameters for the annular flow regime, which were used as input parameters for a three-layer, feed-forward, back-propagation neural network. The output of the neural network was the boiling number at dryout. The developed ANN-FPM was shown to predict the data quite well.

6.2 Recommendations

Further investigations with respect to the application of artificial neural network techniques to flow regime identification and the application of hybrid ANN-FPM to boiling heat transfer are recommended as follows:

1. Multiphase flow phenomena, including two and three-phase flow regimes and their transition conditions, are known to be generally sensitive to system scale. The flow regimes and flow regime transition maps obtained in this study should therefore be applied to much larger prototypical systems with caution. Flow regime and gas holdup tests, and other hydrodynamics measurements, in larger and prototypical systems are therefore recommended.
2. This study indicated that an ANN-aided flow regime classifier based on a single pressure sensor may be feasible for industrial systems. However, experimental verification in industrial systems, which are typically much larger than the test section used in this study, will be important and necessary. Transportability with respect to multiple similar sensors applied to the same system scale was also considered in this study. Transportability with respect to sensors that are significantly different, and transportability with respect to systems with different

size scales remains to be resolved, however, and further investigations are recommended.

3. This study addressed the application of ANN-FPM to dryout critical heat transfer and its performance. Extending and testing ANN-FPM to other important types of CHF, in particular departure from nucleate boiling, in micro/mini channels is recommended.

APPENDIX I

VOID FRACTION DATA

Table I-1: Void fraction data for 0.5% pulp consistency

				Void Fraction					
#	Superficial liquid velocity (cm/s)	Superficial gas velocity (cm/s)	Flow regime	left 2cm	left 1cm	center	right 1cm	right 2cm	Cord-Average
1	22.38	0.18	B3	0.004	0.003	0.004	0.002	-0.003	0.002
2	22.31	0.50	P	-0.003	0.010	0.016	0.015	0.002	0.010
3	22.87	0.73	P	-0.008	0.014	0.025	0.023	0.009	0.015
4	22.84	0.97	P	-0.004	0.023	0.037	0.035	0.017	0.024
5	23.34	1.83	C	-0.012	0.036	0.068	0.066	0.032	0.043
6	22.22	3.73	C	0.006	0.097	0.123	0.121	0.083	0.093
7	22.61	5.99	C	0.009	0.111	0.163	0.155	0.094	0.116
8	23.40	8.86	S	0.028	0.154	0.201	0.195	0.125	0.151
9	22.77	16.23	S	0.070	0.239	0.307	0.302	0.210	0.240
10	23.22	22.85	S	0.095	0.302	0.358	0.353	0.267	0.291
11	32.55	0.27	B2	0.001	0.000	0.004	0.002	0.001	0.002
12	32.22	0.49	B2	0.001	0.004	0.011	0.012	0.009	0.008
13	32.39	0.55	B3	-0.003	0.003	0.008	0.012	0.002	0.005
14	32.32	0.68	B3	-0.009	0.005	0.015	0.019	0.007	0.009
15	32.52	0.82	B3	-0.008	0.008	0.020	0.020	0.008	0.011
16	32.79	1.19	P	-0.011	0.017	0.033	0.036	0.022	0.022
17	32.79	1.92	P	-0.005	0.036	0.059	0.059	0.031	0.040
18	33.07	2.65	P	0.003	0.057	0.086	0.084	0.048	0.061
19	32.26	3.60	C	0.009	0.070	0.113	0.106	0.063	0.078
20	32.49	5.90	C	-0.025	0.085	0.125	0.119	0.057	0.082
21	32.83	8.57	C	-0.011	0.125	0.168	0.160	0.092	0.118
22	32.93	11.33	S	0.013	0.169	0.216	0.209	0.126	0.159
23	32.92	18.10	S	0.012	0.216	0.282	0.269	0.164	0.205
24	32.05	23.59	S	0.032	0.243	0.318	0.312	0.209	0.240
25	42.07	0.11	B1	0.004	0.001	0.005	0.005	0.005	0.004
26	42.07	0.27	B2	0.008	0.009	0.006	0.006	0.007	0.007
27	41.87	0.52	B2	0.006	0.005	0.011	0.011	0.012	0.009
28	42.41	0.83	B3	0.006	0.012	0.018	0.020	0.022	0.016
29	42.17	1.04	B3	0.009	0.019	0.026	0.031	0.027	0.023
30	42.44	1.21	B3	0.009	0.022	0.034	0.037	0.032	0.028
31	42.35	1.79	P	-0.011	0.012	0.040	0.043	0.030	0.025
32	40.97	3.10	P	-0.005	0.042	0.069	0.074	0.045	0.049
33	41.14	4.27	P	-0.002	0.056	0.099	0.094	0.053	0.066
34	42.11	5.17	C	0.006	0.069	0.111	0.107	0.058	0.077
35	41.90	8.31	C	0.015	0.110	0.150	0.142	0.089	0.110
36	42.00	11.86	C	0.023	0.147	0.201	0.194	0.117	0.148
37	41.01	14.41	S	0.035	0.178	0.232	0.224	0.140	0.174
38	41.66	19.15	S	0.050	0.214	0.285	0.271	0.175	0.214

39	41.01	24.07	S	0.059	0.251	0.311	0.298	0.203	0.240
40	53.85	0.22	B1	0.007	0.002	0.005	0.004	0.003	0.004
41	51.90	0.34	B1	0.010	0.005	0.005	0.007	0.009	0.007
42	51.64	0.61	B2	0.009	0.004	0.005	0.005	0.005	0.006
43	51.44	0.85	B2	0.001	0.006	0.007	0.012	0.012	0.008
44	51.25	1.11	B3	0.005	0.005	0.014	0.019	0.017	0.012
45	51.07	1.37	B3	0.004	0.012	0.023	0.031	0.025	0.020
46	51.29	1.54	B3	0.005	0.014	0.025	0.033	0.028	0.022
47	51.55	2.59	P	0.004	0.029	0.049	0.063	0.047	0.040
48	51.50	4.99	P	-0.004	0.039	0.085	0.094	0.056	0.059
49	51.38	7.23	P	-0.004	0.062	0.111	0.114	0.064	0.076
50	51.60	10.97	C	0.022	0.116	0.168	0.164	0.105	0.124
51	52.83	12.59	C	0.026	0.123	0.182	0.176	0.109	0.133
52	50.89	14.66	C	0.030	0.151	0.206	0.203	0.128	0.154
53	51.62	17.73	S	0.045	0.174	0.235	0.223	0.150	0.177
54	50.98	21.04	S	0.062	0.195	0.264	0.257	0.173	0.203
55	51.15	24.72	S	0.063	0.214	0.288	0.277	0.189	0.220

Table I-2: Void fraction data for 1.0% pulp consistency

				Void Fraction					
#	Superficial liquid velocity (cm/s)	Superficial gas velocity (cm/s)	Flow regime	left 2cm	left 1cm	center	right 1cm	right 2cm	Cord-Average
1	22.14	0.49	B2	0.011	0.031	0.014	0.002	-0.010	0.011
2	23.11	0.69	B2	0.017	0.040	0.022	0.012	0.003	0.020
3	22.24	0.96	B3	0.029	0.049	0.032	0.021	0.016	0.031
4	22.03	1.12	B3	0.027	0.054	0.038	0.028	0.010	0.034
5	23.30	1.43	P	0.033	0.060	0.052	0.040	0.031	0.045
6	22.60	2.00	P	0.038	0.073	0.067	0.050	0.036	0.055
7	22.15	2.48	P	0.040	0.078	0.086	0.081	0.061	0.072
8	23.05	3.76	C	0.057	0.112	0.130	0.120	0.086	0.106
9	22.94	4.97	C	0.074	0.122	0.151	0.151	0.103	0.126
10	22.83	7.21	C	0.106	0.168	0.186	0.181	0.137	0.161
11	23.24	10.37	S	0.122	0.213	0.252	0.239	0.181	0.210
12	23.26	15.48	S	0.160	0.247	0.303	0.303	0.251	0.261
13	23.59	19.23	S	0.161	0.308	0.347	0.337	0.285	0.299
14	22.13	23.56	S	0.201	0.322	0.387	0.376	0.354	0.336
15	32.98	0.51	B1	-0.005	0.036	0.027	0.003	-0.010	0.013
16	32.68	0.81	B2	0.024	0.042	0.033	0.014	0.001	0.025
17	31.91	1.06	B2	0.052	0.050	0.038	0.018	0.011	0.034
18	31.73	1.20	B3	0.033	0.053	0.044	0.026	0.021	0.037
19	31.52	1.36	B3	0.021	0.051	0.043	0.025	0.009	0.032
20	32.22	1.76	P	0.023	0.062	0.058	0.039	0.024	0.044
21	31.61	2.70	P	0.036	0.084	0.087	0.068	0.043	0.068
22	30.87	3.80	P	0.047	0.108	0.120	0.104	0.060	0.093
23	31.67	5.81	C	0.075	0.127	0.147	0.140	0.090	0.121
24	31.96	8.34	C	0.086	0.149	0.201	0.176	0.135	0.156
25	32.30	11.24	C	0.114	0.202	0.251	0.230	0.172	0.203

26	32.02	14.81	S	0.144	0.237	0.279	0.270	0.231	0.240
27	31.65	18.01	S	0.157	0.279	0.321	0.303	0.250	0.272
28	31.33	20.86	S	0.157	0.295	0.344	0.344	0.268	0.293
29	30.94	24.13	S	0.162	0.295	0.374	0.348	0.293	0.306
30	42.34	0.09	B1	-0.011	0.022	0.013	-0.002	-0.026	0.002
31	42.00	0.26	B1	-0.004	0.029	0.016	0.003	-0.020	0.007
32	40.80	0.42	B1	0.004	0.035	0.022	0.005	-0.015	0.013
33	42.03	0.64	B2	0.011	0.036	0.024	0.007	-0.008	0.016
34	41.61	0.89	B2	0.020	0.044	0.035	0.019	0.001	0.026
35	43.66	1.16	B2	0.021	0.050	0.035	0.021	0.009	0.029
36	41.86	1.64	B2	0.023	0.055	0.042	0.032	0.013	0.035
37	41.42	2.23	P	0.029	0.066	0.060	0.046	0.030	0.049
38	41.20	3.90	P	0.045	0.085	0.100	0.087	0.058	0.079
39	42.07	6.13	P	0.066	0.115	0.130	0.121	0.087	0.108
40	41.05	9.10	C	0.079	0.153	0.178	0.179	0.131	0.150
41	41.84	13.43	C	0.123	0.211	0.249	0.228	0.182	0.206
42	41.95	16.75	C	0.129	0.227	0.268	0.271	0.218	0.231
43	41.34	19.54	S	0.142	0.254	0.319	0.310	0.261	0.267
44	42.54	22.50	S	0.196	0.274	0.329	0.332	0.276	0.289
45	42.77	25.61	S	0.155	0.286	0.354	0.345	0.295	0.298
46	52.15	0.55	B1	0.009	0.041	0.020	0.005	-0.020	0.014
47	52.17	0.74	B1	0.015	0.045	0.025	0.008	-0.017	0.018
48	52.15	0.90	B1	0.017	0.042	0.027	0.013	-0.014	0.019
49	51.78	1.15	B2	0.015	0.046	0.026	0.013	-0.013	0.020
50	53.03	1.44	B2	0.026	0.052	0.033	0.022	0.002	0.029
51	52.79	1.62	B2	0.024	0.056	0.039	0.029	0.011	0.034
52	52.56	1.91	B2	0.022	0.061	0.048	0.037	0.019	0.040
53	51.75	2.95	P	0.024	0.066	0.066	0.054	0.024	0.051
54	50.71	5.64	P	0.044	0.104	0.109	0.108	0.069	0.092
55	51.01	8.49	P	0.053	0.123	0.143	0.133	0.097	0.116
56	51.10	11.76	C	0.079	0.156	0.186	0.183	0.134	0.154
57	51.49	14.71	C	0.097	0.188	0.222	0.216	0.149	0.183
58	50.81	17.56	C	0.101	0.238	0.242	0.231	0.178	0.208
59	51.84	20.20	S	0.115	0.238	0.274	0.270	0.211	0.231
60	51.60	22.63	S	0.129	0.247	0.299	0.298	0.218	0.249
61	51.01	25.83	S	0.131	0.256	0.319	0.313	0.254	0.265

Table I-3: Void fraction data for 1.5% pulp consistency

				Void Fraction					
#	Superficial liquid velocity (cm/s)	Superficial gas velocity (cm/s)	Flow regime	left 2cm	left 1cm	center	right 1cm	right 2cm	Cord-Average
1	22.31	0.52	B2	0.013	0.007	0.010	0.012	0.029	0.013
2	22.65	0.79	B2	0.017	0.012	0.016	0.025	0.044	0.021
3	22.38	1.03	B3	0.023	0.016	0.021	0.029	0.043	0.026
4	23.37	1.44	P	0.037	0.028	0.032	0.040	0.052	0.037
5	22.86	3.14	P	0.060	0.083	0.090	0.097	0.091	0.086
6	22.41	4.89	P	0.090	0.111	0.130	0.130	0.103	0.115

7	22.61	6.44	C	0.098	0.135	0.160	0.157	0.134	0.140
8	23.26	8.06	C	0.121	0.150	0.181	0.176	0.162	0.161
9	22.90	9.38	C	0.160	0.187	0.208	0.206	0.170	0.190
10	22.92	12.16	S	0.169	0.232	0.261	0.253	0.208	0.231
11	22.92	17.65	S	0.183	0.272	0.321	0.307	0.249	0.275
12	23.03	23.24	S	0.217	0.318	0.380	0.366	0.307	0.327
13	33.90	0.50	B1	0.004	0.012	0.015	0.016	0.007	0.012
14	34.49	0.78	B2	0.027	0.013	0.020	0.021	0.016	0.019
15	32.09	0.98	B2	0.021	0.016	0.020	0.025	0.026	0.021
16	32.19	1.19	B2	0.041	0.026	0.025	0.034	0.026	0.030
17	31.33	1.75	P	0.048	0.041	0.040	0.053	0.045	0.045
18	30.49	4.02	P	0.077	0.090	0.101	0.098	0.091	0.093
19	33.86	5.95	P	0.114	0.102	0.129	0.131	0.116	0.119
20	31.79	7.67	C	0.107	0.135	0.156	0.153	0.118	0.137
21	31.98	9.36	C	0.129	0.155	0.183	0.180	0.145	0.162
22	32.29	11.39	C	0.141	0.181	0.221	0.216	0.182	0.193
23	33.36	14.32	S	0.173	0.224	0.260	0.259	0.177	0.226
24	32.40	19.26	S	0.179	0.268	0.306	0.302	0.256	0.270
25	34.74	23.76	S	0.197	0.303	0.353	0.331	0.252	0.298
26	39.59	0.44	B1	0.025	0.011	0.011	0.017	0.018	0.015
27	42.15	0.71	B1	0.022	0.010	0.011	0.011	0.016	0.013
28	42.72	0.89	B2	0.025	0.012	0.018	0.020	0.026	0.019
29	43.30	1.19	B2	0.031	0.015	0.019	0.025	0.034	0.023
30	43.10	1.34	B2	0.036	0.023	0.028	0.032	0.043	0.031
31	43.37	1.49	B2	0.046	0.026	0.025	0.034	0.043	0.033
32	41.83	2.24	P	0.051	0.034	0.034	0.040	0.052	0.041
33	40.21	4.21	P	0.072	0.078	0.081	0.087	0.087	0.081
34	41.18	6.70	P	0.102	0.112	0.123	0.126	0.118	0.117
35	40.84	9.87	C	0.128	0.147	0.166	0.171	0.141	0.153
36	43.72	12.45	C	0.119	0.166	0.200	0.188	0.166	0.172
37	44.54	14.39	C	0.171	0.201	0.232	0.215	0.178	0.204
38	43.52	16.97	S	0.180	0.219	0.255	0.254	0.204	0.228
39	42.43	20.77	S	0.207	0.236	0.301	0.285	0.250	0.261
40	41.76	24.02	S	0.195	0.275	0.327	0.309	0.261	0.281
41	49.76	0.56	B1	0.018	0.019	0.013	0.008	0.006	0.013
42	53.91	0.69	B1	0.027	0.019	0.019	0.015	0.013	0.018
43	50.33	0.93	B1	0.045	0.031	0.031	0.022	0.018	0.029
44	52.16	1.14	B2	0.041	0.032	0.031	0.023	0.028	0.031
45	53.00	1.39	B2	0.057	0.033	0.032	0.028	0.033	0.035
46	48.53	1.64	B2	0.053	0.035	0.037	0.032	0.049	0.040
47	52.77	1.89	B2	0.062	0.043	0.040	0.036	0.045	0.044
48	52.93	3.20	P	0.067	0.058	0.057	0.062	0.066	0.061
49	50.58	6.59	P	0.090	0.106	0.115	0.109	0.099	0.105
50	52.50	9.40	P	0.114	0.140	0.151	0.148	0.125	0.138
51	52.47	11.68	C	0.145	0.155	0.184	0.179	0.150	0.165
52	53.83	15.56	C	0.145	0.198	0.229	0.211	0.167	0.196
53	51.85	18.39	C	0.161	0.224	0.254	0.265	0.206	0.228
54	50.84	20.44	S	0.180	0.227	0.280	0.271	0.211	0.240
55	52.51	22.86	S	0.184	0.267	0.300	0.278	0.224	0.259
56	52.49	25.53	S	0.185	0.270	0.309	0.299	0.234	0.268

APPENDIX II

ANN DATA FOR FLOW REGIME IDENTIFICAION

Table II-1: ANN data from pressure fluctuation measurements

Sample	Consistency	U_{LS} (cm/s)	U_{GS} (cm/s)	Bubbly	Plug	Churn	Slug
1	0.5%	22.20	0.41	1	0	0	0
2	0.5%	22.20	0.55	1	0	0	0
3	0.5%	22.20	0.80	1	0	0	0
4	0.5%	22.20	1.09	1	0	0	0
5	0.5%	22.20	1.38	1	0	0	0
6	0.5%	22.20	1.73	0	1	0	0
7	0.5%	22.20	2.14	0	1	0	0
8	0.5%	22.20	2.46	0	1	0	0
9	0.5%	22.20	3.26	0	0	1	0
10	0.5%	22.20	4.55	0	0	1	0
11	0.5%	22.20	7.07	0	0	1	0
12	0.5%	22.20	8.22	0	0	0	1
13	0.5%	22.20	13.90	0	0	0	1
14	0.5%	22.20	20.64	0	0	0	1
15	0.5%	22.20	26.19	0	0	0	1
16	0.5%	32.07	0.25	1	0	0	0
17	0.5%	32.07	0.41	1	0	0	0
18	0.5%	32.07	0.53	1	0	0	0
19	0.5%	32.07	0.67	1	0	0	0
20	0.5%	32.07	0.78	1	0	0	0
21	0.5%	32.07	1.13	1	0	0	0
22	0.5%	32.07	1.37	1	0	0	0
23	0.5%	32.07	1.53	1	0	0	0
24	0.5%	32.07	1.94	0	1	0	0
25	0.5%	32.07	2.50	0	1	0	0
26	0.5%	32.07	3.13	0	1	0	0
27	0.5%	32.07	4.03	0	0	1	0
28	0.5%	32.07	6.25	0	0	1	0
29	0.5%	32.07	7.65	0	0	1	0
30	0.5%	32.07	10.85	0	0	0	1
31	0.5%	32.07	16.03	0	0	0	1
32	0.5%	32.07	21.79	0	0	0	1
33	0.5%	32.07	25.98	0	0	0	1
34	0.5%	41.94	0.10	1	0	0	0
35	0.5%	41.94	0.27	1	0	0	0
36	0.5%	41.94	0.58	1	0	0	0
37	0.5%	41.94	0.76	1	0	0	0
38	0.5%	41.94	1.23	1	0	0	0

39	0.5%	41.94	1.47	1	0	0	0
40	0.5%	41.94	1.84	1	0	0	0
41	0.5%	41.94	2.27	0	1	0	0
42	0.5%	41.94	3.29	0	1	0	0
43	0.5%	41.94	4.69	0	1	0	0
44	0.5%	41.94	5.51	0	0	1	0
45	0.5%	41.94	8.55	0	0	1	0
46	0.5%	41.94	11.59	0	0	1	0
47	0.5%	41.94	14.72	0	0	0	1
48	0.5%	41.94	18.83	0	0	0	1
49	0.5%	41.94	22.20	0	0	0	1
50	0.5%	41.94	26.23	0	0	0	1
51	0.5%	51.80	0.25	1	0	0	0
52	0.5%	51.80	0.39	1	0	0	0
53	0.5%	51.80	0.58	1	0	0	0
54	0.5%	51.80	0.73	1	0	0	0
55	0.5%	51.80	1.06	1	0	0	0
56	0.5%	51.80	1.23	1	0	0	0
57	0.5%	51.80	1.60	1	0	0	0
58	0.5%	51.80	2.14	1	0	0	0
59	0.5%	51.80	2.88	0	1	0	0
60	0.5%	51.80	5.34	0	1	0	0
61	0.5%	51.80	6.83	0	1	0	0
62	0.5%	51.80	10.44	0	0	1	0
63	0.5%	51.80	12.58	0	0	1	0
64	0.5%	51.80	15.05	0	0	1	0
65	0.5%	51.80	17.60	0	0	0	1
66	0.5%	51.80	21.22	0	0	0	1
67	0.5%	51.80	23.27	0	0	0	1
68	0.5%	51.80	26.40	0	0	0	1
69	1.0%	22.20	0.25	1	0	0	0
70	1.0%	22.20	0.55	1	0	0	0
71	1.0%	22.20	0.74	1	0	0	0
72	1.0%	22.20	0.90	1	0	0	0
73	1.0%	22.20	1.23	1	0	0	0
74	1.0%	22.20	1.64	0	1	0	0
75	1.0%	22.20	2.30	0	1	0	0
76	1.0%	22.20	2.88	0	1	0	0
77	1.0%	22.20	3.86	0	0	1	0
78	1.0%	22.20	5.34	0	0	1	0
79	1.0%	22.20	7.15	0	0	1	0
80	1.0%	22.20	9.62	0	0	0	1
81	1.0%	22.20	14.47	0	0	0	1
82	1.0%	22.20	20.80	0	0	0	1
83	1.0%	22.20	26.56	0	0	0	1
84	1.0%	32.07	0.13	1	0	0	0
85	1.0%	32.07	0.35	1	0	0	0
86	1.0%	32.07	0.58	1	0	0	0
87	1.0%	32.07	0.74	1	0	0	0

88	1.0%	32.07	1.07	1	0	0	0
89	1.0%	32.07	1.32	1	0	0	0
90	1.0%	32.07	1.97	0	1	0	0
91	1.0%	32.07	2.80	0	1	0	0
92	1.0%	32.07	3.95	0	1	0	0
93	1.0%	32.07	5.92	0	0	1	0
94	1.0%	32.07	7.32	0	0	1	0
95	1.0%	32.07	9.29	0	0	1	0
96	1.0%	32.07	13.98	0	0	0	1
97	1.0%	32.07	18.09	0	0	0	1
98	1.0%	32.07	22.20	0	0	0	1
99	1.0%	32.07	26.31	0	0	0	1
100	1.0%	41.94	0.16	1	0	0	0
101	1.0%	41.94	0.41	1	0	0	0
102	1.0%	41.94	0.71	1	0	0	0
103	1.0%	41.94	0.82	1	0	0	0
104	1.0%	41.94	0.99	1	0	0	0
105	1.0%	41.94	1.32	1	0	0	0
106	1.0%	41.94	1.73	1	0	0	0
107	1.0%	41.94	2.22	0	1	0	0
108	1.0%	41.94	3.86	0	1	0	0
109	1.0%	41.94	5.18	0	1	0	0
110	1.0%	41.94	8.22	0	0	1	0
111	1.0%	41.94	10.85	0	0	1	0
112	1.0%	41.94	14.23	0	0	1	0
113	1.0%	41.94	16.94	0	0	0	1
114	1.0%	41.94	21.38	0	0	0	1
115	1.0%	41.94	26.31	0	0	0	1
116	1.0%	51.80	0.16	1	0	0	0
117	1.0%	51.80	0.33	1	0	0	0
118	1.0%	51.80	0.44	1	0	0	0
119	1.0%	51.80	0.66	1	0	0	0
120	1.0%	51.80	0.78	1	0	0	0
121	1.0%	51.80	0.90	1	0	0	0
122	1.0%	51.80	1.15	1	0	0	0
123	1.0%	51.80	1.32	1	0	0	0
124	1.0%	51.80	1.73	1	0	0	0
125	1.0%	51.80	2.38	0	1	0	0
126	1.0%	51.80	4.44	0	1	0	0
127	1.0%	51.80	6.41	0	1	0	0
128	1.0%	51.80	9.37	0	0	1	0
129	1.0%	51.80	13.40	0	0	1	0
130	1.0%	51.80	17.27	0	0	1	0
131	1.0%	51.80	20.56	0	0	0	1
132	1.0%	51.80	23.02	0	0	0	1
133	1.0%	51.80	26.31	0	0	0	1
134	1.5%	22.20	0.25	1	0	0	0
135	1.5%	22.20	0.46	1	0	0	0
136	1.5%	22.20	0.79	1	0	0	0

137	1.5%	22.20	1.19	1	0	0	0
138	1.5%	22.20	1.81	0	1	0	0
139	1.5%	22.20	3.78	0	1	0	0
140	1.5%	22.20	5.26	0	1	0	0
141	1.5%	22.20	7.98	0	0	1	0
142	1.5%	22.20	9.87	0	0	1	0
143	1.5%	22.20	12.25	0	0	1	0
144	1.5%	22.20	14.80	0	0	0	1
145	1.5%	22.20	18.01	0	0	0	1
146	1.5%	22.20	22.70	0	0	0	1
147	1.5%	22.20	26.23	0	0	0	1
148	1.5%	32.07	0.29	1	0	0	0
149	1.5%	32.07	0.50	1	0	0	0
150	1.5%	32.07	0.67	1	0	0	0
151	1.5%	32.07	0.90	1	0	0	0
152	1.5%	32.07	1.15	1	0	0	0
153	1.5%	32.07	1.40	1	0	0	0
154	1.5%	32.07	2.06	0	1	0	0
155	1.5%	32.07	3.95	0	1	0	0
156	1.5%	32.07	6.74	0	1	0	0
157	1.5%	32.07	9.79	0	0	1	0
158	1.5%	32.07	11.51	0	0	1	0
159	1.5%	32.07	14.23	0	0	1	0
160	1.5%	32.07	16.53	0	0	0	1
161	1.5%	32.07	21.63	0	0	0	1
162	1.5%	32.07	25.98	0	0	0	1
163	1.5%	41.94	0.29	1	0	0	0
164	1.5%	41.94	0.56	1	0	0	0
165	1.5%	41.94	0.75	1	0	0	0
166	1.5%	41.94	1.07	1	0	0	0
167	1.5%	41.94	1.23	1	0	0	0
168	1.5%	41.94	1.32	1	0	0	0
169	1.5%	41.94	1.48	1	0	0	0
170	1.5%	41.94	1.81	1	0	0	0
171	1.5%	41.94	2.47	0	1	0	0
172	1.5%	41.94	4.11	0	1	0	0
173	1.5%	41.94	7.48	0	1	0	0
174	1.5%	41.94	10.20	0	0	1	0
175	1.5%	41.94	12.91	0	0	1	0
176	1.5%	41.94	15.54	0	0	1	0
177	1.5%	41.94	18.09	0	0	0	1
178	1.5%	41.94	23.02	0	0	0	1
179	1.5%	41.94	26.31	0	0	0	1
180	1.5%	51.80	0.16	1	0	0	0
181	1.5%	51.80	0.41	1	0	0	0
182	1.5%	51.80	0.62	1	0	0	0
183	1.5%	51.80	0.79	1	0	0	0
184	1.5%	51.80	1.23	1	0	0	0
185	1.5%	51.80	1.64	1	0	0	0

186	1.5%	51.80	1.89	1	0	0	0
187	1.5%	51.80	2.22	1	0	0	0
188	1.5%	51.80	2.63	1	0	0	0
189	1.5%	51.80	3.62	0	1	0	0
190	1.5%	51.80	6.50	0	1	0	0
191	1.5%	51.80	10.11	0	1	0	0
192	1.5%	51.80	14.80	0	0	1	0
193	1.5%	51.80	17.43	0	0	1	0
194	1.5%	51.80	19.65	0	0	1	0
195	1.5%	51.80	21.38	0	0	0	1
196	1.5%	51.80	24.01	0	0	0	1
197	1.5%	51.80	26.31	0	0	0	1

Table II-1 (Continued)

Sample	T200	T100	T50	T20	T10	T5	T2	stdev	skewness	kurtosis
1	1235	1247	1268	1237	1427	1555	1272	0.0298	0.0554	-0.2901
2	1138	1230	1344	1223	1281	1471	1270	0.0355	-0.0007	-0.1575
3	1172	1241	1313	1268	1321	1512	1295	0.0381	0.0136	-0.2688
4	1174	1263	1314	1262	1314	1511	1271	0.0385	0.0517	-0.3514
5	1199	1207	1290	1266	1425	1499	1293	0.0355	-0.0127	-0.2034
6	1175	1240	1250	1368	1457	1373	1311	0.0308	-0.0442	0.1415
7	1149	1187	1230	1231	1292	1264	1313	0.0303	0.0116	0.0130
8	1142	1220	1224	1261	1288	1279	1369	0.0330	-0.0602	0.0608
9	1184	1237	1272	1301	1314	1294	1397	0.0389	-0.1234	0.0664
10	1157	1216	1211	1267	1315	1298	1522	0.0486	-0.2571	-0.0332
11	1132	1276	1170	1246	1326	1369	1542	0.0615	-0.4447	0.4836
12	1080	1204	1239	1210	1266	1339	1552	0.0679	-0.0892	0.9929
13	1116	1233	1227	1239	1322	1490	1716	0.1078	-0.2881	0.1812
14	1151	1154	1214	1228	1300	1491	1723	0.1251	-0.1072	0.1718
15	1221	1290	1380	1370	1310	1457	1718	0.1479	-0.2112	-0.3092
16	1182	1244	1219	1324	1317	1421	1290	0.0221	0.1331	-0.1971
17	1136	1213	1243	1289	1303	1360	1261	0.0233	0.1971	-0.0303
18	1133	1223	1275	1353	1315	1398	1402	0.0289	0.0972	-0.3582
19	1105	1182	1200	1276	1319	1403	1336	0.0368	0.1026	-0.2483
20	1104	1173	1228	1372	1254	1491	1503	0.0376	0.0143	-0.3211
21	1124	1187	1252	1358	1254	1399	1478	0.0362	0.0328	-0.1326
22	1155	1196	1255	1318	1304	1397	1301	0.0297	-0.0257	-0.2411
23	1134	1193	1231	1264	1329	1357	1282	0.0301	0.0723	0.1390
24	1194	1204	1279	1270	1332	1304	1299	0.0293	-0.0284	-0.0006
25	1114	1236	1271	1294	1307	1324	1314	0.0340	-0.0063	-0.0070
26	1098	1202	1232	1273	1234	1258	1347	0.0370	-0.0077	0.2886
27	1116	1204	1168	1226	1256	1260	1385	0.0389	-0.0763	0.2523
28	1127	1171	1223	1269	1276	1299	1470	0.0467	-0.1965	0.2067
29	1142	1223	1219	1276	1238	1278	1462	0.0556	0.0228	1.2889
30	1103	1198	1261	1250	1274	1352	1577	0.0761	-0.2934	0.8050
31	1121	1243	1271	1335	1299	1442	1660	0.0957	-0.2130	0.1252

32	1118	1187	1265	1316	1262	1427	1648	0.1084	-0.2688	-0.2205
33	1139	1175	1297	1353	1253	1399	1656	0.1144	-0.1833	-0.0490
34	1174	1218	1241	1291	1287	1378	1279	0.0244	0.1831	-0.2227
35	1185	1248	1276	1346	1289	1422	1303	0.0249	0.1026	-0.3263
36	1103	1210	1214	1289	1278	1423	1410	0.0275	0.0580	-0.1142
37	1119	1214	1256	1322	1302	1524	1493	0.0306	0.0267	-0.2264
38	1147	1232	1279	1294	1337	1394	1333	0.0286	0.0732	-0.1594
39	1141	1201	1225	1233	1302	1352	1247	0.0256	-0.0325	-0.0254
40	1107	1182	1233	1270	1355	1291	1304	0.0277	0.1584	0.2158
41	1161	1233	1253	1289	1303	1301	1310	0.0286	-0.0061	-0.0553
42	1148	1211	1219	1248	1296	1263	1296	0.0363	-0.1146	0.0929
43	1161	1221	1265	1269	1299	1310	1375	0.0412	0.0581	-0.1809
44	1198	1248	1260	1278	1310	1306	1471	0.0465	-0.1376	-0.0723
45	1154	1243	1258	1264	1295	1336	1484	0.0543	-0.0987	-0.0385
46	1093	1192	1197	1226	1262	1360	1573	0.0741	-0.2052	0.4165
47	1198	1232	1242	1299	1297	1367	1549	0.0790	-0.1625	-0.0049
48	931	1073	1128	1176	1145	1285	1484	0.0989	-0.3696	0.2318
49	1131	1215	1316	1290	1260	1364	1627	0.0986	-0.2664	-0.1124
50	1082	1160	1228	1242	1193	1430	1678	0.1145	-0.3707	0.6662
51	1250	1223	1332	1235	1391	1544	1255	0.0278	0.0534	-0.4029
52	1132	1201	1253	1259	1321	1429	1256	0.0274	0.1045	-0.2740
53	1200	1210	1290	1290	1289	1486	1400	0.0312	0.1265	-0.2388
54	1134	1225	1322	1232	1373	1568	1289	0.0344	0.0257	-0.4258
55	1155	1177	1287	1226	1300	1495	1333	0.0318	0.1793	-0.1557
56	1122	1204	1316	1228	1326	1547	1323	0.0323	0.0307	-0.2705
57	1200	1245	1324	1220	1366	1438	1278	0.0299	-0.1396	-0.1398
58	1180	1214	1264	1253	1318	1325	1290	0.0334	-0.0083	-0.0232
59	1099	1208	1256	1271	1314	1317	1300	0.0408	0.0061	0.1513
60	1091	1166	1225	1275	1247	1264	1413	0.0445	-0.0716	0.1885
61	1136	1169	1186	1263	1275	1255	1408	0.0469	-0.0734	0.1604
62	1152	1226	1308	1264	1311	1338	1526	0.0662	-0.1605	-0.2821
63	1134	1280	1254	1315	1330	1361	1563	0.0743	-0.1555	-0.1364
64	1153	1250	1312	1278	1304	1346	1588	0.0830	-0.1948	-0.1851
65	1173	1272	1268	1262	1291	1325	1561	0.0866	-0.1693	-0.0852
66	1084	1144	1180	1238	1272	1341	1579	0.0935	-0.1498	0.2363
67	1197	1250	1266	1297	1267	1341	1604	0.0950	-0.1602	0.0013
68	1153	1255	1274	1295	1316	1377	1612	0.0979	-0.2595	-0.0369
69	1112	1163	1187	1210	1395	1385	1245	0.0361	0.1623	0.0123
70	1170	1283	1203	1246	1443	1424	1241	0.0396	0.0686	-0.3390
71	1219	1274	1278	1338	1537	1426	1276	0.0376	0.0083	-0.4818
72	1204	1244	1285	1315	1487	1353	1266	0.0369	0.0386	-0.3811
73	1217	1302	1324	1359	1527	1459	1288	0.0390	-0.0561	-0.5355
74	1109	1218	1273	1300	1420	1428	1277	0.0427	0.1454	0.3797
75	1216	1252	1277	1291	1351	1369	1349	0.0418	0.0471	-0.2742
76	1153	1136	1169	1197	1226	1235	1347	0.0411	-0.0899	0.7642
77	1081	1200	1186	1241	1227	1253	1440	0.0478	0.2597	0.9563
78	1026	1128	1125	1130	1151	1158	1261	0.0616	0.1838	5.1963
79	1065	1087	1121	1159	1208	1255	1413	0.0780	-0.0435	3.6318
80	1085	1222	1265	1270	1299	1388	1535	0.1032	-0.1653	0.4464

81	1151	1254	1254	1248	1329	1438	1586	0.1342	-0.2152	-0.1294
82	1208	1249	1246	1215	1369	1480	1615	0.1519	-0.3530	0.3235
83	1071	1105	1189	1167	1283	1477	1655	0.1579	-0.3092	0.1452
84	1179	1296	1340	1357	1592	1580	1311	0.0451	0.0728	-0.5786
85	1216	1300	1323	1336	1593	1602	1272	0.0512	0.0023	-0.7009
86	1172	1252	1298	1292	1514	1510	1254	0.0385	0.0144	-0.3243
87	1162	1338	1339	1370	1626	1640	1275	0.0569	-0.0185	-0.8003
88	1101	1241	1313	1313	1447	1448	1302	0.0342	-0.0119	-0.1572
89	1173	1237	1314	1358	1478	1467	1315	0.0396	0.1123	-0.3107
90	1138	1194	1226	1244	1317	1327	1290	0.0404	-0.1024	0.5969
91	1011	1096	1151	1180	1207	1277	1298	0.0443	1.0333	12.6834
92	1040	1111	1177	1210	1194	1231	1327	0.0444	0.1307	2.1694
93	1054	1058	1081	1116	1156	1214	1346	0.0687	-0.0235	1.8796
94	1102	1160	1188	1205	1207	1275	1373	0.0732	0.2810	3.8437
95	1092	1126	1182	1228	1234	1311	1460	0.0854	0.0755	0.8502
96	1187	1194	1272	1321	1234	1380	1527	0.1142	0.0046	0.3328
97	1134	1236	1202	1261	1364	1445	1575	0.1304	-0.1568	0.1621
98	1129	1170	1215	1244	1270	1417	1577	0.1452	-0.1980	0.2374
99	1202	1232	1272	1250	1362	1458	1629	0.1726	-0.0968	0.0237
100	1169	1273	1305	1268	1426	1495	1279	0.0323	0.1645	-0.1303
101	1211	1277	1384	1317	1544	1579	1303	0.0475	-0.0429	-0.5442
102	1251	1243	1292	1298	1517	1580	1262	0.0462	0.0957	-0.2039
103	1284	1310	1339	1284	1491	1492	1299	0.0382	0.2134	-0.0174
104	1434	1306	1399	1353	1615	1724	1271	0.0583	-0.0401	-0.8820
105	1238	1282	1330	1339	1506	1541	1300	0.0448	-0.0069	-0.4433
106	1172	1205	1259	1291	1339	1329	1332	0.0351	-0.0121	-0.0798
107	1127	1229	1278	1277	1340	1369	1305	0.0415	0.0633	-0.1072
108	1084	1201	1179	1194	1214	1204	1342	0.0435	0.0676	0.6654
109	1109	1131	1144	1173	1222	1208	1344	0.0498	0.0588	1.6936
110	1026	1121	1181	1142	1194	1227	1349	0.0706	-0.5352	3.7958
111	1079	1191	1224	1260	1216	1299	1404	0.0908	-0.2161	0.6373
112	1073	1157	1210	1277	1247	1308	1466	0.1128	0.2470	1.7489
113	1114	1211	1253	1274	1274	1382	1538	0.1173	-0.1745	0.6436
114	1187	1247	1316	1343	1309	1402	1576	0.1382	-0.1266	0.0318
115	1163	1220	1325	1306	1253	1391	1595	0.1447	-0.0887	0.2286
116	1114	1176	1214	1210	1260	1247	1274	0.0250	0.4035	0.8592
117	1191	1234	1290	1301	1310	1327	1236	0.0223	0.1582	-0.1169
118	1081	1178	1244	1272	1295	1322	1276	0.0215	0.1906	0.1974
119	1151	1222	1264	1223	1286	1216	1246	0.0218	0.3914	0.7916
120	1150	1255	1270	1264	1295	1294	1248	0.0232	0.1862	0.0295
121	1100	1204	1251	1237	1271	1279	1298	0.0235	0.1379	-0.0366
122	1104	1146	1176	1226	1204	1186	1321	0.0262	0.2869	1.1124
123	1089	1174	1207	1248	1247	1232	1312	0.0268	0.0530	0.9129
124	1088	1152	1197	1231	1233	1245	1316	0.0281	0.0578	0.2512
125	1134	1188	1206	1245	1268	1212	1302	0.0367	-0.1262	0.2757
126	1120	1163	1232	1252	1216	1255	1356	0.0472	-0.0250	0.3719
127	1095	1142	1173	1224	1183	1176	1314	0.0607	-0.0168	2.6368
128	1166	1183	1272	1256	1248	1285	1438	0.0783	-0.0855	0.3944
129	1048	1130	1174	1179	1142	1272	1418	0.0999	-0.0837	0.8733

130	1054	1126	1215	1237	1241	1302	1424	0.1079	0.0393	0.5175
131	1133	1168	1165	1241	1223	1343	1503	0.1192	-0.4326	0.4275
132	1152	1261	1203	1275	1253	1361	1533	0.1405	-0.1020	0.5941
133	1203	1238	1302	1341	1292	1380	1543	0.1346	-0.2383	-0.0487
134	1014	1158	1250	1144	1212	1345	1644	0.0610	1.0522	1.8370
135	1225	1244	1251	1311	1337	1494	1741	0.0669	0.4603	0.6268
136	1011	1279	1392	1405	1487	1582	1787	0.0859	0.8761	0.3319
137	1161	1242	1270	1282	1340	1460	1701	0.0608	0.5690	0.6630
138	1052	1074	1141	1172	1307	1416	1713	0.0685	1.1040	2.1301
139	1106	1075	1142	1247	1274	1383	1626	0.0712	0.8879	2.4307
140	1117	1087	1199	1240	1228	1291	1501	0.0751	0.5114	1.0043
141	1034	1045	1089	1122	1213	1287	1523	0.0890	0.6746	1.8668
142	1108	1145	1185	1158	1171	1279	1494	0.0998	0.3494	2.1931
143	1067	1166	1230	1226	1237	1290	1511	0.1178	0.2177	0.8105
144	1096	1167	1223	1257	1234	1326	1469	0.1231	0.0869	0.5013
145	1117	1215	1246	1264	1299	1380	1503	0.1417	0.0772	-0.0262
146	1172	1233	1273	1300	1292	1355	1449	0.1733	0.0715	0.1877
147	1059	1184	1193	1228	1256	1334	1465	0.1852	0.1038	0.6795
148	981	1091	1205	1203	1199	1341	1648	0.0602	0.8560	0.6153
149	1180	1253	1381	1394	1420	1447	1690	0.0672	0.5545	0.0867
150	1260	1382	1342	1414	1401	1502	1749	0.0757	0.2691	-0.4382
151	1208	1335	1394	1355	1421	1466	1716	0.0739	0.1981	-0.4883
152	1106	1085	1235	1274	1340	1448	1721	0.0746	0.5539	0.3147
153	1052	1167	1183	1226	1213	1331	1649	0.0708	0.8326	0.4166
154	1138	1211	1215	1354	1391	1402	1685	0.0735	0.6902	0.0968
155	1050	1093	1235	1204	1282	1298	1582	0.0777	0.6354	0.7792
156	1088	1180	1278	1257	1260	1356	1577	0.0909	0.3062	0.4099
157	1089	1161	1219	1260	1260	1361	1503	0.0996	0.0964	0.4932
158	1096	1155	1208	1187	1202	1338	1527	0.1048	0.1576	0.5933
159	1160	1162	1128	1245	1225	1351	1507	0.1178	0.0542	0.5554
160	1149	1166	1243	1209	1231	1344	1488	0.1309	-0.0018	0.5904
161	996	1060	1125	1079	1086	1238	1352	0.1652	0.1635	0.1872
162	1112	1202	1244	1161	1289	1335	1480	0.1736	0.0646	0.8595
163	1120	1261	1306	1394	1412	1447	1641	0.0621	0.7319	-0.2462
164	1096	1181	1181	1270	1292	1300	1511	0.0489	0.6232	0.6197
165	1001	1060	1142	1166	1137	1213	1440	0.0491	0.7879	1.0083
166	1110	1162	1191	1366	1343	1366	1575	0.0590	0.7017	0.3280
167	1156	1124	1199	1236	1261	1253	1501	0.0550	0.5576	0.5675
168	979	1090	1126	1144	1219	1189	1508	0.0546	0.9181	1.0641
169	1079	1188	1223	1290	1292	1262	1486	0.0543	0.4835	0.4281
170	1153	1207	1211	1227	1234	1270	1526	0.0584	0.5155	0.5828
171	1205	1205	1281	1344	1381	1422	1648	0.0755	0.4063	-0.3003
172	1119	1210	1252	1316	1349	1422	1584	0.0770	0.3047	-0.0961
173	1063	1099	1151	1201	1196	1261	1422	0.0821	0.2543	0.6064
174	1104	1126	1156	1174	1232	1264	1436	0.1024	0.0801	1.2740
175	1102	1124	1196	1190	1189	1222	1426	0.1129	0.4379	0.8864
176	1085	1113	1134	1209	1212	1277	1448	0.1230	0.2471	0.7728
177	1086	1175	1175	1206	1221	1225	1336	0.1341	-0.1438	2.4302
178	1081	1155	1259	1234	1229	1312	1497	0.1616	0.0566	0.3151

179	1043	1129	1181	1206	1280	1362	1495	0.1692	-0.0406	0.8416
180	1062	1083	1150	1210	1226	1309	1453	0.0467	0.9476	1.1180
181	958	1065	1130	1152	1160	1183	1400	0.0458	1.0394	1.9533
182	1053	1100	1102	1144	1115	1154	1351	0.0427	0.9083	1.7698
183	926	1050	1122	1206	1267	1313	1479	0.0471	1.2062	2.5674
184	1001	1024	991	1097	1169	1188	1410	0.0483	1.1517	2.0688
185	1044	1042	1159	1186	1116	1199	1395	0.0470	1.1222	2.6750
186	991	1108	1114	1169	1142	1164	1393	0.0538	0.8422	1.3098
187	1032	1107	1168	1156	1129	1178	1385	0.0520	0.9828	2.0045
188	1122	1126	1168	1183	1243	1271	1445	0.0587	0.6489	0.6846
189	1087	1166	1114	1187	1244	1267	1460	0.0619	0.4370	0.8486
190	1114	1098	1160	1162	1209	1191	1364	0.0701	0.5118	1.0895
191	1122	1173	1149	1225	1212	1231	1406	0.0894	0.1231	0.8204
192	1063	1155	1191	1204	1216	1257	1436	0.1156	0.1476	0.7112
193	1087	1155	1202	1289	1244	1288	1396	0.1204	-0.1079	0.4433
194	1064	1124	1147	1198	1208	1230	1346	0.1310	-0.0522	1.4013
195	1140	1135	1207	1243	1237	1299	1446	0.1497	0.0565	0.6343
196	1154	1191	1245	1291	1257	1321	1430	0.1529	-0.0113	0.5314
197	1105	1185	1218	1246	1274	1326	1419	0.1660	-0.0112	0.5813

Table II-1 (Continued)

Sample	Average_f	Sigma_f	0.0<f<3.0	3.0<f<8.0	8.0<f<13.0	13.0<f<25.0	25.0<f<30.0
1	13.464	8.472	0.0881	0.0324	0.5974	0.0497	0.1963
2	17.455	9.235	0.0552	0.0169	0.4390	0.0626	0.4033
3	18.063	9.017	0.0353	0.0310	0.4122	0.0964	0.4000
4	17.867	9.091	0.0392	0.0219	0.4273	0.0756	0.4051
5	15.362	9.145	0.0551	0.0348	0.5259	0.1310	0.2042
6	13.103	10.186	0.1112	0.1009	0.5100	0.1446	0.0466
7	12.422	11.582	0.2094	0.1516	0.3577	0.1091	0.0516
8	11.912	11.670	0.2324	0.1773	0.3265	0.0784	0.0751
9	11.519	12.072	0.2785	0.1926	0.2551	0.0893	0.0530
10	7.959	11.389	0.4393	0.1820	0.1231	0.0670	0.0301
11	7.542	11.128	0.4429	0.2071	0.0951	0.0660	0.0279
12	7.036	9.935	0.4565	0.2662	0.0822	0.0641	0.0236
13	4.584	7.647	0.5337	0.2723	0.0514	0.0420	0.0084
14	3.901	6.467	0.5972	0.2009	0.0651	0.0347	0.0078
15	4.292	6.422	0.6767	0.1836	0.0559	0.0423	0.0063
16	18.669	10.030	0.0487	0.0519	0.2942	0.1135	0.4311
17	18.405	10.443	0.0742	0.0473	0.2980	0.0913	0.4272
18	21.855	9.689	0.0349	0.0398	0.1675	0.1444	0.5441
19	19.756	10.545	0.0790	0.0246	0.1891	0.1331	0.4947
20	21.793	8.994	0.0388	0.0281	0.1928	0.1058	0.5966
21	22.530	8.176	0.0262	0.0232	0.1512	0.1364	0.6361
22	17.106	10.329	0.0589	0.0351	0.3750	0.1293	0.3046
23	14.872	11.028	0.0685	0.0605	0.4125	0.1641	0.1375

24	13.515	10.230	0.0950	0.0920	0.4985	0.1737	0.0221
25	15.328	12.662	0.0929	0.1863	0.3453	0.1505	0.0539
26	13.536	12.699	0.2018	0.2277	0.2097	0.1306	0.0857
27	14.063	13.708	0.2140	0.2040	0.1970	0.0954	0.0633
28	9.061	11.138	0.3615	0.2538	0.1568	0.0783	0.0323
29	8.983	11.726	0.4528	0.1954	0.1071	0.0824	0.0433
30	9.472	12.048	0.3430	0.3366	0.0788	0.0892	0.0344
31	5.224	7.387	0.4971	0.3455	0.0609	0.0502	0.0094
32	5.399	7.520	0.4614	0.3521	0.0677	0.0552	0.0118
33	5.251	6.836	0.4575	0.3391	0.1034	0.0547	0.0106
34	19.312	11.912	0.0724	0.0773	0.2065	0.0445	0.4674
35	20.332	11.144	0.0550	0.0807	0.2461	0.0424	0.4843
36	21.818	10.548	0.0537	0.0527	0.1565	0.0915	0.5398
37	23.032	8.887	0.0282	0.0380	0.1438	0.0933	0.6552
38	18.662	10.871	0.0768	0.0870	0.2570	0.1071	0.4007
39	16.999	11.869	0.0723	0.0832	0.3331	0.1355	0.2325
40	12.447	11.951	0.1558	0.1037	0.3582	0.1230	0.0554
41	14.433	11.889	0.1210	0.1517	0.3275	0.2099	0.0321
42	14.857	13.129	0.1470	0.2152	0.2500	0.1409	0.0685
43	12.474	12.497	0.1998	0.2560	0.2408	0.0963	0.0405
44	10.600	12.353	0.3198	0.2995	0.1238	0.0915	0.0417
45	9.179	10.691	0.2800	0.3549	0.1404	0.0942	0.0383
46	6.697	9.140	0.3623	0.4049	0.0668	0.0642	0.0195
47	7.040	9.103	0.3540	0.4099	0.0730	0.0811	0.0187
48	6.426	8.917	0.4566	0.3035	0.0905	0.0753	0.0122
49	5.955	8.286	0.3785	0.4119	0.0710	0.0572	0.0140
50	4.736	6.796	0.5682	0.2771	0.0496	0.0553	0.0087
51	16.752	10.536	0.0399	0.0542	0.5368	0.0348	0.2525
52	18.527	11.419	0.0551	0.0629	0.3924	0.0435	0.3312
53	21.663	9.692	0.0357	0.0576	0.2034	0.0705	0.5772
54	17.060	9.559	0.0336	0.0362	0.5115	0.0598	0.3092
55	20.287	10.261	0.0433	0.0380	0.2889	0.0589	0.4889
56	19.981	9.438	0.0201	0.0528	0.3345	0.0737	0.4852
57	14.657	9.534	0.0474	0.0721	0.5867	0.1199	0.0997
58	14.684	10.753	0.0837	0.1035	0.4822	0.1664	0.0415
59	14.974	12.285	0.0844	0.1589	0.4104	0.1382	0.0345
60	11.787	12.421	0.1699	0.3636	0.2185	0.0890	0.0307
61	11.614	12.611	0.2172	0.3154	0.1720	0.0875	0.0323
62	7.892	9.631	0.2355	0.4709	0.1212	0.0795	0.0223
63	7.075	8.824	0.2945	0.4783	0.0811	0.0718	0.0190
64	6.430	9.002	0.3131	0.4816	0.0620	0.0533	0.0182
65	6.651	8.435	0.2322	0.5460	0.0724	0.0676	0.0162
66	6.679	8.432	0.3798	0.3979	0.0811	0.0842	0.0150
67	6.234	7.915	0.3437	0.4393	0.0767	0.0755	0.0117
68	7.339	9.870	0.3512	0.4342	0.0637	0.0773	0.0141
69	13.687	9.482	0.0706	0.0388	0.4572	0.1114	0.2100
70	14.260	8.015	0.0508	0.0387	0.5789	0.1386	0.1627
71	13.303	7.410	0.0513	0.0375	0.6420	0.1346	0.1057
72	13.003	8.192	0.0842	0.0500	0.5374	0.1630	0.1085

73	12.258	8.316	0.0596	0.0696	0.6925	0.0872	0.0169
74	11.956	8.259	0.0641	0.1052	0.6658	0.0578	0.0374
75	11.116	9.084	0.1310	0.1299	0.5354	0.0614	0.0547
76	11.848	11.484	0.2061	0.2149	0.3112	0.1103	0.0306
77	10.685	12.601	0.2949	0.2775	0.1817	0.0738	0.0270
78	12.855	14.087	0.3027	0.2308	0.0996	0.1166	0.0532
79	9.556	13.136	0.4580	0.1217	0.0995	0.1033	0.0287
80	9.460	12.441	0.4846	0.1523	0.0913	0.1053	0.0398
81	6.697	10.502	0.5969	0.1122	0.0621	0.0827	0.0213
82	7.027	10.913	0.6068	0.1085	0.0818	0.0835	0.0224
83	5.610	9.298	0.6551	0.1332	0.0653	0.0584	0.0128
84	11.246	6.311	0.0535	0.0348	0.7635	0.0467	0.0484
85	11.472	6.566	0.0580	0.0340	0.7225	0.0505	0.0822
86	13.316	7.792	0.0501	0.0482	0.6346	0.0929	0.1344
87	11.593	5.747	0.0337	0.0291	0.8006	0.0493	0.0580
88	11.976	8.791	0.0766	0.0877	0.5951	0.1061	0.0342
89	11.966	8.491	0.0599	0.1007	0.6587	0.0683	0.0235
90	13.098	10.735	0.0735	0.1263	0.5329	0.0847	0.0427
91	11.859	11.343	0.1884	0.2314	0.3022	0.1100	0.0353
92	14.807	13.710	0.1838	0.1830	0.2722	0.1232	0.0463
93	13.188	14.584	0.3204	0.1707	0.1267	0.1216	0.0424
94	9.970	12.339	0.4386	0.1684	0.1044	0.1110	0.0276
95	12.215	13.848	0.3756	0.1590	0.1070	0.1230	0.0455
96	10.448	13.433	0.3907	0.2682	0.0786	0.1015	0.0236
97	9.117	12.858	0.5217	0.1236	0.1109	0.0842	0.0184
98	6.627	10.057	0.6065	0.1512	0.0609	0.0763	0.0154
99	6.862	10.946	0.5882	0.1262	0.0840	0.0707	0.0140
100	13.374	8.284	0.0666	0.0617	0.5935	0.0926	0.1391
101	12.443	6.771	0.0383	0.0534	0.7009	0.0727	0.1082
102	11.739	6.935	0.0669	0.0583	0.6998	0.0533	0.0830
103	12.043	7.296	0.0778	0.0616	0.6669	0.0721	0.0850
104	11.927	5.703	0.0286	0.0242	0.8284	0.0391	0.0587
105	11.097	6.542	0.0803	0.0748	0.7386	0.0421	0.0342
106	12.505	9.446	0.0708	0.1351	0.5568	0.1183	0.0225
107	11.651	9.633	0.0891	0.1843	0.4971	0.0967	0.0254
108	13.837	12.765	0.1591	0.2110	0.2478	0.1491	0.0397
109	12.329	12.805	0.2437	0.2278	0.1593	0.1468	0.0533
110	11.664	14.017	0.3828	0.1718	0.0877	0.1217	0.0396
111	10.268	12.869	0.4021	0.1670	0.0917	0.1253	0.0283
112	9.905	12.305	0.3716	0.2680	0.0941	0.1100	0.0280
113	8.683	11.745	0.4497	0.2319	0.0800	0.0891	0.0212
114	6.371	9.072	0.5117	0.2454	0.0923	0.0755	0.0153
115	7.008	9.692	0.5018	0.2390	0.0808	0.0817	0.0235
116	12.874	11.041	0.1592	0.2005	0.2585	0.0692	0.2148
117	16.163	11.361	0.1045	0.1398	0.2158	0.1023	0.3420
118	12.259	10.528	0.1752	0.1998	0.2447	0.0997	0.1992
119	13.087	11.824	0.2122	0.1367	0.1336	0.1228	0.2508
120	14.449	11.520	0.1627	0.1552	0.1827	0.1346	0.2563
121	14.745	11.538	0.1158	0.1948	0.2543	0.1627	0.1604

122	11.740	11.654	0.1786	0.2046	0.2218	0.1586	0.0557
123	13.184	13.539	0.1988	0.1041	0.1737	0.1905	0.0500
124	14.633	12.743	0.1193	0.2060	0.2626	0.1752	0.0505
125	14.367	12.790	0.1265	0.2580	0.2144	0.1777	0.0456
126	12.608	12.516	0.1148	0.3345	0.2258	0.1139	0.0420
127	13.967	14.016	0.1471	0.3239	0.1586	0.1275	0.0305
128	11.117	12.616	0.2278	0.3659	0.1054	0.1106	0.0413
129	10.551	13.175	0.3660	0.2636	0.0733	0.1241	0.0263
130	9.930	11.692	0.3218	0.3053	0.0917	0.1459	0.0266
131	7.792	10.245	0.3981	0.3349	0.0614	0.0970	0.0247
132	8.200	11.666	0.5368	0.1812	0.0692	0.0912	0.0228
133	9.170	11.996	0.4126	0.2587	0.0800	0.1138	0.0220
134	12.767	9.623	0.0719	0.0302	0.5671	0.0190	0.1794
135	17.826	9.012	0.0525	0.0115	0.4716	0.0407	0.3898
136	15.383	9.111	0.0256	0.0333	0.4329	0.0532	0.3776
137	15.818	9.010	0.0412	0.0241	0.5157	0.0218	0.3635
138	17.254	9.096	0.0522	0.0405	0.5120	0.0441	0.2728
139	11.954	11.271	0.1978	0.1728	0.3366	0.1029	0.0405
140	11.404	11.247	0.2032	0.1689	0.3026	0.0871	0.0837
141	10.784	11.318	0.2677	0.1898	0.2529	0.0695	0.0477
142	11.452	11.183	0.2893	0.1802	0.2316	0.0761	0.0532
143	7.542	11.128	0.4348	0.2121	0.0891	0.0550	0.0218
144	6.944	9.367	0.4614	0.2834	0.0778	0.0524	0.0179
145	4.684	7.451	0.5018	0.2570	0.0702	0.0394	0.0113
146	4.015	6.237	0.6012	0.2278	0.0637	0.0422	0.0084
147	5.434	8.921	0.6339	0.1548	0.0662	0.0325	0.0070
148	19.346	9.586	0.0536	0.0268	0.2780	0.1211	0.4542
149	20.338	10.779	0.0327	0.0378	0.2661	0.1002	0.4064
150	21.106	9.237	0.0782	0.0413	0.1972	0.1295	0.5160
151	18.353	8.999	0.0551	0.0367	0.1877	0.1033	0.4817
152	21.174	10.022	0.0365	0.0316	0.2030	0.0997	0.5520
153	20.667	8.187	0.0346	0.0304	0.1413	0.1236	0.5903
154	17.280	10.119	0.0765	0.0422	0.2614	0.1027	0.4241
155	14.240	12.362	0.1144	0.2497	0.3018	0.1535	0.0605
156	13.536	10.909	0.1973	0.2534	0.1841	0.1262	0.1001
157	8.886	10.478	0.4029	0.3334	0.1062	0.0553	0.0476
158	10.051	11.107	0.2737	0.2019	0.2618	0.0782	0.0344
159	10.283	11.267	0.2468	0.1859	0.2488	0.0702	0.0517
160	5.389	10.478	0.3821	0.2976	0.0532	0.0944	0.0452
161	9.214	7.270	0.4822	0.3312	0.0429	0.0404	0.0176
162	5.116	6.530	0.4693	0.3849	0.0513	0.0312	0.0079
163	16.365	10.892	0.0435	0.0757	0.2477	0.0540	0.4425
164	23.783	10.224	0.0649	0.0708	0.2219	0.0918	0.4527
165	18.562	9.485	0.0432	0.0718	0.1772	0.0878	0.5014
166	20.315	9.737	0.0448	0.0212	0.1627	0.1022	0.5986
167	19.427	11.820	0.0404	0.0653	0.1980	0.0905	0.4996
168	17.533	11.429	0.0731	0.0817	0.2556	0.1232	0.3401
169	17.339	8.773	0.0628	0.0544	0.2318	0.1032	0.2829
170	14.324	10.993	0.0537	0.0724	0.2067	0.0915	0.4741

171	15.124	10.858	0.0842	0.0704	0.2108	0.0803	0.3852
172	17.315	10.363	0.0320	0.0651	0.2530	0.0412	0.3327
173	11.421	13.026	0.3322	0.2356	0.1352	0.0916	0.0348
174	11.585	12.115	0.3300	0.3016	0.1513	0.0787	0.0266
175	10.113	12.398	0.2970	0.3214	0.1458	0.0741	0.0353
176	5.516	9.412	0.3883	0.4010	0.0563	0.0579	0.0123
177	6.115	10.024	0.3230	0.4121	0.0617	0.0835	0.0175
178	6.074	10.121	0.4298	0.3328	0.0462	0.0768	0.0203
179	6.825	9.006	0.3615	0.4123	0.0377	0.0539	0.0235
180	15.689	12.091	0.0503	0.0462	0.1978	0.0887	0.4373
181	17.645	10.135	0.0402	0.0377	0.2108	0.1127	0.5010
182	13.355	10.708	0.1466	0.2479	0.2821	0.1134	0.0586
183	11.152	10.176	0.1970	0.1453	0.2068	0.1726	0.0365
184	13.288	10.162	0.2030	0.1646	0.1829	0.1635	0.0326
185	12.634	10.378	0.2317	0.1933	0.2466	0.1874	0.0321
186	14.286	8.358	0.1653	0.2714	0.2777	0.1439	0.0803
187	13.602	11.313	0.1935	0.2047	0.2714	0.1669	0.0582
188	11.414	9.912	0.1878	0.1538	0.2707	0.1473	0.0606
189	12.783	9.726	0.1761	0.2347	0.2637	0.1369	0.0582
190	10.637	11.685	0.2586	0.3132	0.0893	0.1294	0.0233
191	12.343	11.705	0.1892	0.2162	0.2915	0.1417	0.0658
192	12.139	12.709	0.1351	0.2387	0.2695	0.1438	0.0492
193	10.947	12.552	0.1701	0.2119	0.2457	0.1281	0.0838
194	10.776	12.038	0.2659	0.3382	0.0945	0.1348	0.0276
195	9.135	10.286	0.4379	0.3505	0.0516	0.0724	0.0205
196	6.886	11.099	0.3412	0.4044	0.0974	0.0475	0.0183
197	6.599	12.194	0.3843	0.3908	0.0746	0.0518	0.0293

APPENDIX III

HYBRID NEURAL NETWORK-FIRST PRINCIPLE MODELING OF CRITICAL HEAT FLUX

III.1 Introduction

The hybrid artificial neural network-first principle modeling (ANN-FPM) is a powerful and flexible methodology that can be particularly useful for complex multi-phase flow processes. In this method the flow state variables are obtained from the solution of conservative equations using first principle-based closure relations whenever possible, and using trained artificial neural networks for poorly-understood rate processes.

The importance of forced-flow critical heat flux (CHF), its extreme complexity, and the need for reliable and accurate methods for its prediction are well recognized. A multitude of thermal-hydraulic and geometric parameters influence forced-flow CHF, and CHF may occur due to several different mechanisms under different flow patterns, all contributing to its complexity (Weisman, 1992; Katto, 1994). The vast experimental data and numerous correlations that have been published in the past have been partially reviewed and qualified only recently (Hall and Mudawar, 1997; 2000a; 2000b). Semi-theoretical methods have been reasonably successful in predicting CHF for some flow conditions. The main mechanism leading to subcooled CHF, for example, is qualitatively well understood (Galloway and Mudawar, 1993), and accordingly phenomenological methods for the prediction of subcooled boiling have been published (Katto, 1992; Celata et al., 1994). Successful semi-theoretical methods are also available for CHF in

subcooled and low-quality flow (Weisman, 1992; Hall and Mudawar, 2000b; Weisman and Ileslamlous, 1988); and for dryout in annular dispersed flow regime (Hewitt and Govan, 1990; Sugawara, 1990). These semi-theoretical methods, however, utilize a large number of empirical closure relations, and may have serious limitations with respect to their applicability to conditions outside the experimental databases that have been used for their validation and adjustment. This is particularly true for dryout heat flux, where complex liquid film hydrodynamics and droplet entrainment and impingement occur. Empirical correlations are therefore often applied. For water in vertical, upward flow in circular pipes, for example, table look-up methods (Groeneveld et al., 1986; Groeneveld et al., 1996), and a purely empirical correlation for subcooled boiling (Hall and Mudawar, 2000b) provide more accurate predictions than the semi-theoretical models. Empirical correlations with wide parameter ranges that cover different CHF modes are also available (Shah, 1987; Caira et al., 1995).

CHF in horizontal channels, in particular at low flow conditions, is also quite complex. Data and analysis can be found in (Cumo et al., 1978; Jensen and Bergles, 1981; Leontiev et al., 1981; Mrilo, 1977; Merilo, 1979; Ahmad et al., 1982; Wong et al., 1990; Balino and Converti, 1994)). At high flow rates the effect of channel orientation is unimportant. In large horizontal channels, annuli and rod bundles, at low flow conditions, stratified two-phase flow regime can occur and cause dryout at the upper channel surfaces, leading to significantly lower CHF values than vertical channels. A criterion, based on an appropriately defined Froude number, has been suggested to determine whether vertical channel models and correlations can be applied to the horizontal configuration (Jensen and Bergles, 1981; Kefer et al., 1989). Empirical correlations based

on the method of compensated distortions (Merilo, 1979; Ahmad, 1973; Stoddard et al., 2002), and semi-theoretical method based on using vertical channel correlations along with a correlation factor (Celata et al., 1994; Wong et al., 1990; Stoddard et al., 2002), all with limited success when applied outside their data bases (Hall and Mudawar, 2000a; Wong et al., 1990) have been suggested in the past.

Table III-1: Summary of the experimental data used in this study

	Lezzi et al. (1994)	Lowdermilk et al. (1958)	Weatherhead (1963)	Roach et al. (1999)
Number of data points	86	63	22	43
D (mm)	1.0	1.3	1.14	1.168~1.448
L (m)	0.239~0.975	0.065~0.325	0.114	0.16
P (bar)	19~70	1.0	13.8	3.4~10.4
G (kg/m^2s)	816~2,738	149~5,110	3,900~7,800	250~1,000
x_e	0.66~0.99	0.20~0.98	0.11~0.33	0.35~0.99

Critical heat flux in mini-channels (channels with $D_H \approx 1$mm) has also been investigated extensively, mostly under high mass flux and highly subcooled liquid conditions representative of the cooling systems of the plasma-facing fusion reactor components (Ghiaasiaan and Abdel-Khalik, 2001). Although mini-channel-range experimental data are included in the databases of some empirical correlations and mechanistic models (e.g., Celata et al., 1994; Shah, 1987; Caira et al., 1995), the adequacy of these predictive methods for mini-channels is questionable. Figure III.1 and III.2 are examples to this point. In these figures the experimental data of (Lezzi et al., 1994; Lowdermilk et al., 1958; Weatherhead, 1963; Roach et al., 1999), which are included in the critically reviewed and qualified PU-BTPFL CHF database (Hall and

Mudawar, 1998), are compared with the widely-used and well-recognized empirical correlations of Shah (1987) and Caira et al. (1995), respectively. The parametric ranges of these data are summarized in Table III-1, and in light of their high equilibrium vapor qualities, they all can be assumed to represent dryout-type CHF. Agreement among the depicted data and the aforementioned correlations is evidently poor. Furthermore, the discrepancy between either correlations or data is clearly dependent of data source. For example, the correlation of Shah (1987) consistently and quite significantly under-predicts the data of (Lezzi et al., 1994; Lowdermilk et al., 1958; Weatherhead, 1963). The correlation of Caira et al. (1995), on the other hand, systematically and significantly under-predicts the data (Lezzi et al., 1994), and systematically over-predicts the remainder of the data.

Empirical correlations for CHF are generally in terms of macroscopic flow and geometric parameters, for obvious reasons. Mechanistic and phenomenological models, however, need to use local thermal and hydrodynamic parameters that represent thermal and/or mechanical non-equilibrium. Examples to this point include local pressure and quality in subcooled CHF (Katto, 1992; Celata et al., 1994); and void fraction, phase velocities, entrainment and deposition rates, etc., in annular film dryout (Hewitt and Govan, 1990; Sugawara, 1990). These local parameters evidently need to be calculated by a thermal-hydraulic model, and this essentially fine-tunes the CHF model to the thermal-hydraulic model, and limits the applicability of the CHF models to the range of applicability of the thermal-hydraulic model. In the case of dryout, where the film and entrained droplet hydrodynamics play crucial roles, the interdependence of the CHF model and the multi-fluid model that predicts these local hydrodynamic parameters is

overwhelming (Hewitt and Govan, 1990; Sugawara, 1990; Lin and Pei, 1992) and renders these models essentially hybrid thermal-hydraulic-CHF methods. The significance of the interplay among thermal-hydraulic and dryout phenomena becomes more evident by the fact that the aforementioned dryout models well predict experimental data despite significant differences in their hydrodynamic modeling details.

Recently published descriptions of ANN fundamentals include (Maren, 1990; Anderson, 1995). Neural networks are now well-accepted non-classical alternatives for mechanistic and/or empirical models for highly non-linear processes. Recent applications of ANNs in multi-phase flow modeling include (Cai et al., 1994; Mi et al., 1998), where the pattern-recognative capabilities of ANNs have been utilized for objective identification of flow regimes in multiphase flow systems, and (Moon and Chang, 1994), where the non-linear mapping capability of ANNs have been used for correlating CHF data. In other applications ANNs have even been used as fast calculation alternatives for well-understood but time-consuming theoretical models (Jambunathan et al., 1996) and equations of states (Normandin et al., 1993).

Using the Korea Advanced Institute of Science and Technology (KAIST) database, Moon et al. (1996) developed a ANN-based method for predicting CHF in round, vertical and uniformly heated channels with water. They trained ANNs for using, as input, parameters representing the heated channel inlet, exit, or local conditions. In a follow-up paper, Lee et al. (2000) used an innovative ANN-based technique for deriving an expression for the effect of the heated length on CHF.

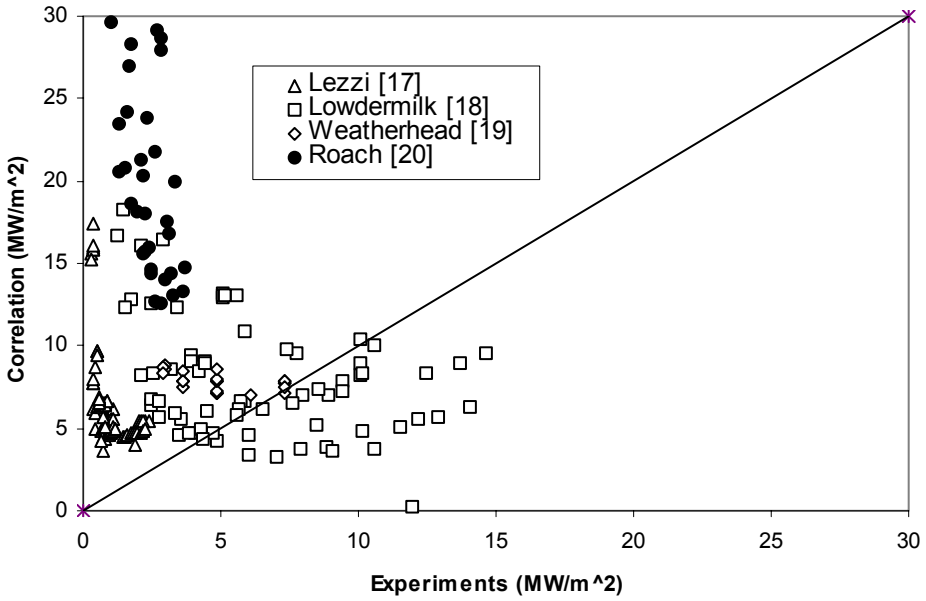

Figure III.1: Comparison of the CHF data of (Lezzi et al., 1994; Lowdermilk et al., 1958; Weatherhead, 1963; Roach et al., 1999) with the correlation of Shah (1987). Plotted data represent q''_{CHF}.

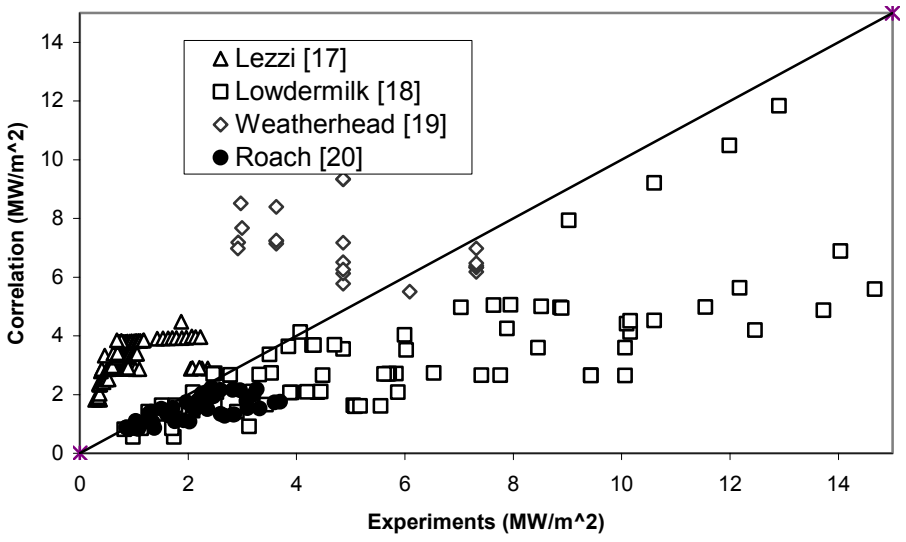

Figure III.2: Comparison of the CHF data of (Lezzi et al., 1994; Lowdermilk et al., 1958; Weatherhead, 1963; Roach et al., 1999) with the correlation of Caira (1995). Plotted data represent q''_{CHF}.

The objective of this study is to propose a methodology for hybrid artificial neural network-first principle modeling (ANN-FPM) of CHF. In what follows, the essence of the proposed model is first described. The methodology is then applied to a set of experimental data dealing with CHF in a thin, horizontal annulus and the available qualified dryout heat flux data representing uniformly-heated circular mini-channels (channels with diameters of around or slightly larger than 1mm), separately.

III.2 Hybrid ANN-FPM Methodology

The hybrid, ANN-FPM method is a simple way of modeling complex processes that are highly non-linear functions of local parameters that themselves must be calculated from the solution of conservation equations. In this method the conservation equations are solved using primarily first principles with minimal assumptions introduced in the development and closure of these conservation equations. The complex and poorly understood closure relations, in particular the rate-controlling transport processes, which are typically poorly understood non-linear functions of local state variables, are represented by trained neural networks. The training of the neural networks is of course done using experimental data. However, the training is performed using the hybrid ANN and FPM; whereby the local state variables predicted by FPM, and the experimentally-measured quantities, are used as the ANN input and output, respectively. The restriction of the model to first principles can evidently provide for compatibility among separately developed models and minimize fine-tuning effects. Recent applications of hybrid ANN-FPM include (Qi et al, 1999; Fullana et al., 1999; Molga and Cherbanski, 1999; Gupta et al., 1999). In (Gupta et al., 1999), for example, Gupta et al. used a simple one-

dimensional first principle model for the analysis of a flotation column, while four different trained ANNs provided the needed closure relations, two for the prediction of bubble size and void fraction respectively, and two for the floatation rate constants.

We propose that the hybrid ANN-FPM methodology offers a promising technique for the development of simple, flexible, highly accurate, modular, and fast-running thermal-hydraulic codes in the future. In addition, such codes will be easy to modify and enhance without compromising compatibility and objectivity.

In the forthcoming sections the hybrid ANN-FPM method is applied to a set of experimental data representing CHF in a thin horizontal annular channel (Stoddard et al., 2002) and the qualified PU-BTPFL CHF database in mini-channels (Hall and Mudawar, 1998). The data are few in number, and were obtained under low-flow conditions that can cause the dryout process to be hydrodynamically controlled, leading to complicated coupling among local thermal and two-phase hydrodynamic processes. It will be shown that the ANN-FPM method can provide a model that captures the patterns in the major parametric dependencies, and well predicts all the trends in the data.

III.3 The First-Principle Model

Figure III.3 is a schematic of the modeled systems. On Figure III.3(a), the studied system is a horizontal thin annular channel. On Fig. III.3(b), a mini-channel with subcooled liquid at inlet, and annular flow regime near its exit, is the system of interest. The one-dimensional conservation equations will be presented below for a channel with an arbitrary orientation. In accordance with the ANN-FPM method, the conservation equations are cast in simple forms, with the following assumptions:

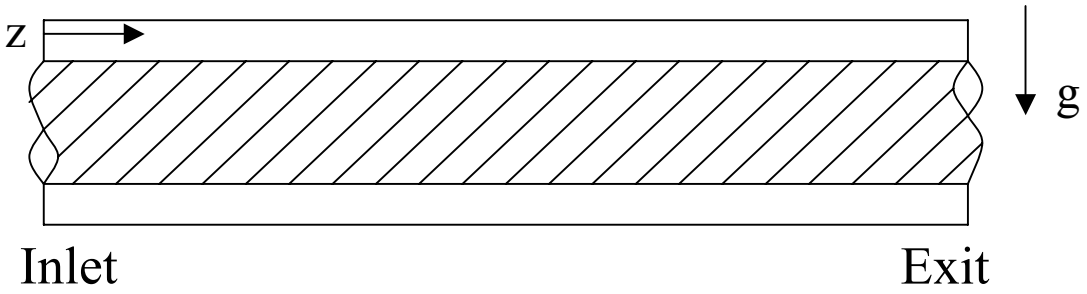

(a)

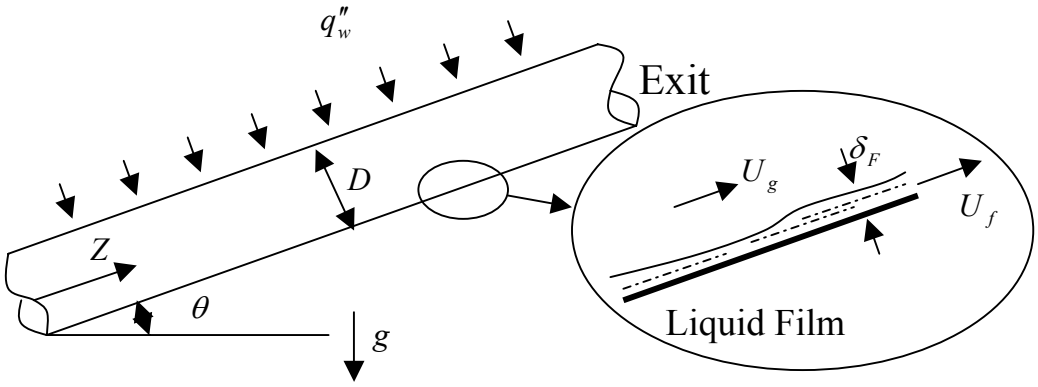

(b)

Figure III.3: Schematic of the modeled systems: (a) a thin annular channel; (b) a mini-channel

1. One-dimensional, steady state flow in a constant cross-sectional area channel;
2. The fluid mixture is at thermal equilibrium everywhere;
3. Velocity difference between the liquid and vapor phases can be represented by a velocity slip ratio correlation.

The coolant can be subcooled liquid at inlet, requiring the solution of the following single-phase momentum and energy conservation equations:

$$G^2 \frac{d}{dz}\left(\frac{1}{\rho_L}\right) = -\frac{dP}{dz} - \rho_L g \sin\theta - \frac{\tau_w p_f}{A} \tag{III-1}$$

$$G\frac{d}{dz}(h_L) = -\frac{q'' p_H}{dz} - Gg\sin\theta \tag{III-2}$$

Two-phase flow is assumed to start when $h_L \geq h_f(P)$, where the mixture mass, momentum and energy conservation equations are:

$$\frac{d}{dz}\left[\rho_f U_f (1-\alpha) + \rho_g U_g \alpha\right] = 0 \tag{III-3}$$

$$\frac{d}{dz}\left[\rho_f (1-\alpha) U_f{}^2 + \rho_g \alpha U_g{}^2\right] = -\frac{dP}{dz} - \left[\rho_f (1-\alpha) + \rho_g \alpha\right] g\sin\theta - \frac{\tau_w p_f}{A} \tag{III-4}$$

$$\frac{d}{dz}\left[\rho_f U_f (1-\alpha)(h_f + \frac{U_f{}^2}{2} + gz\sin\theta) + \rho_g U_g \alpha (h_g + \frac{U_g{}^2}{2} + gz\sin\theta)\right] = \frac{q'' p_H}{A} \tag{III-5}$$

Consistent with assumption 3 above, the vapor and liquid mean velocities are related according to:

$$U_g / U_f = S \tag{III-6}$$

The closure relations for the above equations are now briefly described.

For liquid single-phase flow, the wall friction factor f is calculated using the Colebrook-White correlation (Colebrook, 1939), whereby

$$\tau_w = f_{Lo} \frac{G^2}{2\rho_L} \tag{III-7}$$

$$\frac{1}{\sqrt{f_{Lo}}} = 3.48 - 4\log_{10}\left[2\frac{\varepsilon}{D_H} + \frac{9.35}{\mathrm{Re}_{Lo}\sqrt{f}}\right] \tag{III-8}$$

For the two-phase flow conditions, the correlation of Beattie and Whalley (1982) was used, according to which Equation (III-6) and (III-7) apply provided that ρ_L is replaced with ρ_h and Re_{Lo} is replaced with Re_{TP}, where:

$$\rho_H = \alpha_h \rho_g + (1-\alpha_h)\rho_f \tag{III-9}$$

$$\mathrm{Re}_{TP} = GD_H / \mu_{TP} \tag{III-10}$$

$$\mu_{TP} = \alpha_h \mu_g + (1-\alpha_h)(1+2.5\alpha_h)\mu_f \tag{III-11}$$

$$\alpha_h = \frac{\alpha U_g}{\alpha U_g + (1-\alpha)U_f} \tag{III-12}$$

Adiabatic two-phase flow experiments have shown that the gas-liquid velocity slip is insignificant in bubbly and plug/slug flow regimes, while significant slip is likely in froth and annular flow regimes (Triplett et al, 1999a; 1999b). Little is known about liquid-vapor velocity slip during boiling in minichannels. For simplicity, the slip ratio is everywhere calculated using the correlation of Chisholm (Chisholm, 1972), which agrees with experimental data representing water boiling systems well (Whalley, 1996):

$$S = \left[1 - x(1-\rho_f/\rho_g)\right]^{1/2} \tag{III-13}$$

The numerical solution method for the above equations is now discussed.

The above conservation equations were expanded using appropriate thermodynamic relations, following the methodology described elsewhere (Ghiaasiaan et al., 1995), in order to derive a set of coupled ordinary differential equations in the form

$$\mathbf{A}\frac{d\mathbf{Y}}{dz} = \mathbf{C} \tag{III-14}$$

For the liquid single-phase region $\mathbf{Y} = (P, h_L)^T$, and for the vapor-liquid mixture $\mathbf{Y} = (P, U_f, \alpha)^T$. The resulting sets of ordinary differential equations were numerically integrated using the DVODE (Petzold and Hindmarsh, 1997) solver package, which offers a variable-order robust technique for the numerical solution of stiff systems. The water and steam properties were calculated using the property routines described in (Ghiaasiaan et al., 1995).

III.4 ANN-FPM Modeling and Results For Horizontal Annulus

III.4.1 Experimental Data

The CHF experimental data have been presented and discussed in detail in (Stoddard et al., 2002), and will be explained only briefly here.

The experiments were performed using water as the working fluid, in a horizontal, uniformly-heated annular test section with 6.45 and 7.77 mm inner and outer diameters, respectively. The heated segment of the test section was 18.5 cm long. The test section was part of a carefully designed and fully-instrumented flow loop capable of providing stable and well-controlled coolant flow rates, at desired pressures and temperatures, covering a wide range of test parameters. Four thermocouples were installed near the test section exit, three on the outer surface of the annular test section at 120^o angular

intervals, and one on the inner surface. The occurrence of CHF would cause an abrupt temperature rise in any of these thermocouples. In the experiments, as expected, CHF always occurred first at the test channel top, leading to CHF values considerably lower than the values expected for a vertical channel operating under similar local conditions.

Table III-2 is a summary of the experimental results. As noted, only 35 data points were generated covering the following parameter range: test section exit pressure: 0.344-1.034 MPa; coolant (water) mass flux: 100-380 $Kg/m^2 \cdot s$; wall heat flux: 0.231-1.068 MW/m^2; water inlet temperature: 30-65 ^oC.

Table III-2: Summary of CHF Data

Run Number	$T_{inlet}\,(^{o}C)$	$P_{exit}\,(kPa)$	Mass Flux $(kg/m^2 \cdot s)$	Heat Flux (MW/m^2)
1	30.1	690	207.74	0.4689
2	48.4	694	179.38	0.4409
3	65.1	688	187.34	0.4343
4	50.0	344	198.86	0.3940
5	50.2	1033	187.63	0.4986
6	30.0	689	106.28	0.3167
7	50.0	690	100.68	0.2625
8	64.5	692	99.19	0.2309
9	49.6	354	102.01	0.2392
10	50.1	1037	99.42	0.3606
11	31.8	695	291.15	0.7671
12	49.7	687	290.25	0.7668
13	65.8	690	293.57	0.5340
14	51.4	345	294.68	0.6209
15	49.2	1039	297.63	0.8004
16	29.8	692	151.16	0.3958
17	49.8	689	146.59	0.3383
18	65.3	691	150.97	0.3419
19	48.9	351	153.14	0.3031
20	50.1	1033	146.74	0.3861
21	30.6	694	248.22	0.6422
22	49.5	688	246.55	0.5818
23	65.6	689	241.67	0.5412
24	50.3	349	245.44	0.5302
25	49.4	1040	247.55	0.6867
26	31.4	700	338.46	0.8629
27	51.0	684	331.58	0.8348
28	63.9	710	328.99	0.7366
29	52.5	343	339.69	0.7716
30	49.8	1029	338.09	1.0142
31	32.2	705	375.14	1.0674
32	49.5	686	371.22	0.9253
33	61.9	717	366.80	0.7869
34	51.3	343	373.54	0.7786
35	49.2	1031	379.39	1.0686

III.4.2 The Artificial Neural Network

A schematic of the ANN that was designed and used is shown in Figure III.4. The commercial software Neuroshell 2 was used for the design and training of the ANN. The principles of ANNs have been described in numerous publications including (Maren, 1990; Anderson, 1995), and will not be repeated here - only the major characteristics of the designed ANN will be described. The ANN is feed-forward, and has three neuron layers. The neurons in the inlet layer have a piecewise linear activation function, while the neurons in the hidden and the output layers use the sigmoidal activation function. The back-propagation learning paradigm was used.

Two different ANN schemes were used. In one scheme, the input parameters to the ANN were Re_{fo}, x_e, and δ_F^*, the latter representing the local dimensionless average liquid film thickness in the annular two-phase flow regime, where:

$$\mathrm{Re}_{fo} = GD_H / \mu_f \tag{III-15}$$

$$\delta_F^* = \delta_F \sqrt{\tau_w / \rho_f} / \nu_f \tag{III-16}$$

In the second ANN scheme, the input parameters were Re_{fo}, x_e, and the Martinelli factor X_{tt} defined as:

$$X_{tt} = \left(\frac{1-x_e}{x_e}\right)^{0.9} \left(\frac{\mu_f}{\mu_g}\right)^{0.1} \left(\frac{\rho_g}{\rho_f}\right)^{0.5} \tag{III-17}$$

For both schemas, the output was the critical heat flux, non-dimensionalized as:

$$Bo_{CHF} = q''_{CHF} / (G * \hat{h}_{fg}) \tag{III-18}$$

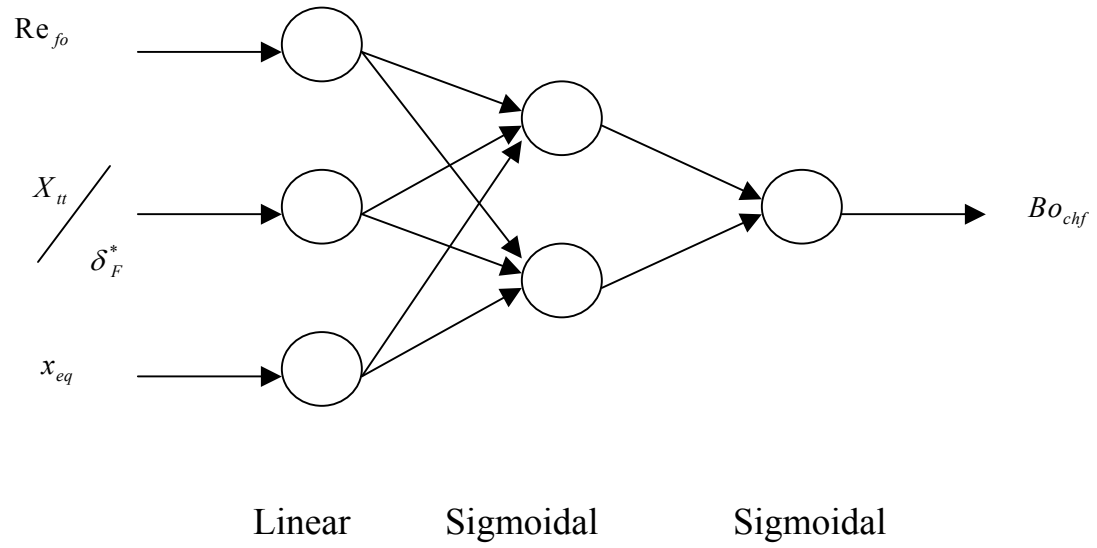

Figure III.4: Schematic of the neural network

The rationale for the selection of the above input parameters was as follows. We assume that CHF occurs due to the combined effects of local hydrodynamic processes and flow history. Furthermore, we hypothesize that the local hydrodynamic parameters predicted by the one-dimensional first-principle model, although unlikely to be accurate in comparison with their physical counterparts, are related to the hydrodynamic parameters of the modeled physical system through an (unknown) one-to-one mapping. Geometric parameters were not included since the modeled experimental data all represented the same geometry. Either of parameters δ_F^* and X_{tt} can be assumed to be a good indicator of conditions that can lead to disruption of the contiguous film and the occurrence of dryout. Parameter X_{tt}, furthermore, can account for the details of the two-phase flow regime. Parameters Re_{fo} and δ_F^* were of course properly normalized to render the orders-of-magnitude of all input parameters equal to one.

III.4.3 Results and Discussions

Training, calibration and testing of the ANNs were all based on the values of the above-described input parameters for the experimental data of Table III-2, as predicted by the afore-mentioned first-principle model. For training, 23 randomly selected data points were used, while calibration and testing were done using 7 and 5 data points, respectively. Training and testing were repeated a few times using different data points for each task. ANNs with 2, 3 and 4 hidden neurons were tried. In view of the small number of data points, our purpose was to find the smallest number of hidden neurons that would lead to adequate ANN performance, and that was achieved with 3 hidden neurons, where only one data point did not fall into 5% error range. For comparison purpose, a neural network using raw data including inlet temperature, channel exit pressure, and mass flux as inputs was also designed and trained. The comparison is given in Figure III.5, which shows that the neural network using raw data has a poor performance and there is no apparent generic relation between the raw data and the critical heat flux. Following completion of the training and testing, the trained ANNs were coupled with the first-principle model, and the coupled system was applied for parametric studies. In a hybrid ANN-FPM system the trained ANN should be applied over the entire boiling length of the modeled system in order to predict the local q''_{CHF}, and CHF occurs at the first point along the channel where the local heat flux exceeds the local q''_{CHF}. To provide for parametric calculations that were consistent with the experiments, however, only CHF at the exit of the simulated systems was considered.

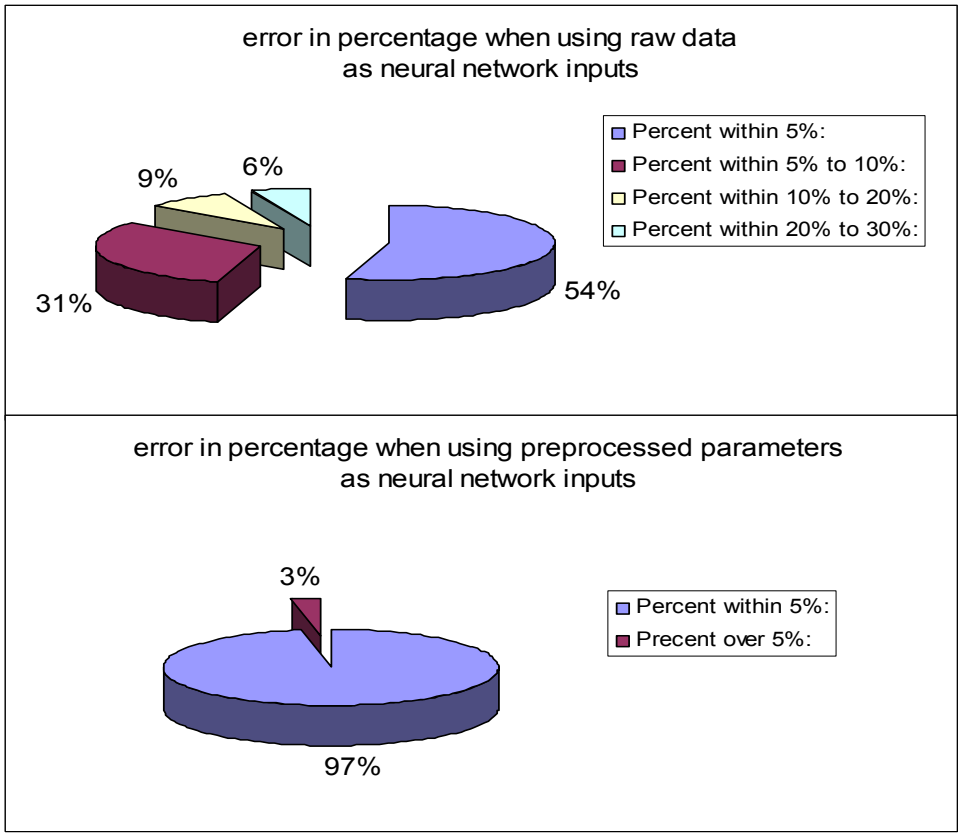

Figure III.5: Comparison of two neural network performances

Figures III.6 and III.7 compare the predictions of the hybrid model with experimental data. In Figure III.6, Re_{fo}, x_e, and δ_F^* are the input parameters for the ANN; and Re_{fo}, x_e, and the Martinelli factor X_{tt} are the ANN input parameters for Figure III.7. The agreement between model and data is very good, and each hybrid model provides smooth predictions of CHF that correctly account for the expected parametric trends. These data and model predictions, it should be emphasized, show the parametric

dependencies of CHF in a channel with a constant length-over-diameter ratio. Accordingly, q''_{CHF} monotonically increases with Re_{fo}. It also increases with increasing pressure and inlet subcooling.

Some parametric calculation results, obtained with the hybrid model that uses X_{tt} as an input to the ANN, are depicted in Figs. III.8 and III.9, where the effect of the heated annulus width on the predicted CHF is shown. In Fig. III.8, the geometric characteristics of the afore-mentioned experimental test section are all maintained, except for the outer diameter of the test section, D_o. The latter parameter was adjusted to provide an annulus width of 1 mm in a group of parametric runs, and 0.83 mm, in another group of runs. In Figure III.9, furthermore, the channel-heated length was assumed to be half the length of the afore-mentioned experimental test section. Artificial neural networks are in general not appropriate tools for extrapolation. The calculated results displayed in Figs. III.8 and III.9, however, include model predictions that were only slightly outside the range of parameters of the experimental data used for training the ANNs. Since the input parameters to the trained ANNs only consisted of local dimensionless parameters that did not include geometric dimensions, application of the hybrid model to horizontal annuli with slightly modified geometric dimensions may be justified, as long as the dimensionless input and output ANN parameters remain within the original data base. Only slight deviations of these dimensionless parameter ranges were allowed. According to Figs. III.8 and III.9, with $L/D_H = \text{constant}$, the hybrid model predicts an increasing q''_{CHF} with decreasing the annulus width. These predicted trends of course need to be verified experimentally before non-mechanistic models such as those proposed here can be applied outside their basic databases with confidence.

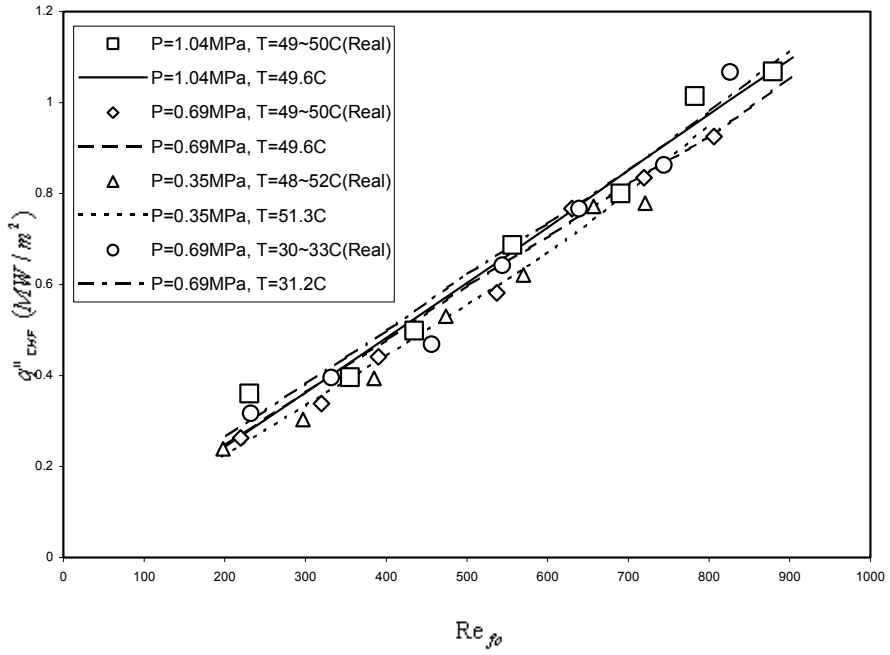

Figure III.6: Experimental data and the trained ANN predictions when δ_F^* was used as an input

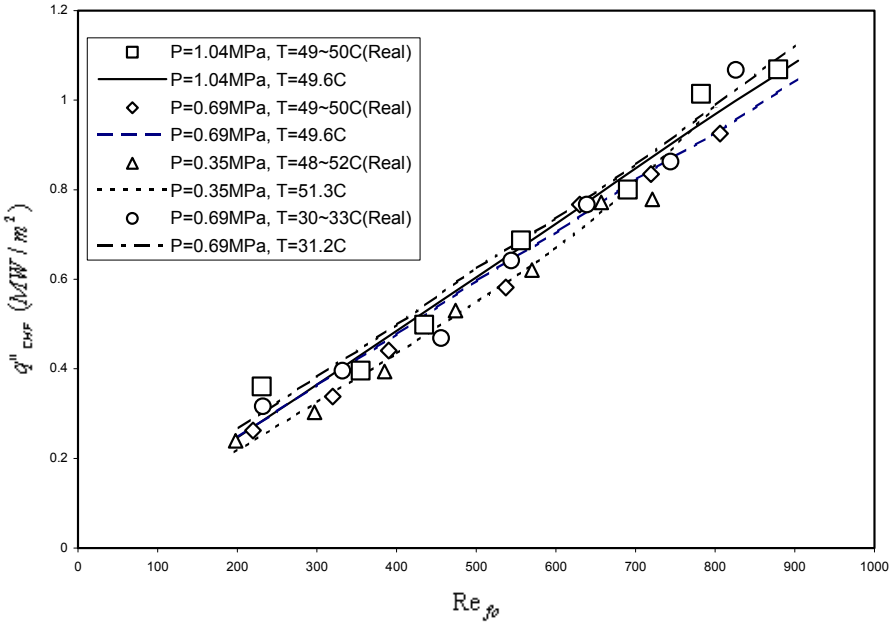

Figure III.7: Experimental data and the trained ANN predictions when X_{tt} was used as an input

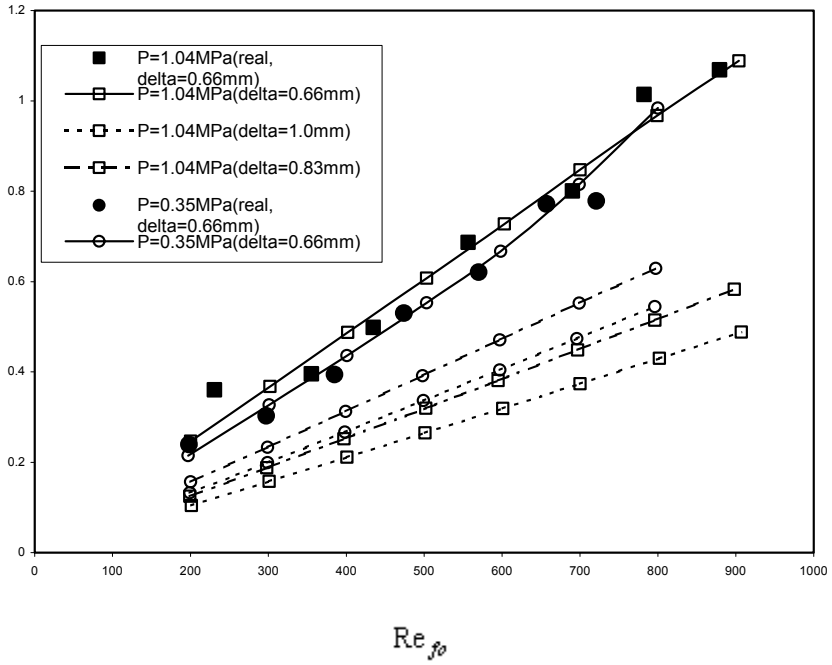

Figure III.8: Some parametric calculation results using the hybrid model with X_{tt} as a neural network input

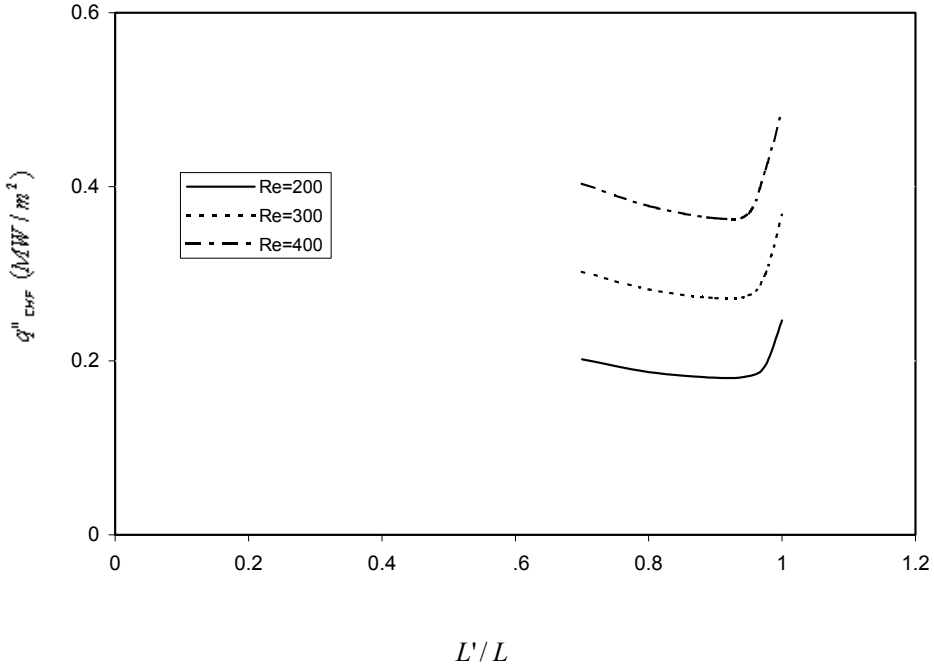

Figure III.9: calculation results for different tube length using the hybrid model with X_{tt} as a neural network input

III.5 ANN-FPM Modeling and Results For Mini-channels

III.5.1 Experimental Data

The dryout data associated with water flow in circular mini-channels (with diameters of around or slightly larger than 1 mm) in the PU-BTPFL CHF database (Hall and Mudawar, 1998) were used for model development and comparison.

III.5.2 The Artificial Neural Network

A schematic of the ANN that was designed and used is shown in Figure III.10. The commercial software Neuroshell 2 was used for the design and training of the ANN. The ANN is feed-forward, and has three neuron layers. The neurons in the inlet layer

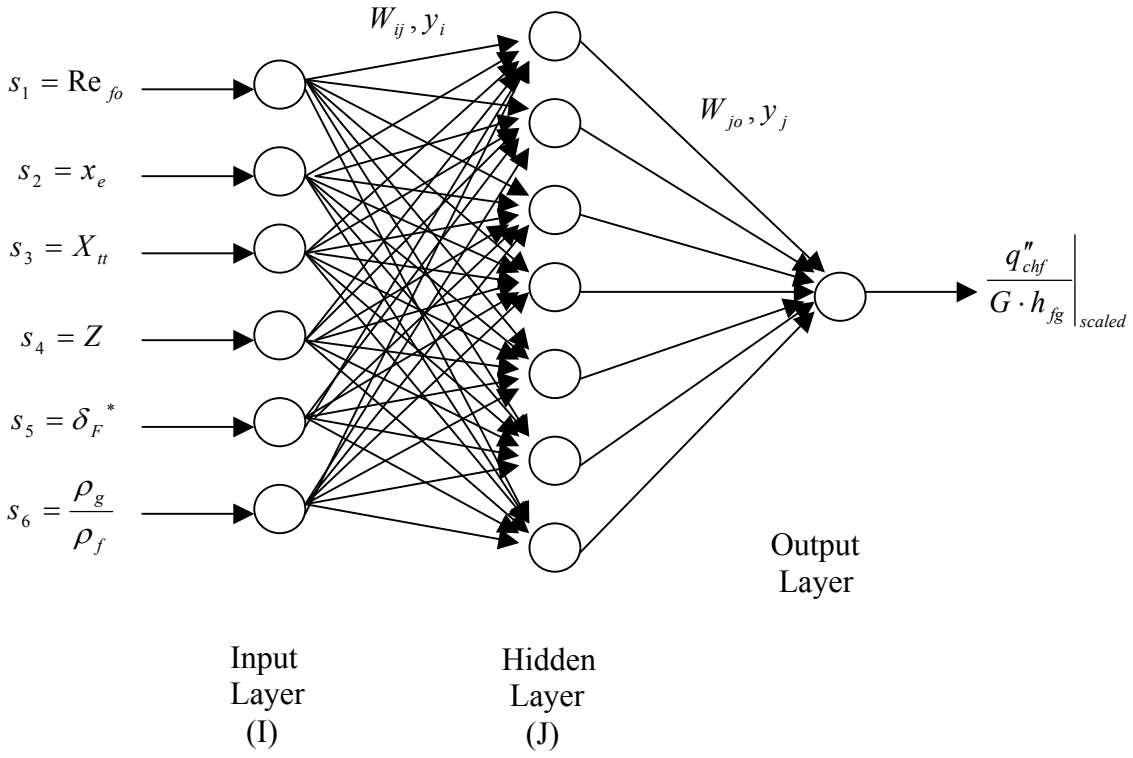

Figure III.10: Schematic of the artificial neural network

have a piecewise linear activation function, while the neurons in the hidden and the output layers use the sigmoidal activation function. The back-propagation learning paradigm was used.

Since dryout is of interest, the ANN input parameters should represent important characteristics of the annular two-phase flow regime at the vicinity of the dryout point. Dryout is caused by the disruption of the contiguous liquid film on the heated surface. The input parameters to the ANN were thus chosen to be Re_{fo}, x_e, X_{tt}, Z, ρ_g / ρ_f and δ_F^*, the latter representing the local dimensionless average liquid film thickness in the annular two-phase flow regime, where:

$$\mathrm{Re}_{fo} = GD_H / \mu_f \tag{III-19}$$

$$\delta_F^* = \delta_F \sqrt{\tau_w / \rho_f} / \nu_f \tag{III-20}$$

$$Z = \mu_f / [\sigma D \rho_f]^{\frac{1}{2}} \tag{III-21}$$

$$X_{tt} = \left(\frac{1-x_e}{x_e}\right)^{0.9} \left(\frac{\mu_f}{\mu_g}\right)^{0.1} \left(\frac{\rho_g}{\rho_f}\right)^{0.5} \tag{III-22}$$

The disruption of the contiguous liquid film, which leads to dryout, is strongly influenced by droplet impingement and entrainment phenomena in macro scale (Hewitt and Govan, 1990; Sugawara, 1990; Sugawara, 1990). The role of droplets in mini-channel dryout is not clear, however. Gu and Mudawar (2002) studied boiling and two-phase flow in 12 geometrically-similar parallel mini-channels with triangular cross-sections ($D_H \approx 195 \mu m$). Bubbly flow was hard to sustain in their experiments and slug flow, which developed shortly after boiling incipience, appeared to be the dominant

regime. The regime transitions were strongly influenced by the parallel-channel instability phenomenon, however, and oscillations between slug and annular-dispersed flow regime could be seen under high heat flux conditions. Dryout conditions were not approached in these tests, furthermore. On the other hand, adiabatic two-phase flow experiments with circular cross-section mini-channels do not definitely support the occurrence of significant droplet phenomena (Triplett et al., 1999a; 1999b). For simplicity, therefore, the film thickness, δ_F, was calculated assuming that all liquid was in the film. The output of the ANN is the critical heat flux, which is non-dimensionalized as:

$$Bo_{CHF} = q''_{CHF} / (G * \hat{h}_{fg}) \tag{III-23}$$

Parameters Re_{fo}, δ_F^*, x_e, and X_{tt} are used as input for the ANN since they are important for the annular flow regime hydrodynamics. Parameter Z is added in order to better account for the effect of liquid viscosity (Ahmad, 1973; Merilo, 1979). These parameters, together, are thus assumed to determine the conditions that would lead to the disruption of the contiguous liquid film. Parameters Re_{fo}, Z, and δ_F^* were of course properly normalized to render the orders-of-magnitude of all input parameters equal to one.

III.5.3 Results and Discussions

Training, calibration and testing of the ANN were all based on the values of the above-described ANN input parameters for the experimental data of Table III-1, as predicted by the afore-mentioned first-principle model. The total number of data points was 214. For training, 128 randomly selected data points were used, while calibration and

testing were done using 43 and 43 data points, respectively. Training and testing were repeated a few times using different data points for each task. ANNs with various number of hidden neurons were tried, with purpose of finding the number of hidden neurons that would lead to the best ANN performance, and that was achieved with 7 hidden neurons.

Table III-3 displays the values of the weight coefficients and bias parameters of the trained ANN, depicted schematically in Fig. III.10. The trained ANN calculated the scaled critical heat flux (between 0.1 and 0.9) from:

$$\left.\frac{q''_{CHF}}{Gh_{fg}}\right|_{scaled} = \left\{1+\exp\left[-\left(\sum_{j=1}^{N_J}(W_{jo}y_j)+d_{jo}\right)\right]\right\}^{-1},\ N_J = 7 \tag{III-24}$$

where y_j is the output of neuron j in the hidden layer, and is obtained from:

$$y_j = \left\{1+\exp\left[-\left(\sum_{i=1}^{N_I}(W_{ij}y_i)+d_j\right)\right]\right\}^{-1},\ N_I = 6 \tag{III-25}$$

where y_i, the output of neuron i in the input layer is found from:

$$y_i = \frac{s_i - s_{i,\min}}{s_{i,\max} - s_{i,\min}} \tag{III-26}$$

Prediction of the trained ANN are compared with the experimental data in Figures III.11(a) and III.11(b). Good agreement is evident, without any apparent systematic dependence of the discrepancy on data source. The mean and standard deviation of the following statistic were -11% and 44%, respectively:

$$\zeta = 1 - q''_{CHF,ANN} / q''_{CHF,\exp} \tag{III-27}$$

Table III-3: Values of weight coefficients and bias parameters for the trained artificial neural network

w_{ij}	i=1	i=2	i=3	i=4	i=5	i=6		d_j
j=1	1.785739	-0.12722	-0.99330	0.373166	-0.20679	0.463420		0.073745
j=2	2.575928	-0.94074	-1.58306	1.016416	-0.74226	0.765880		-0.35566
j=3	0.671711	-6.66186	-0.51020	7.11533	-2.08856	-3.54702		-1.13997
j=4	-9.71730	5.481012	0.802244	-1.69341	0.182384	-7.77232		-3.32172
j=5	2.869205	-1.21671	-1.75378	1.677428	-1.81993	1.220381		-1.10540
j=6	0.966522	-0.07374	-0.10125	0.087973	0.419783	0.450487		0.842642
j=7	6.527212	0.945040	-3.94147	5.442292	2.838725	5.818459		-2.42598
w_{jo}	j=1	j=2	j=3	j=4	j=5	j=6	j=7	d_{jo}
	0.798448	1.506487	4.650515	3.760493	2.023981	-0.03378	-3.49346	-0.59707

Following completion of the training and testing, the trained ANN was coupled with the first-principle model, and the coupled system was applied for parametric studies. In a hybrid ANN-FPM system the trained ANN should be applied over the entire boiling length of the modeled system in order to predict the local q''_{CHF}, and CHF occurs at the first point along the channel where the local heat flux exceeds the local q''_{CHF}. To provide for parametric calculations that were consistent with the experiments, however, only CHF at the exit of the simulated systems was considered.

Some parametric calculation results, obtained with the hybrid model, are now presented and discussed. The parametric results are generally consistent with known experimental trend. The experimental test sections of Roach et al. (1999) are used as the basis in these calculations. In all these calculations dryout occurs at channel exit.

The effect of channel inlet subcooling is depicted in Fig. III.12. Dryout heat flux increases with increasing inlet subcooling. It also evidently increases with mass flux. The dependence of the dryout heat flux on mass flux and pressure are also displayed in Fig. III.13. The dryout heat flux is reduced as the pressure is increased. Generally, when CHF

occurs under low local quality conditions, it is known to increase as mass flux is increased. This trend is reversed in common large channels when dryout takes place at high local qualities, however, (the "inverse mass flux effect" (Tong and Tang, 1997)), due to strong droplet entrainment caused by very high vapor velocity (Bennet et al., 1963; Griffel and Bonilla, 1965). As noted earlier, however, the present model is based on the assumption of insignificant droplet entrainment during annular flow in mini-channels, with appears to be consistent with adiabatic experimental data dealing with two-phase flow regimes in mini-channels (Triplett et al., 1999a; 1999b).

Figure III.14 depicts the effect of channel diameter on the dryout heat flux, as predicted by the model. Note that the abscissa in this figure is the channel diameter normalized with a reference diameter of 1.17 mm. The dryout heat flux increases as the channel diameter is increased. The dependence of CHF on channel diameter in small channels is complicated, and depends on quality. For CHF under locally-subcooled or $x_e \geq 0$ conditions (i.e., departure from nucleate boiling), q''_{CHF} increases as channel diameters is decreased (Bergles, 1962; Vandervort et al., 1994; Celata et al., 1993). This trend is reversed, however, for CHF occurring when $x_e > 0$ (Nariai et al., 1987; 1989).

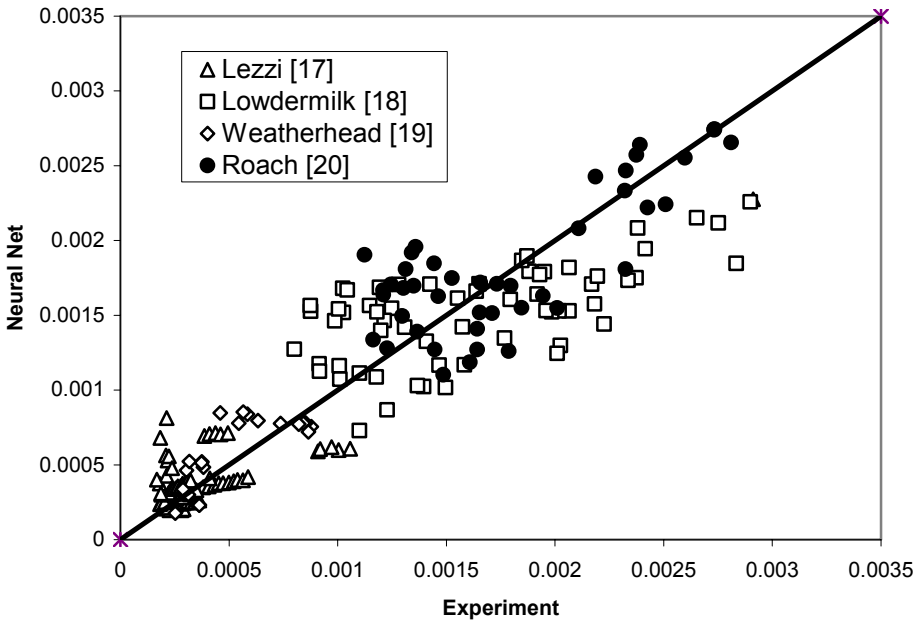

(a)

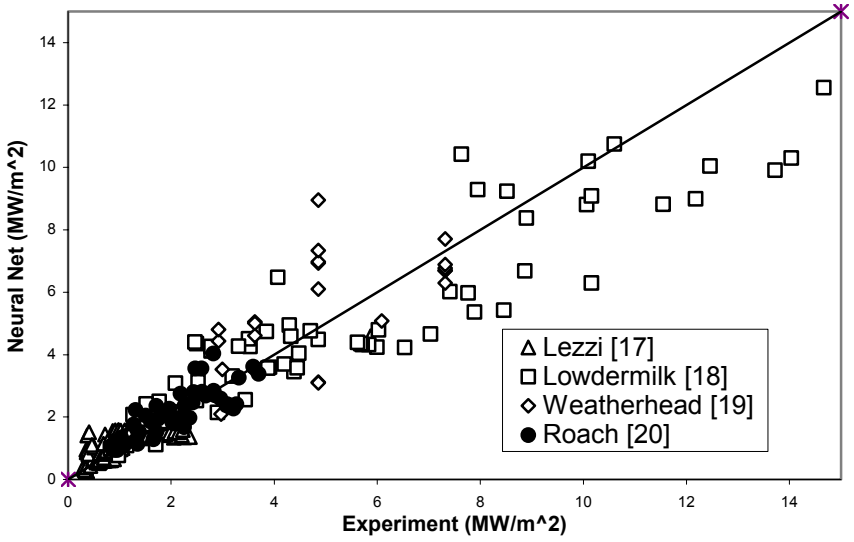

(b)

Figure III.11: Comparisons of model predictions with the experimental data: (a) in terms of q''_{CHF} / Gh_{fg}; (b) in terms of q''_{CHF}.

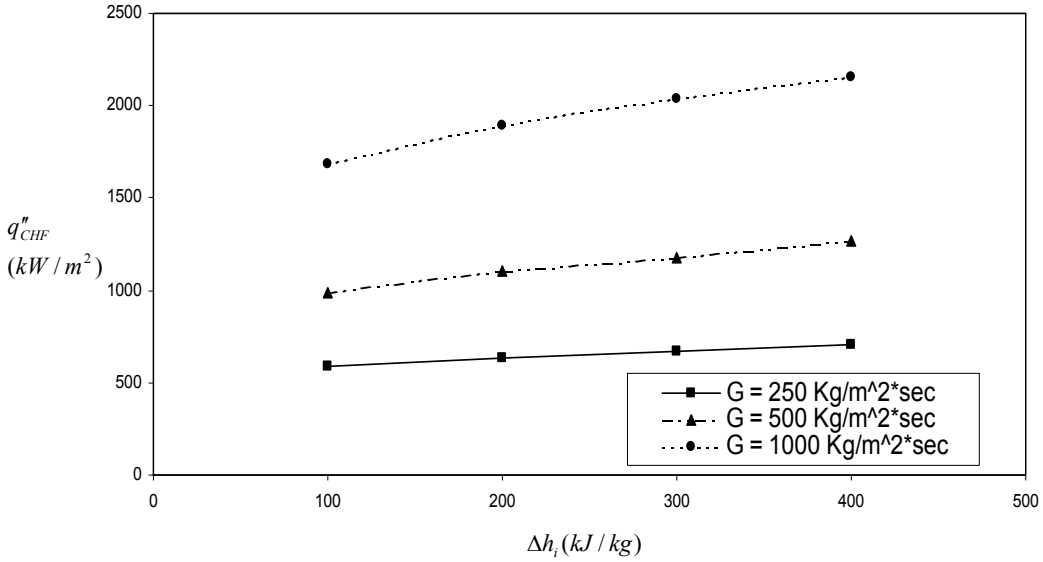

Figure III.12: Effect of inlet subcooling as predicted by the model (L=0.117m, D=1.17mm, P=1.0MPa) Note: q''_{CHF} = channel heat flux that gives CHF at exit.

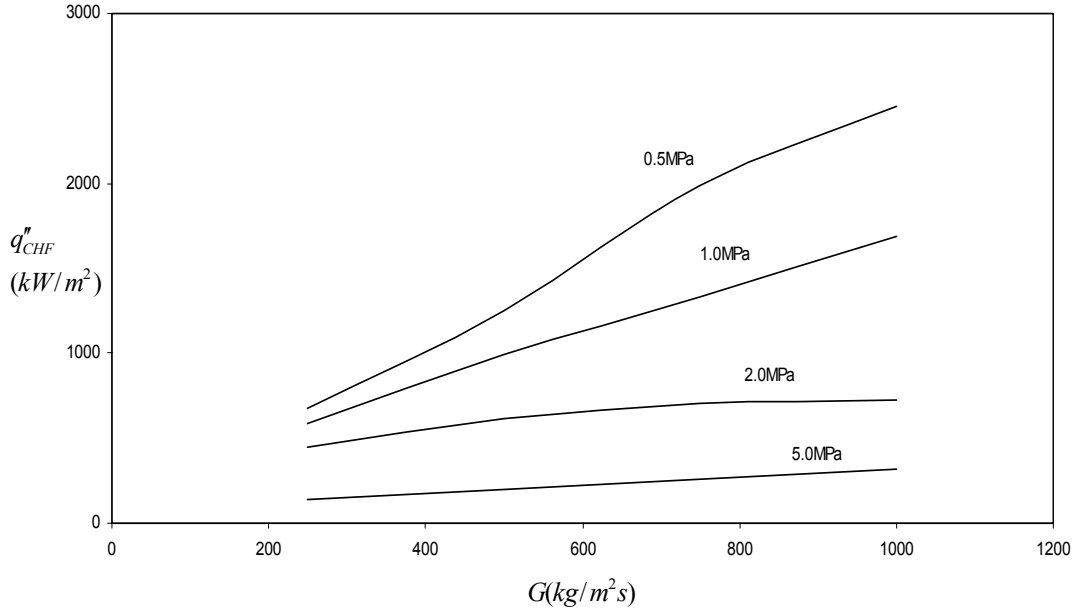

Figure III.13: Effects of mass flux and inlet pressure as predicted by the model (L=0.117m, D=1.17mm, $\Delta h_i = 100 kJ/kg$)

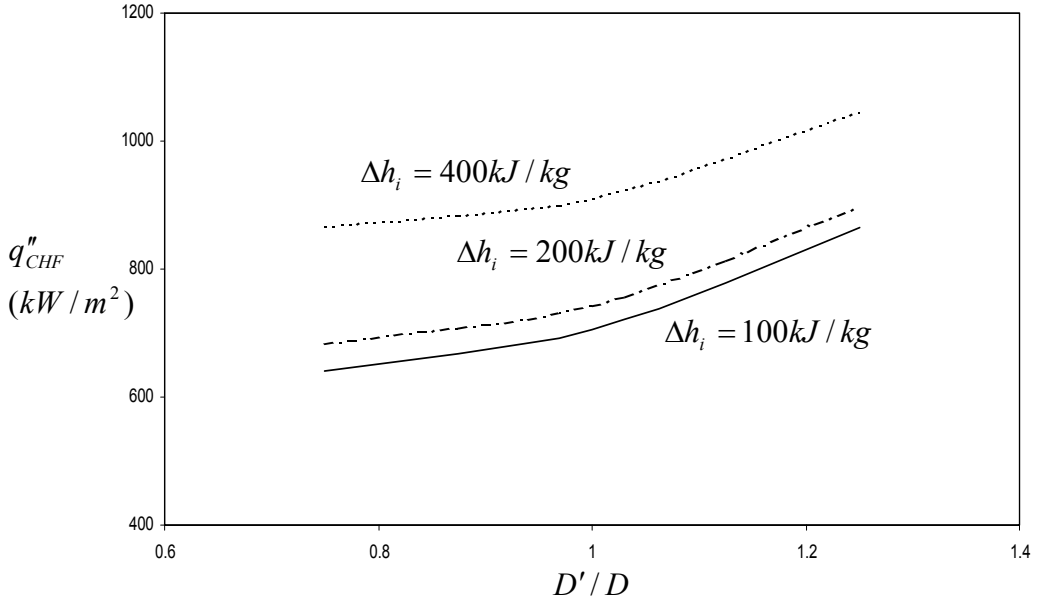

Figure III.14: Effect of diameter as predicted by the model
(L=0.117m, D=1.17mm, P=2.0Mpa, G= $0.5\times10^3\,kg/m^2s$)

III.6 Concluding Remarks

The applicability of the hybrid artificial neural network-first principle modeling (ANN-FPM) methodology to complex boiling and two-phase flow was addressed in this chapter. It was argued that the methodology may be particularly useful for multi-phase flow problems with phase change where the rate processes are poorly understood.

The methodology was first applied to a small set of experimental critical heat flux data previously obtained in a heated horizontal, thin annular test section cooled with water, with good results.

Next, another hybrid artificial neural network-first principle model (ANN-FPM) was developed for the prediction of dryout heat flux in mini-channels cooled with water. The first-principle component was based on a simple slip-flow modeling. The thermal and hydrodynamic parameters predicted by the first-principle component for the annular flow regime were used as input parameters for a three-layer, feed-forward, back-propagation neural network, the output of which was the boiling number at dryout. The dryout data associated with water flow in circular mini-channels (with diameters of around or slightly larger than 1 mm) in the PU-BTPFL CHF database (Hall and Mudawar, 1998) were used for model development and comparison. The developed ANN-FPM was shown to predict the data quite well. The developed model was also used for some parametric calculations.

APPENDIX IV

SOURCE CODE FOR CRITICAL HEAT FLUX PROBLEMS

```
$debug
c  This routine solves 1-d equations using homogeneous velocities
c  It is appropriate for NNW-CHF problem
c  The NNW program affect film flow subroutine
C     Uses DVODE integrator.
C
      PROGRAM SETUP
      implicit double precision (A-H,O-Z)
      EXTERNAL FUNC
      EXTERNAL FUNC2
      EXTERNAL FUNC3
      external func2f
      external jac
      double precision MV,MN
C
      COMMON /INPUT3/ MN,MV,WIDE,HIGH,tubel,din,dout,theta,PIN
C
      COMMON /INP1/ P1,GG,U1,XE1,QW,TIN,ZHEATS,ZHEATF,XEOSV
      COMMON /INP2/ ELOSSIRR,ELOSSREV,H1,akexp
      COMMON /INP4/ UF1,UG1,ALF1,P1ALF1,PSATVAP,slip, tauw,xlm,bo
C
      COMMON /PRP1A/ TG,RHOV,RHOG
      COMMON /PRP2/ RHOL,EMUL,CPL,EKL,PRNTL,RHOL2,beta
      COMMON /PRP2A/ EMUG,CPG,EKG,PRNTG,HF,HG,VFG,SIG
      COMMON /PRP3/ HFG,DHVDP,RAD
C
      COMMON /CALC/ ALPHA,ZPRNT,HENT,ITP,ZTWOPH,IVP,ZVAPPH
      COMMON /OSV/ IOSVFLG,ZOSV,IFLAG
C
      COMMON /CONSTS/ RGAS,G,PI
      common/hydro/ UG(395),UF(395),ALF(395),P1ALF(395)
C
C     --- FOR: INPUT PARAMETERS, CONSTITUENT RELATIONS, AND
C     ---      OTHER REQUIRED QUANTITIES.
      OPEN (5,FILE='chfDAT.DAT')
      OPEN (6,FILE='chfOUT.OUT')
C
C-----INPUT DATA
C
      idata=1
101   continue
      idata=idata+1
c      WRITE (6,*) 'PROGRAM INPUT DATA'
c      WRITE (6,2000)
c 2000 FORMAT(///,3x,'Molecular Weights of Noncondensibles',
c     1 ' and Water',/)
      READ (5,*) MN,MV,wide, high,din,dout,tubel,THETA
c      WRITE (6,2001)MN,MV
```

```
c 2001 FORMAT (3x,'MN = ',F10.4,5X,'MV = ',F10.4,/)
c      WRITE (6,2002) din,dout,tubel,theta
c 2002 FORMAT (3x,'Din  ',5x,'     Dout',3x,
c     1 'Height',3x,'Angle of Inclination',/,5x,F6.4,13x,F6.4,
c     1 8x,F6.4,5x,F10.4,/)
      READ (5,*) TIN,PIN,V1
      WRITE (6,*) 'Inlet Conditions'
      WRITE (6,2003) TIN,PIN,V1
 2003 FORMAT (5X,'Temperature',6x,'Pressure',8x,'Velocity',
     1 /,5x,'(Deg C)',10x,'(Pa)',15x,'(m/s)',/,5x,F10.6,3x,
     1 F15.6,3x,F10.6,/)
c---- QW=heat input rate per unit channel length
      READ (5,*) QW,ZHEATS,ZHEATF
c      WRITE (6,*) ' QW,ZHEATS,ZHEATF',QW,ZHEATS,ZHEATF
      write (6,2004) QW,ZHEATS,ZHEATF
 2004 format (/,2x,'Heat Input = ',e12.6, '  W/m',
     1       /,2x,' Heating starts at z = ',f8.6, ' m ',
     2       /,2x,' Heating ends at z = ',f8.6, ' m')
      READ (5,*) ELOSSIRR,ELOSSREV
c      WRITE (6,*) ' ELOSSIRR,ELOSSREV',ELOSSIRR,ELOSSREV
c      write (6,2005)  ELOSSIRR,ELOSSREV
c 2005 format (/,2x,' Inlet irreversible loss coefficient = ', f6.3,
c     3  /,2x,'Inlet reversible loss coefficient = ', f6.3)
      read (5,*) beta
c      write (6,*) 'beta = ', beta
c      write (6,2006) beta
c 2006 format (2x,'Thermal expansion coef. of liquid = ',1pe12.5,
c     1  ' 1/K' )
      read (5,*) zprnt
c      write (6,*) 'zprnt = ', zprnt
c      Write (6,2007) zprnt
c 2007 format (2x,' Print interval = ',1pe12.5, ' m')
      area=3.1416*(din**2)/4.
      perim=3.1416*din
      ZSTART = 0.0
      zinit = 0.0
      ITP = 0
      ivp=0
      IFLAG=0
      ztp=1.e8
      ztwoph=1.e8
      ZVAPPH=1.E8
      NUMPRNT=((TUBEL-ZSTART)/ZPRNT)+1
      QWORIG = QW
      V1ORIG = V1
      U1 = V1
      CALL MARCH(PEX)
      write(*,*) 'itp=', itp
      IF (ITP.EQ.0) GO TO 505
      CALL MARCH2(PEX, xe,rel)
      write(*,*) 'ivp=', ivp
      IF (IVP.EQ.0) GO TO 505
      CALL MARCH3(PEX)
 505  CONTINUE
      del=area*(1.-alpha)/perim
      vstr=dsqrt(tauw/rhol)
```

```
      delstr=rhol*del*vstr/emul
      zboil=emul/(dsqrt(sig*rhol*din))
      rhogl=RHOG/RHOL
      write (6,*) ' Tauw=',tauw
       write (6,*) ' del=',del
      write (6,*) ' vstr=',vstr
       write (6,*) ' alpha=',alpha
      write (6,*) ' delstr=',delstr
      write (6,*) ' U_g=', ug1
      write (6,*) ' U_f=', ufl
      write (6,*) 'slip ratio =', slip
      write (6,*) ' Bo=', bo
      write (6,*) ' Re=',rel
      write (6,*) ' xe=',xe
      write (6,*) 'X_LM=', xlm
      write (6,*) 'zboil=', zboil
      write (6,*) 'delstr=', delstr
      write (6,*) 'rhogl=', rhogl
      call nrlfive(rel,xe,xlm,zboil,rhogl,qchf)
      write (6,*) 'from netfive: dimensionless qchf = ',qchf
      qchf=qchf*(gg*hfg)*0.000001
      qdd=qw/perim*0.000001
      write (6,*) 'for netfive: qdd (real),and qchf=',qdd,qchf
c     call nrlxlm (rel,xlm,xe,qchf)
c     qchf=qchf*(gg*hfg)*0.000001
c     qdd=qw/perim*0.000001
      write (*,*) 'for netfive: qdd (real),and qchf=',qdd,qchf
c      write (6,*) 'for xlm: qdd (real),and qchf=',qdd,qchf
       if (idata.lt.1000) go to 101
      END
C=======================================================================
C
      SUBROUTINE MARCH (PEXIT)
C
      IMPLICIT double precision (A-H,O-Z)
      EXTERNAL FUNC
      external jac
      DOUBLE PRECISION ATOL,Rpar,rtol,RWORK,ZINIT,ZIP,YIN
      double precision MV,MN
C
      COMMON /INPUT3/ MN,MV,wide,high,tubel,din,dout,theta,PIN
C
      COMMON /INP1/ P1,GG,U1,XE1,QW,TIN,ZHEATS,ZHEATF,XEOSV
      COMMON /INP2/ ELOSSIRR,ELOSSREV,H1,akexp
      COMMON /INP4/ UF1,UG1,ALF1,P1ALF1,PSATVAP,slip, tauw,xlm,bo
      COMMON /OTHER/TINK
C
      COMMON /PRP1A/ TG,RHOV,RHOG
      COMMON /PRP2/ RHOL,EMUL,CPL,EKL,PRNTL,RHOL2,beta
      COMMON /PRP2A/ EMUG,CPG,EKG,PRNTG,HF,HG,VFG,SIG
      COMMON /PRP3/ HFG,DHVDP,RAD
      COMMON /OSV/ IOSVFLG,ZOSV,IFLAG
      COMMON/OUT/zstp(400),h(400),p(400),ZSTP2(400),ZSTP3(400)
      COMMON/OUT3/H3(400),P3(400)
C
      COMMON /CALC/ ALPHA,ZPRNT,HENT,ITP,ZTWOPH,IVP,ZVAPPH
```

```
      COMMON /CALC2/ATOL(4),RWORK(100),IWORK(35)
C
      COMMON /CONSTS/ RGAS,G,PI
C
      common /hydro/ UG(395),UF(395),ALF(395),P1ALF(395)
      DIMENSION YIN(2),YOUT(2),EU(2),EL(2),dydz(2)
      DATA RGAS,G,PI/8314.34,9.81,3.14159265/
C
      TINK = TIN + 273.15
C-------------------------------------------------------------
C -------------------- MAIN PROGRAM--------------------------
C
C
C     --- SET INITIAL CONDITIONS (INLET-PARAMETERS) ---
C           CHANNEL CONSISTS OF THREE REGIONS WITH THREE DIFFERENT
C           FLOW REGIMES - COMPRESSED LIQUID,TWO-PHASE LIQUID/VAPOR,
C           AND SATURATED VAPOR
C
C-------------------------------------------------------------
C           FIRST REGION            -  COMPRESSED LIQUID
C-------------------------------------------------------------
C
C------INLET FLUID IS COMPRESSED LIQUID-----------------------
C
C     CALCULATE THE PRESSURE DROP AT THE TUBE INLET
C     FIND THE INLET DENSITY (AT TSAT)
C     THE FUNCTION VFT RETURNS DENSITY IN KG/M3.
C
      VFIN = VFT(TINK)
      RHOMS = VFIN
C
C     CALCULATE LOSSES
C
      ELOSS = ELOSSIRR+ELOSSREV
      GG = U1*RHOMS
c     write (*,*) ' G at the beginning ',gg
C     PRESSURE LOSS ENTERING CHANNEL
      PINF = PIN
      P1 = PINF - (ELOSS*(GG**2)/(2.0*RHOMS))
C
C     SET INITIAL VALUES OF OTHER VARIABLES; P AND H
C
C     CALCULATE THE EQUILIBRIUM QUALITY FROM ENTHALPY
C     FIND THE TUBE INLET ENTHALPY, NEED PROPERTIES AT INFINITY
      PSATS = PSATF(TINK)
      CALL PRPSAT(PSATS,TSAT1,RHOLS,EMUL,CPL,EKL,PRNTL,
     1        EMUG,CPG,EKG,PRNTG,HFINF,HG,VFG,HFG,SIG,DHVDP,CPA,HA)
      RHOL = RHOLS
      HINF = HFINF + (P1-PSATS)/RHOLS
      HIN = HINF - (0.5*ELOSSIRR*((GG/RHOL)**2))
C
C     ASSUME THE SUBCOOLED ENTHALPY REMAINS CONSTANT
C     AND COMPARE CURRENT ENTHALPY WITH THIS TO DETERMINE
C     ONSET OF TWO-PHASE FLOW
C
      HENT = HIN
```

```
      XE1 = (HIN - hfpsat(p1/1.e5))/HFG
      H1 = HIN
C
      ZSTART = 0.0
      IOSVFLG = 0
C
      NEQ = 2
C
      YIN(1) = H1
      YIN(2) = P1
C
C---------------------------------------------------------------------
C-----------------PREPARATION FOR SOLVING ODE
C----------------------INPUT FOR DVODE
C---------------------------------------------------------------------
C
      write (6,125)
  125 format (//,3x,'Liquid Single Phase Results',/,5x,'    z (m)   '
     1  '   T (K)     P (Pa)     Xeq (--)   ',/)
      ZSTPUP = 0.0
      NUMPRNT=((TUBEL-ZSTART)/ZPRNT)+1
      DO 107 I=1,NEQ
      EU(I) = 0.0
      EL(I) = 0.0
      dydz(i)=0.0
  107  CONTINUE
C
C------------PRINTING LOOP-------------------------------------
C
      z=0.
      xeq=(h1-hfpsat(p1/1.e5))/hfg
      zstp(1)=zprnt
      DO 41 ILOOP = 1,NUMPRNT
      jj = iloop
c      if (jj.eq.1) write (6,126) z,tink,pin,xeq
  126 format (5x, f8.5, 2x, f7.2,2x,1pe12.4,2x,1pe12.4)
c      H(JJ)=H1
c      P(JJ)=P1
      if (jj.gt.1) then
       ZSTP(JJ)= ZSTPUP
       Z = ZSTP(JJ)
      endif
C
C------------CALCULATION LOOP-----------------------------------
C
C     SET UP PARAMETERS FOR DVODE SOLVER
C
      ITOL = 1
      RTOL = 1.0D-13
      ATOL(1) = 1.0D-13
      ATOL(2) = 1.0D-13
      ITASK = 1
      ISTATE = 1
      IOPT = 0
      LRW = 100
      LIW = 35
```

```
      MF = 22
      ZIP = ZINIT + ZPRNT
C
      CALL dvode(FUNC,NEQ,YIN,ZINIT,ZIP,ITOL,RTOL,ATOL,ITASK,
     1                  ISTATE,IOPT,RWORK,LRW,IWORK,LIW,JAC,mf,rpar,ipar)
C
C     IDENTIFY WHETHER THE FLOW IS 2-PHASE YET
C     IF SO, GO BACK TO THE MAIN PROGRAM AND INTO
C     THE MARCH 2 SUBROUTINE.         MUST RETAIN Z ALONG TUBE
C     FOR NEXT PART OF PROGRAM.
c
C     CHECK TO SEE IF THE FLOW IS TWO-PHASE
      pb=p1/(1.e5)
      hfsat=hfpsat(pb)
      H1 = YIN(1)
      P1 = YIN(2)
      x=(h1-hfsat)/hfg
      if(h1.gt.hfsat) then
      tg=tsatf(pb)
      rhog=(1.e3)/vgpt(pb,tg)
      alf1=x/(x+((rhog/rhol)*(1.-x)))
      if (alf1.ge.0.0025) then
       itp=1
       ztwoph=zip
      write (6,128)zip
  128 format (/4x,' **  Boiling Started at z = ', f7.4, ' (m)')
       go to 626
      endif
      endif
      ZSTPUP = ZIP
      zinit = zip
      DO I=1,NEQ
      YOUT(I) = YIN(I)
      ENDDO
      H1 = YIN(1)
      P1 = YIN(2)
      H(JJ)=YOUT(1)
      P(JJ)=YOUT(2)
      ZSTP(JJ) = ZIP
c  estimate the local water temperature
      pb=p1/(1.e5)
      temp=tsatf(pb)-273.15-1.
      call cplt (pb,temp,cpl)
      cpl=cpl*1000.
      tl=tsatf(pb)-(hf-h1)/cpl
      write (6,129) zip,tl,p1,x
  41   CONTINUE
      pexit=p(jj)-((akexp*(gg**2))/rhol2)
      IF (ZIP.GE.TUBEL) P(JJ) = PEXIT
  626  CONTINUE
c  recalculate velocity using saturated liquid density, for consistency
      p1alf1=p1
      rho2p=(rhog*alf1)+rhol*(1.-alf1)
      u1=gg/rho2p
      UG1 = U1*1.001
      UF1 = U1*0.999
```

```
      RETURN
  129 format (5x, f8.5, 2x, f7.2,2x,1pe12.4,2x,1pe12.4)
      END
C-----------------------------------------------------------------------
C                              SUBROUTINE MARCH2
C
C
C                    CALCULATIONS FOR TWO-PHASE FLOW REGIME
C
C
      SUBROUTINE MARCH2 (PEXIT, xe,rel)
C
      IMPLICIT double precision (A-H,O-Z)
      external func2
      external func2f
      external jac
      DOUBLE PRECISION ATOL,Rpar,rtol,RWORK,ZIP,zipend,YIN2
      double precision MV,MN
C
      COMMON /INPUT3/ MN,MV,wide,high,tubel,din,dout,theta,PIN
C
      COMMON /INP1/ P1,GG,U1,XE1,QW,TIN,ZHEATS,ZHEATF,XEOSV
      COMMON /INP2/ ELOSSIRR,ELOSSREV,H1,akexp
      COMMON /INP4/ UF1,UG1,ALF1,P1ALF1,PSATVAP,slip, tauw,xlm,bo
      COMMON /OTHER/TINK
C
      COMMON /PRP1A/ TG,RHOV,RHOG
      COMMON /PRP2/ RHOL,EMUL,CPL,EKL,PRNTL,RHOL2,beta
      COMMON /PRP2A/ EMUG,CPG,EKG,PRNTG,HF,HG,VFG,SIG
      COMMON /PRP3/ HFG,DHVDP,RAD
      COMMON /OSV/ IOSVFLG,ZOSV,IFLAG
      COMMON/OUT/zstp(400),h(400),p(400),ZSTP2(400),ZSTP3(400)
      COMMON/OUT3/H3(400),P3(400)
      COMMON /CALC2/ATOL(4),RWORK(100),IWORK(35)
C

      COMMON /CALC/ ALPHA,ZPRNT,HENT,ITP,ZTWOPH,IVP,ZVAPPH
C
      COMMON /CONSTS/ RGAS,G,PI
C
      common /hydro/ UG(395),UF(395),ALF(395),P1ALF(395)
      DIMENSION YIN2(8),YOUT2(8),EU(8),EL(8)
      DIMENSION DYDZ2(8)
      DATA RGAS,G,PI/8314.34,9.81,3.14159265/
C-------------------------------------------------------------
C ---------- MAIN PROGRAM----------
C
C
C     --- SET INITIAL CONDITIONS (INLET-PARAMETERS) ---
C           CHANNEL CONSISTS OF THREE REGIONS WITH THREE DIFFERENT
C           FLOW REGIMES - COMPRESSED LIQUID, SATURATED LIQUID, AND
C           TWO-PHASE LIQUID/VAPOR
C
C-------------------------------------------------------------
C           SECOND REGION        -  TWO-PHASE FLOW
C-------------------------------------------------------------
```

```
C
C------ INLET FLUID IS TWO-PHASE FROM FIRST PART OF PROGRAM --
C
C
      area=3.1416*(din**2)/4.
      perim=3.1416*din
c     perim=2.*(wide+high)
      dh=4.*area/perim
C
C     CONVERT UNITS TO KG-M-S SYSTEM
C     PRESSURE IS IN PASCALS
C
C
C     MUST USE PROPERTIES AND Z LOCATION FROM FIRST PART
C
      HNEW = h1
      PNEW = p1
      ZLOC = ZTWOPH
C
C     CALCULATE THE EQUILIBRIUM QUALITY FROM ENTHALPY AND PRESSURE
C
      PSATS = PNEW
C
      CALL PRPSAT(PSATS,TSAT1,RHOf,EMUL,CPL,EKL,PRNTL,
     1         EMUG,CPG,EKG,PRNTG,HF,HG,VFG,HFG,SIG,DHVDP,CPA,HA)
C
C      CALCULATE THE QUALITY AT THIS POINT
C
      XE1 = (HNEW-HF)/HFG
C     BEGIN 2-PHASE REGION AT ALPHA = 1E-3
C     first find alfa
      slip=ug1/uf1
      alf1=xe1/(xe1+((rhog*slip/rhol)*(1.-xe1)))
      if(alf1.lt.0.001) alf1=0.001
C
C     INITIALIZE VARIABLES FROM FIRST PART
C
      ZSTART = ZLOC
      NEQ = 4
      YIN2(1) = p1
      YIN2(2) = UG1
      YIN2(3) = UF1
      YIN2(4) = ALF1
C
C-------------------------------------------------------------------
C-----------------PREPARATION FOR SOLVING ODE
C---------------------INPUT FOR RKAMS
C-------------------------------------------------------------------
C
      write (6,125)
  125 format (3x,'Boiling Region Results',/,7x,
     1  'z (m)     P (Pa)      Xeq (--)     Void (--)     Ug (m/s)  ',
     2  '      Uf (m/s)'/)
      ZSTPUP2 = ZLOC
      numprnt=((tubel-zstart)/zprnt)+1
c
```

```
C             SETUP PARAMETERS FOR DVODE SOLVER
C
      ITOL = 1
      RTOL = 1.0D-13
      ATOL(1) = 1.0D-13
      ATOL(2) = 1.0D-13
      ITASK = 1
      ISTATE = 1
      IOPT = 0
      LRW = 100
      LIW = 35
      MF = 22
      DO 107 I=1,NEQ
      EU(I) = 0.0
      EL(I) = 0.0
      dydz2(I)=0.0
 107  CONTINUE
C
C------------PRINTING LOOP---------------------------------------
C
      z=ZLOC
      zstp2(1)=zprnt + ZLOC
      DO 41 ILOOP = 1,NUMPRNT
      JJ = ILOOP
      P1ALF(JJ)=P1ALF1
      UG(JJ)=UG1
      UF(JJ)=UF1
      ALF(JJ)=ALF1
      if (jj.gt.1) then
      ZSTP2(JJ)= ZSTPUP2
      Z = ZSTP2(JJ)
      endif
      ZIP = Z
      zipend = z+zprnt
C
C------------CALCULATION LOOP-----------------------------------
c
c     CALL DVODE SOLVER
c
      CALL dvode(FUNC2,NEQ,YIN2,Zip,ZIPEND,ITOL,RTOL,ATOL,ITASK,
     1                   ISTATE,IOPT,RWORK,LRW,IWORK,LIW,JAC,mf,rpar,ipar)
c
      pb=yin2(1)/1.e5
      psaths = yin2(1)
      CALL PRPSAT(PSAThs,TSAT1,RHOf,EMUL,CPL,EKL,PRNTL,
     1        EMUG,CPG,EKG,PRNTG,HF,HG,VFG,HFG,SIG,DHVDP,CPA,HA)
      tg=tsatf(pb)
      rhog=1.e3/vgpt(pb,tg)
      xe=rhog*ug1*alf1
      xe=xe/(xe+(rhol*uf1*(1.-alf1)))
c     if ((xe.gt.0.2).and.(yin2(4).gt.0.95)) then
      if ((xe.gt.0.9).and.(yin2(4).gt.0.95)) then
c the above on August 02
       write (6,127) zipEND
  127  format (/,3x,'Switch to Film Flow at z = ', f7.4,'(m)'/)
       go to 1997
```

```
      endif
      ZSTPUP2 = ZIPEND
      DO I=1,NEQ
      YOUT2(I) = YIN2(I)
      ENDDO
      P1ALF1 = YIN2(1)
      UG1 = YIN2(2)
      UF1 = YIN2(3)
      ALF1 = YIN2(4)
      gmass=rhol*uf1*(1.-alf1)+rhog*ug1*alf1
      write (6,128) zipEND,p1alf1,xe,alf1,ug1,uf1
  128 format (3x,f8.5,2x,1pe12.4,2x,1pe12.4,2x,1pe12.4,2x,1pe12.4
     1    ,2x,1pe12.4,1x)
      P1ALF(JJ)=YOUT2(1)
       UG(JJ)=YOUT2(2)
            UF(JJ)=YOUT2(3)
             ALF(JJ) = YOUT2(4)
      ZSTP2(JJ) = ZIPEND
c
c  Now check and see if chf has happened, using the trained neural network
c
      xlm=((1.-xe)/xe)**0.9
      xlm=xlm*((emul/emug)**0.1)*((rhog/rhol)**0.5)
      write(*,*) 'gg=', gg
      write(*,*) 'dh=', dh
      rel=gg*dh/emul
      zboil=emul/(dsqrt(sig*rhol*dh))
      bo=9.81*(rhol-rhog)*(dh**2)/sig
c  Set the upper limit on Xlm from experiments
c      xlmmax=4.15e-5
c      write (6,619)  xlm, rel, zboil, bo
619   format (1x,'xlm,rel=',2e12.5,2x,'zboil,Bo=',2e12.5)
c      if (xlm.gt.xlmmax) go to 41
c       call neural (xlm, rel, bo, zboil,qchf)
c       qchf=qchf*(hfg*gg)
 620  FORMAT ('Z=',e9.4,2x,'PRESSURE=',e14.6,2x,/,
     1           'GAS VELOCITY=',e14.6,2x 'LIQUID VELOCITY=',e14.9,2x,/,
     1      'VOID FRACTION=',e9.4,/)
c      qchfl=qchf*perim
c      write (6,625) qchf,qchfl
c      write (*,625) qchf,qchfl
 625  format (3x,' Qchf = ', 1pe13.5,1x,'W/m2  Qchfl='1pe13.5,' W/m')
c      if (qchfl.lt.qw) then
c       write (6,628) z, Qchfl
 628  format (2x, 'CHF Happened at z=',f8.4, 1x, 'Qchfl=', 1pe13.5)
c      stop
c      endif
 41   CONTINUE
C
C      CALCULATE THE PRESSURE LOSS AT CHANNEL EXIT IF NEEDED
C
      AKEXP = 0.5
      ALPHA = ALF1
      PHIEXP = ((((1.0-Xe)**2)/(1.0-ALPHA))+(RHOF*(Xe**2))
     *             /(RHOG*ALPHA))
      PEXIT = P1alf1-(PHIEXP*AKEXP*(GG**2)/(RHOF))
```

```
      WRITE (6,655) PEXIT
 655  FORMAT ('PEXIT=',e9.3)
      return
c  Now we are in the high-quality film evaporation region
 1997 CONTINUE
      zstrt=zipEND
      neq=3
      yin2(1)=p1alf1
      yin2(2)=ug1
      yin2(3)=xe
      write (6,1251)
 1251 format (3x,'Film Region Results',/,7x,
     1  'z (m)     P (Pa)      Xeq (--)     Void (--)     Ug (m/s)  ',
     2  '      Uf (m/s)'/)
      ZSTPUP2 = ZipEND
      numprnt=((tubel-zstart)/zprnt)+1
c
c     Set up parameters for DVODE solver
c
      ITOL = 1
      RTOL = 1.0D-13
      ATOL(1) = 1.0D-13
      ATOL(2) = 1.0D-13
      ITASK = 1
      ISTATE = 1
      IOPT = 0
      LRW = 100
      LIW = 35
      MF = 22
      DO 1071 I=1,NEQ
      EU(I) = 0.0
      EL(I) = 0.0
      dydz2(I)=0.0
 1071  CONTINUE
C
C------------PRINTING LOOP---------------------------------------
C
      zstp2(1)=zprnt + Zip
      DO 141 ILOOP = 1,NUMPRNT
      JJ = ILOOP
      if (jj.gt.1) then
      ZSTP2(JJ)= ZSTPUP2
      Z = ZSTP2(JJ)
      endif
      ZIP = Z
      ZIPEND = Z+ZPRNT
C
C------------CALCULATION LOOP-----------------------------------
c
C     CALL dvode SOLVER
C
      CALL dvode(FUNC2f,NEQ,YIN2,ZIP,ZIPEND,ITOL,RTOL,ATOL,ITASK,
     1                  ISTATE,IOPT,RWORK,LRW,IWORK,LIW,JAC,mf,rpar,ipar)
C--------
      gmass=rhol*uf1*(1.-alf1)+rhog*ug1*alf1
      pb=yin2(1)/1.e5
```

```
      tg=tsatf(pb)
      P1ALF1 = YIN2(1)
      UG1 = YIN2(2)
      xe = YIN2(3)
      YIN2(4)=alf1
      if (xe.gt.0.999) then
       write (6,1271) zipEND
 1271  format (/,3x,'Complete Evaporation at z = ', f7.4,'(m)'/)
       ivp = 1
      psatvap = p1alf1
      zvapph  = ZIPEND
       go to 2997
      endif
      ZSTPUP2 = ZIPEND
      gmass=rhol*uf1*(1.-alf1)+rhog*ug1*alf1
c      write (6,1281) zipEND,p1alf1,xe,alf1,ug1,uf1
 1281 format (3x,f8.5,2x,1pe12.4,2x,1pe12.4,2x,1pe12.4,2x,1pe12.4
     1    ,2x,1pe12.4,1x)
      ZSTP2(JJ) = ZIPEND
1620   FORMAT ('Z=',e9.4,2x,'PRESSURE=',e14.6,2x,/,
     1          'GAS VELOCITY=',e14.6,2x 'LIQUID VELOCITY=',e14.9,2x,/,
     1          'VOID FRACTION=',e9.4,/)
c
c  Now check and see if chf has happened, using the trained neural network
c  This part needs updating, if meant to be used. Need to call neural2 now
c      xlm=((1.-xe)/xe)**0.9
c      xlm=xlm*((emul/emug)**0.1)*((rhog/rhol)**0.5)
c  Set the upper and lower limits for the experimental data
c      rel=gg*dh/emul
c      zboil=emul/(dsqrt(sig*rhol*dh))
c      bo=9.81*(rhol-rhog)*(dh**2)/sig
c      write (6,619)  xlm, rel, zboil, bo
c      if (xlm.lt.xlmmax) go to 141
c  Here need to calculate delstr.
c      call neural2 (rel,xe,delstr,qchf)
c      qchf=qchf*(hfg*gg)
c      qchfl=qchf*perim
c      write (6,725) qchf,qchfl
c      write (*,725) qchf,qchfl
 725  format (3x, ' Qchf = ',1pe13.5,1x,'W/m2 Qchfl='1pe13.5,'W/m')
c      if (qchfl.lt.qw) then
c       write (6,728) z, Qchfl
 728  format (2x, 'CHF Happened at z=',f8.4, 1x, 'Qchfl=', 1pe13.5)
c      stop
c      endif
 141   CONTINUE
C
C      CALCULATE THE PRESSURE LOSS AT CHANNEL EXIT IF NEEDED
C
      AKEXP = 0.5
      ALPHA = ALF1
      PHIEXP = ((((1.0-Xe)**2)/(1.0-ALPHA))+(RHOf*(Xe**2))
     *             /(RHOG*ALPHA))
      PEXIT = P1alf1-(PHIEXP*AKEXP*(GG**2)/(RHOf))
      WRITE (6,1625) PEXIT
1625  FORMAT ('PEXIT=',e9.3)
```

```
      return
 2997 CONTINUE
      RETURN
      END
C
C-------------------------------------------------------
C                              SUBROUTINE MARCH3
C-------------------------------------------------------
C
C            CALCULATIONS FOR SATURATED VAPOR FLOW REGIME
C
C
      SUBROUTINE MARCH3(PEXIT)
c
      IMPLICIT double precision (A-H,O-Z)
      EXTERNAL FUNC3
      external jac
      DOUBLE PRECISION ATOL,Rpar,rtol,RWORK,ZIpend,ZIP,YIN3
      double precision MV,MN
C
      COMMON /INPUT3/ MN,MV,wide,high,tubel,din,dout,theta,PIN
C
      COMMON /INP1/ P1,GG,U1,XE1,QW,TIN,ZHEATS,ZHEATF,XEOSV
      COMMON /INP2/ ELOSSIRR,ELOSSREV,H1,akexp
      COMMON /INP4/ UF1,UG1,ALF1,P1ALF1,PSATVAP,slip , tauw,xlm,bo
      COMMON /OTHER/TINK
C
      COMMON /PRP1A/ TG,RHOV,RHOG
      COMMON /PRP2/ RHOL,EMUL,CPL,EKL,PRNTL,RHOL2,beta
      COMMON /PRP2A/ EMUG,CPG,EKG,PRNTG,HF,HG,VFG,SIG
      COMMON /PRP3/ HFG,DHVDP,RAD
      COMMON /OSV/ IOSVFLG,ZOSV,IFLAG
      COMMON/OUT/zstp(400),h(400),p(400),ZSTP2(400),ZSTP3(400)
      COMMON/OUT3/H3(400),P3(400)
C

      COMMON /CALC/ ALPHA,ZPRNT,HENT,ITP,ZTWOPH,IVP,ZVAPPH
      COMMON /CALC2/ATOL(4),RWORK(100),IWORK(35)
C
      COMMON /CONSTS/ RGAS,G,PI
C
      common /hydro/ UG(395),UF(395),ALF(395),P1ALF(395)
      DIMENSION YIN3(8),YOUT3(8),EU(8),EL(8)
      DIMENSION DYDZ3(8)
      DATA RGAS,G,PI/8314.34,9.81,3.14159265/
C
C-------------------------------------------------------------
C ---------- MAIN PROGRAM----------------------------
C
C
C     --- SET INITIAL CONDITIONS (INLET-PARAMETERS) ---
C           CHANNEL CONSISTS OF THREE REGIONS WITH THREE DIFFERENT
C           FLOW REGIMES - COMPRESSED LIQUID, TWO-PHASE LIQUID/VAPOR
C           AND SUPERHEATED VAPOR
C
C-------------------------------------------------------------
```

```
C            THIRD REGION           -  SINGLE-PHASE VAPOR
C-------------------------------------------------------------
C
C-- INLET FLUID BECOMES SINGLE PHASE FROM SECOND PART OF PROGRAM --
C
C     CONVERT UNITS TO KG-M-S SYSTEM
C     PRESSURE IS IN PASCALS
C
C     MUST USE PROPERTIES AND Z LOCATION FROM SECOND PART OF PROGRAM
C     STARTS OUT AS SATURATED VAPOR
C
      PNEW3 = PSATVAP
      ZSTART = ZVAPPH
C----CALCULATE THE EQUILIBRIUM QUALITY FROM ENTHALPY AND PRESSURE
      CALL PRPSAT(PNEW3,TSAT1,RHOF,EMUL,CPL,EKL,PRNTL,
     1        EMUG,CPG,EKG,PRNTG,HF,HG,VFG,HFG,SIG,DHVDP,CPA,HA)
      HNEW3 = HG
      NEQ = 2
      YIN3(1) = HNEW3
      YIN3(2) = PNEW3
C---------------------------------------------------------------------
C----------------PREPARATION FOR SOLVING ODE
C---------------------INPUT FOR RKAMS
C---------------------------------------------------------------------
      write (6,149)
 149  format (//,3x,'Superheated Single Phase Results',/,8x,'z (m)'
     1       '   T (K)     P (Pa)     H (J/kg)  (--)   ',/)
      ZSTPUP3 = ZSTART
      NUMPRNT=((TUBEL-ZSTART)/ZPRNT)+1
c
C             SETUP PARAMETERS FOR DVODE SOLVER
C
      ITOL = 1
      RTOL = 1.0D-13
      ATOL(1) = 1.0D-13
      ATOL(2) = 1.0D-13
      ITASK = 1
      ISTATE = 1
      IOPT = 0
      LRW = 100
      LIW = 35
      MF = 22
      DO 107 I=1,NEQ
      EU(I) = 0.0
      EL(I) = 0.0
      dydz3(I)=0.0
 107  CONTINUE
C------------PRINTING LOOP-------------------------------------
      z=ZSTART
      zstp3(1)=zprnt + ZSTART
      DO 41 ILOOP = 1,NUMPRNT
      JJ = ILOOP
      H3(JJ)=HNEW3
      P3(JJ)=PNEW3
      if (jj.gt.1) then
      ZSTP3(JJ)= ZSTPUP3
```

```
      Z = ZSTP3(JJ)
      endif
      ZIP = Z
      ZIPEND = Z+ZPRNT
C
C------------CALCULATION LOOP----------------------------------
C
C     CALL DVODE SOLVER
C
      CALL dvode(FUNC3,NEQ,YIN3,ZIP,ZIPEND,ITOL,RTOL,ATOL,ITASK,
     1                  ISTATE,IOPT,RWORK,LRW,IWORK,LIW,JAC,mf,rpar,ipar)
C
      ZSTPUP3 = ZIPEND
      DO I=1,NEQ
      YOUT3(I) = YIN3(I)
      ENDDO
      HNEW3 = YIN3(1)
      PNEW3 = YIN3(2)
       H3(JJ)=YOUT3(1)
            P3(JJ)=YOUT3(2)
      ZSTP3(JJ) = ZIPEND
      WRITE (6,620) ZSTP3(JJ),TG,P3(JJ),H3(JJ)
 620  format (5x, f8.5, 2x, f7.2,2x,1pe12.4,2x,1pe12.4)
 41   CONTINUE
C---- CALCULATE THE PRESSURE LOSS AT CHANNEL EXIT
      AKEXP = 0.5
      PEXIT = P3(JJ)-(AKEXP*(GG**2)/(RHOG))
      WRITE (6,625) PEXIT
 625  FORMAT ('PEXIT=',e9.3)
 1997 CONTINUE
      RETURN
      END
C-----------------------------------------------------------------------
C---------------- FORMATION OF FUNCTION ------------
      SUBROUTINE FUNC (neq,ZA,Y,DYDZ,rpar,ipar)
      IMPLICIT double precision (A-H,O-Z)
      double precision MV,MN
      external jac
      COMMON /INP1/ P1,GG,U1,XE1,QW,TIN,ZHEATS,ZHEATF,XEOSV
      COMMON /INP2/ ELOSSIRR,ELOSSREV,H1,akexp
      COMMON /INP4/ UF1,UG1,ALF1,P1ALF1,PSATVAP,slip, tauw,xlm,bo
      COMMON /PRP1A/ TG,RHOV,RHOG
      COMMON /PRP2/ RHOL,EMUL,CPL,EKL,PRNTL,RHOL2,beta
      COMMON /PRP2A/ EMUG,CPG,EKG,PRNTG,HF,HG,VFG,SIG
      COMMON /PRP3/ HFG,DHVDP,RAD
      COMMON /INPUT3/ MN,MV,wide,high,tubel,din,dout,theta,PIN
      COMMON /CALC/ ALPHA,ZPRNT,HENT,ITP,ZTWOPH,IVP,ZVAPPH
      COMMON /CALC2/ATOL(4),RWORK(100),IWORK(35)
      COMMON /OTHER/TINK
      COMMON /CONSTS/ RGAS,G,PI
      DOUBLE PRECISION ZA,Y,DYDZ
      DIMENSION Y(8),DYDZ(8),AINPUT(8,8),AIN(8,8),X(8)
      common /hydro/ UG(395),UF(395),ALF(395),P1ALF(395)
      DIMENSION CM(8), AM(8,8)
      COMMON /OSV/ IOSVFLG,ZOSV,IFLAG
c     AREA = WIDE*HIGH
```

```
c  on August 02
      area=3.1416*(din**2)/4.
      perim=3.1416*din
c       perim=2.*(wide+high)
      dh=4.*area/perim
C---------------------------------------------------------------
C --------PROPERTIES CALCULATION----------------------
C
      H1= Y(1)
      P1 = Y(2)
      QWN = QW
c       find saturation properties
      CALL PRPSAT (P1,TGSAT,RHOL,EMUL,CPL,EKL,PRNTL,EMUG,CPG,
     1          EKG,PRNTG,HF,HG,VFG,HFG,SIG,DHVDP,CPA,HA)
C  now estimate subcooled local properties (sbscript 2)
      tl=-(hf-h1)/cpl+tgsat
      if (tl.gt.tgsat) tl=tgsat
      if (tl.lt.(tgsat-150.)) tl=tgsat-150.
      psat2=psatf(tl)
      call prpsat (psat2,t2,rhol2,emul2,cpl2,ekl2,prntl2,emug2,cpg2,
     1       ekg2,prntg2,hf2,hg2,vfg2,hfg2,sig2,dhvdp2,cpa2,ha2)
c   adjust velocity to account for liquid density change
      u1=gg/rhol2
      IF ((ZA.LT.ZHEATS).OR.(ZA.GE.ZHEATF)) QWN=0.0
c 29   CONTINUE
C     INITIALIZE MATRIX TO ZERO
      DO 111 I1=1,neq
            CM(I1)=0.0
      DO 101 J1=1,neq
 101  AM(I1, J1)=0.0
 111  CONTINUE
C
      AM(1,1) = 1.0
      AM(1,2) = 0.0
C-----COEFFICIENTS A's
C
      am(1,1)=1.0
      am(1,2)=0.0
      am(2,1) = (gg**2)*beta/(rhol2*cpl2)
      AM(2,2) = 1.0
      CM(1) = ((QWN/(AREA))-9.81*SIN(THETA/180.0*PI)*GG)/GG
C     FOR C2, NEED TO CALCULATE THE WALL FRICTION
c      DH = 2.0*(WIDE*HIGH)/(wide+high)
      REN = (GG*(DH))/EMUL2
C
C     LAMINAR FLOW
C
      IF(REN.LE.2300.0) THEN
      GALPHA = dmin1(wide,high)/dmax1(wide,high)
C      WRITE(6,*) 'GALPHA=',GALPHA
      TERM = (24.0)*(1.0-(1.3553*GALPHA)+(1.9467*(GALPHA**2))
     1           -(1.7012*(GALPHA**3))+(0.9564*(GALPHA**4))
     1           -(0.2537*(GALPHA**5)))
      F=TERM/REN
c  on August 02
      f=16./ren
```

```
      ELSE
      FTERM = 1.7372*DLOG(REN/(1.964*DLOG(REN)-3.8215))
      F = (1.0875-0.1125*GALPHA)/(FTERM**(2.0))
c  August 02
      f=0.079/(ren**0.25)
      END IF
      TAUW = (F*(GG**2)/RHOL2)/2.0
      DRHOLDT= -BETA*RHOL
      CM(2) = -RHOL2*G*SIN(THETA/180.0*PI)-(TAUW*perim/(WIDE*HIGH))
      GO TO 15
 10   CONTINUE
C     CALL FRIEDEL(FW)
C       RELO = REN
C       FLO = 0.079*(RELO**(-0.25))
C       FWLO = (4.0*FLO*(GG**2))/(2.0*RAD*2.0*RHOL2)
C       PHILOSQ = ((1.0 + (XLOCAL*((EMUL2-EMUG)/EMUG)))**(-0.25))*
C      1     (1.0 + XLOCAL*((RHOL2/RHOG)-1.0))
C       FW = (FWLO)*(PHILOSQ**2)
C       WRITE (6,*) ' FW = ', FW
C       WRITE (6,*) 'RELO, RHOH, FW', RELO, RHOH, FW
C       CM(2) = -RHOH*G*SIN(THETA/180.0*PI)-FW
c       WRITE (6,*) ' C2 WITH FW =', C(2)
 15   CONTINUE
C
C       CM(3) = (4.0*QWN/(2.0*RAD)) + (4.0*U1*TAUW/(2.0*RAD))
C       WRITE (6,*) ' QW, RAD, U1, TAUW', QWN, RAD, U1, TAUW
C
C-----MATRIX INVERSE
      N=2
      DO 103 I2=1,2
      DO 102 J2=1,2
 102  AINPUT(I2, J2)=AM(I2,J2)
 103  CONTINUE
C
      CALL INVER(AINPUT,AIN,N,DET)
C
C     --- GET VALUES FOR THE TWO DERIVATIVE EQNS. ---
C
      DO 17 I=1,N
      X(I)=0.0
      DO 11 J=1,N
 11   X(I)=X(I)+ AIN(I,J)*CM(J)
 17   CONTINUE
C     --- ASSIGN VALUES TO THE DERIVATIVES ---
      DENTH=X(1)
      DP=X(2)
      DYDZ(1) = DENTH
      DYDZ(2) = DP
      RETURN
      END
C-------------------------------------------------------------------------
C---------------- FORMATION OF FUNCTION2 ------------
      SUBROUTINE FUNC2 (neq,ZA,Y2,DYDZ2,rpar,ipar)
      IMPLICIT double precision (A-H,O-Z)
      double precision MV,MN
      external jac
```

```
C
      COMMON /INP1/ P1,GG,U1,XE1,QW,TIN,ZHEATS,ZHEATF,XEOSV
      COMMON /INP2/ ELOSSIRR,ELOSSREV,H1,akexp
      COMMON /INP4/ UF1,UG1,ALF1,P1ALF1,PSATVAP,slip, tauw,xlm,bo
      COMMON /PRP1A/ TG,RHOV,RHOG
      COMMON /PRP2/ RHOL,EMUL,CPL,EKL,PRNTL,RHOL2,beta
      COMMON /PRP2A/ EMUG,CPG,EKG,PRNTG,HF,HG,VFG,SIG
      COMMON /PRP3/ HFG,DHVDP,RAD
      COMMON /INPUT3/ MN,MV,wide,high,tubel,din,dout,theta,PIN
      COMMON /CALC/ ALPHA,ZPRNT,HENT,ITP,ZTWOPH,IVP,ZVAPPH
      COMMON /OTHER/TINK
      COMMON /CONSTS/ RGAS,G,PI
      COMMON /CALC2/ATOL(4),RWORK(100),IWORK(35)
C
      DIMENSION Y2(8),DYDZ2(8),AINPUT2(8,8),AIN2(8,8),X2(8)
      common /hydro/ UG(395),UF(395),ALF(395),P1ALF(395)
      DIMENSION CM2(8), AM2(8,8)
      COMMON /OSV/ IOSVFLG,ZOSV,IFLAG
C
      AREA = WIDE*HIGH
      perim=2.*(high+wide)
c  August 02
      area=3.1416*(din**2)/4.
      perim=3.1416*din
      dh=4.*area/perim
C---------------------------------------------------------------------
C --------PROPERTIES CALCULATION-----------------------
      P1ALF1= Y2(1)
      UG1 = Y2(2)
            UF1 = Y2(3)
             ALF1 = Y2(4)
             alpha=alf1
      QWN = QW
      CALL PRPSAT (P1ALF1,TGSAT,RHOF,EMUf,CPf,EKf,PRNTf,EMUG,CPG,
     1          EKG,PRNTG,HF,HG,VFG,HFG,SIG,DHgDP,CPA,HA)
c  Below is a simplifying assumption
      dhfdp=0.0
c  since liquid is saturated, therefore:
      rhol=rhof
      emul=emuf
C
      IF ((ZA.LT.ZHEATS).OR.(ZA.GE.ZHEATF)) QWN=0.0
c  29   CONTINUE
C
C    CALCULATE THE LOCAL VALUE OF X, XLOCAL USING ZUBER
C
C      XLOCAL = (XE1-XEOSV*QX)/(1.0-XEOSV*QX)
C      WRITE (6,*) 'IOSVFLG INTO FRIEDEL=', IOSVFLG
C      WRITE (6,*) ' XLOCAL USING ZUBER = ', XLOCAL
C      DXDXE =(1.0- XEOSV*QX - QX + XE1*QX)/
C     1         ((1.0-XEOSV*QX)**2)
C      ELSE
C      XLOCAL = 0.0
C      DXDXE = 0.0
C
C      ENDIF
```

```
C
C      WRITE (6,*) 'MAKES IT TO POINT 1'
C---------------------------------------
C ---------------------------------------
C     INITIALIZE MATRIX TO ZERO
C
      DO 111 I1=1,neq
            CM2(I1)=0.0
      DO 101 J1=1,neq
 101  AM2(I1, J1)=0.0
 111  CONTINUE
C    CALCULATE THE MATRIX COEFFICIENTS
      TG = TGSAT
      PGAS = PSATF(TG)
      PBG = PGAS/(1.E+5)
      rhog=1000./VGPT(PBG,TG)
      rhoh=(rhog*alf1)+(rhof*(1.-alf1))
C      CALCULATE NEEDED QUANTITIES AND THEN MATRIX COEFFICIENTS
C      FIRST GROUP ARE ALL TIMES DP/DZ
C
      DRHOGDP= MV/(RGAS*TG)
      DRHOFDP= 0.0
      AM2(1,1) =(UF1*(1-ALPHA)*DRHOFDP+UG1*ALPHA*DRHOGDP)
      AM2(2,1) =(DRHOFDP*(1-ALPHA)*(UF1**2))+(1-ALPHA)
     1         -0.5*(UF1+UG1)*(UF1*(1-ALPHA)*DRHOFDP)
c Change on august 02
      am2(2,1)=0.0
      AM2(3,1) = ((DRHOFDP*(1-ALPHA)*(UF1**2))+(DRHOGDP*ALPHA*
     1          (UG1**2))+1)
      EF = HF + (UF1**2)/2.0 + G*Za*SIN(THETA/180.0*PI)
      EG = HG + (UG1**2)/2.0 + G*Za*SIN(THETA/180.0*PI)
      AM2(4,1) = (DRHOFDP*(UF1*(1-ALPHA)*EF)+(RHOF*UF1*(1-ALPHA)*DHFDP)
     1                   +(DRHOGDP*UG1*ALPHA*EG)+(RHOG*UG1*ALPHA*DHVDP))
C
C-----COEFFICIENTS A21,A22,A23,A24
C     FOR DUG/DZ
C
      AM2(1,2) = RHOG*ALPHA
      CVM = ALPHA*(1-ALPHA)*(RHOF*(1-ALPHA)+(RHOG*ALPHA))
      AM2(2,2) = (-CVM*UG1)
c Change on august 02
      am2(2,2)=1.0
      AM2(3,2) = (2*RHOG*ALPHA*ug1)
      AM2(4,2) = (RHOG*ALPHA*EG+RHOG*(ug1**2)*ALPHA)
C
C     CALCULATE COEFFICIENTS A31,A32,A33,A34
C     FOR DUF/DZ
C
      AM2(1,3) = RHOF*(1-ALPHA)
      AM2(2,3) = 2.0*RHOF*(1-ALPHA)*uf1+(CVM*UF1)-
     1         0.5*(UF1+UG1)*(RHOF*(1-ALPHA))
c Change on august 02
      Slip=slipr (rhof,rhog,alpha,ug1,uf1,dh,emul,emug,sig)
c      write (*,*) ' 1, slip=',slip
      am2(2,3)=-Slip
      AM2(3,3) = 2*RHOF*(1-ALPHA)*uf1
```

```
      AM2(4,3) = (RHOF*(1-ALPHA)*EF+RHOF*(uf1**2)*(1-ALPHA))
C     FOR THIS CODE, SET DH/DP AND DHFG/DP = 0.0
C      DHDP = 0.0
C      DHFGDP = 0.0
C
C     CALCULATE COEFFICIENTS A41,A42,A43,A44
C     FOR DALPDZ
C
      AM2(1,4) = (RHOG*UG1-RHOF*UF1)
      AM2(2,4) = (-RHOF*(UF1**2)+0.5*(UF1+UG1)*(RHOF*UF1))
c Change on august 02
      am2(2,4)=0.0
      AM2(3,4) = (RHOG*(UG1**2)-RHOF*(UF1**2))
      AM2(4,4) = (-RHOF*UF1*EF+RHOG*UG1*EG)
C
C     MATRIX C1, C2, C3, C4
C
      CM2(1) = 0.0
      C1 = CM2(1)
C
C     FOR C2, NEED TO CALCULATE THE WALL FRICTION
C
C     CALCULATE THE REYNOLDS NUMBER
C     USING THE HYDRAULIC DIAMETER, DH
c      DH = 2.0*(WIDE*HIGH)/(wide+high)
      RAD = DH/2.0
      YME = (RHOG*UG1*ALPHA)/(RHOG*UG1*ALPHA+RHOF*Uf1*(1-ALPHA))
      ALPHAH = (YME/RHOG)/((YME/RHOG)+((1-YME)/RHOF))
      eMUTP =ALPHAH*eMUG+(1-ALPHAH)*(1+2.5*ALPHAH)*eMUF
      RETP = (GG*(DH))/eMUTP
C  LAMINAR FLOW
      IF(REtp.LE.2300.0) THEN
      GALPHA =dmin1(wide,high) /dmax1(wide,high)
      TERM = (24.0)*(1.0-(1.3553*GALPHA)+(1.9467*(GALPHA**2))
     1          -(1.7012*(GALPHA**3))+(0.9564*(GALPHA**4))
     1          -(0.2537*(GALPHA**5)))
      F=TERM
c  August 02
      f=16./retp
      ELSE
C  Turbulent flow
      FTERM = 1.7372*LOG(RETP/(1.964*LOG(RETP)-3.8215))
      F = (1.0875-0.1125*GALPHA)*(FTERM**(-2.0))
c  August 02
      f=0.079/(retp**0.25)
      END IF
      tauw=0.5*f*(gg**2)/((rhog*alphah)+((1.-alphah)*rhof))
c      area=wide*high
c  Now determine flow regime, and get interfacial perimenter/area, perim,
c  and factor for interfacial force/area, fi.
c  First set void fractions for regime transition.
c      alphab=0.2
c      alphaa=0.8
c      If (alpha.lt.alphaa) then
c       webcr=3.0
c       dbbl=sig*webcr/(rhof*((ug1-uf1)**2))
```

```
c       dbbl2=0.5*dmin1(high,wide)
c       dbbl=dmin1(dbbl,dbbl2)
c       vbbl=3.1416*(dbbl**3)/6.
c       reb=rhof*dabs(ug1-uf1)*dbbl/emuf
c       cd=(1.+0.15*(reb**0.687))*24./reb
c       if (alpha.le.alphab) then
c        fi=0.75*rhof*alpha*cd*dabs(ug1-uf1)/dbbl
c        enb=alpha/vbbl
c       else
c        fib=0.75*rhof*alphab*cd*dabs(ug1-uf1)/dbbl
c        enb=alphab/vbbl
c       endif
c       perimi=enb*3.1416*(dbbl**2)*area
c       perimib=perimi
c      Endif
c      If (alpha.gt.alphab) then
cc  estimate film thickness in annular flow
c       del=0.5*(1.-alpha)*area/(wide+high)
c       if (alpha.lt.alphaa) then
c        del=0.5*(1.-alphaa)*area/(wide+high)
c       endif
c       cfi=0.005*(1.+180.*del/dmin1(wide,high))
c       perimi=2.*((wide-2.*del)+(high-2.*del))
c       fi=perimi*cfi*0.5*dabs(ug1-uf1)/area
c       perimia=perimi
c       fia=fi
c       if(alpha.lt.alphaa) then
c        param=(alpha-alphab)/(alphaa-alphab)
c        fi=fib+param*(fia-fib)
c        perimi=perimib+param*(perimia-perimib)
c       endif
c      Endif
c  August 02 ------------------
      fi=perim*0.05*0.5*dabs(ug1-uf1)/area
      fI=fI*1.e8
c ----------------------
c  The above statement added on July 29, 01 to render homogeneous
      CM2(2) = -RHOF*G*SIN(THETA/180.0*PI)*(1-ALPHA)+FI*(ug1-uf1)
     1        -(1-ALPHA)*
     1        F*(GG**2)*(perim/area)/(2*(ALPHA*RHOG+(1-ALPHA)*RHOF))
c Change on august 02
      cm2(2)=0.0
 10   CONTINUE
C     CALL FRIEDEL(FW)
C       RELO = REN
C       FLO = 0.079*(RELO**(-0.25))
C       FWLO = (4.0*FLO*(GG**2))/(2.0*RAD*2.0*RHOL2)
C       PHILOSQ = ((1.0 + (XLOCAL*((EMUL2-EMUG)/EMUG)))**(-0.25))*
C      1     (1.0 + XLOCAL*((RHOL2/RHOG)-1.0))
C
      CM2(3) =-(RHOF*(1.0-ALPHA)+RHOG*ALPHA)*G*SIN(THETA/180.0*PI)
     1             -(F*(GG**2))/(2.0*(RHOG*ALPHA+(1-ALPHA)*RHOF))
C
      CM2(4) = (QWN/area) - (RHOF*UF1*(1-ALPHA)*G*SIN(THETA/180.0*PI))
     1        -(RHOG*UG1*ALPHA*G*SIN(THETA/180.0*PI))
C
```

```
C-----MATRIX INVERSE
C
      N=4
      DO 103 I2=1,4
      DO 102 J2=1,4
 102  AINPUT2(I2,J2)=AM2(I2,J2)
 103  CONTINUE
C
      CALL INVER(AINPUT2,AIN2,N,DET)
C
C     --- GET VALUES FOR THE four DERIVATIVE EQNS. ---
C
      DO 17 I=1,N
      X2(I)=0.0
      DO 11 J=1,N
 11   X2(I)=X2(I)+ AIN2(I,J)*CM2(J)
 17   CONTINUE
C
C     --- ASSIGN VALUES TO THE DERIVATIVES ---
C
       DP1ALF=X2(1)
       DUG=X2(2)
       DUF=X2(3)
            DALF=X2(4)
      DYDZ2(1) = DP1ALF
      DYDZ2(2) = DUG
      DYDZ2(3) = DUF
      DYDZ2(4) = DALF
c      write (*,*) ' dpz,dug,duf,dalf',DP1ALF,dug,duf,dalf
      RETURN
      END
C
      SUBROUTINE FUNC2f (neq,ZA,Y2,DYDZ2,rpar,ipar)
      IMPLICIT double precision (A-H,O-Z)
      double precision MV,MN
      external jac
C
C
      COMMON /INP1/ P1,GG,U1,XE1,QW,TIN,ZHEATS,ZHEATF,XEOSV
      COMMON /INP2/ ELOSSIRR,ELOSSREV,H1,akexp
      COMMON /INP4/ UF1,UG1,ALF1,P1ALF1,PSATVAP,slip, tauw,xlm,bo
      COMMON /PRP1A/ TG,RHOV,RHOG
      COMMON /PRP2/ RHOL,EMUL,CPL,EKL,PRNTL,RHOL2,beta
      COMMON /PRP2A/ EMUG,CPG,EKG,PRNTG,HF,HG,VFG,SIG
      COMMON /PRP3/ HFG,DHVDP,RAD
      COMMON /INPUT3/ MN,MV,wide,high,tubel,din,dout,theta,PIN
      COMMON /CALC/ ALPHA,ZPRNT,HENT,ITP,ZTWOPH,IVP,ZVAPPH
      COMMON /CALC2/ATOL(4),RWORK(100),IWORK(35)
      COMMON /OTHER/TINK
      COMMON /CONSTS/ RGAS,G,PI
C
      DIMENSION Y2(8),DYDZ2(8),AINPUT2(8,8),AIN2(8,8),X2(8)
      common /hydro/ UG(395),UF(395),ALF(395),P1ALF(395)
      DIMENSION CM2(8), AM2(8,8)
      COMMON /OSV/ IOSVFLG,ZOSV,IFLAG
      neq=3
```

```
      AREA = WIDE*HIGH
      perim=2.*(wide+high)
c  August 02
      area=3.1416*(din**2)/4.
      perim=3.1416*din
      dh=4.*area/perim
C-----------------------------------------------------------------
C --------PROPERTIES CALCULATION----------------------
C
      P1ALF1= Y2(1)
      ug1= Y2(2)
        xe = Y2(3)
             alpha=alf1
      QWN = QW
      CALL PRPSAT (P1ALF1,TGSAT,RHOF,EMUf,CPf,EKf,PRNTf,EMUG,CPG,
     1          EKG,PRNTG,HF,HG,VFG,HFG,SIG,DHgDP,CPA,HA)
c  Below is a simplifying assumption
      dhfdp=0.0
c since liquid is saturated, therefore:
      rhol=rhof
      emul=emuf
C
C     ACCOUNT FOR THE FACT THAT THE TUBE IS HEATED ON THE BOTTOM
C
      IF ((ZA.LT.ZHEATS).OR.(ZA.GE.ZHEATF)) QWN=0.0
C     INITIALIZE MATRIX TO ZERO
C
      DO 111 I1=1,neq
             CM2(I1)=0.0
      DO 101 J1=1,neq
 101  AM2(I1, J1)=0.0
 111  CONTINUE
C
C    CALCULATE THE MATRIX COEFFICIENTS
C
      TG = TGSAT
      PGAS = PSATF(TG)
      PBG = PGAS/(1.E+5)
      rhog=1000./VGPT(PBG,TG)
      rhoh=(rhog*alf1)+(rhof*(1.-alf1))
C      CALCULATE NEEDED QUANTITIES AND THEN MATRIX COEFFICIENTS
C      FIRST GROUP ARE ALL TIMES DP/DZ
      DRHOGDP= MV/(RGAS*TG)
      DRHOFDP= 0.0
      EF = HF + (UF1**2)/2.0
      EG = HG + (UG1**2)/2.0
c      alf1=(((high-delta)*(wide-delta))/(wide*high))
c       uf1=gg*(1.-xe)/(rhof*(1.-alf1))
c      uf1=dmin1((0.1*ug1),5.0)
c  use a slip relation
      ss=(rhof/rhog)**0.333
c  The change below rendered on July 29, 2001
      slip=0.9999
c  And it was changed once again on August 02
      Slip=slipr (rhof,rhog,alpha,ug1,uf1,dh,emul,emug,sig)
c      write (*,*) ' 2,slip=',slip
```

```
c      pause
       uf1=ug1/slip
       alf1=1.-(((1.-xe)*gg)/(rhof*uf1))
       am2(1,1)=drhogdp/rhog
       am2(1,2)=1./ug1
       am2(1,3)=-1./xe
       am2(2,1)=-alf1
       am2(2,2)=-gg*xe
       am2(2,3)=0.5*gg*(uf1-ug1)
       am2(3,1)=((1.-xe)*dhfdp+xe*dhgdp)*gg
       am2(3,2)=gg*xe*ug1
       am2(3,3)=(-ef+eg)*gg
C      FOR C2, NEED TO CALCULATE THE WALL FRICTION
C      CALCULATE THE REYNOLDS NUMBER
C      USING THE HYDRAULIC DIAMETER, DH
c      DH = 2.0*(WIDE*HIGH)/(wide+high)
       RAD = DH/2.0
       YME = (RHOG*UG1*ALPHA)/(RHOG*UG1*ALPHA+RHOF*Uf1*(1-ALPHA))
       ALPHAH = (YME/RHOG)/((YME/RHOG)+((1-YME)/RHOF))
       eMUTP =ALPHAH*eMUG+(1-ALPHAH)*(1+2.5*ALPHAH)*eMUF
       RETP = (GG*(DH))/eMUTP
C
C      LAMINAR FLOW
C
       IF(REtp.LE.2300.0) THEN
       GALPHA =dmin1(wide,high) /dmax1(wide,high)
       TERM = (24.0)*(1.0-(1.3553*GALPHA)+(1.9467*(GALPHA**2))
      1           -(1.7012*(GALPHA**3))+(0.9564*(GALPHA**4))
      1           -(0.2537*(GALPHA**5)))
       F=TERM
c  August 02
       f=16./retp
       ELSE
       FTERM = 1.7372*LOG(RETP/(1.964*LOG(RETP)-3.8215))
       F = (1.0875-0.1125*GALPHA)*(FTERM**(-2.0))
c  August 02
       f=0.079/(retp**0.25)
       ENDIF
       tauw=0.5*f*(gg**2)/((rhog*alphah)+((1.-alphah)*rhof))
       cfi=f
c      temporarily use f for cfi, and width for interphase perim
       perimi=wide
c  August 02
       perimi=perim
       FI = CFI*0.5*(dABS(UG1-Uf1))*(perimi/area)
 10    CONTINUE
       cm2(1)=0.0
       cm2(2)=rhog*alf1*g*sin(theta/180.0*PI)+fi*(ug1-uf1)
c      cm2(2)=cm2(2)+alf1*f*(gg**2)*(perim/area)/
c     1   (2.*(alf1*rhog+(1.-alf1)*rhof))
       cm2(3)=qwn/area
C      CALL FRIEDEL(FW)
C        RELO = REN
C        FLO = 0.079*(RELO**(-0.25))
C        FWLO = (4.0*FLO*(GG**2))/(2.0*RAD*2.0*RHOL2)
C        PHILOSQ = ((1.0 + (XLOCAL*((EMUL2-EMUG)/EMUG)))**(-0.25))*
```

```
C     1     (1.0 + XLOCAL*((RHOL2/RHOG)-1.0))
C
C-----MATRIX INVERSE
C
      N=neq
      DO 103 I2=1,neq
      DO 102 J2=1,neq
 102  AINPUT2(I2,J2)=AM2(I2,J2)
 103  CONTINUE
C
      CALL INVER(AINPUT2,AIN2,N,DET)
C
C     --- GET VALUES FOR THE four DERIVATIVE EQNS. ---
      DO 17 I=1,N
      X2(I)=0.0
      DO 11 J=1,N
 11   X2(I)=X2(I)+ AIN2(I,J)*CM2(J)
 17   CONTINUE
C
C     --- ASSIGN VALUES TO THE DERIVATIVES ---
C
       DP1ALF=X2(1)
       DUG=X2(2)
            Dxe=X2(3)
      DYDZ2(1) = DP1ALF
      DYDZ2(2) = DUG
      DYDZ2(3) = Dxe
      RETURN
      END
C
C-------------------------------------------------------------------------
C---------------- FORMATION OF FUNCTION 3------------
C
      SUBROUTINE FUNC3 (NEQ,ZA,Y3,DYDZ3,RPAR,IPAR)
      IMPLICIT double precision (A-H,O-Z)
      double precision MV,MN
      external jac
C
      COMMON /INP1/ P1,GG,U1,XE1,QW,TIN,ZHEATS,ZHEATF,XEOSV
      COMMON /INP2/ ELOSSIRR,ELOSSREV,H1,akexp
      COMMON /INP4/ UF1,UG1,ALF1,P1ALF1,PSATVAP,slip, tauw,xlm,bo
      COMMON /PRP1A/ TG,RHOV,RHOG
      COMMON /PRP2/ RHOL,EMUL,CPL,EKL,PRNTL,RHOL2,beta
      COMMON /PRP2A/ EMUG,CPG,EKG,PRNTG,HF,HG,VFG,SIG
      COMMON /PRP3/ HFG,DHVDP,RAD
      COMMON /INPUT3/ MN,MV,wide,high,tubel,din,dout,theta,PIN
      COMMON /CALC/ ALPHA,ZPRNT,HENT,ITP,ZTWOPH,IVP,ZVAPPH
      COMMON /CALC2/ATOL(4),RWORK(100),IWORK(35)
      COMMON /OTHER/TINK
      COMMON /CONSTS/ RGAS,G,PI
      DIMENSION Y3(8),DYDZ3(8),AINPUT3(8,8),AIN3(8,8),X3(8)
      common /hydro/ UG(395),UF(395),ALF(395),P1ALF(395)
      DIMENSION CM3(8), AM3(8,8)
      COMMON /OSV/ IOSVFLG,ZOSV,IFLAG
C
c     AREA = WIDE*HIGH
```

```
c      perim=2*(wide+high)
c  August 02
      area=3.1416*(din**2)/4.
      perim=3.1416*din
      dh=4.*area/perim
C
C     CHECK FOR OSV USING PE AND H
C
C---------------------------------------------------------------
C --------PROPERTIES CALCULATION----------------------
C
      H3= Y3(1)
      P3 = Y3(2)
      QWN = QW
c      find saturation properties
C     START OF THIS SECTION IS SATURATED VAPOR
C
      IF (IFLAG.EQ.0) THEN
      CALL PRPSAT (P3,TGSAT,RHOL,EMUL,CPL,EKL,PRNTL,EMUG,CPG,
     1          EKG,PRNTG,HF,HG,VFG,HFG,SIG,DHVDP,CPA,HA)
C      WRITE(6,*)'P3,TGSAT,RHOL IN FUNC',P3,TGSAT,RHOL
      PBG = P3/(1.E+5)
      tg=tsatf(PBG)
      rhog=1.e3/vgpt(pbG,tg)
C      WRITE(6,*)'SAT TEMP ON FIRST PASS IS',TG
      ELSE
C
      ZIPIT = ZA-ZLAST
C      WRITE (6,*) 'ZA, ZLAST,ZIPIT',ZA,ZLAST,ZIPIT
      DELTAT = (DENTH/CPG)*ZIPIT
      TG = TG + DELTAT
C---- SPECIFIC HEAT FROM LOOK-UP FUNCTION-------
      CPGN = CPGAS(TG)
      CPG = CPGN
      RHOG = (P3*MV)/(RGAS*TG)
      ENDIF
C      WRITE (6,*) 'ZA USED BY PROGRAM TO INTEGRATE IS', ZA
c
C     ACCOUNT FOR THE FACT THAT THE TUBE IS HEATED ON THE BOTTOM
C
      IF ((ZA.LT.ZHEATS).OR.(ZA.GE.ZHEATF)) QWN=0.0
C
c  29   CONTINUE
C
C     INITIALIZE MATRIX TO ZERO
C
      DO 111 I1=1,neq
            CM3(I1)=0.0
      DO 101 J1=1,neq
 101  AM3(I1, J1)=0.0
 111  CONTINUE
C
C-----COEFFICIENTS A's
C
      am3(1,1)=(GG**2)/(RHOG*CPG*TG)
      am3(1,2)= (1-((GG**2)/(RHOG*P3)))
```

```
      am3(2,1) = GG
      AM3(2,2) = 0.0
C
C     FOR C1 MUST CALCULATE THE WALL FRICTION
C
c     DH = 2.0*(WIDE*HIGH)/(wide+high)
      RAD = DH/2.0
C
C     MUG FROM SUTHERLAND'S KINETIC THEORY
C
      TO = 350.0
      S = 1064.0
      EMUG = (1.12E-5)*((TG/TO)**1.5)*((TO+S)/(TG+S))
      REN = (GG*(DH))/EMUG
C
C     LAMINAR FLOW
C
      IF(REN.LE.2300.0) THEN
      GALPHA = dmin1(wide,high)/dmax1(wide,high)
      TERM = (24.0)*(1.0-(1.3553*GALPHA)+(1.9467*(GALPHA**2))
     1           -(1.7012*(GALPHA**3))+(0.9564*(GALPHA**4))
     1           -(0.2537*(GALPHA**5)))
      F=TERM/REN
c  August 02
      f=64./ren
      ELSE
      FTERM = 1.7372*DLOG(REN/(1.964*DLOG(REN)-3.8215))
      F = (1.0875-0.1125*GALPHA)/(FTERM**2)
c  August 02
      f=0.316/(ren**0.25)
      END IF
      TAUW = (F*(GG**2)/RHOG)/2.0
      DRHOLDT= -BETA*RHOL
      CM3(1) = -RHOG*G*SIN(THETA/180.0*PI)-(TAUW*perim/(AREA))
      CM3(2) = (QWN/(AREA))-G*GG*SIN(THETA/180.0*PI)
C
      GO TO 15
 10   CONTINUE
C     CALL FRIEDEL(FW)
C       RELO = REN
C       FLO = 0.079*(RELO**(-0.25))
C       FWLO = (4.0*FLO*(GG**2))/(2.0*RAD*2.0*RHOL2)
C       PHILOSQ = ((1.0 + (XLOCAL*((EMUL2-EMUG)/EMUG)))**(-0.25))*
C      1     (1.0 + XLOCAL*((RHOL2/RHOG)-1.0))
C       FW = (FWLO)*(PHILOSQ**2)
C       WRITE (6,*) ' FW = ', FW
C       WRITE (6,*) 'RELO, RHOH, FW', RELO, RHOH, FW
C       CM(2) = -RHOH*G*SIN(THETA/180.0*PI)-FW
c      WRITE (6,*) ' C2 WITH FW =', C(2)
 15   CONTINUE
C
C       CM(3) = (4.0*QWN/(2.0*RAD)) + (4.0*U1*TAUW/(2.0*RAD))
C       WRITE (6,*) ' QW, RAD, U1, TAUW', QWN, RAD, U1, TAUW
C
C-----MATRIX INVERSE
      N=2
```

```
      DO 103 I2=1,2
      DO 102 J2=1,2
  102  AINPUT3(I2, J2)=AM3(I2,J2)
  103  CONTINUE
C
      CALL INVER(AINPUT3,AIN3,N,DET)
C
C     --- GET VALUES FOR THE TWO DERIVATIVE EQNS. ---
C
      DO 17 I=1,N
      X3(I)=0.0
      DO 11 J=1,N
   11   X3(I)=X3(I)+ AIN3(I,J)*CM3(J)
   17   CONTINUE
C
C     --- ASSIGN VALUES TO THE DERIVATIVES ---
C
      DENTH=X3(1)
      DP=X3(2)
      DYDZ3(1) = DENTH
      DYDZ3(2) = DP
C
C     USE SUPERHEATED PROPERTIES AFTER FIRST PASS THROUGH
C     NEED A FLAG TO MARK THIS
C
      IFLAG = 1
      ZLAST = ZA
C      WRITE (6,*) 'TG AT END OF FUNC3',TG
      RETURN
      END
C
C-------------------------------------------------------
C     SUBROUTINES TO BE USED
C-------------------------------------------------------
C
C     THIS SUBROUTINE INTERPOLATES
C
      SUBROUTINE POLINT (XA,YA,N,X,Y,DY)
      IMPLICIT REAL*8 (A-H,O-Z)
C

            PARAMETER (NMAX=60)
      REAL*8 XA(N),YA(N),C(NMAX),D(NMAX)
C
      NS=1
      DIF=DABS(X-XA(1))
      DO 11 I=1,N
        DIFT=DABS(X-XA(I))
           IF(DIFT.LT.DIF) THEN
          NS=I
          DIF=DIFT
           END IF
        C(I)=YA(I)
        D(I)=YA(I)
   11   CONTINUE
      Y=YA(NS)
```

```
      NS=NS-1
      DO 13 M=1,N-1
        DO 12 I=1,N-M
          HO=XA(I)-X
          HP=XA(I+M)-X
          W=C(I+1)-D(I)
          DEN=HO-HP
              IF(DEN.NE.0.0D0) GO TO 16
              WRITE (*,*)'ERROR IN POLINT'
              STOP
   16         DEN=W/DEN
          D(I)=HP*DEN
          C(I)=HO*DEN
   12   CONTINUE
        IF (2*NS.LT.N-M)THEN
          DY=C(NS+1)
        ELSE
          DY=D(NS)
          NS=NS-1
             END IF
        Y=Y+DY
      DY1=DABS(DY)
      IF ((ISTOP.EQ.2).OR.(DY1.LT.0.01)) GO TO 14
        ISTOP=ISTOP+1
   13   CONTINUE
C
   14   CONTINUE
C
      RETURN
      END
C
C     ---------------------------------------------------------------
C
      SUBROUTINE INVER(A,AINV,N,DET)
      IMPLICIT REAL*8 (A-H,O-Z)
C
      DIMENSION A(8,8),AINV(8,8)
C
C     ------------------------------------------------
C     USES A STANDARD GAUSS-JORDAN ELIMINATION TECH.
C     --- DEFINITION OF VARIABLES ---
C     A(N,N)-------- INPUT SQUARE MATRIX
C     AINV(N,N) ---- INVERSE OF SQUARE MATRIX
C     DET ---------- DETERMINANT OF MATRIX A(N,N)
C     IRROW -------- INDEX OF MATRIX ROW, FROM 1 TO N
C     IROW --------- INDEX OF MATRIX ROW, FROM 1 TO N
C     ICOL --------- INDEX OF MATRIX COLUM, FROM 1 TO N
C     ------------------------------------------------
C
      DET=1.0
C
C     --- INITIALLY SET AINV(N,N)=UNIT MATRIX
C
      DO 10 I=1,N
        DO 10 J=1,N
          IF (I .EQ. J) THEN
```

```
            AINV(I,I)=1.0
          ELSE
            AINV(I,J)=0.0
          END IF
   10 CONTINUE
C
      DO 90 IRROW = 1,N
C     --- FIND THE LARGEST ELEM. IN THE ROWS OF A SPEC. COLUMN
        IMAX=IRROW
       DO 21 IROW=IRROW,N
          IF (DABS (A(IROW,IRROW)) .GT. DABS (A(IMAX,IRROW))) THEN
             IMAX=IROW
          END IF
   21  CONTINUE
C     --- SWAP THE ELEMENTS OF ROW IRROW & ROW IMAX FOR MATRIX A,AINV
      IF (IMAX .NE. IRROW ) THEN
        DO 30 ICOL=1,N
          RESV=AINV(IRROW,ICOL)
          AINV(IRROW,ICOL)=AINV(IMAX,ICOL)
          AINV(IMAX,ICOL)=RESV
           IF (ICOL .GE. IRROW) THEN
             RESV = A(IRROW,ICOL)
             A(IRROW,ICOL) = A(IMAX,ICOL)
             A(IMAX,ICOL) = RESV
           END IF
   30    CONTINUE
      END IF
C     --- THE DETERMINANT IS THE PRODUCT OF DIAGO. ELEMENTS FOR
C     --- A DIAGONAL MATRIX
      AIRR=A(IRROW,IRROW)
      DET=DET*AIRR
C     --- IF THE DETERMINANT IS ZERO: THE MATRIX IS SINGULAR ---
       IF (DET .EQ. 0.0) THEN
         WRITE (6,69)
   69    FORMAT(/' SINGULAR MATRIX, CHECK INPUT MATRIX')
         STOP
       END IF
C     --- SUBTRACTING ONE ROW FROM EACH OF THE OTHERS, WITH PROPER
C     --- NORMALIZATION, TO ELIMINATE ALL THE ELEMS. OF THE COLUMN
C     --- EXCEPT FOR ONE ELEMENT
       DO 11 ICOL =1,N
         AINV(IRROW,ICOL)=AINV(IRROW,ICOL)/AIRR
          IF (ICOL .GE. IRROW) THEN
             A(IRROW,ICOL)=A(IRROW,ICOL)/AIRR
          END IF
   11   CONTINUE
C     --- SET THE NORMALIZATION FACTOR
       DO 40 IROW =1,N
         IF (IROW .NE. IRROW) THEN
           FAC =A(IROW,IRROW)
         END IF
       DO 50 ICOL =1,N
         IF (IROW .NE. IRROW) THEN
           AINV(IROW,ICOL) = AINV(IROW,ICOL)-FAC*AINV(IRROW,ICOL)
           A(IROW,ICOL) = A(IROW,ICOL)-FAC*A(IRROW,ICOL)
         END IF
```

```
C      WRITE(*,*) 'IROW,ICOL,A(IROW,ICOL) (INPUT)',
C     1   IROW,ICOL,A(IROW,ICOL)
C      WRITE(*,*) 'IROW,ICOL,AINV(IROW,ICOL) INVERSE',
C     1   IROW,ICOL,AINV(IROW,ICOL)
  50  CONTINUE
  40  CONTINUE
  90 CONTINUE
C
      RETURN
      END
C
C---------------------------------------------------------------

C ***************************************************************
C
C     BLOCK PRPSAT: PRPSAT AND ANOTHER 18 SUBROUTINES OR FUNCTIONS
C     CALCULATE PROPERTIES AT SATURATE CONDITION
C
C ***************************************************************
C     ---------------------------------------------------------

C
      SUBROUTINE PRPSAT (PR1,TGSAT,RHOL,EMUL,CPL,EKL,PRNTL,
     1          EMUG,CPG,EKG,PRNTG,HF,HG,VFG,HFG,SIG,DHVDP,CPA,HA)
      IMPLICIT REAL*8 (A-H,O-Z)
      REAL*8 MV,MN

C
c     COMMON /INP1/ P1,GG,U1,XE1,QW,TIN,ZHEATS,ZHEATF,XEOSV
      COMMON /INP2/ ELOSSIRR,ELOSSREV,H1,akexp
      COMMON /INP4/ UF1,UG1,ALF1,P1ALF1,PSATVAP,slip, tauw,xlm,bo
c     COMMON /PRP1A/ TG,RHOV,RHOG
      COMMON /INPUT3/ MN,MV,wide,high,tubel,din,dout,theta,PIN

      DATA XGA1,YGA1/0.0,0.0/
C
C     --- P,XE ARE ALREADY KNOWN ---
C     --- CHANGE P FROM PASCAL TO BAR,  T FROM K TO C ---
C
      PB= PR1/(1.E+5)
C     WRITE (*,*) 'PB,PR1 IN SUB PRPSAT', PB,PR1
C
C IN THIS SUBROUTINE, BNM CHANGED ALL THE "PVB" TO "PB"
C  5/7/97
C
C     --- (1): GET TSAT FROM PVB ---
      TGSAT= TSATF (PB)
C     --- CHANGE TSAT FROM K TO C ---
      TGSATC= TGSAT-273.15
C
C     --- CHANGE P FROM BAR TO PSIA & H FROM KJ/KG TO BTU/LBM ---
C     --- SP. VOL. IS IN FT3/LBM ---
C
      PSI= PB*(1.E+5)/6895.
C          WRITE (*,*) 'PSI PRESS', PSI
C
```

```
C     --- (2): RHOF ---
C           FIND VF FOR TSAT, AND THEN RHOF ---
C           VF IN CM3/G ==> 1.E-3 M3/KG ---
C
C     CHANGED BY BNM ON 7-9-97 TO BE A DIRECT TABLE LOOK-UP
C     FUNCTION RETURNS RHOL DIRECTLY.
C
C      VF= VFT(TGSAT)
C      VF= VF*1.E-3
C      RHOL= 1./VF
C      VF = 1./RHOL
C
C     LINE BELOW WAS ADDED 7-9-97 BY BNM
C
      RHOL = VFT(TGSAT)
      vf=1./rhol
C      write (*,*) 'rhol in subroutine', rhol

C
C     --- TO GET HFG FROM HF AND HG ---
C
      HF= HFPSAT (PB)
      HG= HGPSAT (PB)
C
      HFG= HG - HF
C-----        HFG=HFG*10000.
C
C     --- (3): GET VISCOSITY FROM TSAT AND RHOL ---
C           EMU (1.E-6 KG/M-SEC), T IN K, RHOL IN KG/M3 ---
C
C     THIS SUBROUTINE ALSO MODIFIED TO BE A TABLE LOOK-UP BY BNM.
C
      CALL VISCOL (TGSAT,EMU)
C
      EMUL= EMU
C      write (*,*) 'viscosity in subroutine', emul
C
C     ---- (4): GET SP. HEAT FROM P AND T ---
C            P IN BAR, T IN C, CP IN KJ/KG K ---
      CALL CPLT (PB,TGSATC,CP)
C
      CPL= CP*1.E+3
C
C     --- (5): GET CONDUCTIVITY FROM T, RHOL ---
C           T IN K, RHOL IN KG/M3, EKL IN W/K-M ---
C
      CALL THCND (TGSAT,RHOL,EKL)
C
C     --- (6): TO FIND PRANDTL NUMBER, FROM CP, MU, AND K ---
C
      PRNTL= CPL*EMUL/EKL
C
C     --- ALL VAPOR-PROPERTIES ARE AT PV ---
C     --- GET VGV FROM RHOV ---
C
C     BNM ADDED THE FOLLOWING 3 LINES, PER HAINING'S PROGRAM
```

```
C     5/7/97
C
C
      TG1 = TSATF(PB)
      VV1 = VGPT(PB,TG1)
      VV1 = VV1*1.E-3
      RHOV= 1./VV1
C
C     THE REST WAS HERE
C
      VGV= 1./RHOV
      VFG = VGV-VF
C
C     --- (7): TO GET CPG FROM PV (?) AND TSAT ---
C              CP IN J/G-K ==> J/KG-K ---
C
      CPGV= CPVPT (PB,TGSAT)
      CPGV= CPGV*1.E+3
C
C     --- FIND DHVDP ---
C
       PSI=PB*(1.E+5)/6895.
C      WRITE (*,*) 'PSI IN 2ND PLACE IN PRPSAT', PSI
      DHVDP=DHGPSAT(PSI)
C
C     --- CHANGE DHVDP FROM (BTU/LB PER PSI) TO (J/KG PER PA) ---
C     --- 2326. FROM BTU/LB TO J/KG AND 6895. FROM PSI TO PA ---
C
      DHVDP=DHVDP*(2326./6895.)
C
C     ---- (12): TO FIND SIG FROM TSAT ---
C               TSAT IN K, SIG IN 1.E-3 N/M (DYNE/CM) ---
C
      SIG= SIGTF (TGSAT)
      SIG= SIG * 1.E-3


C     --- EMUV IN PA S ---
      CALL VISCOV (PB,TGSAT,EMU)
C
      EMUGV= 1.E-6 * EMU
C     --- EKV IN W/K M ---
      CALL THCONV (PB,TGSAT,EK)
C
      EKGV= 1.E-3 * EK
C
C     --- NON-CONDENSABLE PROPS: CPA, HA, EKN, AND EMUN ---
C
      IF (MN.EQ.29) THEN
            CPA=CPA28 (TGSAT)
             CPA=962.2+(TGSAT*(.06781+(.0001656*TGSAT)
     1                    -(6.78E-8*(TGSAT**2.))))
              HA=HAT28(TGSAT)
C     --- CURVE-FITS FOR EKN AND EMUN: FROM SECTION 4;
C     --- THERMO-PHYSICAL PROPERTIES OF AIR.
      EKN=(3.227E-3)+(TGSAT*((8.3894E-5)-(TGSAT*(1.958E-8))))
```

```
      EMUN=(6.109E-6)+(TGSAT*((4.604E-8)-(TGSAT*(1.051E-11))))
C
            ELSEIF (MN.EQ.4) THEN
C
             CPA= 5200.
              HA=CPA*TGSAT
               EKN=EKNTHE(TGSAT)
                EMUN=EMUNTHE(TGSAT)
      END IF
C
C     --- DEFINE MIXTURE-PROPS ---
C
      FRMASV=1.0-XGA1
            FRMASN=XGA1
      FRMOLV=1.0-YGA1
            FRMOLN=YGA1
C
      CPG=(FRMASV*CPGV)+(FRMASN*CPA)
C
            UP12= (1.+(((MN/MV)**0.25)*((EMUGV/EMUN)**0.5)))**2.
            DN12=(8.+(8.*(MV/MN)))**0.5
      PHI12=UP12/DN12
C
            UP21= (1.+(((MV/MN)**0.25)*((EMUN/EMUGV)**0.5)))**2.
            DN21=(8.+(8.*(MN/MV)))**0.5
      PHI21=UP21/DN21
C
            DNTRM1=FRMOLV+(FRMOLN*PHI12)
             DNTRM2=FRMOLN+(FRMOLV*PHI21)
C
      EKG=((FRMOLV*EKGV)/DNTRM1)+((FRMOLN*EKN)/DNTRM2)
C
      EMUG=((FRMOLV*EMUGV)/DNTRM1)+((FRMOLN*EMUN)/DNTRM2)
C
            HA0=0.
      HG=((1.-XGA1)*HG)+(XGA1*(HA-HA0))
C     --- PRNTV ---
      PRNTG = (EMUG * CPG) / EKG
C
C
  10  FORMAT (3X,'SUBCOOLED LIQUID  ***  DO NOT USE VAPOR PROPERTIES')
C
C      WRITE (6,*) PB,TGSAT,CPV,EMUV,EKV,PRNTV
C
C
      RETURN
      END
C
C     ----------------------------------------------------------------
C
C     ----------------------------------------------------------------
C
      FUNCTION TSATF(PB)
      IMPLICIT REAL*8 (A-H,O-Z)
C
C     --- GIVE SAT TEMP. TSAT FOR THE PRESS. P IN BAR ---
```

```
C       PA IS PRESS. ARRAY, TA IS TEMP. ARRAY ---
C
      DIMENSION PA(44),TA(44)
C
      DATA PA/ 0.05,0.075,.1,0.15,
     *        .2,0.25,0.30,0.35,0.40,0.45,
     *        .5,0.60,0.70,0.80,0.90,0.95,
     *        1.,1.5,2.0,2.5,3.0,3.5,4.0,
     *        5., 10., 20., 30., 40., 50.,
     1        60.,70.,80.,90.,100.,110.,120.,130.,140.,150.,
     2       160.,170.,180.,190.,200./
C
      DATA TA/ 32.88,40.3,45.82,53.98,
     *       60.07,64.98,69.11,72.7,75.88,78.74,
     *       81.34,85.95,89.96,93.51,96.71,98.2,
     *       99.63,111.38,120.24,127.44,133.55,138.89,143.64,
     1       151.87,179.92,212.42,233.89,250.39,263.98,
     2       275.62,285.86,295.04,303.38,311.03,
     3       318.11,324.71,330.89,336.70,342.19,
     4       347.39,352.34,357.04,361.52,365.80/
C
      N= 44
       PB1=PB
C
      CALL POLINT (PA,TA,N,PB1,TSATC,DY)
C
      TSATQ= TSATC + 273.15
      TSATF= TSATQ
      RETURN
      END
C
C     FOUND THAT THIS SUBROUTINE DOESN'T WORK FOR 50 DEGREES C
C     SO AM REPLACING IT! AM COMMENTING THIS ONE OUT. OOPS,
C     PUT VISCOL WHERE RHO CALC SUBROUTINE WAS.
C
C
C      DIMENSION D(4)
C
C     --- T IN K, VF IN CM3/G ---
C
C      DATA D / -4.4267, 3.598E-2, -8.0055E-5, 6.1163E-8/
C
C      SEG1= 0.
C
C      write (*,*) 'tsat in subroutine vft', tsat
C      DO 10 I=1,4
C  10    SEG1= SEG1 + D(I)*(TSAT**(I-1))
C
C      VFT= SEG1
C      write (*,*) 'vft in sub vft =', vft
C
C      RETURN
C      END
C -------------------------------------------------------------------
C       NEW SUBROUTINE FOR DENSITY OF WATER ONLY(BNM, 7-9-97)
C
```

```
      FUNCTION VFT(TGSAT)
C       MAKE DATA TABLES USING TEMPERATURE AND DENSITY (KG/M3)
       IMPLICIT REAL*8(A-H,O-Z)
       DIMENSION TAP(16),RHOTAB(16)
C
      DATA TAP/ 273.16,293.16,313.16,333.16,353.16,
     *        373.16,393.16,413.16,433.16,453.16,
     *        473.16,493.16,513.16,533.16,553.16,
     *        573.16/
C
      DATA RHOTAB/1002.28,1000.52,994.59,985.46,974.08,
     *        960.63,945.25,928.27,909.69,889.03,
     *        866.76,842.41,815.66,785.87,752.55,
     *        714.26/
      N= 16
C       WRITE(*,*) "HOWDY, I'M IN FUNCTION VFT"
      TAINT = TGSAT
C
      CALL POLINT (TAP,RHOTAB,N,TAINT,RHOLUP,DY)
C
      VFT = RHOLUP
C       WRITE (*,*) "VFT= RHO",VFT
C
C
      RETURN
      END
C
C-----------------------------------------------------------------
C       NEW SUBROUTINE FOR VISCOSITY OF WATER ONLY(BNM, 7-9-97)
       SUBROUTINE VISCOL(TSAT,EMU)
       IMPLICIT REAL*8 (A-H,O-Z)
C
C
C     --- GIVE VISCOSITY MU GIVEN THE TEMPERATURE IN K ---
C         TA IS TEMP. ARRAY, AMUA IS TEMP. ARRAY ---
C
      DIMENSION TAQ(32),AMUA(32)
C
      DATA TAQ/ 0.0,20.0,40.0,60.0,80.0,
     *        100.0,120.0,140.0,160.0,180.0,
     *        200.0,220.0,240.0,260.0,280.0,
     *        300.0,320.0,340.0,360.0,380.0,
     *        400.0,420.0,440.0,460.0,480.0,
     *        500.0,520.0,540.0,560.0,580.0,
     *        600.0,620.0/
C
      DATA AMUA/ 1.7921E-2,1.0065E-2,6.5442E-3,4.7105E-3,
     *       3.5457E-3,2.8243E-3,2.3348E-3,1.9865E-3,
     *       1.7284E-3,1.5380E-3,1.3868E-3,1.2636E-3,
     *       1.1664E-3,1.0766E-3,1.0159E-3,9.6425E-4,
     *       5.7700E-4,4.2000E-4,3.2400E-4,2.6000E-4,
     *       2.1700E-4,1.8500E-4,1.6200E-4,1.4300E-4,
     *       1.2900E-4,1.1800E-4,1.0800E-4,1.0100E-4,
     *       0.9400E-4,0.8800E-4,0.8100E-4,0.7200E-4/
C
      N= 32
```

```
      TAINT=TSAT
C
      CALL POLINT (TAQ,AMUA,N,TAINT,AMUINT,DY)
C
      EMU= AMUINT
C
C
      RETURN
      END
C
C     ---------------------------------------------------------------
C
      FUNCTION PSATF (T)
      IMPLICIT REAL*8 (A-H,O-Z)
C
C     --- GIVE SAT PRESSURE PSAT FOR THE TEMP. T IN K ---
C         PA IS PRESS. ARRAY, TA IS TEMP. ARRAY ---
C
      DIMENSION PA(47),TA(47)
C
      DATA PA/ 0.02,0.03,0.04,0.05,0.075,.1,0.15,
     *        .2,0.25,0.30,0.35,0.40,0.45,
     *        .5,0.60,0.70,0.80,0.90,0.95,
     *        1.,1.5,2.0,2.5,3.0,3.5,4.0,
     *        5., 10., 20., 30., 40., 50.,
     1        60.,70.,80.,90.,100.,110.,120.,130.,140.,150.,
     2       160.,170.,180.,190.,200./
C
      DATA TA/ 17.5,24.1,29.0,32.88,40.3,45.82,53.98,
     *       60.07,64.98,69.11,72.7,75.88,78.74,
     *       81.34,85.95,89.96,93.51,96.71,98.2,
     *       99.63,111.38,120.24,127.44,133.55,138.89,143.64,
     1       151.87,179.92,212.42,233.89,250.39,263.98,
     2       275.62,285.86,295.04,303.38,311.03,
     3       318.11,324.71,330.89,336.70,342.19,
     4       347.39,352.34,357.04,361.52,365.80/
C
      N= 44
      T1=T-273.15
C     WRITE(6,*) 'T1 IN PSAT',T1
C
      CALL POLINT (TA,PA,N,T1,PSAT,DY)
C
C     WRITE(6,*) 'BACK FROM POLINT'
      PSATF= PSAT*1.0E5
C     WRITE(6,*) 'PSATF IN PSAT SUB',PSATF
C
C
      RETURN
      END
C
C-----------------------------------------------------------------
C
      FUNCTION HFPSAT (PB)
      IMPLICIT REAL*8 (A-H,O-Z)
C
```

```
C     --- GIVE SAT. ENTHALPY IN J/KG  FOR A GIVEN P IN BAR ---
C         XA IS PRESS. ARRAY AND YA IS ENTHALPY ARRAY ---
C         RANGE: .1 BAR TO 200 BAR  ---
C
      DIMENSION XA(20),YA(20)
C
      DATA XA/.1, .5, 1., 5.,10.,20.,40.,60.,70.,80.,
     1       90.,100.,110.,120.,130.,140.,150.,160.,180.,200./
C
      DATA YA/191.8,340.5,417.5,640.4,762.9,
     1        908.7,1087.,1213.,1266.,1316.,
     2         1363.,1407.,1449.,1490.,1530.,
     3          1570.,1610.,1649.,1732.,1827./
C
C
      N=20
C
      CALL POLINT (XA,YA,N,PB,HFSAT,DY)
C
      HFPSAT= HFSAT * 1.E+3
C
C
      RETURN
      END
C
C     ----------------------------------------------------------------

C
      FUNCTION HGPSAT (PB)
      IMPLICIT REAL*8 (A-H,O-Z)
C
C     --- VAPOR SAT. ENTHALPY IN J/KG  FOR A GIVEN P IN BAR ---
C         XA IS PRESS. ARRAY AND YA IS ENTHALPY ARRAY ---
C         RANGE: .1 BAR TO 200 BAR  ---
C
      DIMENSION XA(20),YA(20)
C
      DATA XA/.1, .5, 1., 5.,10.,20.,40.,60.,70.,80.,
     1       90.,100.,110.,120.,130.,140.,150.,160.,180.,200./
C
      DATA YA/ 2584., 2645., 2675., 2748., 2777.,
     1         2798., 2800., 2783., 2771., 2757.,
     2          2742., 2724., 2705., 2684., 2661.,
     3           2637., 2610., 2580., 2510., 2413. /
C
C
      N=20
C
      CALL POLINT (XA,YA,N,PB,HGSAT,DY)
C
      HGPSAT= HGSAT * 1.E+3
C
C
      RETURN
      END
C
```

```
C    ---------------------------------------------------------------
C
C    COMMENTING OUT THIS SUBROUTINE, NOT GOOD FOR T = 50 DEGREES C
C
C     SUBROUTINE VISCOL (T,RHOL,EMU)
C     IMPLICIT REAL*8 (A-H,O-Z)
C
C     DIMENSION AP(4),BIJ(6,5)
C
C    --- T IN K, RHOL IN KG/M3, EMU IN MICRO PA-S (1.E-6 KG/MS) ---
C
C     DATA AP / 0.0181583, 0.0177624, 0.0105287, -0.0036744/
C     DATA TCRT, RHOC / 647.27, 317.763 /
C     DATA BIJ/ .501938, .162888, -.130356, .907919, -.551119, .146543,
C    2         .235622, .789393, .673665, 1.207552, .0670665, -.084337,
C    3        -.274637, -.743539,-.959456,-.687343,-.497089, .195286,
C    4       .145831, .263129, .347247, .213486, .100754, -.032932,
C    5      -.027045,-.025309,-.026776,-.082290, .060225, -.020259/
C
C
C     SUM1= 0.
C     SUM2= 0.
C
C     DO 10 K=1,4
C  10    SUM1= SUM1 + (AP(K)*((TCRT/T)**(K-1)))
C
C     EMUO= (1.E-6) * ((T/TCRT)**.5) * (1./SUM1)
C
C     DO 20 I=1,6
C      DO 20 J= 1,5
C  20  SUM2=SUM2+BIJ(I,J)*(((TCRT/T)-1.)**(I-1))*
C     1 (((RHOL/RHOC)-1.)**(J-1))
C
C     EMU= EMUO * EXP((RHOL/RHOC)*SUM2)
C
C     RETURN
C     END
C
C    ---------------------------------------------------------------
C
      SUBROUTINE CPLT (X1,X2,Y)
      IMPLICIT REAL*8 (A-H,O-Z)
C
C    ----------------------------- CPT -----------------------------
C    --- TO FIND SUBCOOLED LIQUID SP. HEAT FROM PRESS. & TEMP. ---
C        PRESSURE IN BAR AND TEMPERATURE IN DEGREE CELSIUS
C        X1 = GIVEN PRESS. ,  X2 = GIVEN TEMP. , Y = SP. HEAT CALC.
C    ---------------------------------------------------------------
C
C     OPEN (6,FILE='H.OUT')
C
C    --- READ X1 (PRESS), AND X2 (TEMP) TO FIND Y (SP. HEAT) ---
C     SUBROUTINE POLIN2 (X1,X2,Y,DY)
C
      PARAMETER (M=10,N=10,NMAX=10,MMAX=10)
      DIMENSION X1A(M),X2A(N),YA(M,N), X1B(M),X2B(N),YB(M,N),
```

```
     1 YNTMP(NMAX),YMTMP(MMAX)
C
C     --- X1A:  PRESSURE HAS 10 VALUES FROM 1 TO 100 BAR ---
C     --- X2A:  TEMPERATURE HAS 10 VALUES FROM 0 TO 300 C ---
C
      DATA X1A/1.,5.,10.,25.,50.,60.,70.,80.,90.,100./
      DATA X2A/10.,20.,40.,60.,80.,100.,150.,200.,250.,300./
C
      DATA X1B/80.,90.,100.,110.,120.,130.,140.,160.,180.,200./
      DATA X2B/10.,20.,40.,80.,100.,150.,200.,250.,300.,350./
C
C     --- YA: SP. HEAT HAS (10 X 10) VALUES  IN KJ/KG K ---
C
      DATA YA/4.188,4.186,4.184,4.178,4.17,4.165,4.16,4.158,4.154,4.15,
     1    4.183,4.182,4.180,4.176,4.168,4.165,4.162,4.159,4.156,4.153,
     2    4.182,4.181,4.180,4.176,4.171,4.168,4.166,4.164,4.161,4.159,
     3    4.183,4.182,4.181,4.177,4.172,4.170,4.168,4.166,4.163,4.161,
     4    4.194,4.193,4.192,4.189,4.183,4.181,4.179,4.177,4.175,4.173,
     5    4.216,4.216,4.215,4.212,4.206,4.204,4.201,4.199,4.197,4.195,
     6    4.312,4.312,4.310,4.305,4.298,4.294,4.291,4.288,4.285,4.282,
     7    4.484,4.484,4.484,4.484,4.469,4.464,4.458,4.453,4.448,4.442,
     8    4.843,4.843,4.843,4.843,4.843,4.830,4.817,4.804,4.792,4.780,
     9    5.724,5.724,5.724,5.724,5.724,5.724,5.724,5.724,5.724,5.676/
C
C     --- TABLE 2. YB: SP. HEAT (80 TO 200 BAR, 10 TO 350 C) ---
C
      DATA YB/4.158,4.154,4.15,4.147,4.143,4.14,4.136,4.129,4.123,4.116,
     1    4.159,4.156,4.153,4.15,4.147,4.145,4.142,4.136,4.131,4.125,
     2    4.164,4.161,4.159,4.157,4.154,4.152,4.15,4.146,4.141,4.137,
     3    4.177,4.175,4.173,4.171,4.169,4.167,4.165,4.161,4.157,4.153,
     4    4.199,4.197,4.195,4.193,4.19,4.188,4.186,4.182,4.178,4.174,
     5    4.288,4.285,4.282,4.279,4.276,4.273,4.271,4.265,4.259,4.254,
     6    4.453,4.448,4.442,4.437,4.432,4.427,4.422,4.412,4.403,4.394,
     7    4.804,4.792,4.78,4.768,4.757,4.746,4.735,4.714,4.694,4.674,
     8    5.724,5.724,5.676,5.63,5.586,5.546,5.507,5.435,5.37,5.311,
     9    9.702,9.702,9.702,9.702,9.702,9.702,9.702,9.702,9.025,8.138/
C
C     ---------------------------------------------------------------
C
      P=X1
      T=X2+273.15
C
      TSAT= TSATF (P)
C
C       IF (T.GT.TSAT) WRITE (6,10)
C  10  FORMAT (3X,' LIQUID SATURATED  ***  USE SATURATED PROPS')
C
      IF (P.GT.90.) GO TO 20
C
      DO 12 J=1,M
        DO 11 K=1,N
          YNTMP(K)=YA(J,K)
   11   CONTINUE
        CALL POLINT(X2A,YNTMP,N,X2,YMTMP(J),DY)
   12   CONTINUE
      CALL POLINT(X1A,YMTMP,M,X1,Y,DY)
```

```
C
      RETURN
C
C
  20  CONTINUE
      DO 22 J=1,M
        DO 21 K=1,N
      YNTMP(K)=YB(J,K)
  21  CONTINUE
      CALL POLINT (X2B,YNTMP,N,X2,YMTMP(J),DY)
  22  CONTINUE
      CALL POLINT (X1B,YMTMP,M,X1,Y,DY)
C
C
      RETURN
      END
C
C     ----------------------------------------------------------------
C
      SUBROUTINE THCND (T,RHOL,CND)
      IMPLICIT REAL*8 (A-H,O-Z)
C
      DIMENSION A(4),B(3),C(6),D(4)
C
C     --- T IN K, RHOL IN KG/M3, CND IN W/K-M ---
C
      DATA TCRT, RHOC / 647.3, 317.7 /
      DATA B11, B22 / -.171587, 2.39219 /
      DATA A / 1.02811E-2, 2.99621E-2, 1.56146E-2, -4.22464E-3/
      DATA B / -3.9707E-1, 4.00302E-1, 1.06/
      DATA C/6.42757E-1,-4.11717,-6.17937,3.08976E-3,8.22994E-2,1.00932/
      DATA D / 7.01309E-2, 1.1852E-2, 1.69937E-3, -1.02 /
C
C
      S1=0.
C
      DO 10 I=1,4
   10   S1= S1 + A(I) * ((T/TCRT)**(I-1))
      CKO= ((T/TCRT)**.5) * S1
C
      CKBAR=B(1)+B(2)*(RHOL/RHOC)+B(3)*EXP(B11*(((RHOL/RHOC)+B22)**2.))
C
      F1= D(1)*((TCRT/T)**10.) + D(2)
       F2= C(1)*(1.-((RHOL/RHOC)**2.8))
C
      DTC= DABS((T/TCRT)-1.) + C(4)
      Q= 2. + C(5) * (DTC**(-.6))
      R= Q + 1.
C
      RTTC= T/TCRT
      IF (RTTC.GE. 1.) THEN
        S= DTC**(-1.)
       ELSE
        S= C(6)*(DTC**(-.6))
      END IF
C
```

```
      F3= (Q/R)*(1.-((RHOL/RHOC)**R))
       F4= C(2)*((T/TCRT)**1.5) + C(3)*((RHOC/RHOL)**5.)
C
      CKDEL= F1*((RHOL/RHOC)**1.8)*EXP(F2) + D(3)*S*((RHOL/RHOC)**Q)
     1 *EXP(F3) + D(4)*EXP(F4)
C
      CND = CKO + CKBAR + CKDEL
C
      RETURN
      END
C
C     ----------------------------------------------------------------

      FUNCTION CPVPT (PB,T)
      IMPLICIT REAL*8 (A-H,O-Z)
C
      DIMENSION C(3),Y(11)
C
C     --- P IN BAR, T IN K, CPG IN KJ/G-K ---
C
      DATA C / 1.7524, 2.4936E-4, 3.0978E-7 /
      DATA Y / 1.112E+1, 5.211E+1, -1.0089E-1, 4.5463E-5, 4.3768E-1,
     * -1.5544E-3, 1.2808E-6, -4.9183E-2, 7.2632E-5, -3.5782E-8, 2.9971/
C
      CPG= C(1) + T*(C(2) + C(3)*T) +
     1      ( (PB*(Y(1)*(PB**2.)+ T*(Y(2) +
     2      Y(3)*T + Y(4)*(T**2.) + Y(5)*PB + Y(6)*PB*T +
     3      Y(7)*PB*(T**2.) + Y(8)*(PB**2.) + Y(9)*(PB**2.)*T +
     4      Y(10)*(PB**2.)*(T**2.) )) )
     5          / ((T-Y(11)*PB)**2.) )

      CPVPT= CPG
C
      RETURN
      END
C
C     ----------------------------------------------------------------

      FUNCTION DHGPSAT (P)
C     ---------------
      IMPLICIT REAL*8 (A-H,O-Z)
C
C     ----- CAL. THE DERV. OF VAPOR-ENTHALPY VS. PRESSURE -----
C     -----        ( P IN  PSIA,  AND H IN BTU/LBM. )   -----
C
      DIMENSION CG1(12), CG2(9), CG3(7)
C
C  ---   0.1 < P < 1500. PSIA
C
      DATA CG1/.1105836875E+04, .1436943768E+02, .8018288621E+00,
     * .1617232913E-01,-.1501147505E-02,  4*0.,
     *-.1237675562E-04, .3004773304E-05,-.2062390734E-06/
C
C  ---  1100. < P < 2650. PSIA
C
      DATA CG2/-.2234264997E+07, .1231247634E+07,-.1978847871E+06,
```

```
     * .1859988044E+02,-.2765701318E+01, .1036033878E+04,
     *-.2143423131E+03, .1690507762E+02,-.4864322134E+00/
C
C  ---  2550. < P < 3208. PSIA
C
      DATA CG3/.9059978254E+03, .5561957539E+01, .3434189609E+01,
     *-.6406390628E+00, .5918579484E-01,-.2725378570E-02,
     * .5006336938E-04/
C
C     ----------------------------------------------------------------
C
C                       -----  VAPOR REGION  -----
C
C       WRITE (6,*) 'P IN SUBROUTINE DHGPSAT', P
       ALNP=DLOG(P)
       DP=(3208.-P)**.41
C
      DHGSAT=0.
C
      IF (P.GE..1.AND.P.LE.1500.) GO TO 10
       IF (P.GE.1100..AND.P.LE.2650.) GO TO 20
        IF (P.GE.2550..AND.P.LE.3208.) GO TO 30
C
  10  CONTINUE
C
      DO 11 I=1,12
C      WRITE (*,*) 'DHGSAT,CG1(1),I,ALNP,P',DHGSAT,CG1(1),I,P
  11  DHGSAT=DHGSAT+(CG1(I)*(I-1)*(ALNP**(I-2))*(1./P))
       DHGPSAT=DHGSAT
       RETURN
C
  20  CONTINUE
      DO 21 J=1,9
  21   DHGSAT=DHGSAT+(CG2(J)*(J-1)*(ALNP**(J-2))*(1./P))
       DHGPSAT=DHGSAT
       RETURN
C
  30  CONTINUE
      DO 31 K=1,7
  31   DHGSAT=DHGSAT+(CG3(K)*(K-1)*(DP**(K-2))*
     1              (-.41*((3208.-P)**(.41-1.))))
       DHGPSAT=DHGSAT
C
      RETURN
      END
C
C     ----------------------------------------------------------------
C
      FUNCTION SIGTF (T)
      IMPLICIT REAL*8 (A-H,O-Z)
C
      DIMENSION A(5)
C
      DATA A / 1.1609368E-1, 1.1214047E-3, -5.7528052E-6,
     1         1.2862746E-8, -1.1497193E-11/
      DATA TCRT, BETA / 647.3, 0.83 /
```

```
C
      SUM1=0.
      DCRTT= TCRT -T
C
      DO 10 N=2,5
   10   SUM1= SUM1 + A(N) * (DCRTT**N)
      SIG= ((A(1)*(DCRTT**2.)) / (1. + BETA*DCRTT)) + SUM1
      SIGTF= SIG
C
C
      RETURN
      END
C
C     ----------------------------------
C     ------------------------------------------------------------------
C
      SUBROUTINE VISCOV (X1,X2,Y)
      IMPLICIT REAL*8 (A-H,O-Z)
C
C     --- GIVE VAPOR VISCOSITY FOR PRESS. P AND TEMP. T ---
C        P IN BAR, T IN K, AND EMUV IN PA S ---
C        X1A IS PRESSURE, X2A IS TEMP., AND YA IS VAPOR VISCOSITY ---
C        RANGE: X1A ==> 1 TO 80 BAR,  X1B ==> 60 TO 200 BAR
C              X2A ==> 100 TO 375 C ,  X2B ==> 275 TO 600 C
C              YA ==> VISCOSITY     ,  YB  ==> VISCOSITY
C
      PARAMETER (M=10,N=10,NMAX=10,MMAX=10)
      DIMENSION X1A(M),X2A(N),YA(M,N),X1B(M),X2B(N),YB(M,N),
     1          YNTMP(NMAX),YMTMP(MMAX)
C
C     --- PRESSURE RANGE IN BAR ---
C
      DATA X1A/1.,5.,10.,20.,30.,40.,50.,60.,70.,80./
      DATA X1B/60.,70.,80.,90.,100.,120.,140.,160.,180.,200./
C
C     --- TEMPERATURE RANGE IN C ---
C
      DATA X2A/100.,150.,200.,225.,250.,275.,300.,325.,350.,375./
      DATA X2B/275.,300.,325.,350.,375.,400.,425.,450.,475.,500./
C
C     (TABLE1): VAPOR VISCOSITY IN MICRO PA S, 1 TO 80 BAR & 100 TO 375 C
C
      DATA YA/12.28, 12.3,12.3,12.3,12.3, 12.3,12.3,12.3,12.3,12.3,
     1     14.19,14.08,14.08,14.08,14.08,14.08,14.08,14.08,14.08,14.08,
     2     16.18,16.07,15.93,15.93,15.93,15.93,15.93,15.93,15.93,15.93,
     3     17.20,17.11,17.00,16.79,16.79,16.79,16.79,16.79,16.79,16.79,
     4     18.22,18.15,18.07,17.91,17.75,17.61,17.61,17.61,17.61,17.61,
     5     19.25,19.20,19.14,19.01,18.89,18.78,18.67,18.61,18.61,18.61,
     6     20.29,20.25,20.20,20.10,20.01,19.93,19.86,19.80,19.76,19.73,
     7     21.33,21.30,21.26,21.19,21.12,21.07,21.02,20.98,20.96,20.95,
     8     22.37,22.35,22.32,22.27,22.22,22.18,22.16,22.14,22.13,22.13,
     9     23.41,23.39,23.37,23.34,23.31,23.29,23.27,23.27,23.27,23.28/
C
C     (TABLE2): VAPOR VISCO. IN MICRO PA S, 60 TO 200 BAR & 275 TO 600 C
C
      DATA YB/18.61,18.6,18.6,18.6,18.6, 18.6,18.6,18.6,18.6,18.6,
```

```
     1    19.80,19.76,19.73,19.73,19.73,19.73,19.73,19.73,19.73,19.73,
     2    20.98,20.96,20.95,20.96,21.00,21.23,21.23,21.23,21.23,21.23,
     3    22.14,22.13,22.13,22.15,22.18,22.33,22.64,23.35,23.35,23.35,
     4    23.27,23.27,23.28,23.31,23.35,23.47,23.69,24.04,24.64,25.79,
     5    24.38,24.39,24.42,24.45,24.49,24.61,24.79,25.05,25.43,25.96,
     6    26.57,26.60,26.63,26.67,26.72,26.85,27.01,27.21,27.46,27.77,
     7    28.71,28.75,28.79,28.84,28.90,29.02,29.18,29.36,29.57,29.82,
     8    30.80,30.85,30.79,30.95,31.01,31.15,31.03,31.47,31.67,31.89,
     9    32.85,32.91,32.96,33.02,33.08,33.22,33.37,33.54,33.72,33.82/
C
C    ----------------------------------------------------------------
C
C
      P=X1
      T=X2
C       TSAT= TSATF (P)
C
C       WRITE (6,*) P,TSAT
C
C       IF (T.LT.TSAT) THEN
C         Y=1.0000
C         WRITE (6,10)
C   10   FORMAT (3X,'SUBCOOLED *** DONOT USE VAPOR PROPERTIES ')
C         RETURN
C       END IF
C
      X2C = X2 - 273.15
C
      IF (P.GT.65.) GO TO 20
C
C
      DO 12 J=1,M
        DO 11 K=1,N
      YNTMP(K)= YA(J,K)
   11 CONTINUE
      CALL POLINT (X2A,YNTMP,N,X2C,YMTMP(J),DY)
   12 CONTINUE
C
      CALL POLINT (X1A,YMTMP,M,X1,Y,DY)
C
      RETURN
C
   20 CONTINUE
C
      DO 22 J=1,M
        DO 21 K=1,N
      YNTMP(K)= YB(J,K)
   21 CONTINUE
      CALL POLINT (X2B,YNTMP,N,X2C,YMTMP(J),DY)
   22 CONTINUE
C
      CALL POLINT (X1B,YMTMP,M,X1,Y,DY)
C
C
      RETURN
      END
```

```
C
C    ---------------------------------------------------------------
C
      SUBROUTINE THCONV (X1,X2,Y)
      IMPLICIT REAL*8 (A-H,O-Z)
C
C     --- GIVE VAPOR CONDUCTIVITY FOR PRESS. P AND TEMP. T ---
C         P IN BAR, T IN K, AND EK IN 1.E-3 W/K M ---
C         X1A IS PRESSURE, X2A IS TEMP., AND YA IS VAPOR CONDUCTIVITY.
C         RANGE: X1A ==> 1 TO 80 BAR,  X1B ==> 60 TO 200 BAR
C              X2A ==> 100 TO 375 C ,  X2B ==> 275 TO 600 C
C              YA ==> CONDUCTIVITY  ,  YB  ==> CONDUCTIVITY
C
      PARAMETER (M=10,N=10,NMAX=10,MMAX=10)
      DIMENSION X1A(M),X2A(N),YA(M,N),X1B(M),X2B(N),YB(M,N),
     1          YNTMP(NMAX),YMTMP(MMAX)
C
C     --- PRESSURE RANGE IN BAR ---
C
      DATA X1A/1.,5.,10.,20.,30.,40.,50.,60.,70.,80./
      DATA X1B/60.,70.,80.,90.,100.,120.,140.,160.,180.,200./
C
C     --- TEMPERATURE RANGE IN C ---
C
      DATA X2A/100.,150.,200.,225.,250.,275.,300.,325.,350.,375./
      DATA X2B/275.,300.,325.,350.,375.,400.,425.,450.,475.,500./
C
C     (TABLE1): CONDUCTIVITY IN 1.E-3 W/K M, 1 TO 80 BAR & 100 TO 375 C
C
      DATA YA/24.78,24.8,24.8,24.8,24.8,24.8,24.8,24.8,24.8,24.8,
     1     28.80,28.8,28.8,28.8,28.8,28.8,28.8,28.8,28.8,28.8,
     2     33.37,34.24,36.06,36.06,36.06,36.06,36.06,36.06,36.06,36.06,
     3     35.78,36.44,37.64,41.45,41.45,41.45,41.45,41.45,41.45,41.45,
     4     38.28,38.81,39.69,42.22,45.95,45.95,45.95,45.95,45.95,45.95,
     5     40.85,41.30,42.01,43.86,46.37,49.71,54.13,54.13,54.13,54.13,
     6     43.49,43.89,44.49,45.95,47.81,50.14,53.04,56.67,61.27,67.28,
     7     46.19,46.57,47.09,48.32,49.80,51.58,53.70,56.23,59.25,62.91,
     8     48.97,49.32,49.79,50.86,52.11,53.55,55.22,57.14,59.37,61.96,
     9     51.81,52.14,52.57,53.53,54.60,55.79,57.11,58.58,60.21,62.03/
C
C     (TABLE2): CONDUCT. IN 1.E-3 W/K M, 60 TO 200 BAR & 275 TO 600 C
C
      DATA YB/59.98,60.0,60.0,60.0,60.0, 60.0,60.0,60.0,60.0,60.0,
     1    56.67,61.27,67.28,67.28,67.28,67.28,67.28,67.28,67.28,67.28,
     2    56.23,59.25,62.91,67.41,73.05,90.69,90.69,90.69,90.69,90.69,
     3    57.14,59.37,61.96,65.00,68.58,78.07,92.86,121.0,121.0,121.0,
     4    58.58,60.21,62.03,64.08,66.38,72.01,79.62,90.64,108.6,145.4,
     5    60.80,62.20,63.73,65.41,67.26,71.56,76.86,83.50,92.04,103.4,
     6    65.82,66.89,68.04,69.26,70.57,73.44,76.72,80.48,84.81,89.81,
     7    71.44,72.34,73.30,74.29,75.34,77.59,80.07,82.80,85.81,89.14,
     8    77.43,78.24,79.07,79.93,80.83,82.73,84.78,86.98,89.37,91.93,
     9    83.71,84.44,85.19,85.96,86.75,88.42,90.20,92.09,94.10,96.23/
C
C    ---------------------------------------------------------------
C
C
```

```
      P=X1
      T=X2
C       TSAT= TSATF (P)
C
C       WRITE (6,*) P,TSAT
C
C       IF (T.LT.TSAT) THEN
C         Y=1.0000
C         WRITE (6,10)
C    10   FORMAT (3X,'SUBCOOLED *** DONOT USE VAPOR PROPERTIES ')
C         RETURN
C       END IF
C
      X2C = X2 - 273.15
C
      IF (P.GT.70.) GO TO 20
C
C
      DO 12 J=1,M
        DO 11 K=1,N
      YNTMP(K)= YA(J,K)
   11 CONTINUE
      CALL POLINT (X2A,YNTMP,N,X2C,YMTMP(J),DY)
   12 CONTINUE
C
      CALL POLINT (X1A,YMTMP,M,X1,Y,DY)
C
      RETURN
C
   20 CONTINUE
C
      DO 22 J=1,M
        DO 21 K=1,N
      YNTMP(K)= YB(J,K)
   21 CONTINUE
      CALL POLINT (X2B,YNTMP,N,X2C,YMTMP(J),DY)
   22 CONTINUE
C
      CALL POLINT (X1B,YMTMP,M,X1,Y,DY)
C
C
      RETURN
      END
C
C -------------------------------------------------------
      FUNCTION VGPT (PB,T)
      IMPLICIT REAL*8 (A-H,O-Z)
C
      DIMENSION ZX(10)
C
C     --- P IN BAR, T IN K, VG IN CM3/G ---
C
      DATA R / 4.619/
      DATA ZX/ 1.0001, -5.3391, 6.1322E-3, -7.4961E+1, .25547,
     *         -2.058E-4, -8.901E-3, 4.3505E-6, 6.1847, -1.4715E+3/
C
```

```
      VG= R * ( (ZX(1)*(T/PB)) + ZX(2) + ZX(3)*T + ZX(4)*(PB/T) +
     1          PB * (ZX(5) + ZX(6)*T + ZX(7)*PB + ZX(8)*PB*T +
     2          ZX(9)*(PB/T) + ZX(10)*(PB/(T*T))) )
C     WRITE (6,*) 'FIRST TERM', ZX(1)*(T/PB)
C     WRITE (6,*) 'SECOND TERM', ZX(2)
C     WRITE (6,*) 'THIRD TERM', ZX(3)*T
C     WRITE (6,*) 'FOURTH TERM', ZX(4)*(PB/T)
C     WRITE (6,*) 'FIFTH TERM, PB', PB
C     WRITE (6,*) 'ZX(5)', ZX(5)
C     WRITE (6,*) 'ZX(6)*T', ZX(6)*T
C     WRITE (6,*) 'ZX(7)*PB', ZX(7)*PB
C     WRITE (6,*) 'ZX(8)*PB*T', ZX(8),PB,T
C     WRITE (6,*) 'ZX(9)*(PB/T)', ZX(9)*(PB/T)
C     WRITE (6,*) 'ZX(10)*(PB/(T*T))', ZX(10)*(PB/(T*T))
C
      VGPT= VG
C     WRITE (6,*) 'VGPT IN SUBROUTINE', VGPT
C
C
      RETURN
      END
C
C     ---------------------------------------------------------------
C
      FUNCTION PSS (TSC1)
      IMPLICIT REAL*8 (A-H,O-Z)
C
C -----HERE TSC1 IN C
C -----PSS IN 0.1MPA
C
      TS2=TSC1
      PSS=(-6.15739E-1)+((2.87130E-2)*TS2)+((-4.46449E-4)*(TS2**2))+
     1  (3.22211E-6)*(TS2**3)
C
      RETURN
      END
C   ---------------------------------------------------------------
C
      FUNCTION CPA28 (T)
      IMPLICIT REAL*8 (A-H,O-Z)
C
      REAL*8 MN,MV
      COMMON /INPUT3/ MN,MV,wide,high,tubel,din,dout,theta,PIN
      COMMON /CONSTS / RGAS,G,PI
C
C     --- T IN K (300 K TO 1000K), CPA IN ? ---
C
       A= 3.675
        B= - 1.208 * (1.E-3)
         C= 2.324 * (1.E-6)
          D= - 0.632 * (1.E-9)
           E= - 0.226 * (1.E-12)
C
      CPA0= A + (B*T) + (C*(T**2.)) + (D*(T**3.)) + (E*(T**4.))
C
      CPA28=(RGAS/MN)*CPA0
```

```
C
      RETURN
      END
C
C     ----------------------------------------------------------------
      FUNCTION CPGAS(TG)
      IMPLICIT REAL*8 (A-H,O-Z)
C
C     --- GIVE SPECIFIC HEAT AT CONSTANT PRESS. FOR TEMP.---
C           SUPERHEATED STEAM, TEMP IN DEGREES K, CP IN J/(KG-K)
C           TA IS TEMP. ARRAY, CP IS SPECIFIC HEAT ARRAY
C
      DIMENSION TCP(37),CPG(37)
C
      DATA TCP/ 200.0,250.0,300.0,350.0,400.0,450.0,500.0,
     *          550.0,600.0,650.0,700.0,750.0,800.0,850.0,900.0,
     *          950.0,1000.0,1050.0,1100.0,1150.0,1200.0,1250.0,
     *          1300.0,1350.0,1400.0,1450.0,1500.0,1550.0,1600.0,
     *          1650.0,1700.0,1750.0,1800.0,1850.0,1900.0,1950.0,
     *          2000.0/
C
      DATA CPG/1851.2,1856.8,1864.9,1879.4,1901.8,1927.1,1955.3,
     *          1985.1,2016.3,2048.4,2081.3,2115.0,2149.3,2184.3,
     *          2219.6,2255.2,2290.7,2326.1,2361.1,2395.6,2429.5,
     *          2462.6,2494.8,2526.1,2556.4,2585.7,2613.9,2641.1,
     *          2667.2,2692.2,2716.3,2739.4,2761.5,2782.7,2803.0,
     *          2822.3,2840.9/
C
      N= 37
      TEMPIN = TG
C
      CALL POLINT (TCP,CPG,N,TEMPIN,CPBACK,DY)
C
      CPGAS= CPBACK
      RETURN
      END
C     ----------------------------------------------------------------
C
      FUNCTION EKNTHE (T)
      IMPLICIT REAL*8 (A-H,O-Z)
C
C     --- NONCONDESABLE HE: COND. (W/MK)  VS. TEMP. (K) ---
C     --- XA IS TEMP. ARRAY AND YA IS COND. ARRAY ---
C     --- TEMP. RANGE: 200 - 500 K ---
C
      DIMENSION XA(5),YA(5)
C
      DATA XA/200., 250., 300., 400., 500./
C
      DATA YA/0.116, 0.133, 0.149, 0.178, 0.205/
C
C
      N=5
C
      CALL POLINT (XA,YA,N,T,EKNHE,DY)
C
```

```
      EKNTHE=EKNHE
C
C
      RETURN
      END
C
C     ---------------------------------------------------------------
C
      FUNCTION EMUNTHE (T)
      IMPLICIT REAL*8 (A-H,O-Z)
C
C     --- NONCONDESABLE HE: VISCOSITY (KG/MS)  VS. TEMP. (K) ---
C     --- XA IS TEMP. ARRAY AND YA IS VISC. ARRAY ---
C     --- TEMP. RANGE: 200 - 500 K ---
C
      DIMENSION XA(5),YA(5)
C
      DATA XA/200., 250., 300., 400., 500./
C
      DATA YA/1.5616, 1.794, 2.014, 2.436, 2.825/
C
C
      N=5
C
      CALL POLINT (XA,YA,N,T,EMUHE,DY)
C
      EMUNTHE=EMUHE*1.E-5
C
C
      RETURN
      END
C
C     ---------------------------------------------------------------
C
C     ---------------------------------------------------------------
C
      FUNCTION HAT28 (T)
      IMPLICIT REAL*8 (A-H,O-Z)
C
C     --- NONCONDESABLE N2: ENTHALPY (KJ/KG) VS. TEMP. (K) ---
C     --- XA IS TEMP. ARRAY AND YA IS ENTHALPY ARRAY ---
C     --- TEMP. RANGE: 100 - 1050 K ---
C
      DIMENSION XA(20),YA(20)
C
      DATA XA/100.,150.,200.,250.,300.,350.,400.,450.,500.,550.,
     1       600.,650.,700.,750.,800.,850.,900.,950.,1000.,1050./
C
      DATA YA/ 103.59,155.57,207.51,259.45,311.42,
     1         363.43,415.55,467.88,520.50,573.51,
     2         626.99,681.02,735.61,790.80,846.59,
     3          903.01,960.0,1017.6,1075.7,1134.3/
C
C
      N=20
C
```

```
      CALL POLINT (XA,YA,N,T,HA1,DY)
C     --- CHANGE TO J/KG ---
      HAT28= HA1 * 1.E+3
C
C
      RETURN
      END
C     ---------------------------------------------------------------
C
      FUNCTION HENRY(T)
      IMPLICIT REAL*8 (A-H,O-Z)
C
C     --- HENRY'S CONSTANT FOR N2 IN WATER.
C     --- HENRY'S CONSTANT IN ATM/(MOLE FRACTION)
C     --- TEMPERATURE K
C
      DIMENSION XA(16),YA(16)
C
      DATA XA/0.0,5.0,10.0,15.0,20.0,25.0,30.0,35.0,40.0,
     *       45.0,50.0,60.,70.0,80.0,90.0,100.0/
C
      DATA YA/5.29, 5.97, 6.68, 7.38, 8.04, 8.65, 9.24,
     *       9.85, 10.4, 10.9, 11.3, 12.0, 12.5, 12.6,
     *       12.6, 12.6 /
C
C
      N=16
C
      THERE = T-273.15
      IF(THERE.GT.100) THERE=100.0
      CALL POLINT (XA,YA,N,THERE,HEN,DY)
C
      HENRY = HEN*10000.0
C
C
      RETURN
      END
C
C     ---------------------------------------------------------------
C
C END OF BLOCK PRPSAT
C ********************************************************************
C
          SUBROUTINE FRIEDEL(FW)
C
C      CALCULATE WALL FRICTION FROM FRIEDEL MODEL
C
          IMPLICIT REAL*8 (A-H,O-Z)
          REAL*8 MV,MN

          COMMON /INP1/ P1,GG,U1,XE1,QW,TIN,ZHEATS,ZHEATF,XEOSV
       COMMON /INP2/ ELOSSIRR,ELOSSREV,H1,akexp
       COMMON /INP4/ UF1,UG1,ALF1,P1ALF,PSATVAP,slip, tauw,xlm,bo
C
          COMMON /PRP1A/ TG,RHOV,RHOG
       COMMON /PRP2/ RHOL,EMUL,CPL,EKL,PRNTL,RHOL2,beta
```

```
      COMMON /PRP2A/ EMUG,CPG,EKG,PRNTG,HF,HG,VFG,SIG

          COMMON /PRP3/ HFG,DHVDP,RAD
C
          COMMON /CALC/ ALPHA,ZPRNT,HENT,ITP,ZTWOPH,IVP,ZVAPPH
C
      COMMON /INPUT3/ MN,MV,wide,high,tubel,din,dout,theta,PIN
          COMMON /CONSTS/ RGAS,G,PI
C
          ENUL=EMUL/RHOL
          ENUG=EMUG/RHOG
C
      UG1 = U1*1.001
      UL1 = U1*.999
          EJL=UL1*(1.-ALPHA)
          EJG=UG1*ALPHA
C
C      CALCULATION OF WALL FRICTION IN TERMS OF
C      METHOD DEVELOPED BY FRIEDEL
C
          XX = RHOG*EJG/(RHOG*EJG + RHOL*EJL)
          GG =EJL*RHOL+EJG*RHOG
C
          RHOTP = 1.0/(XX/RHOG + (1.0-XX)/RHOL)
          FRNO = GG*GG/(9.81*2.0*RAD*RHOTP**2.0)
          SIGMA = SIG
          WENO = GG*GG*2.0*RAD/(RHOTP*SIGMA)
C
          FRENOL = GG*(2.0*RAD)/EMUL
          FRENOG = GG*(2.0*RAD)/EMUG
          IF (FRENOL.LE.1055.0) THEN
            FFRCL = 16.0/FRENOL
          ELSE
            FFRCL = 0.25*(0.86859*DLOG(FRENOL/(1.964*
     *      DLOG(FRENOL)-3.8215)))**(-2.0)
          END IF
C
          IF (FRENOG.LE.1055.0) THEN
            FFRCG = 16.0/FRENOG
          ELSE
            FFRCG = 0.25*(0.86859*DLOG(FRENOG/(1.964*
     *      DLOG(FRENOG)-3.8215)))**(-2.0)
          END IF
C
          CF1 = (1.0-XX)**2.0 + XX*XX*(RHOL/RHOG)*
     *    (FFRCG/FFRCL)
C
          CF2 = (XX**0.78)*((1.0-XX)**0.224)*
     *      ((RHOL/RHOG)**0.91)
     *      *((EMUG/EMUL)**0.19)*((1.0-EMUG/EMUL)**0.7)
          FAIS = CF1 + 3.24*CF2*
     *      (FRNO**(-0.0454))*(WENO**(-0.035))
C
          FDPDZFL=FFRCL*GG*GG/(RAD*RHOL)
          FW = FAIS*FDPDZFL
c         write(*,*) "ffrcg,ffrcl,fais",ffrcg,ffrcl,fais
```

```
C
          RETURN
          END
C
C-------------------------------------------------------------
C     ---------------------------------------------------
C
C     USE RKAMS INTEGRATION SUBROUTINE
C
      SUBROUTINE RKAMS (XDP,HDP,VAR,DER,AUXSUB,N,OPT,
     1  EU,EL,HMAX,HMIN,ICNT,NH)
      IMPLICIT REAL*8 (A-H,O-Z)
      EXTERNAL AUXSUB
      DIMENSION VAR(N),DER(N),EU(N),EL(N),TEMPS(8,8)
      NN=N
      IC=ICNT
C  TRANSFER ON R-K ONLY OPTION
      IF (OPT.NE.0.) GO TO 200
C  IF COUNTER .GT. 2--TRANSFER FOR ADAMS-MOULTON STEP
      IF (IC.GT.2) GO TO 300
      IF (IC.NE.0) GO TO 200
C  STORE INITIAL CONDITIONS
  100 DO 110 I=1,NN
      TEMPS(4,I)=VAR(I)
  110 TEMPS(3,I)=DER(I)
C  INTEGRATE ONE STEP WITH RUNGE-KUTTA
  200 K=0
      B=.5*HDP
      A=B
  210 XDP=XDP+B
  220 DO 240 I=1,NN
      IF (K.NE.0) GO TO 230
      TEMPS(2,I)=VAR(I)
      TEMPS(1,I)=DER(I)
      GO TO 240
  230 TEMPS(1,I)=TEMPS(1,I)+2.*DER(I)
  240 VAR(I)=TEMPS(2,I)+A*DER(I)
      CALL AUXSUB(XDP,VAR,DER)
      K=K+1
      IF (K-2) 220,250,260
  250 A=HDP
      GO TO 210
  260 A=HDP/6.
      DO 270 I=1,NN
  270 VAR(I)=TEMPS(2,I)+(DER(I)+TEMPS(1,I))*A
      CALL AUXSUB(XDP,VAR,DER)
      IF (OPT.NE.0.) RETURN
      IC=IC+1
      GO TO 600
C  INTEGRATE ONE STEP WITH ADAMS-MOULTON AND TEST STEP SIZE
  300 A=HDP/24.
      XDP=XDP+HDP
      DO 310 I=1,NN
      TEMPS(1,I)=A*(55.*TEMPS(3,I)-59.*TEMPS(4,I)
     1  +37.*TEMPS(5,I)-9.*TEMPS(6,I))
  310 VAR(I)=TEMPS(2,I)+TEMPS(1,I)
```

```
      CALL AUXSUB(XDP,VAR,DER)
      K=0
      DO 320 I=1,NN
      B=A*(9.*DER(I)+19.*TEMPS(3,I)-5.*TEMPS(4,I)+TEMPS(5,I))
      C=ABS(B-TEMPS(1,I))
      IF (C.LT.EL(I)) GO TO 320
      K=1
      IF (C.LT.EU(I)) GO TO 320
      IF (ABS(HDP).GT.2.*HMIN) GO TO 500
  320 VAR(I)=TEMPS(2,I)+B
      CALL AUXSUB(XDP,VAR,DER)
      IF (IC.GT.3) GO TO 330
      IC=4
  330 IF (K.EQ.0) GO TO 340
      IC=4
      GO TO 600
  340 IC=IC+1
      IF (IC.LT.7) GO TO 600
      IF (ABS(HDP).GT..5*HMAX) GO TO 600
C  DOUBLING PROCESS--REARRANGE DERIVATIVES AND EXIT
  400 IC=4
      HDP=HDP*2.
      DO 410 I=1,NN
      TEMPS(5,I)=TEMPS(6,I)
  410 TEMPS(6,I)=TEMPS(8,I)
      GO TO 700
C  HALVING PROCESS
C  COUNTER .LT. 4--BACK 3 STEPS--RESTART R-K WITH H/2
C  COUNTER .GE. 4--INTERPOLATE--REDO LAST STEP WITH H/2
  500 NH=I
      A=HDP
      HDP=.5*HDP
      IF (IC.GE.4) GO TO 520
      IC=0
      XDP=XDP-4.*A
      DO 510 I=1,NN
      VAR(I)=TEMPS(7,I)
  510 DER(I)=TEMPS(6,I)
      GO TO 100
  520 XDP=XDP-A
      IC=4
      DO 530 I=1,NN
      A=(5.*(TEMPS(3,I)+3.*TEMPS(4,I)-TEMPS(5,I))+TEMPS(6,I))/16.
      TEMPS(6,I)=(9.*(TEMPS(4,I)+TEMPS(5,I))-TEMPS(3,I)
     1  -TEMPS(6,I))/16.
      TEMPS(5,I)=TEMPS(4,I)
  530 TEMPS(4,I)=A
      GO TO 300
C  MOVE PAST DATA
  600 DO 610 J=1,5
      K=9-J
      DO 610 I=1,NN
  610 TEMPS(K,I)=TEMPS(K-1,I)
C  STORE NEW VALUES OF VAR AND DER FOR NEXT STEP
  700 DO 710 I=1,NN
      TEMPS(2,I)=VAR(I)
```

```
  710 TEMPS(3,I)=DER(I)
      ICNT=IC
      RETURN
      END
C  Added on August 02
      function slipr (rhof,rhog,alf,ug,uf,dh,emul,emug,sig)
c  This function calculates the slip ration from Premoli correlation
      implicit real*8(a-h,o-z)
      beta=(ug*alf)/(ug*alf+((1.-alf)*uf))
      gg=(ug*rhog*alf)+(uf*rhof*(1.-alf))
      rel0=gg*dh/emul
      wel0=(GG**2)*dh/(sig*rhof)
      b1=1.578*((rhof/rhog)**0.22)/(rel0**0.19)
      b2=(rel0**0.51)*((rhof/rhog)**0.08)
      b2=0.0273*wel0/b2
      y=(1.-beta)/beta
      slipr=(y/(1.+(y*b2)))-(y*b2)
      slipr=b1*dsqrt(dabs(slipr))+1.
c      slipr=b1*(dsqrt(dabs((y/(1.+(y*b2)))-(y*b2))))+1.
c     write (*,*) ' rhof,rhog,alf,uf,ug', rhof,rhog,alf,uf,ug
c      write (*,*) ' dh,emul,emug,sig',  dh,emul,emug,sig
c      write (*,*) ' y,beta,b1,b2,slipr', y,beta,b1,b2,slipr
      return
      end
```

APPENDIX V

DRYOUT DATA FOR MICROCHANNELS

Table V-1: Lezzi et al. (1994) horizontal CHF data

Test No.	Tube Dimensions								CHF
	D (mm)	L/D	t_ω (mm)	$G \infty 10^{-3}$ ($kg\,m^{-2}\,s^{-1}$)	$P \infty 10^{-5}$ ($N\,m^{-2}$)	T_t (°C)	x_t	x_o	$q_\mu \infty 10^{-6}$ ($W\,m^{-2}$)
1	1.00	239	0.25	1.480	70.1	258.6	-0.10	0.82	2.052
2	1.00	239	0.25	1.480	69.7	230.4	-0.19	0.82	2.257
3	1.00	239	0.25	1.475	70.3	213.2	-0.24	0.82	2.363
4	1.00	241	0.25	1.491	69.6	249.0	-0.13	0.81	2.079
5	1.00	241	0.25	1.496	69.6	230.1	-0.19	0.80	2.206
6	1.00	502	0.25	1.485	70.5	266.8	-0.08	0.72	0.869
7	1.00	502	0.25	1.475	70.5	248.1	-0.14	0.71	0.914
8	1.00	502	0.25	1.475	70.3	230.1	-0.19	0.71	0.976
9	1.00	502	0.25	1.464	70.3	213.2	-0.25	0.71	1.021
10	1.00	502	0.25	1.464	70.0	190.1	-0.31	0.71	1.098
11	1.00	502	0.25	2.270	49.8	244.0	-0.09	0.72	1.431
12	1.00	502	0.25	2.270	49.7	223.1	-0.15	0.72	1.534
13	1.00	502	0.25	2.270	50.3	200.5	-0.21	0.71	1.628
14	1.00	502	0.25	2.270	50.2	181.5	-0.26	0.70	1.704
15	1.00	502	0.25	2.270	49.8	161.4	-0.32	0.69	1.783
16	1.00	502	0.25	2.270	49.8	140.0	-0.37	0.69	1.886
17	1.00	502	0.25	2.270	50.0	120.6	-0.43	0.68	1.968
18	1.00	502	0.25	2.303	50.0	102.5	-0.47	0.67	2.067
19	1.00	502	0.25	2.281	50.3	81.2	-0.53	0.67	2.138
20	1.00	502	0.25	2.281	50.3	60.8	-0.58	0.66	2.227
21	1.00	502	0.25	2.738	50.3	198.6	-0.23	0.66	1.873
22	1.00	975	0.25	0.776	54.5	268.6	-0.01	0.90	0.285
23	1.00	975	0.25	0.782	50.8	238.8	-0.09	0.97	0.338
24	1.00	975	0.25	0.782	49.6	219.0	-0.13	0.99	0.364
25	1.00	975	0.25	0.782	50.4	199.2	-0.20	0.97	0.374
26	1.00	975	0.25	0.816	45.4	245.0	-0.05	0.90	0.324
27	1.00	975	0.25	0.838	36.6	248.3	-0.01	0.96	0.350
28	1.00	975	0.25	0.906	19.0	221.5	0.00	0.88	0.369
29	1.00	975	0.25	1.100	72.0	288.0	-0.01	0.87	0.359
30	1.00	975	0.25	1.123	70.4	283.6	-0.02	0.82	0.355
31	1.00	975	0.25	1.109	69.3	271.1	-0.06	0.84	0.375
32	1.00	975	0.25	1.160	52.9	268.9	-0.01	0.92	0.436
33	1.00	975	0.25	1.230	28.4	239.7	-0.01	0.89	0.488
34	1.00	975	0.25	1.230	29.3	242.2	-0.01	0.90	0.491
35	1.00	975	0.25	1.421	71.0	285.1	-0.02	0.71	0.387
36	1.00	975	0.25	1.470	70.5	291.0	0.00	0.74	0.407
37	1.00	975	0.25	1.475	53.1	273.1	0.00	0.86	0.509

38	1.00	975	0.25	1.475	52.9	266.6	-0.03	0.90	0.542
39	1.00	975	0.25	1.475	50.2	241.2	-0.09	0.90	0.591
40	1.00	975	0.25	1.475	50.3	221.7	-0.15	0.90	0.624
41	1.00	975	0.25	1.475	50.4	199.7	-0.21	0.88	0.650
42	1.00	975	0.25	1.475	50.5	184.3	-0.25	0.88	0.674
43	1.00	975	0.25	1.475	50.7	162.0	-0.31	0.87	0.706
44	1.00	975	0.25	1.480	50.2	140.2	-0.37	0.87	0.742
45	1.00	975	0.25	1.480	49.9	121.8	-0.42	0.86	0.763
46	1.00	975	0.25	1.480	49.7	102.8	-0.46	0.87	0.800
47	1.00	975	0.25	1.480	50.7	81.0	-0.53	0.86	0.832
48	1.00	975	0.25	1.485	49.9	59.2	-0.58	0.86	0.867
49	1.00	975	0.25	1.480	49.4	40.4	-0.62	0.86	0.892
50	1.00	975	0.25	1.496	40.1	246.6	-0.04	0.92	0.603
51	1.00	975	0.25	1.518	39.0	260.4	0.00	0.87	0.552
52	1.00	975	0.25	1.528	39.0	256.3	-0.01	0.92	0.598
53	1.00	975	0.25	1.544	33.1	251.9	-0.01	0.87	0.576
54	1.00	975	0.25	1.544	33.0	248.4	-0.02	0.90	0.604
55	1.00	975	0.25	1.765	30.0	248.0	-0.02	0.91	0.695
56	1.00	975	0.25	1.810	69.5	292.5	0.00	0.69	0.461
57	1.00	975	0.25	1.822	50.3	222.1	-0.16	0.83	0.718
58	1.00	975	0.25	1.817	50.4	204.3	-0.21	0.82	0.748
59	1.00	975	0.25	1.827	50.1	179.6	-0.27	0.81	0.796
60	1.00	975	0.25	1.827	50.3	159.3	-0.33	0.81	0.831
61	1.00	975	0.25	1.827	49.6	141.2	-0.37	0.81	0.871
62	1.00	975	0.25	1.832	50.6	119.8	-0.43	0.79	0.902
63	1.00	975	0.25	1.827	49.5	102.0	-0.47	0.79	0.930
64	1.00	975	0.25	1.832	49.4	80.7	-0.53	0.79	0.973
65	1.00	975	0.25	1.832	50.2	60.8	-0.58	0.79	1.016
66	1.00	975	0.25	1.832	50.3	38.7	-0.64	0.77	1.039
67	1.00	975	0.25	1.832	50.1	22.9	-0.68	0.75	1.059
68	1.00	975	0.25	1.870	50.5	276.0	0.00	0.83	0.621
69	1.00	975	0.25	1.878	25.5	245.0	-0.02	0.85	0.694
70	1.00	975	0.25	2.178	31.5	255.7	-0.01	0.78	0.719
71	1.00	975	0.25	2.178	31.4	252.0	-0.02	0.79	0.737
72	1.00	975	0.25	2.173	50.0	242.6	-0.10	0.75	0.736
73	1.00	975	0.25	2.173	49.3	219.9	-0.16	0.77	0.808
74	1.00	975	0.25	2.173	50.1	200.2	-0.22	0.75	0.838
75	1.00	975	0.25	2.173	50.5	189.6	-0.25	0.74	0.855
76	1.00	975	0.25	2.173	50.1	181.0	-0.27	0.74	0.879
77	1.00	975	0.25	2.173	50.1	161.9	-0.33	0.74	0.922
78	1.00	975	0.25	2.178	49.7	143.2	-0.38	0.73	0.958
79	1.00	975	0.25	2.178	50.1	120.0	-0.44	0.72	1.003
80	1.00	975	0.25	2.184	50.5	100.6	-0.49	0.70	1.038
81	1.00	975	0.25	2.184	50.6	79.8	-0.54	0.70	1.083
82	1.00	975	0.25	2.173	50.5	60.5	-0.59	0.69	1.117
83	1.00	975	0.25	2.184	50.1	40.0	-0.64	0.69	1.170
84	1.00	975	0.25	2.189	49.8	24.6	-0.68	0.66	1.179
85	1.00	975	0.25	2.205	27.9	233.8	-0.06	0.77	0.767
86	1.00	975	0.25	2.230	50.0	277.5	0.00	0.78	0.687

Table V-2: Lowdermilk et al. (1958) vertical CHF data

Test No.	Tube Dimensions							CHF
	D (mm)	L/D	t_w (mm)	$G \infty 10^{-3}$ ($kg\,m^{-2}\,s^{-1}$)	$P \infty 10^{-5}$ ($N\,m^{-2}$)	T_i (°C)	x_o	$q_m \infty 10^{-6}$ ($W\,m^{-2}$)
1	1.30	50.0	0.84	0.9494	1.01	23.3	0.410	5.868
2	1.30	50.0	0.84	1.3427	1.01	23.3	0.360	7.760
3	1.30	50.0	0.84	2.0479	1.01	23.3	0.290	10.063
4	1.30	50.0	0.84	2.5497	1.01	23.3	0.290	12.461
5	1.30	50.0	0.84	3.1465	1.01	23.3	0.240	13.723
6	1.30	50.0	0.84	3.8110	1.01	23.3	0.200	14.669
7	1.30	100.0	0.84	0.1492	1.01	23.3	0.970	0.978
8	1.30	100.0	0.84	0.2712	1.01	23.3	0.950	1.703
9	1.30	100.0	0.84	0.5561	1.01	23.3	0.780	2.902
10	1.30	100.0	0.84	0.6917	1.01	23.3	0.750	3.439
11	1.30	100.0	0.84	0.9494	1.01	23.3	0.680	4.385
12	1.30	100.0	0.84	1.3969	1.01	23.3	0.680	6.530
13	1.30	100.0	0.84	2.0479	1.01	23.3	0.590	8.454
14	1.30	100.0	0.84	2.4955	1.01	23.3	0.570	10.158
15	1.30	100.0	0.84	3.2414	1.01	23.3	0.480	11.546
16	1.30	100.0	0.84	3.8517	1.01	23.3	0.410	12.177
17	1.30	100.0	0.84	5.1130	1.01	23.3	0.340	14.038
18	1.30	150.0	0.84	0.2712	1.01	23.3	0.960	1.136
19	1.30	150.0	0.84	0.5696	1.01	23.3	0.830	2.082
20	1.30	150.0	0.84	0.6917	1.01	23.3	0.810	2.492
21	1.30	150.0	0.84	0.9629	1.01	22.2	0.730	3.186
22	1.30	150.0	0.84	1.3427	1.01	22.2	0.740	4.480
23	1.30	150.0	0.84	1.9937	1.01	22.2	0.660	6.025
24	1.30	150.0	0.84	2.5904	1.01	22.2	0.660	7.887
25	1.30	150.0	0.84	3.2279	1.01	22.2	0.590	8.864
26	1.30	200.0	0.84	0.2577	1.01	23.3	0.980	0.820
27	1.30	200.0	0.84	0.5154	1.01	23.3	0.860	1.451
28	1.30	200.0	0.84	0.6781	1.01	22.2	0.780	1.767
29	1.30	200.0	0.84	0.9494	1.01	22.2	0.790	2.524
30	1.30	200.0	0.84	1.3969	1.01	22.2	0.750	3.533
31	1.30	200.0	0.84	2.0208	1.01	22.2	0.700	4.858
32	1.30	200.0	0.84	2.4141	1.01	22.2	0.740	5.994
33	1.30	200.0	0.84	3.2279	1.01	22.2	0.630	7.035
34	1.30	250.0	0.84	0.5561	1.01	23.3	0.870	1.262
35	1.30	250.0	0.84	0.6781	1.01	23.3	0.840	1.514
36	1.30	250.0	0.84	0.9494	1.01	23.3	0.830	2.082
37	1.30	250.0	0.84	1.3427	1.01	23.3	0.780	2.776
38	1.30	250.0	0.84	1.8716	1.01	23.3	0.680	3.502
39	1.30	250.0	0.84	2.4955	1.01	23.3	0.570	4.069
40	1.30	100.0	0.84	1.3834	1.01	21.1	0.610	5.836
41	1.30	100.0	0.84	1.3834	1.01	50.6	0.650	5.710
42	1.30	100.0	0.84	1.3834	1.01	78.9	0.690	5.678
43	1.30	100.0	0.84	1.3834	1.01	96.1	0.720	5.615
44	1.30	100.0	0.84	0.9494	1.01	51.7	0.640	3.912

45	1.30	100.0	0.84	0.9494	1.01	76.7	0.680	3.880
46	1.30	100.0	0.84	0.9629	1.01	93.3	0.760	4.196
47	1.30	100.0	0.84	0.9629	1.01	26.7	0.690	4.448
48	1.30	100.0	0.84	3.2143	1.01	22.2	0.480	8.896
49	1.30	100.0	0.84	3.2685	1.01	55.6	0.450	8.517
50	1.30	100.0	0.84	3.3228	1.01	77.8	0.420	7.950
51	1.30	100.0	0.84	3.3228	1.01	95.6	0.400	7.634
52	1.30	200.0	0.84	2.1293	1.01	22.2	0.640	4.700
53	1.30	200.0	0.84	2.1293	1.01	60.0	0.640	4.290
54	1.30	200.0	0.84	2.1293	1.01	80.0	0.690	4.322
55	1.30	200.0	0.84	2.1022	1.01	100.0	0.650	3.849
56	1.30	200.0	0.84	1.3969	1.01	100.0	0.630	2.492
57	1.30	200.0	0.84	1.3834	1.01	82.2	0.720	2.461
58	1.30	200.0	0.84	1.3562	1.01	54.4	0.640	2.776
59	1.30	200.0	0.84	1.3562	1.01	26.7	0.730	3.312
60	1.30	50.0	0.84	1.3427	1.01	21.1	0.340	7.413
61	1.30	50.0	0.84	2.7396	1.01	26.7	0.190	10.095
62	1.30	50.0	0.84	2.8345	1.01	44.4	0.230	10.599
63	1.30	50.0	0.84	2.8345	1.01	93.3	0.310	10.158

Table V-3: Weatherhead (1963) vertical CHF data

Test No.	Tube Dimensions							CHF
	$D \infty 10^3$ (m)	L/D	$t_\omega \infty 10^3$ (m)	$G \infty 10^{-3}$ (kg m^{-2} s^{-1})	$P \infty 10^{-5}$ (N m^{-2})	$h_o \infty 10^{-3}$ (J kg^{-1})	x_o	$q_\mu \infty 10^{-6}$ (W m^{-2})
1	1.14	100	0.25	5.18	13.8	1238.4	0.210	7.32
2	1.14	100	0.25	4.52	13.8	1296.5	0.239	7.32
3	1.14	100	0.25	4.37	13.8	1347.7	0.265	7.32
4	1.14	100	0.25	4.52	13.8	1310.5	0.246	7.32
5	1.14	100	0.25	4.57	13.8	1301.2	0.242	7.32
6	1.14	100	0.25	4.67	13.8	1326.8	0.255	7.32
7	1.14	100	0.25	3.72	13.8	1473.3	0.329	6.09
8	1.14	100	0.25	4.69	13.8	1270.9	0.226	4.86
9	1.14	100	0.25	7.78	13.8	1157.0	0.168	4.86
10	1.14	100	0.25	7.80	13.8	1154.6	0.167	4.86
11	1.14	100	0.25	3.97	13.8	1402.4	0.293	4.86
12	1.14	100	0.25	4.31	13.8	1305.8	0.244	4.86
13	1.14	100	0.25	4.45	13.8	1289.6	0.236	4.86
14	1.14	100	0.25	5.38	13.8	1173.3	0.176	4.86
15	1.14	100	0.25	6.71	13.8	1091.8	0.135	3.63
16	1.14	100	0.25	5.44	13.8	1166.3	0.173	3.63
17	1.14	100	0.25	5.34	13.8	1161.6	0.170	3.63
18	1.14	100	0.25	5.47	13.8	1131.4	0.155	3.63
19	1.14	100	0.25	5.91	13.8	1061.6	0.119	3.00
20	1.14	100	0.25	6.85	13.8	1032.5	0.105	2.97
21	1.14	100	0.25	5.40	13.8	1116.3	0.147	2.92

22	1.14	100	0.25	5.18	13.8	1138.4	0.159	2.92

Table V-4: Roach et al. (1999) CHF data

Test No.	Tube Dimensions								CHF
	D (mm)	L/D	t_ω (mm)	$G \infty 10^{-3}$ ($kg\,m^{-2}\,s^{-1}$)	$P \infty 10^{-5}$ ($N\,m^{-2}$)	T_ι (°C)	x_ι	x_o	$q_\mu \infty 10^{-6}$ ($W\,m^{-2}$)
1	1.168			0.256	3.46	138.5		0.73	0.904
2	1.168			0.379	3.44	138.3		1.01	1.752
3	1.168			0.499	3.42	138.1		0.66	1.611
4	1.168			0.621	3.36	137.5		0.54	1.711
5	1.168			0.768	3.44	138.3		0.56	2.186
6	1.168			0.852	3.43	138.2		0.57	2.466
7	1.168			0.991	3.48	138.7		0.55	2.820
8	1.168			0.279	3.48	138.7		0.64	0.860
9	1.168			0.552	3.48	138.7		0.47	1.314
10	1.168			0.607	3.48	138.7		0.77	2.138
11	1.168			0.993	3.46	138.5		0.53	2.590
12	1.168			0.284	6.87	164.2		0.58	0.861
13	1.168			0.384	6.90	164.4		0.48	1.034
14	1.168			0.511	6.90	164.4		0.43	1.274
15	1.168			0.603	6.87	164.2		0.43	1.508
16	1.168			0.734	6.89	164.3		0.48	1.966
17	1.168			0.858	6.82	163.9		0.51	2.419
18	1.168			0.986	6.84	164.1		0.56	2.957
19	1.168			0.266	6.89	164.3		0.72	0.957
20	1.168			0.356	7.41	167.3		0.74	1.304
21	1.168			0.491	6.79	163.8		0.69	1.716
22	1.168			0.594	6.92	164.5		0.82	2.354
23	1.168			0.753	7.20	166.1		0.85	3.077
24	1.168			0.886	7.47	167.6		0.72	3.209
25	1.168			1.001	7.13	165.7		0.63	3.263
26	1.168			0.256	10.37	181.5		0.88	1.083
27	1.168			0.363	10.41	181.7		0.74	1.346
28	1.168			0.504	10.40	181.6		0.62	1.657
29	1.168			0.634	10.42	181.7		0.62	2.078
30	1.168			0.752	10.20	180.8		0.54	2.253
31	1.168			0.911	10.37	181.5		0.40	2.257
32	1.168			1.037	10.41	181.7		0.36	2.436
33	1.448			0.379	3.44	138.3		0.93	2.027
34	1.448			0.516	3.48	138.7		0.86	2.596
35	1.448			0.625	3.49	138.8		0.84	3.094
36	1.448			0.742	3.45	138.2		0.83	3.595
37	1.448			0.500	6.76	163.6		0.97	2.829
38	1.448			0.617	6.86	164.2		0.92	3.317
39	1.448			0.752	6.91	164.5		0.81	3.698

40	1.448			0.278	6.90	164.4		0.83	1.378
41	1.448			0.403	7.01	165.0		0.79	1.917
42	1.448			0.480	6.99	164.9		0.96	2.673
43	1.448			0.502	10.29	181.2		0.97	2.851

APPENDIX VI

LIST OF PUBLISHED PAPERS

Xie, T., Ghiaasiaan, S. M., Karrila, S., and McDonough, T., 2003a, "Flow regimes and gas holdup in paper pulp-water-gas three-phase slurry flow", *Chem. Eng. Sci.*, *58*, 1417-1430.

Xie, T., Ghiaasiaan, S. M., and Karrila, S., 2003b, "Flow regime identification in gas-liquid-pulp fiber slurry flows based on pressure fluctuations using artificial neural networks", *Industrial and Engineering Chemistry Research*, *42*, 7017-7024.

Xie, T., Ghiaasiaan, S. M., and Karrila, S., 2004, "Artificial neural network approach for flow regime classification in gas-liquid-fiber flows based on frequency domain analysis of pressure signals", *Chem. Eng. Sci.*, *59*, 2241-2251.

Xie, T., Ghiaasiaan, S. M., Karrila, S., and McDonough, T., "Hybrid neural network-first principle modeling of critical heat flux in a thin annular channel", *ASME 2002 International Mechanical Engineering Congress*, New Orleans, Nov. 2002.

BIBLIOGRAPHY

Ahmad, S. Y., 1973, "Fluid to fluid modeling of critical heat flux: a compensated distortion model*", Int. J. Heat Mass Transfer, 16*, 641-662.

Ahmad, S. Y., Nnickerson, J. R., and Midvidy, W. I., 1982, "Critical heat flux in a horizontal 37-element bundle cooled by water and Freon", *Proc. 7th International Heat Transfer Conference*, Hemisphere, New York, 261-266.

Anderson, James A., "An introduction to neural networks", MIT Press, Cambridge, Massachusetts, 1995.

Armand, A. A., and Treshchev, G. G., 1959, "Investigation of the resistance during the movement of steam-water mixtures in heated boiler pipe at high pressure", *AERE Lib/Trans, 81*.

Balaban, M. O., Korel, F., Odabasi, A. Z., and Folkes, G., 2000, "Transportability of data between electronic noses: mathematical methods", *Sensors and Actuators*, B 71, 203-211.

Balino, J. L., Converti, J., 1994, "Critical heat flux in horizontal annular channels with variable eccentricity", *Int. Comm. Heat Mass Transfer*, *18*, 659-667.

Bankoff, S. G., 1960, "A variable sensity single fluid model for two-phase flow with particular reference to steam-water flow", *J. Heat Transfer, 82*, 265-273.

Beattie, D. R. H., and Whalley, P. B., 1982, "A simple two-phase fractional pressure drop calculation method", *Int. J. Multiphase Flow*, *8*, 83-87.

Bennet, A. W., Collier, J. G., and Lacey, P. M. C., 1963, "Heat transfer mixture of high pressure steam and water in an annulus, Part III: The effect of system pressure on the burnout heat flux for an internally heated unit", *AERE-R-3934*, Harwell, England.

Bennington, C. P. J., Kerekes, R. J., and Grace, J. R., 1989, "Mixing in pulp bleaching", *J. Pulp Paper Science*, *15*, 186-195.

Bennington, C. P. J., Azevedo, G., John, D. A., Birt, S. M., and Wolgast, B. H., 1995, "The yield-stress of medium- and high-consistency mechanical pulp fiber suspensions at high gas contents", *J. Pulp Paper Science*, *21*, 111-118.

Bennington, C. P. J., Owusu, G., and Francis, D. W., 1997, "Gas-liquid mass transfer in pulp suspension mixing operations", *Can. J. Chem. Eng.*, *75*, 53-61.

Bergles, A. E., 1962, "Subcooled burnout in tubes of small diameter", ASME Paper 63-WA-182.

Bin, A. K., Duczmal, B., and Machniewski, P. (2001). Hydrodynamics and ozone mass transfer in a tall bubble column, *Chem. Eng. Sci*., *56*, 6233-6240.

Bishop, C. M., and James, G. D., 1993, "Analysis of multiphase flows using dual-energy gamma densitomery and neural networks", *Nuclear Instruments and Methods in Physics Research, A327*, 580-593.

Bose, F., Ghiaasiaan, S. M., Heindel, J. T., 1997, "Hydrodynamics of dispersed liquid droplets in agitated synthetic fibrous slurries", *Ind. Eng. Chem. Res*., *36*, 5028-5036.

Burns, A. P., Russell, D., Sheppard, C. P., and Gent, C. R., 1993, "The application of neural network pattern recognition technology to non-intrusive multi-phase metering", *Control Engineering Parctice, 1, no. 2*, 299-304.

Cai, S., Toral, H., Qiu, J., and Archer, J. S., 1994, "Neural network based objective flow regime identification in air-water two-phase flow", *Can. J. Chem. Eng*., *72*, 440-445.

Cai, Y., Wambsganss, M. W., and Jendrzejczyk, J. A., 1996, "Application of chaos theory in identification of two-phase flow patterns and transitions in a small, horizontal, rectangular channel", *J. Fluids Eng.*, *118*, 383-390.

Caira, M., Caruso, G., and Naviglio, A., 1995, "A correlation to predict CHF in subcooled flow boiling", *Int. Comm. Heat Mass Transfer, 22*, 35-45.

Celata, G. P., Cumo, M., Mariani, A., Nariai, H., and Inasaka, F., 1993, "Influence of channel diamter on subcooled flow boiling burnout at high heat fluxes", *Int. J. Heat Mass Transfer, 36*, 3407-3409.

Celata, G. P., Cumo, M., and Mariani, A., 1994, " Assessment of correlations and models for the prediction of CHF in water subcooled flow boiling", *Int. J. of Heat Mass Transfer*, *37*, 237-255.

Chaouki, J., Larachi, F., and Milorad P. Dudukovi´c., Editor, 1997, Non-invasive monitoring of multiphase flows, Amsterdam; New York: Elsevier.

Chen, R. C., Reese, J., and Fan, L.-S., 1994, "Flow structure in a three-dimensional bubble column and three-phase fluidized bed", *AICHE J.*, 40, 1093-1104.

Chisholm, D., 1972, "An equation velocity ratio in two-phase flow", *NEL Report 535*, UK.

Colebrook, C. R., 1939, "Turbulent flow in pipes with particular reference to the transition region between the smooth and rough pipe flows", *J. Inst. Civil Eng*., *11*, 133-156.

Collier, J. G., and Thome, J. R., 1994, *Convective boiling and condensation,* Oxford University Press.

Collier, J. G., and Thome, J. R., 1994, Convective boiling and two-phase flow, *3rd Ed*., *Oxford University Press*, U. K.

Cumo, M., Fabrizi, F., and Palazzi, G., 1978, "The influence of inclination on CHF in steam generation channels", CNEW-RT/ING(78)11, Commitato Nazionale Energia Nucleare, Rome, Italy.

Deckwer, W. D., 1985, Bubble column reactors, *John Wiley and Sons*, New York.

Dence, C. W. and Reeve, D. W., editors, 1996, Pulp bleaching: principles and practice, *TAPPI Press*, Atlanta, GA.

Dix, G. E., 1971, "Vapor void fractions for forced convection with subcooled boiling at low flow rates", NEDO-10491, General Electric Company.

Dosch, J. B., Singh, K. M., Stenuf, T. J., 1986, "Air content of medium and high consistency pulp slurries", 1986 TAPPI Engineering Conference Proceedings, *TAPPI PRESS*, Atlanta, 721.

Drahos, J., and Cermak, J., 1989, "Diagnostics of gas-liquid flow patterns in chemical engineering systems", *Chem. Eng. Process.*, *26*, 147-164.

Drahos, J., Zahradnik, J., Puncochar, M., Fialova, M., Bradka, F., 1991, "Effect of operating conditions on the characteristics of pressure fluctuations in a bubble column", *Chem. Eng. Process*, *29*, 107-115.

Duda, R. O., Hart, P. E., and Stork, D. G., 2000, Pattern classification, 2nd Edition, Wiley-Interscience.

Duffy, G. G., Lee, P. F. W., 1978, "Drag reduction in the turbulent flow of wood pulp suspensions", *Appita*, *31*, 280-286.

Duffy, G. G., Titchener, A. L., 1975, "The disruption shear stress of pulp networks", *Svensk Papperstidn*, *13*, 474-479.

Duffy, G. G., Titchener, A. L., Lee, P. F. W., Moller, K., 1976, "The mechanism of flow of pulp suspensions in pipes", *Appita*, 29, 363-370.

Fang, L. S., Sunil, S., and Wisecarver, K., 1986, "Pressure fluctuation measurements and flow regime transitions in gas-liquid-solid fluidized beds", *AICHE J.*, *32*, 338-340.

Fullana, M., Trabelsi, F., and Recasens, F., 1999, "Use of neural net computing for statistical and kinetic modeling and simulation of supercritical fluid extractors", *Chem. Eng. Sci.*, *54*, 5845-5862.

Galloway, J.E. and Mudawar, I., 1993, "CHF mechanism in flow boiling from a short heated wall - I. Examination of near-wall conditions with the aid of photomicrography and high-speed video imaging", *Int. J. of Heat Mass Transfer*, *36*, 2511-2526.

Garner, A.E., and Heindel, T.J., 2000, "The effect of fiber type on bubble size", *J. Pulp Paper Sci., 26*, 266-269.

Ghiaasiaan, S. M., Kamboj, B. K., and Abdel-Khalik, S. I., 1995, "Two-fluid modeling of condensation in the presence of noncondensables in two-phase channel flows", *Nucl. Sci. Eng*., *119*, 1-17.

Ghiaasiaan, S. M., and Abdel-Khalik, S. I., 2001, Two-phase flow in microchannels*, Adv. Heat Transfer, 34*, 145-254.

Giles, C. L., and Maxwell, T., 1987, "Learning, invariance, and generalization in high-order neural networks", *Applied Optics, 26(23),* 4972-4978.

Govier, G. W., and Aziz, K., 1972, *The flow of complex mixtures in pipes,* Van Nostrand Reinhold Co.

Griffel, J. and Bonilla, C. F., 1965, "Forced convection boiling burnout for water in uniformly heated tubular test sections", *Nucl. Structural Eng., 2*, 1-35.

Groeneveld, D. C., Cheng, S. C., And Doan, T., 1986, "AECL-UO critical heat flux look-up table", *Heat Transfer Eng.*, *7*, 46-62.

Groeneveld, D. C., Leung, L. K. H., Kirillov, P. L., Bobcov, V. P., Smogalev, I. P., Vinogradov, V. N., Huang, X. C., and Royer, E., 1996, "The 1995 look-up table for critical heat flux in tubes", *Nuclear Eng. Design*, *163*, 1-23.

Gu., W. and Mudawar, I., 2002, "Transport phenomena in two-phase microchannel heat sinks", Paper presented in the ASME IMECE-2002 Conf., New Orleans, Nov. 17-22, 2002.

Gullichsen, J., and Harkonem, E., 1981, "Medium consistency technology", *Tappi, 64(6)*, 69-72.

Gupta, S., Liu, P. H., Svoronos, S. A., 1999, "Hybrid first-principles/neural networks model for column flotation", *AICHE J.*, *45*, 557-566.

Hall, David D. and Mudawar, Issam, 1997, "Evaluation of subcooled CHF correlations using the PU-BTPFL CHF database for vertical upflow of water in a uniformly heated round tube", *Nucl. Technol., 117*, 234-246.

Hall, D. A., and Mudawar, I., 1998, "Critical heat flux (CHF) for water flow in tubes", Boiling and Two-phase Flow Laboratory, School of Mechanical Engineering, Purdue University, West Lafayette, Indiana.

Hall, David D. and Mudawar, Issam, 2000, "Critical heat flux (CHF) for water flow in tubes - I. Compilation and assessment of world CHF data", *Int. J. of Heat Mass Transfer*, *43*, 2573-2604.

Hall, David D. and Mudawar, Issam, 2000, "Critical heat flux (CHF) for water flow in tubes - II. Subcooled CHF correlations", *Int. J. of Heat Mass Transfer*, *43*, 2605-2640.

Hayes, M., 1996, *Statistical digital signal processing and modeling*. John Wiley & Sons.

Haykin, S. S., 1999, Neural networks: a comprehensive foundation, Prentice Hall.

Heindel, T.J., 1999, "Bubble size measurement in a quiescent fiber suspension", *J. Pulp Paper Sci.*, *25*, 104-110.

Heindel, T.J., and Garner, A.E., 1999, "The effect of fiber consistency on bubble size", *Nord. Pulp Paper Res. J., 14*, 171-178.

Heindel, T. J., and Monefeldt, J. L, 1997, "Flash X-ray radiography for visualizing gas flows in opaque liquid/fiber suspension", *6th Intl. Symp. Gas-Liquid Two-Phase Flows*, Vancouver, BC, ASME Press, June 22-26.

Hewit, G. F., and Roberts, D. N., 1969, "Studies of two-phase flow patterns by simultaneous x-ray and flash photography", AERE-M2159.

Hewitt, G. F., 1978, Measurement of two phase flow parameters, *Academic Press*: *New York*.

Hewitt, G. F., and Govan, A. H., 1990, "Phenomena and prediction in annular two-phase flow", *ASME Advances in Gas-Liquid Flows*, FED *99*, 41-56.

Honan, T. J., Lahey, R. T., 1978, The measurement of phase separation in wyes and tees, *U.S. Nuclear Regulatory Commission Rep. NUREG/CR-0557*.

Hsu, Y. Y., and Grahm, 1986, *Transport in boiling and two-phase systems,* American Nuclear Society.

Hubbard, M.G. and Dukler, A.E., 1966, "The characterization of flow regimes for horizontal two-phase flow", *Proc., Heat Transfer and Fluid Mech. Inst.*, Standford University Press.

Hydrosonic pump operation manual, *Hydrodynamics Inc*., Rome, GA 30165.

Isler, W., and Widmer, F., 1979, "Formation and separation of air bubbles in technical paper pulp suspensions", *Das Papier, 33(3),* 89-93.

Jain, A. K., Mao, J., and Mohiuddin, K. M., 1996, "Artificial neural networks: a tutorial", *IEEE Computer,* 31-44.

Jambunathan, K., Hartle, S. L., Ashforth-Frost, S., and Fontama, V. N., 1996, "Evaluating convective heat transfer coefficients using neural networks", *Int. J. Heat Mass Transfer*, *39*, 2329-2332.

Jensen, M. K., and Bergles, M. K., 1981, "Critical heat flux in helical coiled tubes", *ASME J. Heat Transfer*, *103*, 660-666.

Jones, A. B., 1961, "Hydrodynamic stability of a boiling channel", KAPL-2170, Knolls Atomis Power Laboratory.

Jones, O. C. and Zuber, N., 1975, "The interrelation between void fraction fluctuations and flow patterns in two-phase flow", *Int. J. Multiphase Flow*, *2*, 273-306.

Justice, A. C., Covinsky, K. E., and Berlin, J. A., 1999, "Assessing the generalizability of prognostic information", *Ann Intern Med.*, 130, 515-524.

Katto, Y., 1992, "A prediction model of subcooled flow boiling CHF for pressure in the range 0.1-20.9 MPa", *Int. J. of Heat Mass Transfer*, *35*, 1115-1123.

Katto, Y., 1994, "Critical heat flux", *Int. J. Multiphase flow, 20*, 53-90.

Kefer, V., Kohler, W., Kastner, W., 1989, "Critical heat flux (CHF) and post-CHF heat transfer in horizontal and inclined evaporator tubes", *Int. J. Multiphase Flow*, *15*, 385-392.

Kerekes, R. J., Soszynski, R. M., Tam Doo, P. A., 1985, "The flocculation of pulp fibers", Transactions of the Eight Fundamental Research Symposium (V. Punton, Ed.), Mechanical Engineering Publications, London, *1*, 265.

Kohonen, T., 1989, *Self organization and associative memory,* Third Edition, Springer-Verlag, New York.

Lahey, R. J., Jr., and Moody, F. J., 1993, The thermal-hydraulics of a boiling water reactor, *2nd Ed*., *American Nuclear Society*, La Grange Park, Illinois.

Lawrence, J., 1994, Introduction to neural networks: design, theory, and applications, California Scientific Software Press.

Lee, P. F. W., Duffy, G. G., 1976, "Relationships between velocity profiles and drag reduction in turbulence fiber suspension flow", *AICHE J*., *22*, 750.

Lee, Y. H., Baek, W.-P., and Chang, S. H., 2000, "A correlation method for heated length effect in critical heat flux prediction", *Nucl. Eng. Design, 199*, 1-11.

Luo, D., and Ghiaasiaan, S. M., 1997, "Liquid-side interphase mass transfer in cocurrent vertical two-phase channel flows", *Int. J. Heat Mass Transfer*, *40*, 641-655.

Leontiev, A. I., Mostinsky, I. L., Polonsky, V. S., Styrikovich, M. A., and Chernika, I. M., 1981, "Experimental investigation of the critical heat flux in horizontal channels with circumferentially variable heating", *Int. J. Heat Mass Transfer*, *24*, 821-828.

Lezzi, A. M., Niro, A., and Beretta, G. P., 1994, "Experimental data on CHF for forced convection water boiling in long horizontal capillary tubes", in: G. F. Hewitt (Ed.), Heat Transfer 1994: Proceeding of the Tenth International Heat Transfer Conference 7 (1994) 491-496, Institution of Chemical Engineering, Rugby, United Kingdom.

Lin, P. Y., and Hanratty, T. J., 1986, "Detection of slug flow regimes in vertical two-phase flow using differential pressure fluctuations", *Nucl. Eng. Design*, *95*, 221-231.

Lin, W.-S., and Pei, B.-S., 1992, "Bundle critical power prediction under normal and abnormal conditions in pressurized water reactors", *Nucl. Technol*., *98*, 354-365.

Lindsay, J. D., Ghiaasiaan, S. M., and Abdel-Khalik, S. I., 1995, "Macroscopic flow structures in a bubbling paper pulp-water slurry", *Ind. Eng. Chem. Research*, *34*, 3342-3354.

Lockhart, R. W., and Martinelli, R. C., 1949, "Proposed of data for isothermal two-phase two-component flow in pipes", *Chem. Eng. Prog., 45, no. 39*.

Longdill, G. R., and Duffy, G. G., 1988, "The shear behavior of medium concentration pulp suspensions", *Appita, 41*, 456-461.

Lowdermilk, W. H., Lanzo, C. D., and Siegel, B. L., 1958, "Investigation of boiling burnout and flow instability of water flowing in tubes", NACA-TN4382.

Mallat, S., and Hang, W. L., 1992, "Singularity detection and process with wavelets", *IEEE Trans. on Information Theory, 38*, 617-643.

Mandhane, J. M., Gregory, G. A., and Aziz, K., 1974, "A flow pattern map for gas-liquid flow in horizontal pipes", *Int. J. Multiphase Flow*, *1*, 537-553.

Maren, A., "Handbook of neural network applications", Academic Press, New York, 1990.

Martinelli, J. M., and Nelson, D. B., 1948, "Prediction of pressure drop during forced circulation boiling of water", *Trans ASME, 70*, 695-704.

MATLAB 6.1 Tutorial, The Mathworks, Inc., 2003.

Matsui, G., 1984, "Identification of flow regimes in vertical gas-liquid two-phase flow using differential pressure fluctuations", *Int. J. Multiphase Flow*, *10*, 711-720.

Matsui, G. 1986, "Automatic identification of flow regimes in vertical two-phase flow using differential pressure fluctuations", *Nucl. Eng. Design, 95*, 221-231.

Matsumoto, S., and Suzuki, M., 1984, "Statistical analysis of fluctuations of froth pressure on perforated plates without downcomers", *Int. J. Multiphase Flow*, *10*, 2, 217-228.

McCulloch, W. S. and Pitts, W., 1943, "A logical calculus of ideas immanent in nervous activity", *Bull. Mathematical Biophysics, 5*, 115-133.

Merilo, M., Dechene, R. L., and Cichowlas, W. M., 1977, "Void fraction measurement with a rotating field conductance gauge", *J. Heat Transfer, Transactions of ASME*, *99*, 330-332.

Merilo, M., 1977, "Critical heat flux experiments in a vertical and horizontal tube with both Freon-12 and water as coolant", *Nuclear Eng. Design*, *44*, 1-16.

Merilo, M., 1979, "Fluid to fluid modeling and correlation of flow boiling crisis in horizontal tubes", *Intl. J. Multiphase Flow*, *5*, 313-325.

Mi, Y., Ishii, M., and Tsoukalas, L. H., 1998, "Vertical two-phase flow identification using advanced instrumentation and neural networks", *Nuclear Eng. Design*, *184*, 409-420.

Mi, Y., Ishii, M., Tsoukalas, L. H., 2001, "Flow regime identification methodology with neural networks and two-phase flow models", *Nuclear Eng. Design*, *204*, 87-100.

Mishima, K., and Ishii, M., 1983, "Flow regime transition criteria for upward two-phase flow in vertical tubes", *Int. J. of Heat and Mass Transfer*, *27*, 723-737.

Molga, E., and Cherbanski, R., 1999, "Hybrid first-principle-neural-networks approach to modeling of the liquid-liquid reactor system", *Chem. Eng. Sci*., *54*, 2467-2473.

Moon, S. K., and Chang, S. H., 1994, "Classification and prediction of the critical heat flux using fuzzy theory and artificial neural networks", *Nucl. Eng. Design*, *150*, 151-161.

Moon, S. K., Baek, W.-P., and Chang, S. H., 1996, "Parametric trends analysis of the critical heat flux based on artificial neural networks", *Nucl. Eng. Design, 163,* 29-49.

Nariai, H., Inasaka, F., and Shimuara, T., 1987, "Critical heat flux of subcooled flow boiling in narrow tube", *Proc. ASME/JSME Thermal Energy Joint Conf. 5*, 455-462.

Nariai, H., Inasaka, F., and Uehara, K., 1989, "Critical heat flux in narrow tubes with uniform heating", *Heating Transfer: Japanese Research, 18*, 21-30.

NeuroShell® 2 release 4.0, Copyright© 1993-1998, Ward Systems Group, Inc, Frederick, MD 21703.

Normandin, A., Grandjean, B. P. A., and Thibanlt, J., 1993, "PVT data analysis using neural network models", *Ind. Eng. Chem. Res*., *32*, 970-975.

Otawara, K, Fan, L. T., Tsutsumi, A., Yano, T., Kuramoto, K., and Yoshida, K., 2002, "An artificial neural network as a model for chaotic behavior of a three-phase fluidized bed", *Chaos, Solitons and Fractals*, *13*, 353-362.

Pelton, R., Piette, R., 1992, "Air bubble hold-up in quiescent wood pulp suspensions", *Can. J. Chem. Eng*., *70*, 660.

Peng, L., Zhang, B., Yao, D., and Xiong Z., 1996, "Recognizing flow pattern of gas/liquid two-component flow using fuzzy logical neural network", Proceedings IWISP '96, 4-7 November 1996, Manchester, U.K., 127-132.

Petzold, L. R., and Hindmarsh, A. C., "LSODA-Livermore Solver for Ordinary Differential Equations, with Automatic Method Switching for Stiff and Non-stiff Problems", Computing and Mathematics Research Division, 1-316, Lawrence Livermore National Laboratory, 1997.

Proakis, J. G., and Manolakis, D. G., 1996, *Digital signal processing: principles, algorithms, and applications*. New Jersey: Prentice-Hall.

Qi, H., Zhou, X.-G., Liu, L.-H., and Yuan, W.-K., 1999, "A hybrid neural network-first principle model for fixed-bed reactor", *Chem. Eng. Sci*., *54*, 2521-2526.

Reese, J., Jiang, P. and Fan, L. -S., 1996, "Bubble characteristics in three-phase systems used for pulp and paper processing", *Chem. Eng. Sci*., *51*, 2501-2510.

Reith, T., and Beck, W. J., 1973, "The oxidation of aqueous sodium sulphite solutions", *Chem. Eng. Sci*., *28*, 1331-1339.

Rewatkar, V. B., and Bennington, C. P. J., 2000, "Gas-liquid mass transfer in low- and medium-consistency pulp suspensions", *Can. J. Chem. Eng*., *78*, 504-512.

Rutkowski, J., 1997, "Environmentally friendly pulp bleaching technologies", *Cellulose Chem. Technol*., *31*, 485-497.

Rezak, S., 2002, Master Thesis, *Institute of Paper Science and Technology*, Atlanta, GA.

Roach, G. M., Jr., Abdel-Khalik, S. I., Ghiaasiaan, S. M., and Jeter, S. M., 1999, "Low-flow critical heat flux in heated microchannels", *Nucl. Sci. Eng., 131*, 411-425.

Robertson, A. A., and Mason, S. G., 1957, "Flow characteristics of dilute fiber suspensions", *Tappi, 40(5),* 326-334.

Sanders, H. T., and Meyer, H., 1971, "Consistency distribution in turbulent tube flow of fiber suspensions", *Tappi, 54(5)*, 722-730.

Shah, M. M., 1987, "Improved general correlation for critical heat flux during upflow in uniformly heated vertical tubes", *Int. J. Heat Fluid Flow, 8*, 326-335.

Smook, G. A., 1992, Handbook for pulp & paper technologists, *2nd Ed*., *Angus Wilde Publications*, Vancouver, British Columbia.

Spedding, P.L. and Spence, D.R., 1993, "Flow regimes in two-phase gas-liquid flow", *Int. J. Multiphase Flow*, *19*, 245-280.

Stoddard, R. M., Blasick, A. M., Ghiaasiaan, S. M., Abdel-Khalik, S. I., Jeter, S. M., and Dowling, M. F., 2002, "Onset of flow instability and critical heat flux in thin horizontal annuli", *Exp. Th. Fluid Sci*., to appear.

Sugawara, S., 1990, "Droplet deposition and entrainment modeling based on the three-fluid model", *Nucl. Eng. Design, 122*, 67-84.

Sugawara, S., 1990, "Analytical prediction of CHF by FIDAS code based on three-fluid and film dryout model", *J. Nucl. Sci. Technol*., *27*, 12-29.

Sun, T., Zhang, H. Hu, C., 2002, "Identification of gas-liquid two-phase flow regime and quality", IEEE Instrumentation and Measurment Technology Conference, Anchorage, AK, USA, 21-23 May 2002, 1471 – 1474.

Taitel, Y., Barnea, D., and Dukler, A. E., 1980, "Modeling flow pattern transitions for steady upward gas-liquid flow in vertical tubes", *AICHE J*., *26*, 345-354.

Taylor, K. E., 1993, An experimental investigation of a bubbling three-phase pool. Master Thesis, G. W. Woodruff School of Mechanical Engineering, Georgia Institute of Technology, Atlanta, GA.

Thibault, J., Leduy, A., and Denis, A., 1990, "Chemical enhancement in the determination of $K_L a$ by the sulfite oxidation method", *Can. J. Chem. Eng*., *68*, 324-326.

Thom, J. R. S., 1964, "Prediction of pressure drop during forced circulation boiling of water", *Int. J. Heat Mass Transfer, 7*, 709-714.

Todreas, N., and Kazimi, M., 1990, *Nuclear systems I, thermal hydrolic fundamentals,* Hemisphere Publishing Corp..

Tong, L. S. and Tang, Y. S., 1997, Boiling heat transfer and two-phase flow, 2nd ed., Taylor & Francis, New York.

Triplett, K. A., Ghiaasiaan, S. M., Abdel-Khalik, S. I., and Sadowski, D. L., 1999, "Gas-liquid two-phase flow in microchannels, Part I: Two-phase flow patterns", *Int. J. Multiphase Flow, 25,* 377-394.

Triplett, K. A., Ghiaasiaan, S. M., Abdel-Khalik, S. I., LeMouel, A., and McCord, B. N., 1999, "Gas-liquid two-phase flow in microchannels, Part II: Void fraction and pressure drop", *Int. J. Multiphase Flow, 25,* 395-410.

Tsoukalas, L. H., and Uhrig, R. E., 1997, Fuzzy and neural approaches in engineering, John Wiley & Sons, New York,.

Xie, T., Ghiaasiaan, S. M., Karrila, S., and McDonough, T., 2003a, "Flow regimes and gas holdup in paper pulp-water-gas three-phase slurry flow", *Chem. Eng. Sci.*, *58*, 1417-1430.

Xie, T., Ghiaasiaan, S. M., and Karrila, S., 2003b, "Flow regime identification in gas-liquid-pulp fiber slurry flows based on pressure fluctuations using artificial neural networks", *Industrial and Engineering Chemistry Research*, *42*, 7017-7024.

Xie, T., Ghiaasiaan, S. M., and Karrila, S., 2004, "Artificial neural network approach for flow regime classification in gas-liquid-fiber flows based on frequency domain analysis of pressure signals", *Chem. Eng. Sci.*, *59*, 2241-2251.

Vandervort, C. L., Bergles, A. E., and Jensen, M. K., 1994, "An experimental study of critical heat flux in very high heat flux subcooled boiling", *Int. J. Heat Mass Transfer, 37 suppl. 1*, 161-173.
Wallis, J. G., 1969, *One-dimensional two-phase flow,* McGraw-Hill.

Whalley, P. B., 1996, "Two-phase flow and heat transfer", Oxford Science Publication, Oxford, UK.

Vince, A. M., Finckle, J. R., 1983, "The relationship between density and void fraction measurement uncertainty in radiation densitometry", *Int. J. Multiphase Flow*, *9*, 449.

Wallis, G. B., 1969, One-dimensional two-phase flow, *McGraw-Hill*, New York.

Walmsley, M. R. W., 1992, "Air bubble motion in wood pulp fiber suspension", *Appita J.*, *45*, 509-515.

Wambsganss, M. W., Jendrzejczyk, J. A., and France, D. M., 1994, "Determination and characteristics of the transition to two-phase slug flow in small horizontal channels", *J. Fluids Eng.*, *116*, 140-146.

Weatherhead, R. J., 1963, "Heat transfer, flow instability, and critical heat flux for water in a small tube at 200psia", ANL-6715, Argonne National Laboratory, Argonne, IL.

Weisman, J., Duncan, O., Gibson, J., and Crawford, T., 1979, "Effect of fluid properties and pipe diameter in two-phase flow patterns in horizontal lines", *Int. J. Multiphase Flow*, *5*, 437-462.

Weisman, J., Ileslamlou, S., 1988, "A phenomenological model for predicion of critical heat flux under highly subcooled conditions", *Fusion Technol.*, *13*, 654-659.

Weisman, J., 1992, "The current status of theoretically based approaches to the prediction of the critical heat flux in flow boiling", *Nucl. Technol.*, *99*, 1-21.

Welch, P. D., 1967, "The use of fast Fourier transform for the estimation of power spectra: a method based on time averaging over short, modified periodograms", *IEEE Trans. Audio Electroacoustics*, AU-15, 70-73.

Wong, Y. L., Groeneveld, D. C., and Cheng, S. C., 1990, "CHF prediction for horizontal tubes", *Int. J. Multiphase Flow*, *16*, 123-138.

Wu, H., Zhou, F., and Wu, Y., 2001, "Intelligent identification system of flow regime of oil-gas-water multiphase flow", *International Journal of Multiphase Flow*, *27*, 459-475.

Zeidenberg, 1991, M., Neural networks in artificial intelligence, Ellis Horwood Limited.

Zhang, J.-P., Grace, J. R., Epstein, N., and Lim, K. S., 1997, "Flow regime identification in gas-liquid flow and three-phase fluidized beds", *Chem. Eng. Science*, *52*, 3979-3992.

Zuber, N., and Findlay, J. A., 1965, "Average volumetric concentration in two-phase flow systems", *J. Heat Transfer, 87*, 453-459.